University of Bath

PHD

The Preparation, Characterisation and Anti-Bacterial Activity of Orally-Viable Tin(II) Salts

Deacon, Paul Robert

Award date:
1994

Awarding institution:
University of Bath

Link to publication

Alternative formats
If you require this document in an alternative format, please contact:
openaccess@bath.ac.uk

Copyright of this thesis rests with the author. Access is subject to the above licence, if given. If no licence is specified above, original content in this thesis is licensed under the terms of the Creative Commons Attribution-NonCommercial 4.0 International (CC BY-NC-ND 4.0) Licence (https://creativecommons.org/licenses/by-nc-nd/4.0/). Any third-party copyright material present remains the property of its respective owner(s) and is licensed under its existing terms.

Take down policy
If you consider content within Bath's Research Portal to be in breach of UK law, please contact: openaccess@bath.ac.uk with the details. Your claim will be investigated and, where appropriate, the item will be removed from public view as soon as possible.

Download date: 04. May. 2023

THE PREPARATION, CHARACTERISATION AND ANTI-BACTERIAL ACTIVITY OF ORALLY-VIABLE TIN(II) SALTS.

Submitted by Paul Robert Deacon

for the degree of PhD

of the University of Bath

1994.

UMI Number: U065506

All rights reserved

INFORMATION TO ALL USERS
The quality of this reproduction is dependent upon the quality of the copy submitted.

In the unlikely event that the author did not send a complete manuscript
and there are missing pages, these will be noted. Also, if material had to be removed,
a note will indicate the deletion.

UMI U065506
Published by ProQuest LLC 2013. Copyright in the Dissertation held by the Author.
Microform Edition © ProQuest LLC.
All rights reserved. This work is protected against
unauthorized copying under Title 17, United States Code.

ProQuest LLC
789 East Eisenhower Parkway
P.O. Box 1346
Ann Arbor, MI 48106-1346

21 03 MAY 1995
Ph. D.
5090510

COPYRIGHT NOTICE.

Attention is drawn to the fact that copyright of this thesis rests with its author. This copy of the thesis has been supplied on condition that anyone who consults it is understood to recognise that its copyright rests with its author and that no quotation from the thesis and no information derived from it may be published without the prior written consent of the author.

This thesis may be made available for consultation within the University Library and may be photocopied or lent to other libraries for the purposes of consultation.

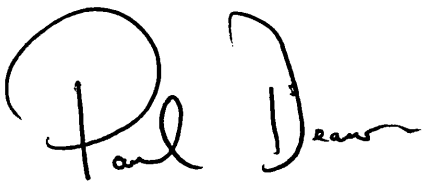

Paul Robert Deacon.

ABSTRACT.

The work described in this thesis has been divided into three main sections. These are the Introduction (Chapter one), the preparation and characterisation of orally-viable stannous compounds (Chapters two to four) and microbiological testing (Chapter five).

Chapter one provides a brief background to the problems associated with the build-up of oral plaque and the methods employed for its removal and prevention of regrowth including the use of metal ions such as Zn^{2+} and, in particular, Sn^{2+}. Following this is an overview of the bonding and structural aspects of general tin(II) chemistry together with a description of ^{119m}Sn Mössbauer and ^{119}Sn NMR spectroscopic techniques used for the characterisation of tin-containing materials. Finally, a review of selected orally-viable compounds containing tin(II) including the halides, phosphorus oxy-acid salts, carboxylates and alkoxides is included.

Chapter two describes in detail the preparation and characterisation of a series of tin(II) phosphates, polyphosphates and related compounds. The spectroscopic data for selected compounds were supplemented with EXAFS structural studies. The interaction of tin(II) pyrophosphate, an important dentifrice anti-microbial active component, with ionic fluorides was investigated in detail.

Chapter three describes the synthesis and characterisation of a series of tin(II) polyolphosphate compounds including the salts of isomeric and anomeric glucose phosphates. As in Chapter two, the spectroscopic analyses were supplemented with EXAFS data. Further examples of carbohydrate compounds were also prepared and characterised including tin(II) salts of selected C_6 aldonic acids. Finally, the interaction of tin(II) α-D-glucose-1-phosphate with an ionic fluoride source was

examined in detail.

Chapter four describes the synthesis and characterisation of a series of tin(II) salts of citric acid and its aliphatic esters. The structures of mono-stannous 1,3-dimethylcitrate mono-methanolate and stannic bis-citrato di-tetramethylammonium heptahydrate are reported, having been determined with X-ray crystallography. Finally, the interaction of di-stannous citrate with a range of ionic fluorides was investigated.

Chapter five describes a series of microbiological experiments that were carried out at Unilever Research Port Sunlight Laboratories. Selected tin(II) compounds from each of the above Chapters were subjected to an lactic acid inhibition assay for the metabolism of α-D-glucose by the important oral organism, *Streptococcus Mutans*. Following this, the inter- and intracellular retention of tin-containing material was examined by TEM. Finally, the adhesion of selected compounds to pellicle-coated spheroidal HAP was determined using ICP-AA.

ACKNOWLEDGEMENTS.

The research project described in this thesis was carried out between January 1991 and December 1993 in the Department of Inorganic Chemistry at the University of Bath.

I am particularly indebted to Dr Kieran Molloy for the help, guidance and continual encouragement that I received throughout the practical work and the writing of this thesis.

I would also like to thank Dr Philip Waterfield, Dr Mike Traudt and Craig Boniface at Unilever Research for the assistance and encouragement that I received during placement visits to the Gum Health Laboratory at Port Sunlight. I would also like to thank Dr Kay Fox of Unilever Research for the many hours spent at Daresbury SRS Laboratories assisting with the EXAFS studies.

My thanks also go to my colleagues in the Inorganic Chemistry Department for their advice, friendship and making my time at Bath humorous and so enjoyable. I would particularly like to thank Rob Harker, Mike Hill, Dr John McGinley and Dr Kim Wong with whom I have shared so many memorable times. My thanks are also extended to Robert, Ahmad and Shiela of the Inorganic Chemistry Department for their technical assistance, Alan Carver for elemental analyses, Dr Mary Mahon for performing the structural X-ray crystallographic analyses and Dave Wood for collecting the majority of the NMR spectra.

Finally, I would like to thank my wife, Joanne, and my family for their untiring support and encouragement throughout the duration of this project.

Financial support for this project from Unilever Research Port Sunlight Laboratories is gratefully acknowledged.

Dedicated to my son, Aaron.

CONTENTS.

ABBREVIATIONS.

br	Broad
^{n}Bu	n-butyl
^{n}BuOH	n-butanol
^{t}Bu	Tertiary butyl
^{t}BuOH	Tertiary butanol
Cit	Citrate
d	Doublet
dd	Doublet of doublets
Ether	Diethyl ether
EtOH	Ethanol
EXAFS	Extended X-ray Absorbance Fine-Structure
αG1P	α-D-glucose-1-phosphate
αG6P	α-D-glucose-6-phosphate
βG6P	β-D-glucose-6-phosphate
HAP	Hydroxyapatite
IR	Infrared spectroscopy
ICP-AA	Inductively-Coupled Plasma Atomic Absorbtion
m	Multiplet
Me	Methyl
MeCN	Acetonitrile
MeOH	Methanol
NMR	Nuclear Magnetic Resonance spectroscopy
^{i}Pr	Iso-propyl
^{i}PrOH	Iso-propanol

q	Quartet
s	Singlet
sh	Sharp
S. Mutans	*Streptococcus Mutans*
st	Strong
t	Triplet
THF	Tetrahydrofuran
w	Weak
ZCT	Zinc Citrate Trihydrate

1. INTRODUCTION.

Stannous fluoride has proven in use to be a highly effective anti-plaque active component of toothpaste formulations. Unfortunately, problems have arisen due to the poor aerial stability and high reactivity of stannous fluoride when incorporated into dentifrice formulations. However, the use of other stannous species in dental care products has attracted very little interest. This project is concerned with extending the range of stannous species that might be succesfully applied as a substitute for stannous fluoride. This thesis describes the preparation, characterisation and anti-microbial evaluation of a range of stannous salts of orally-viable ligands that might offer enhanced long-term stannous stability and activity. Compounds of particular relevance to dental formulation include stannous fluorides, phosphates, carboxylates and chelated polyhydroxyl-alkoxides.

By way of introduction, the oral environment and associated health problems are briefly described. Following this is a summary of the primary types of anti-plaque species that have been applied to reduce or prevent the incidence of periodontol diseases and dental caries. The types of compound described in the literature include organic anti-bacterials, zinc citrate and stannous fluoride, used either independently or in combination. Following this discussion is a review of documented tin(II) chemistry with a particular emphasis on those aspects that are directly related to the further understanding of dental stannous formulation. In this discussion, the stability, preparation, characterisation and structure of known tin(II) compounds is considered. Finally, a summary of the project objectives is included.

The details contained within this introduction are in no way exhaustive and the readers attention is drawn to the further information contained within the literature references cited herein.

1.1 An Overview of Dental Treatment.

Decades of research have been devoted to devising effective means of reducing the incidence of both tooth decay and periodontol, or gum, diseases. The major areas of study have centered on the mechanisms of dental caries, the structure of teeth, the various biological processes taking place in the mouth and the role of diet on dental health. Considerable progress has steadily been made in the understanding of many of the factors that govern an individuals dental health.

In 1923, Dr K H Thoma wrote 'Teeth, Diet and Health' in which he wrote "it is a clean tooth that never ached".[1] As early as 1914 some exciting studies were conducted that proved the hypothesis that good oral hygiene was the major factor responsible for reducing the incidence of tooth decay. Exact details of these studies are lacking, but even assuming significant deviations from currently accepted clinical trial procedures, the results must be considered as being meaningful. The observed reduction in decay in schoolchildren was almost 70% where the children were subjected to rigorous oral hygiene practices. Looking back over the history of dental practice shows that over the course of recorded human activity, the incidence of dental diseases has increased almost proportionally with the advancement of civilisation.[1] The question this generates is: since the earliest days that it has been recognised that dental diseases could be overcome, why haven't appropriate steps been taken to effectively control it? For example, records show that oral hygiene was widely practiced by the ancient Hebrews, who held a good set of teeth in high regard. Regular dental hygiene was also practiced by the Romans and, according to Cicero, clean, white teeth were widely held as a prerequisite of a persons beauty. In fact, the desire for a set of clean, white teeth has been traced to all parts of the world. Study of these varied cultures, as well as current epodemiological surveys clearly reveal that the prevalence of dental diseases is associated with a society's eating habits. An association between diet and dental caries is not a recent finding. The great

philosopher Aristotle suggested that tooth decay was fostered by small particles of sweet foods becoming lodged between the teeth.[1] Caries and gum disease were rampant among the Romans, who regularly dined on sumptuous, sweet foods in spite of their quest for oral hygiene.

There is now strong evidence that a general improvement in oral health in the western world has occurred in recent decades. This improvement is both significant and continuing.[2] Nutritionists may well point to a general improvement in people's dietary habits as the primary cause of this phenomenon, particularly a reduction in sugar consumption. However, increased motivation to preserve ones natural teeth has also become a major factor, as has the ever-increasing efficacy of commercially available dental care products. It is within the grasp of the major manufacturers of dental care products to play an ever-increasing role in the protection of peoples dental health. This can be achieved by providing access to more efficient means to physically clean teeth and providing more effective over-the-counter preparations with therapeutic properties. Products must be developed that are both easier and more pleasant to use, more effective yet still competitively priced in the marketplace. This will help to ensure increasingly widespread product compliance among consumers with the associated improvements to an individuals dental health.

1.2 **The Dental Environment.**

The mouth is the entrance to the alimentary canal, it's major features being the tongue, tonsils, salivary glands, teeth and gums. Once food has been taken into the mouth, it is subjected to two processes, mechanical and chemical, in preparation for its further passage through the alimentary canal. Mechanically, the process of chewing, or mastication, is essential in breaking larger food particles down into smaller fragments. This allows food to be more easily swallowed and the increase in surface area allows it to be further digested more efficiently. Chemically, salivary

enzymes begin the digestive process while the food is still actually within the mouth. Maintainance of the mouth in a healthy state therefore is essential if the digestive process is to function correctly and efficiently. Simple self-applied oral hygiene processes are generally sufficient to ensure continued good health so long as they are applied conscientiously and sufficiently frequently. Since many diseases affecting the mouth originate from the teeth and surrounding tissue, a good oral hygiene programme is essential.

The most obvious symptom of poor oral hygiene is the gradual decay of the teeth. The tooth enamel is the hardest tissue found in the whole body, able to withstand enormous pressures of up to about $10^5 lb/in^2$. It comprises approximately 96% mineral - primarily calcium carbonate, $CaCO_3$, and calcium hydroxyapatite (HAP), $Ca_5(PO_4)_3OH$, with the remaining 4% being organic matter and water. The dental enamel is built up from enamel rods or prisms, rod sheath's, and a cementing interprismatic substance. Around each enamel rod is a rod sheath, a layer which is slightly higher in organic content and slightly less calcified. The sheathed rods are subsequently held together with the interprismatic substance. A cross-section of enamel presents a picture of fine, hexagonal prisms arranged at 90° to the surface and extending to the layer of softer dentin below. Below the layer of dentin is the dental pulp, a highly specialised tissue interspersed with nerves and blood vessels. The teeth are held firmly in the jaw through their roots, although the soft gum tissue also plays a key role in securing the teeth whilst allowing some compliance.

The progressive build up of dental plaque upon the teeth and surrounding gum tissue can lead to caries and periodontol disease respectively, in the absence of a thorough oral care programme.

The teeth and gums are continuously irrigated with freshly produced saliva, excreted from the salivary glands. The role of saliva can be defined in terms of two major functions:-

(i) Digestion and tasting: Solids in dietary food must be dissolved as a

pre-requisite to being tasted. Amylase, a starch-digesting enzyme is a principal component of saliva.

(ii) Protective activity: Saliva acts as a pH buffer to help counter extreme changes in acidity in the mouth. It can buffer both acidic foodstuffs as well as the lactic acid produced as a by-product of bacterial metabolism of sugars and carbohydrates.

Saliva also shows useful detergent properties which can assist with physically clearing the mouth of small food particles, bacterial nutrients and indeed bacteria themselves. Saliva is also supersaturated with hydroxyapatites and fluoroapatites of calcium, i.e. $Ca_5(PO_4)_3OH$ and $Ca_5(PO_4)_3F$ respectively. Consequently, the saliva matrix which contains traces of calcium, phosphorus and fluoride acts as a resevoir which, it is suggested, plays a key role in the continuous maintainance of the surface of the dental enamel.

Crevicular, or gingival fluid is introduced into the saliva stream *via* the gingival crevices at the interface between teeth and gums. Its role in protecting the oral cavity is attributable to its content of potent serum antibodies. Under conditions of good oral health, the detected levels of crevicular fluid are practically non-existent. In the presence of gingivitis and periodontitis, the detected levels of the fluid appear to be directly related to the extent of the condition. This would suggest that the gingival fluid is released into the saliva to combat plaque directly at the gingival margin.

1.3 Oral Accumulations.

The human mouth can play host to a widely varied assortment of accumulations, the removal or prevention of which leads to a healthier oral environment. Thorough and regular toothbrushing, flossing and rinsing will generally keep such accumulations under control and prevent the need for the application of

specialised physical removal.

1.3.1 *Acquired Pellicle.*

As previously described above, the surface of a tooth is made of dental enamel. However, within minutes of being thoroughly cleaned, exposing a clean enamel surface, dental enamel is coated in a sticky organic film. This film is referred to as the acquired pellicle. It consists primarily of proteins laid down by the saliva that continuously irrigates the surface of the teeth and gums and is found to be essentially bacteria-free. Consequently, dental enamel is rarely, if ever, in direct contact with the oral environment, i.e. dental acquired pellicle is the actual surface upon which plaque can form. Unfortunately, as a proteinaceous layer, pellicle is readily stained when exposed to suitable staining agents. Certain dietary components are known to cause rapid discolouration, e.g. tannins in tea and coffee, as well as nicotine from inhaled tobacco smoke. It is widely accepted that the simplest and most effective cure for the largely cosmetic complaint of excessive staining is regular physical scraping by a dental physician. However, it has been suggested that pellicle can act as an effective natural barrier to the acid-attack of the tooth's surface although this remains unproven. Such beneficial protection would be temporarily lost should the acquired pellicle be removed due to excessive staining.

1.3.2 *Dental Plaque.*

Dental plaque is a complex mass of bacteria that forms on the exposed pellicle surface of teeth. It is the single major factor responsible for two of the most prevalent human diseases, namely dental caries and periodontal disease. G V Black can be credited with the earliest written observations on the role of dental plaque.[3] He

observed that a soft, mucinous, water-insoluble deposit formed on the teeth shortly after thorough cleaning had taken place.

The complexity of dental plaque means that much is still to be learned about its precise structure and metabolism, as well as its prevention. Plaque is known to be the cause of periodontol diseases and caries, caused by the bacterial metabolism of dietary carbohydrates with the subsequent generation of lactic acid and it is known that plaque is made up of saliva, bacteria and food particles and it can adhere tenaciously to teeth at points of an irregularity or discontinuity in the surface. The oral bacteria in dental plaque includes many gram-negative and gram-positive micro-organisms embedded in an extra-cellular matrix of insoluble polysaccharides. The colonisation of bacteria to form dental plaque follows an ecological pattern whereby a small number of pioneer aerobic species, mostly gram-positive *Streptococci* such as *S. Mutans*, colonise the surface. The plaque then passes through various stages of increasing microbial complexity, and mature plaque samples removed from protected areas of the mouth, typically contain many potent acid-producing anaerobes.

Plaque control is most commonly effected by methods of physical removal such as toothbrushing and flossing. However, difficulties arise from the fact that the most troublesome, matured plaques often lie in the most inaccesible areas of the mouth where they can do the most damage. Consequently, a more appropriate means of reducing plaque build-up involves the incorporation of potent anti-bacterial agents into commercially available dental care products.

Dental calculus, more commonly known as tartar, is essentially calcified plaque and forms as a hard, unsightly deposit around the gum margin. It can be problematic as it tends to act as an ideal substrate upon which further plaque build-up readily occurs. This can make plaque removal extremely difficult as tartar usually forms around the gum margins in areas of the mouth that are difficult to clean with a conventional toothbrush. Consequently, tartar is considered to be involved in the

onset of gingival problems due to the localised accumulation of plaque build-up around the tooth-gum interface.

The simplest explanation of the formation of calculus is the formation of calcium phosphate crystals ($Ca_3(PO_4)_2$) within the gelatinous plaque matrix. The calcium and phosphate ions are both present in saliva although the exact process by which this crystallisation occurs has yet to be defined in any detail.

1.4 Periodontol Disease and Dental Caries.

An exact definition of what is meant by the term periodontol disease is difficult to give, although most definitions seem to point to inflammatory gingivitis as the earliest indication that periodontol disease is present. This is usually indicated by slight bleeding around the gum margin upon vigorous brushing. It has long been known that the colonies of bacteria present in plaque are the primary cause of gingival health problems and although relatively harmless in itself, if gingivitis is left unchecked it may eventually lead to full periondontitis. This is indicated by the gradual withdrawal of the gums from around the teeth, leading to loosening of the teeth and eventual tooth loss. It is estimated that more teeth are lost in this way than through the actual decay of the teeth. The major factor in controlling this condition is the early and effective removal of plaque, or more effectively, the control of plaque growth upon the teeth. All forms of the disease appear to be caused by bacterial contamination of the gingival margin between teeth and gums, and prevention has emphasised the need to prevent plaque build-up in this critical area. The available information indicates that a large proporton of the population are afflicted by early gingivitis, with many people experiencing slight bleeding around the gum margin during brushing. Improving knowledge about the cause and effect of periodontal diseases should help in the search for an effective prevention and cure for this condition. In particular, improved anti-bacterial agents employed in commercial

toothpastes would be an effective and reliable means of improving gum health.

Dental caries is also a disease primarily caused by plaque that leads to the physical decay and eventual loss of teeth. A major feature in the onset of caries is diet, in particular the sugar consumption of an individual. Briefly, dental caries is a condition caused by bacteria present in the plaque film, whereby they generate lactic acid when metabolising dietary carbohydrates. The acid produced penetrates the acquired pellicle film and reacts with the mineral HAP in the enamel beneath. The acid is said to de-mineralise the tooth enamel leading to calcium deficient apatites according to equation 1.1.

$$Ca_{10}(PO_4)_6(OH)_2 + 2n\,H^+ \longrightarrow n\,Ca^{2+} + Ca_{(10-n)}(HPO_4)_n(PO_4)_{(6-n)}(OH)_{(2-n)}.H_2O \qquad \textbf{(1.1)}$$

The de-mineralised enamel surface is weakened by this process and eventually gives way to the formation of cavities and the eventual destruction of the entire tooth. The associated exposure of nerves within the inner dental pulp can result in severe, painful toothache and discomfort. The regular application of ionic fluorides to the surface of the teeth has had a profound positive effect upon the incidence of caries, and it is for this reason that domestic water supplies are pre-treated with fluoride. Toothpaste formulations also contain a fluoride source (e.g. sodium fluoride) and in extreme cases of decay, dental physicians may prescribe stronger fluoride supplements. The discovery that early carious lesions can be effectively re-mineralised has provided an opportunity to succesfully reverse the effects of dental decay if detected prior to the weakening of the tooth surface has occurred. The exact mechanism of re-mineralisation is currently under study, although the reserves of HAP and fluoride present in saliva are thought to be implicated in this process.

1.5 Formulation of Commercial Dentifrice Products.

A dentifrice, or toothpaste, is designed to fulfil several main objectives:-

(i) Upon application of the paste with suitably designed toothbrushes, the teeth and gums should be thoroughly cleansed. To this end, both abrasive and detergent actions are required, although any abrasive employed should not damage the enamel surface of the tooth.

(ii) The paste should also be formulated to deliver suitably chosen anti-bacterial active ingredients to the plaque deposits. As already described, this can assist in the reduction of both caries and gingivitis, as well as the reduction of calculus build-up.

(iii) The paste should also contain a suitable water-soluble fluoride source, as fluoride is a well documented anti-caries active ingredient. Suitable fluoride sources are sodium fluoride and sodium monofluorophosphate (MFP), $Na_2(FPO_3)$.

(iv) A toothpaste, if it is to be acceptable to the consumer, should have the correct consistency, a pleasant flavour, and should feel right in use, i.e. no grittiness or coarseness of texture.

A commercially available toothpaste may consist of many specific ingredients, but essentially the same basic components are employed in every paste. These are briefly described in Table 1.1 overleaf.

Table 1.1 The components of a typical commercially available dentifrice formulation.

Component	Typical content	Example	Application
Abrasive	15%(w/w)	Silica, Calcium pyrophosphate	Assists the action of brushing in removing deposits from the tooth surface without causing damage to the enamel surface.
Binder	0.5%(w/w)	Sodium carboxy-methyl cellulose, Xantham gum.	Affects the rheology of the finished paste.
Thickener	5%(w/w)	Polyethylene glycol.	Adds structure to the paste.
Detergent	1%(w/w)	Sodium dodecyl sulphate.	Assists the abrasive in cleaning deposits from the teeth.
Opacifier	1%(w/w)	Titanium dioxide.	Gives the desired whiteness to the paste.
Sweetener	<1%(w/w)	Saccharin	Affects the flavour of the product.
Flavouring	1%(w/w)	Peppermint	Produces a desirable flavour.
Humectant	40%(w/w)	Sorbitol	Gives the paste body and holds the ingredients together.
Fluoride	1000ppm	Sodium fluoride	Provides anti-decay protection.
Anti-plaque	1%(w/w)	Zinc / tin(II) salts triclosan.	Provides anti-plaque protection.
Water	To 100%	-	Produces desired consistency.

1.6 Anti-plaque Active Dentifrice Components.

It has previously been described that the primary cause of dental decay and poor gum health is plaque. Consequently, the two main methods of improving dental health are the physical removal of plaque with a mild abrasive action, and the prevention of plaque regrowth by the regular application of suitable anti-plaque active components *via* a dentifrice. Anti-plaque agents that are to be topically administered should have the following basic properties: high intrinsic efficacy against the widest possible range of oral organisms, toxicological and ecological safety, good oral substantivity and no loss due to adverse reactions coupled to good long-term chemical stability.[4] A number of widely varying classes of anti-plaque agent have been identified including positively-charged organic molecules, phenols, enzymes, peroxides, sugar-substitutes, inorganic fluorides, surface-modifying agents and certain metal salts. In the case of dentifrice formulations, various chemical and physical interactions between the proposed anti-plaque agent and the excipient components severely limits compatibility to the non-charged phenolic compounds and metal salts, or a combination of the two. These actives are found to provide a highly effective dosing vehicle, while being efficiently released from the formulation upon application. They also achieve good subsequent retention of the anti-plaque agent in the mouth.[5]

Non-ionic organic anti-bacterial compounds have been found to possess highly effective anti-plaque properties while displaying good compatibility with anionic excipient components commonly found in dentifrice formulations, e.g. surfactants and detergents, fluorides and pyrophosphate or silica abrasives. Such compounds include substituted phenols, such as thymol (**1**) and eucalyptol, halogenated salicylanilides and halogenated hydroxy-diphenylethers such as triclosan (2,4,4′-trichloro-2′-hydroxy-diphenyl ether) (**2**).

Triclosan is a particularly attractive non-ionic anti-bacterial compound

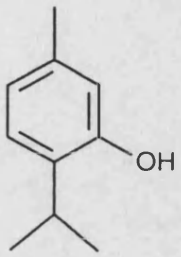

(1)

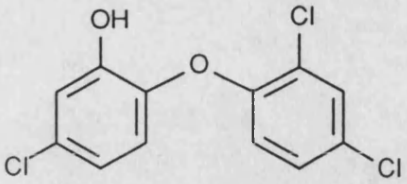

(2)

because it has proven in use to be highly compatible with dentifrice excipients and has a broad anti-microbial activity with no sign that prolonged use produces triclosan-resistant bacterial strains.[6] Triclosan has also shown selective inhibitory activity for gram-negative gingival pathogenic bacteria, and to reduce the ratio of anaerobic to aerobic organisms. This has a profound and positive effect on the quantity of lactic acid produced by glycolytic bacterial metabolism. The efficacy of many antibacterials is greatly influenced by their substantivity, or retention, in the oral cavity. A major determinant of such behaviour is the water-solubility of the compound, and it is here that triclosan is particularly disadvantaged with a very low solubility of about 1ppm in distilled water (at 20°C). Frequently, as a way around this problem, triclosan is emulsified with a suitable surfactant, typically sodium dodecyl sulphate, to form a micellar phase. However, upon dilution in the mouth the surfactant concentration eventually falls below the critical micelle concentration (CMC) and triclosan is precipitated, rendering it biologically inactive. Triclosan that is precipitated in this way is removed either by ingestion or expectoration.

A further disclosed method of improving triclosan delivery is to incorporate a lipophilic copolymer of methoxyethylene and maleic acid into the dentifrice. This has been found to enhance the oral retention of triclosan on both teeth and gum tissue.[7]

The most recently revealed technique for enhancing the activity of triclosan is to exploit the chemical reactivity of the 2′-hydroxyl group.[8] This method involves the

preparation of triclosan-2′-phosphate (**3**) by reaction of triclosan with phosphoryl chloride, $POCl_3$. This compound is ionic and readily water-soluble (> 10%w/w at 20°C), while still showing good levels of chemical stability.

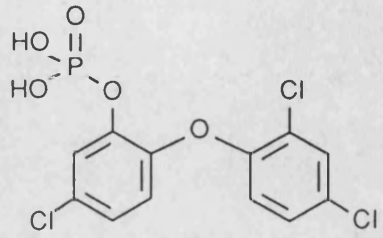

(**3**)

The phosphorylated triclosan is found to be readily soluble in conventional dentifrices, and it is also highly compatible with other active components and excipients. Such an active agent acts as an excellent vehicle for the delivery of triclosan in a bio-active form. A possible explanation for this activity is that (**3**), being readily water-soluble, can diffuse into plaque deposits and bind to phosphatases in saliva, bacterial cell walls and plaque fluids through its phosphate group. The active compound can also bind to phosphatases in gingival lesions and gingival fluid. After binding has occurred, enzymes can process the phosphate groups, thus generating molecular triclosan. The concentration of triclosan increases to effective bacteriocidal levels, thus producing a sustained-release resevoir for triclosan *in situ*. The active triclosan-2′-phosphate is enzymatically degraded to liberate free triclosan primarily in sites of high phosphatase concentration. Since the enzymes are located only in certain specific sites in the oral cavity, subsequent generation of triclosan occurs at these sites only. Fortunately, high phosphatase activity has been identified in plaque samples and certain plaque micro-organisms. This means that the degree of triclosan liberation is found to be directly related to initial plaque levels, and that triclosan is effectively delivered directly to the plaque deposits. One major drawback with triclosan is the current trend for reducing the use of chlorinated organic compounds. Current legislation makes it clear that a more environmentally friendly

alternative to triclosan would be desirable.

Zinc metal ions, Zn^{2+}, are also known to exhibit anti-plaque properties when incorporated into dentifrice formulations. The primary zinc salts that have been used for this purpose have been zinc sulphate, $ZnSO_4$ and zinc citrate trihydrate (ZCT), $Zn_2(C_6H_4O_7).3H_2O$, the exact structure of which is not known. Both of these salts are found to be strongly inhibitory to acid production from sugars and carbohydrates by cell suspensions of *Streptococcus Mutans* (NCTC 10449), a typical oral pathogen. Upon exposure to solutions of these zinc salts, cells of this oral organism are found to contain adsorbed intra-cellular zinc. A good correlation between the degree of acid-inhibition and the level of cellular adsorption of zinc has been established.[9] Clinical-trial data has also shown that continued, regular exposure to mouthwashes containing zinc salts inhibits plaque growth, both *in vivo* and *in vitro*.[10] This encouraging result has also led to use of ZCT in other dentifrice formulations. The use of zinc in this manner has suggested that the main effect of zinc ions is to inhibit the extension of existing plaque, this being of particular benefit to subjects with higher levels of plaque growth.[11] The most common way of utilising ZCT in a dentifrice is in combination with triclosan. The combination of these two anti-plaque agents, themselves both highly effective, is reported to exhibit an additive effect on anti-plaque properties, yielding a particularly potent combination.[12] It has been suggested that the zinc ions induce a lamellar surfactant phase with both triclosan and the sodium dodecyl sulphate surfactant used in the product for detergent purposes. This is said to solubilise the triclosan, overcoming the problems associated with its limited solubility improving the anti-microbial action of the actives. It has also been suggested that there is a direct correlation between the spacing of the lamellar surfactant phase in a triclosan-zinc citrate dentifrice and its overall anti-plaque effect.[13] Several controlled clinical studies have served to confirm the efficacy of combined triclosan-ZCT dentifrices containing typically 0.5% triclosan and 1.0% ZCT. These studies have shown remarkable reductions in plaque accumulations of up

to 50% with prolonged use.[14-17]

The use of such products in commercially available forms has demonstrated significant improvements in plaque build-up, leading to greatly improved gingival health with the associated reduction in calculus levels. A long-term study on a dentifrice containing 0.2% triclosan and 0.5% ZCT showed no evidence of a significant shift in the oral ecology, nor was there any evidence of progressively reduced activity due to the development of bacterial resistance.[18]

A possible explanation for the observed additive levels of activity of such dentifrices is that while zinc ions are more effective on existing plaque, triclosan acts to prevent plaque regrowth. Consequently, the two actives show complementary anti-plaque potential against both existing plaque the formation of new plaque cultures.[19]

Tin(II) fluoride, SnF_2, has also been used in oral preparations since the early 1950's, initially employed as an inorganic fluoride source. In this time stannous fluoride has been reported to be a highly effective agent for treating various dental ailments including plaque, gingivitis, sensitivity, enamel decalcification and periodontitis. Although data is somewhat limited, it is the stannous ion itself, Sn^{2+}, that is now known to be highly effective against oral bacteria and this area has recently been reviewed.[20] Topical applications of stannous fluoride have consistently demonstrated dramatic reductions in dental caries and plaque build-up with minimal side-effects.[21] Traditionally, the mechanism for this effect has been ascribed to the reaction between SnF_2 and HAP at the enamel surface forming a protective layer of a stannous fluoro-phosphate, $Sn_3F_3PO_4$.[22] This product is thought to provide greater resistance to acid attack of the tooth enamel thus reducing the incidence of caries. When studying the reaction between SnF_2 and HAP, a crystalline product can be isolated. An X-ray crystal structure of this compound has been determined, confirming it to be $Sn_3F_3PO_4$.[23] The structure of this compound is discussed later in detail. Evidence has also accumulated that the stannous ion has potent anti-bacterial

properties, which will affect plaque formation and gingivitis as well as influencing its anti-caries properties. Low concentrations of SnF_2, topically applied at frequent intervals have shown significant reductions in *Streptococcus Mutans* levels.[24,25] A significant observation is that the greatest percentage reduction in *Streptococcus Mutans* levels were in subjects displaying the highest initial levels of this oral pathogen. There have been several studies examining the potential anti-plaque properties of SnF_2. Characteristically most of these studies are short term showing that SnF_2 significantly reduces plaque levels.[26-29] These studies have generally used SnF_2 twice daily in concentrations between 0.1 to 0.4%, either as a mouthrinse or dentifrice type formulation, and consistently show 60-80% plaque reduction, i.e. highly effective anti-microbial activity. These anti-plaque results suggest there should be a useful beneficial effect upon gingival health due to regular exposure to SnF_2, however, additional clinical trials are required to further determine the long-term effects of the use of SnF_2 in the treatment of various periodontol diseases.

Most studies that have explored the anti-microbial action of the stannous ion have focussed on alterations to either bacterial growth[30-35] or the levels of bacterial adhesion/ cohesion.[32,36,37] As early as 1956, Lilienthal observed that SnF_2 inhibited oral bacterial acid-production, and it was suggested that this was due to positively-charged tin(II) ions combining with negatively-charged sites on the surface of bacteria preventing the transfer of glucose across the cell membrane.[30] Later investigations have suggested that SnF_2 produces unbalanced bacterial growth,[32] oxidises thiol groups in enzymes involved in glycolysis and sugar transport,[33] reduces the levels of lipoteichoic acid in plaque[27,34] and decreases the rate of bacterial growth.[35] However, a consistent and reproducible finding is that oral bacteria exposed to aqueous solutions of soluble stannous species retain large quantities of tin within the cell.[32,38,39] In the case of *Streptococcus Mutans*, uptake of tin is very rapid with maximum uptake levels of tin occurring after just a few minutes. The level of uptake of tin is not found to be directly proportional to the concentration of stannous

solution to which cells are exposed, a typical set of experimental results that might be obtained are illustrated graphically in Fig. 1.1.

Interestingly, cell suspensions of *Streptococcus Mutans* that had been exposed to a 5mM solution of SnF_2 showed no loss of absorbed tin when thoroughly washed with distilled water or saline.

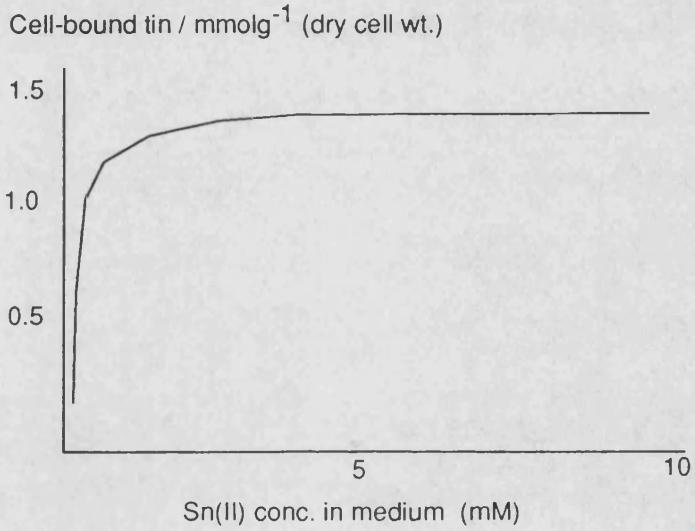

Fig. 1.1 Typical rate of uptake of tin(II) by *Streptococcus Mutans* cell suspensions with varying stannous concentration.

The difficulty in removing the adsorbed tin, together with the high content of tin in the bacteria, as measured by atomic absorption spectrophotometry, suggest that tin(II) ions are actually transported within the cell where they become firmly bound. This can be confirmed by transmission electron microscopy (TEM), which clearly shows large numbers of intracellular, granular tin deposits. The apparent condensation of the tin into granules may be a crude attempt by the individual bacterial cells to minimise the effects of this foreign invader.[40] The intracellular tin accumulation appears to disrupt the metabolism of the *Streptococcus Mutans* cells, as demonstrated by their reduced growth and acid-production, as well as the electron-microscopic evidence of holes in many of the cell walls.

A crucially important point is the apparent lack of analogous behaviour with tin(IV) salts. Compounds such as SnF_4 show an almost complete lack of such activity when tested under the same conditions.[39] No explanation of this phenomenon has been offered, although this observation suggests that the activity of tin(II) species may be due in part to the strongly reducing nature of the stannous ion which is absent in tin(IV) compounds..

Formulating oral health-care products such as mouthwashes and dentifrices containing stannous salts is much more problematic than with zinc compounds. Tin in its lower oxidation state (+2) is particularly susceptible to oxidation and hydrolysis. These processes can render highly active, soluble stannous species inactive, as either stannic compounds or insoluble stannous-hydroxyl species, or a combination of the two. Two stannous salts are currently used in dental formulations, these are stannous fluoride as described in the literature, and stannous pyrophosphate, $Sn_2P_2O_7$. By fine-tuning the actual product formulation it is possible to obtain products that contain stannous species in a soluble, yet aerobically stable state over extended periods and a range of extreme storage conditions. The stannous ion, being highly reactive, can undergo a variety of excipient interactions, including those with flavourings, fluorides, silica and sorbitol once incorporated into a formulation. Many of these interactions will have a profound effect upon the overall level of stannous stability. For example, stannous compounds are known to react with polyhydroxy compounds such as sorbitol and ethylene-glycol.[41] Since a large proportion of a toothpaste consists of sorbitol it is highly probable that a chemical interation will occur. Such an interaction is known to provide a physical barrier to oxidation and hydrolysis, and thus high sorbitol levels should promote stannous stability. This is because stannous ions that are chelated in this manner are physically surrounded and fully coordinated by the multiple hydroxyl groups on the ligand. It is also known that toothpastes formulated with a combination of stannous pyrophosphate and either fluoride or ZCT exhibit quite high levels of soluble stannous, even though the pyrophosphate is known

to be quite insoluble. The structures of the species formed in such pastes are unknown, although the beneficial effect upon stannous stability can be observed experimentally.

A documented method of stabilising stannous compounds in dentifrices is to add a highly specific chelating agent to the product. For example, a copolymer of maleic anhydride and methoxyethylene of molecular weight greater than 30,000 $gmol^{-1}$ is found to form sufficiently strong chelates with stannous fluoride to provide effective protection from oxidation in a similar manner to the situation with sorbitol.[42] Such chelating agents should be carefully selected for their tendancy to chelate calcium as if the chelated calcium species are formed too readily application of the toothpaste may actually deplete calcium ions from the dental enamel causing carious lesions to develop.

A recent approach to formulating stable stannous formulations has involved the incorporation of an effective quantity of an organic anti-oxidant into the product. The exact compound used must be chosen such that it will be readily compatible with the existing ingredients. The compound that has been employed takes the form of an organic radical-inhibitor such as propyl gallate (**4**).

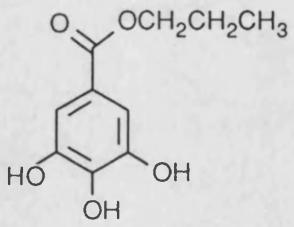

(**4**)

The tendancy for stannous ions to oxidise to stannic species appears to be greatly reduced with levels of this compound as low as 1% incorporated into the paste. This yields net stannous levels that are effectively doubled over the expected values after prolonged storage.[43] It would appear from these experimental results that

the presence of a radical inhibitor such as propyl gallate prevents, or at least drastically inhibits, the major oxidation routes of tin(II) to tin(IV).

1.7 The Chemistry of Potential Orally-viable Tin(II) Compounds.

In this section, various aspects of tin(II) chemistry of particular relevance to the formulation of dental products is considered. These aspects include the preparation and characterisation of stannous compounds, as well as a consideration of the bonding and coordination exhibited by these species. Following this is a description of documented tin(II) phosphates, fluorides, carboxylates and polyhydroxyl-alkoxides. These classes of stannous compound are particularly relevant to the understanding of tin(II) interactions within a formulated dental products.

1.7.1 *Bonding Considerations in Stannous Compounds.*

Tin, a group 14 metal, has the outer electronic configuration $5s^2 5p^2$ and like carbon, silicon, germanium and lead it can form compounds in the +IV and +II oxidation states. There is an abrupt discontinuity in general properties between the first and second row elements followed by a relatively smooth increase in metallic character thereafter in this group of the periodic table. Carbon is non-metallic; silicon essentially non-metallic; germanium is a metalloid; tin and particularly lead are metallic. True divalence is found in carbenes and a few SiX_2 compounds, however the divalent state becomes increasingly stable down the group and is the dominant feature of lead chemistry, i.e. in terms of stability; Pb(II) > Sn(II) > Ge(II) >> Si(II) > C(II). Lead is the only element of this group where the lower valence state is actually favoured. In the case of tin, and particularly germanium, the higher valence state is

favoured and this causes problems in the preparation of tin(II) (and germanium(II)) compounds. When handling tin(II) compounds, particular care is needed to prevent exposure to oxidants and hydrolytic conditions.

Since the properties and structures of many tin(IV) compounds are documented in the literature, this aspect of tin chemistry is well described. However, much of the necessary information on tin(II) compounds has been much less forthcoming. This may well explain why accurate descriptions of their chemistry are less satisfactory. The chemistry of tin(II) compounds can be considered essentially on the valence electronic configuration in the +II oxidation state. This method can be used to explain the chemistry of tin(II) compounds and to predict the general structural features.

Before considering tin(II) chemistry it is worthwhile noting the fact that stannic chloride, $SnCl_4$, is a volatile liquid at room temperature suggesting that the bonding preferred in most tin(IV) compounds is largely covalent and that the properties of most compounds will be explained satisfactorily in terms of sp^3 hybrid covalent bonding. The observed increase in coordination about tin from four to six in complex ions like $SnCl_6^{2-}$, and in adducts such as $SnCl_4$. 2(py) (py = pyridine) can be accounted for by the ease of inclusion of 5*d*-orbitals in the hybridisation process.[44] For certain solid compounds (e.g. Perovskite-type stannates, $MSnO_3$), ionic bonding gives a more convenient picture of the bonding. However, in these materials there is a distortion of the expected regular six-coordinate octahedral geometry toward a four-coordinate tetrahedral environment. This simple approach shows that tin(IV) compounds behave essentially as expected for a metallic element with the $5s^25p^2$ valence electronic configuration.

In treating the bonding in tin(II) compounds we must consider the use of only two of the valence shell electrons. Bonding can be considered from both electrostatic or covalent extremes although it is likely that a somewhat intermediate character will be adopted. On the basis of its outer electronic configuration it is possible to predict

four possible modes of bonding in tin(II) compounds:-

(i) Loss of the two 5*p* electrons to form the stannous ion, Sn^{2+}.

(ii) Use of the two 5*p* electrons for simple covalent bond formation.

(iii) Complex formation, i.e. inclusion of empty 5*p* and low energy 5*d* orbitals in hybridisation to produce acceptor orbitals.

(iv) Overlap of the lone-pair 5*s* orbital with empty orbitals on a suitable acceptor species to form a σ-bonded species, i.e. a 2e Lewis base.

The first and second ionisation energies of tin are 7.43 and 14.63eV respectively.[45] This suggests that the pair of 5*p* electrons can be quite readily lost resulting in the formation of an Sn^{2+} ion of configuration $5s^2 5p^0$. The configuration of this ion means it has a lone pair of *s*-electrons beyond a completed 4*d* shell, resulting in a non-symmetrical charge distribution around the atom. This can be thought of as a stereochemically active lone-pair. Orgel has shown that crystal-field effects on the occupation of the available energy levels of the stannous ion also leads to the prediction of a distorted environment for the tin(II) ion.[46] It is known that the presence of low-lying excited energy levels often leads to a distortion of highly symmetrical ionic coordinations. The first excited state of the stannous ion has the electronic configuration $5s^1 5p^1$, and lies only 6.64eV above the ground state ($5s^2$) energy level. This can yield extra crystal-field stabilisation energy due to *s-p* mixing. Since an *s*-orbital is spherically symmetrical and a *p*-orbital is asymmetric (shaped like a dumbell), stabilisation can only be achieved with the simultaneous formation of more distorted environment about the tin.

As stated, the ground state of tin metal is $5s^2 p^2$, and the element could form covalent bonds in the lower +2 oxidation state by using two unpaired 5*p* electrons. The resulting stereochemistry of the molecule formed will depend upon the type of hybridisation adopted by the valence shell electrons. If the hybridisation of the orbitals is p^2, the bond angles should be 90°. If the lone-pair *s* electrons are incorporated in sp^2 hybridisation, the bond angles should approach 120°.

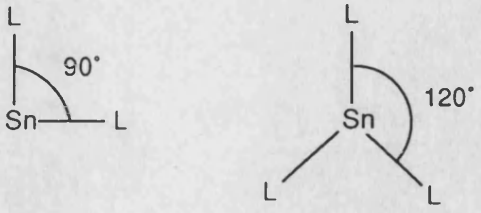

(a) p^2 (b) sp^2

The bond angles will depend heavily on the extent of repulsion between the bonds formed and the highly repulsive effect of the lone-pair electrons leading to the prediction of a distorted geometry in covalent tin(II) compounds. Compounds of this type have an empty p_z orbital of similar energy to those used in bonding, set at right angles to the molecular plane. Therefore, any tin(II) compound with an appreciable covalent character should act as a monofunctional acceptor towards suitable ligands. This will result in the formation of adducts of the type SnX_2.n(ligand). The stereochemistry of these adducts should be based on overlap of a lone-pair on the ligand with the vacant p_z orbital of the stannous molecule but it is also possible that distortion toward sp^3 hybridisation will occur.

The stannous ion, Sn^{2+}, with its empty 5*p* and 5*d* orbitals can also act as an acceptor toward certain ligands. In each case, the electronic configuration of the Sn^{2+} ion leads to hybridisation being adopted in complexes and the lone-pair orbital should be also be included in the hybridisation. The most probable hybrid geometries are illustrated in Fig. 1.2. The resulting complexes are formed by overlap of filled lone-pair orbitals on the incoming ligands with the empty hybrid orbitals on the tin.

If tin(II) species contain a stereochemically active lone-pair, E, as illustrated above, they might also behave as σ-donor ligands. The ability of a lone-pair to act as a donor generally decreases as the atomic weight of the atom increases and in the case of a relatively heavy element like tin, the σ-donor strength of the 5*s* lone-pair orbital should be very low, i.e. stannous species exhibit weak Lewis acidity. Therefore, it should only be possible for the orbital to act as a σ-donor to very powerful electron

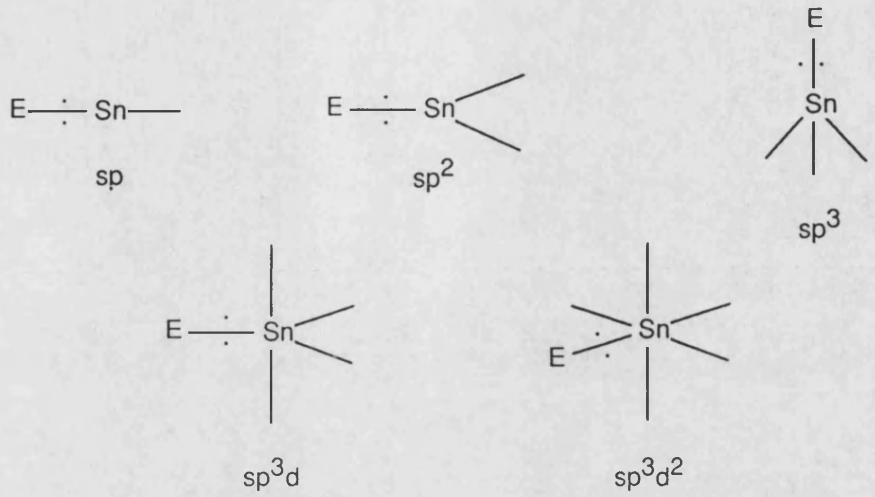

Fig. 1.2 Hybrid orbital geometries around tin(II).

acceptors, particularly if the 5*d* orbitals can utilise synergic ($\sigma + \pi$) effects.

1.7.2 *Common Coordination Numbers and Structures of Tin(II) Compounds.*

Application of simple VSEPR theory predicts an angular geometry for tin(II) compounds, although this is rarely observed. Cases where this simple geometry is observed are the gaseous halides and derivatives where the steric bulk of the ligands precludes a higher coordination number at tin.[47] Bivalent tin compounds more commonly exhibit coordination numbers higher than two, either by complexation, chelation or bridging. The basic coordination unit can usually be identified as a three-coordinate trigonal pyramid (**5**), but additional interactions can lead to distorted pseudo-trigonal bipyramidal (**6**), square-based pyramidal (**7**), octahedral (**8**), distorted octahedral (**9**) or facially-capped trigonal prismatic (**10**) coordination geometries.

This means that stannous species can exhibit coordination numbers in the range 2 through to 9. Distortions from these ideal geometries are frequently encountered, and distinctions between four-coordinate square pyramidal and distorted pseudo-trigonal bipyramidal coordination are often difficult. For the majority of

(5)

(6)

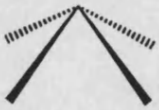

(7)

(8)

(9)

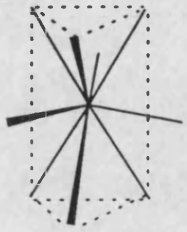

(10)

compounds the tin lone-pair is stereochemically active, indicated by an apparent vacancy in the coordination sphere accompanied by the expected distortion of regular geometries. The coordination geometries exhibited by tin(II) compounds are summarised in Table 1.2, and suitable examples discussed further below.

Angular coordination: A determination of the structure of $Ge(OCBu^t_3)_2$ in the solid-state shows the compound to exist as a simple two coordinate species due to the steric bulk of the ligands. It is claimed from spectroscopic evidence that the tin(II) analogue, $Sn(OCBu^t_3)_2$, is iso-structural with the germanium(II) compound (Fig. 1.3).[48] The molecular structure of $Ge(OCBu^t_3)_2$ has Ge-O bond lengths of 1.896 and 1.832Å and an exceptionally small [O-Ge-O] angle of 85.9°.

Trigonal planar coordination: The structure of $[Cr(CO)_5].Sn[CH(SiMe_3)_2]_2$ consists of a three-coordinate tin with average Sn-C bond-lengths of 2.185Å (Fig. 1.4). This bond-length is shorter than normal, probably due to the π-electron withdrawing effect of the $Cr(CO)_5$ group. The coordination is slightly distorted from the ideal planar arrangement with [C-Sn-C] angles of 98°.

Trigonal pyramidal coordination: The structure of SnS can be described as a badly distorted sodium chloride lattice. The three nearest neighbour atoms are at

Table 1.2 Typical coordination geometries of tin(II) compounds.

Coordination number	Coordination geometry	Example	Ref.
2	Angular	$Sn(OCBu_3^t)_3$	48
3	Trig. planar	R_2Sn: -> $Cr(CO)_5$[a]	49
3	Pyramidal	SnS	50
4	Sq. pyramidal	SnO	51
4	ψ-trig. bipyramid	SnFCl	52
6	Octahedral	Cubic SnSe	53
9	Tri-facially capped trigonal prismatic	$Sn(NCS)_2$	54

[a] $R = CH(SiMe_3)_2$

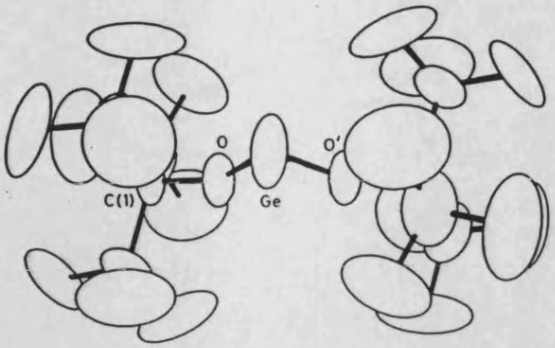

Figure 1.3 The molecular structure of $Ge(OBu_3^t)_2$.

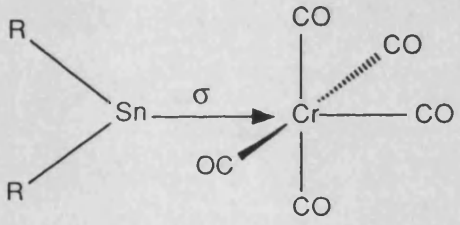

Figure 1.4 The structure of $[Cr(CO)_5].Sn[CH(SiMe_3)_2]_2$.

distances of 2.62-2.68Å from the tin. The next nearest sulphur atom is at 3.27Å, outside the first coordination sphere, and the [S-Sn-S] bond angles for the pyramid containing the three nearest sulphur atoms are 88, 88 and 96° (Fig. 1.5).

The structure of SnS can also be described in terms of -S-Sn-S-Sn- chains, each tin having two bonds to sulphur of 2.68Å in the chain and a further shorter bond to sulphur (2.62Å) completing the pyramidal coordination and linking adjacent chains.[53] The shortest Sn-S distance between layers is 3.39Å. A lead-tin sulphide, $PbSnS_2$ has also been identified although the positions of the atoms were not

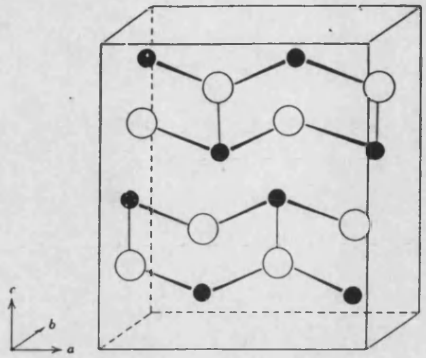

Figure 1.5 The structure of SnS: (•)tin and (○) sulphur.

determined but it was suggested that this material is iso-structural with SnS.[50]

Square pyramidal coordination: Two oxides of tin(II) are known, a highly stable blue-black oxide and a metastable red modification.[55,56] The X-ray crystal structure of the blue-black oxide has been determined showing it to have a layer structure (Fig. 1.6). The tin atom lies at the apex of a square pyramid, the base of which comprises the four nearest neighbour oxygen atoms. The average Sn-O bond distance is 2.21Å with an [O-Sn-O] angle of 75°. The Sn-Sn distance between adjacent layers is only 3.70Å which suggests the presence of Sn-Sn bonding.

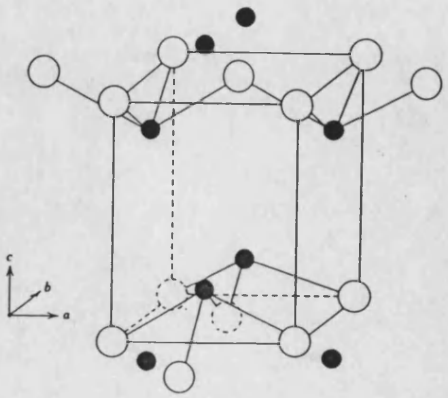

Figure 1.6 The structure of SnO: (•)tin and (○) oxygen.

ψ-Trigonal bipyramidal coordination: A single-crystal structural determination of the mixed halide SnClF (**11**) has been determined, showing the tin to have ψ-trigonal bipyramidal SnF_3ClE geometry, where E represents a stereochemically active lone-pair of electrons. The environment of the tin atom is somewhat perturbed due to the presence of this stereochemical lone-pair and consists of pyramids, subsequently linked to form an infinite $(SnClF)_n$ chain structure.

Octahedral coordination: It has been noted that SnTe and cubic SnSe have the rock-salt structure. These are essentially covalent species in which both lobes of the three *p*-orbitals of the tin(II) bond equally to six neighbours. In the case of cubic SnSe (**12**), the average Sn-Se bond distance is 3.00Å.

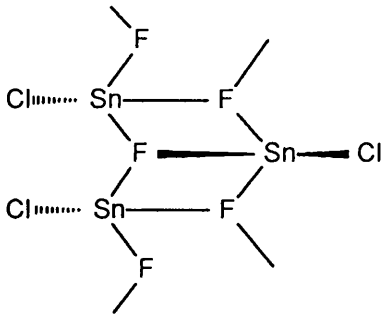

(11)

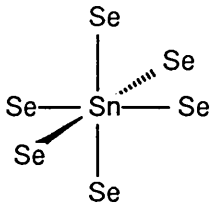

(12)

Tri-facially capped prismatic coordination: Tin(II) thiocyanate has a nine coordinate tin atom with nine distinct thiocyanate groups. Sn-N and Sn-S distances range from 2.20 to 3.85Å and 2.84 to 3.74Å respectively.. Six of these contacts lie at the corner of a trigonal prism, and one outside each of the prism faces.

1.7.3 *Preparation and Characterisation of Tin(II) Compounds.*

The preparation of tin(II) compounds is hampered by the ease of oxidation of stannous tin. It is usually possible to avoid this problem if synthetic procedures are performed in thoroughly deoxygenated solvents under a non-oxidising atmosphere (e.g. nitrogen or argon). The oxidation process is also highly dependant on pH, with

stannous stability favoured at acidic pH's. It is extremely difficult to prevent the formation of stannic by-products if the reaction mixture is pH > 6. Solutions of stannous compounds are found to rapidly oxidise on exposure to air, and many solid compounds slowly decompose upon exposure to atmospheric oxygen.

In the preparation of pure tin(II) species, it is obviously of paramount importance that suitably pure starting materials are used. The most commonly used starting material is probably the dichloride, either the anhydrous or dihydrated form, both of which are commercially available in a highly pure state. Unfortunately, samples prepared from it can be readily contaminated with chloride ions as well as tin(IV) impurities due to the poor stability of stannous chloride in solution. Blue-black tin(II) oxide, tin(II) sulphate and tin(II) bis-methoxide have also found use as suitable, readily available starting materials.[57-60] Other compounds that have been less frequently used as starting materials include $Sn(C_5H_5)_2$, $Sn[N(SiMe_3)_2]_2$ and $Sn(NMe_2)_2$.[48,61] Essentially, all of these starting materials are used in the same way; the chosen ligand to be attached to tin must have a sufficiently acidic proton to facilitate a ligand exchange reaction (e.g. equation 1.2). If the reaction liberates an acid, a quantitative amount of a suitable alkali should be present in solution to form the corresponding salt.

$$2\,HL \xrightarrow[Sn(NMe_2)_2,\ -\ 2\ HNMe_2]{SnCl_2,\ -\ 2\ HCl} SnL_2 \qquad (1.2)$$

The outstanding feature of the chemistry of tin(II) compounds is the ease of oxidation to corresponding tin(IV) materials and this property has resulted in their widespread use as reducing agents in inorganic,[62,63] analytical,[64,65] and organic chemistry.[57,66]

Several of the simple tin(II) salts are water-soluble, the solutions being quite susceptible to oxidation [to tin(IV oxides] and hydrolysis [to hydrous tin(II) oxide]. Electrochemical studies on the stability of $SnCl_2.2H_2O$ in water have served to

confirm that oxidation of Sn^{2+} occurs quite readily.[67] The stability of tin(II) solutions depends largely upon the nature of the anions present as well as the pH. Solutions containing anions such as F^- or $[CH_3CO_2]^-$ that can form strong stannous complexes are usually relatively stable to both hydrolysis and oxidation. The observed increase in the ease of oxidation with pH can be accounted for by the disproportion of tin(II) to tin(0) and tin(IV). A small number of tin(II) compounds are also soluble in polar organic solvents, e.g. $SnCl_2$. This is most easily explained by adduct formation, i.e. $SnX_2.nL$ where L is a coordinating solvent such as methanol, tetrahydrofuran or acetonitrile.

1.7.3.1 *Mössbauer Spectroscopy.*

The phenomenon of the emission or absorption of γ-rays without loss of energy due to recoil of the nucleus is known as the Mössbauer effect, first observed by Rudolph Mössbauer in 1957. The direct application of this effect in chemistry arises from the ability to detect the slight variations in the energy of interaction between the nucleus and extra-nuclear electrons, an interaction that was previously thought to be negligible. Although the Mössbauer effect should be present in all γ-ray excited state-ground state transitions, its magnitude can be so small as to be undetectable. Consequently, there are only about ten elements for which Mössbauer spectroscopy has been developed. Primarily, these include iron and tin as well as antimony, tellurium, iodine, xenon, europium, gold, neptunium, nickel, ruthenium, tungsten and iridium. The applications of this new technique were quickly established with ^{57}Fe, with large resonance effects observed at room temperature. The conditions for the development of ^{119}Sn Mössbauer were not so favourable as the higher γ-ray energy of 23.875Kev meant that low temperatures (e.g. that of liquid nitrogen, 78K) were required to achieve a recoil-free resonance. It is for this reason that ^{119}Sn Mössbauer studies are only suitable for solids and frozen solutions, as

liquids and gases would suffer from enormous recoil levels when the molecules were irradiated. In the case of ^{119}Sn studies, the most suitable radioactive nuclide is the metastable isotope, ^{119m}Sn, which emits a 23.875Kev *K* X-ray. A partial nuclear decay scheme for ^{119}Sn Mössbauer spectroscopy is illustrated in Fig. 1.7.

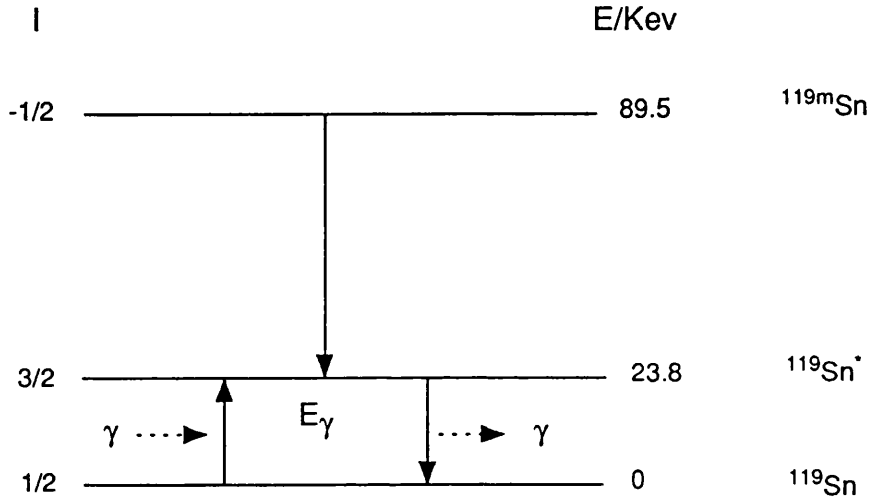

Fig. 1.7 A partial nuclear decay scheme for ^{119}Sn Mössbauer spectroscopy.

The criteria for the observation of a Mössbauer resonance are fulfilled by the 28.3Kev transition from the ground-state (I = 1/2) to the first excited-state (I = 3/2) for ^{119}Sn. The half-life of the ^{119}Sn* state has been measured at 17.8ns which gives a natural resonance half-width half-height (HWHH) linewidth, Γ_{nat}, of 0.325mms^{-1}.[68] The precise value of E_γ is varied in practice to achieve resonance by mechanically oscillating the radioactive source to and fro, thus providing a range of energies due to the Döppler effect.

When the radioactive source and the sample are in different chemical environments, a chemical shift, δ, of the observed spectral line occurs. This shift is due to the effect of the electronic environment of the tin atom upon its nuclear energy levels. Since *s*-orbitals are the only ones which exhibit a finite density at the nucleus, the ^{119}Sn chemical shift is due almost entirely to the 5*s* valence electrons. This effect is largely independent of *p*, *d* and *f* orbital contributions as these have a node (i.e. zero

density) at the nucleus. The reference zero-point for δ is usually measured against standard emitters which have included β-tin, SnO_2 or Mg_2Sn alloy, although data is now standardised and referenced against SnO_2. Because of the sensitivity of δ to the 5*s* electron density, values of isomer shifts can be used to readily distinguish the two oxidation-states of tin, the dividing point being that of α-tin ($2.10 mms^{-1}$) and β-tin ($2.65 mms^{-1}$), as compounds appear to lie either side of these points. The range of observed δ values is approximately as below;-

$$\text{Tin(IV)} \quad -0.5 < \delta < 2.1$$

$$\text{Tin(II)} \quad 2.5 < \delta < 5.0$$

The large difference in δ for the two oxidation states has been shown by MO calculations to be due to the lone-pair orbital which is only present in bivalent tin compounds.[69] In the case of bivalent tin compounds, the isomer shift is found to increase with increasing electronegativity of the attached ligands while the converse is true for tin(IV) species. This is due to the increase in overall charge on the tin. The value of δ can give a useful indication to the coordination geometry at tin in unknown compounds. In the case of stannous compounds it is usual for δ to decrease with increasing coordination number due to the reduced electron density at the nucleus.

Interaction of the nuclear quadrupole moment, Q, with an internal electric field raises the degeneracy of the $^{119}Sn^*$ excited state (*cf.* line broadening in NMR spectra where $I > 1/2$). This phenomenon gives rise to a doublet spectrum, with centre, δ, and quadrupole splitting, Δ. The energy-level splitting effect is illustrated in Fig. 1.8.

Internal electric field gradients of this type can arise from the following sources:-

(i) Non-cubic, or distorted coordination geometries.

(ii) Imbalance in the σ-framework of cubic geometries.

In the case of tin compounds, the value of Δ can provide useful information

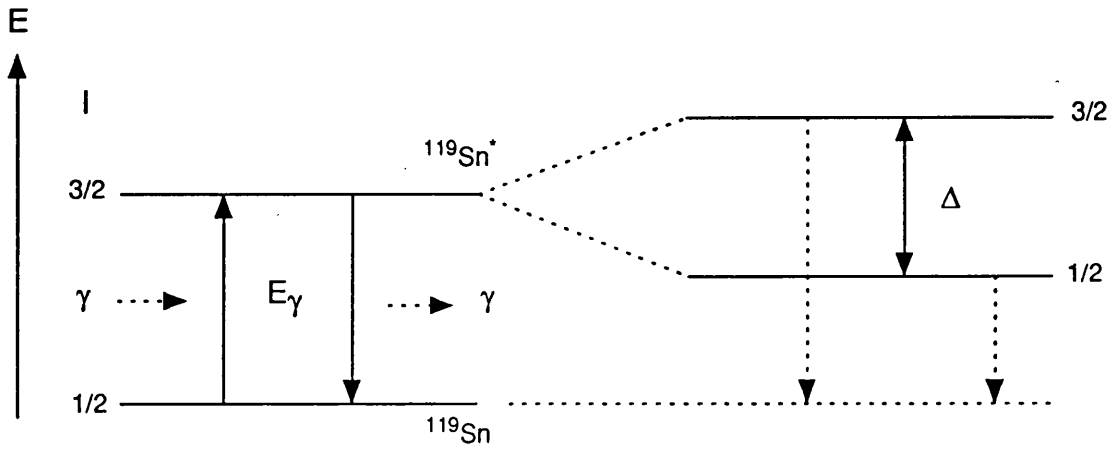

Fig. 1.8 A ^{119}Sn decay scheme illustrating the incidence of quadrupole splitting, Δ.

regarding the overall symmetry of coordination sphere. In general, the magnitude of Δ is related to the differing electronegativities and coordination geometries of the surrounding ligands. For example, with a polymeric dialkyltin dihalide it is possible to distinguish *cis* and *trans*-R_2SnX_4 geometries by comparing Δ values ($\Delta_{cis} < \Delta_{trans}$). These differences arise due to the differing perturbation of the quadrupole moment (Q) about the tin. However, in the case of tin(II) Mössbauer studies, interpretation of observed differences in Δ are less clear cut, rendering the data less useful in assigning coordination geometries. The main reason for this is the presence of the stereochemically active lone-pair which can produce irregular and unpredictable geometries.

The anisotropies in the electric-field gradient in the region of the Mössbauer active nucleus which give rise to the quadrupole splitting, Δ, also cause the nucleus to vibrate in an anisotropic fashion. The net result of this is unequal population of the ±1/2 and ±3/2 energy levels. This in turn gives rise to the observation of unequal peak areas under the two lines of the doublet, known as the Goldanski-Karyagin effect. This feature of a spectrum reflects the variation in the recoil-free fraction of the nucleus with Θ, the angle between the incident γ-ray and the electric field gradient. If, as is often the case, the two lines in a spectrum are of unequal intensity

this may also be caused by the presence of multiple tin environments in the sample.

Mössbauer spectroscopy has been applied to the study of toothpaste formulations containing compounds such as stannous pyrophosphate, $Sn_2P_2O_7$.[70] These studies, carried out on a series of different dentifrice samples with a wide variety of formulations, have allowed a semi-quantitative analysis of the degree of stannous oxidation to be assesssed. The presence of a tin(IV) impurity in these samples can be clearly observed in the Mössbauer spectra due to the differing isomer shifts of the tin(II) and tin(IV) components within the sample. This technique has assisted with establishing links between stannous stability levels and product formulation and storage conditions.

The Mössbauer spectrum of $Sn_2P_2O_7$ (Fig. 1.9a) is typical of a polymeric tin(II) species, i.e. broad linewidths due to the presence of multiple tin environments. The spectrum of $Sn_2P_2O_7$ once incorporated into a fluoride-containing dentifrice (Fig. 1.9b) shows a series of changes to the basic spectral features. The tin(II) component shows a marked reduction in the value of δ, due to tin(II)-excipient interactions. The spectral linewidths are also reduced due to the breakup of the polymeric structure of $Sn_2P_2O_7$. The unidentified tin(IV) spectral component can be clearly observed at $\delta \approx 0 mms^{-1}$, a semi-quantitative estimate of the tin(IV) content can be obtained by comparing the peak areas for each component.

(a)

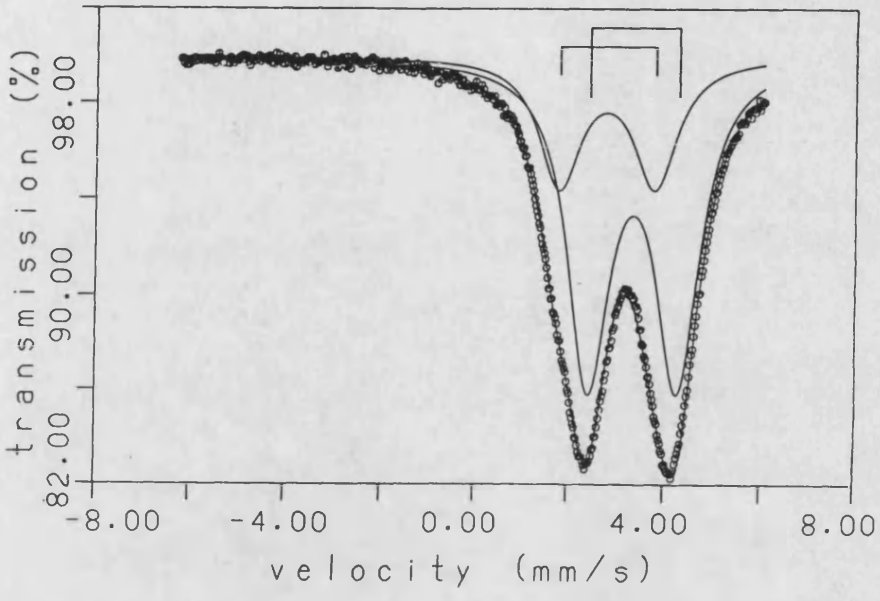

(b)

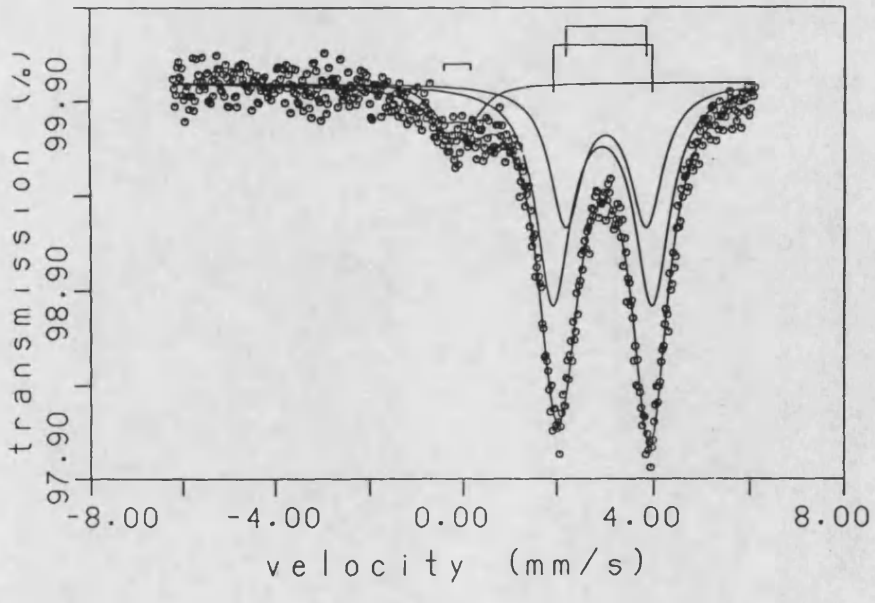

Fig. 1.9 The Mössbauer spectra of (a) solid $Sn_2P_2O_7$ and (b) $Sn_2P_2O_7$ as a dentifrice component.

1.7.3.2 *Nuclear Magnetic Resonance.*

Tin has three naturally occurring isotopes with spin ½, all others having spin = 0. These are ^{115}Sn (abundance 0.35%), ^{117}Sn (abundance 7.61%) and ^{119}Sn (abundance 8.58%). Most commonly tin-NMR studies have used the ^{119}Sn isotope because of its higher natural abundance, and higher receptivity. Today, because of the high sensitivity and relative ease of data accumulation, ^{119}Sn spectra are obtained by Fourier transform methods. Tetramethyltin, $(CH_3)_4Sn$, with an absolute resonance frequency of (37290665 ± 3)Hz is the universally adopted reference standard for ^{119}Sn chemical shifts. The major factors affecting the value of δ are the electronegativity of the ligands attached to tin, coordination number and the geometric distortion of bond angles. Conventionally, negative chemical shift values are upfield from Me_4Sn = 0, with recorded data spanning a very large range of δ (≈4000ppm). Such metal NMR data can prove extremely helpful in the characterisation of compounds, particularly because of the large chemical shift range. Unfortunately, relatively few tin(II) species have been studied by ^{119}Sn NMR. This is probably, in part, due to the relatively low solubilities of such stannous compounds and the properties of the nucleus.

It has already been stated that tin(II) compounds can readily form adducts when dissolved in coordinating solvents and a selection of known adducts of tin(II) halides are shown in scheme 1.1.

The ^{119}Sn NMR shifts of the tin(II) halides has been studied in several donor solvents, the values of δ being solvent, temperature and concentration dependent.[77] The observed δ values become more negative in the order:-

$$SnI_2 < SnBr_2 < SnCl_2 < SnF_2$$

Single NMR peaks were observed in all spectra indicating that rapid exchange among tin species is operative. Thus, the observed shifts represent a time-averaged view of the solvated species present in the sample. The changes in δ due to solvation

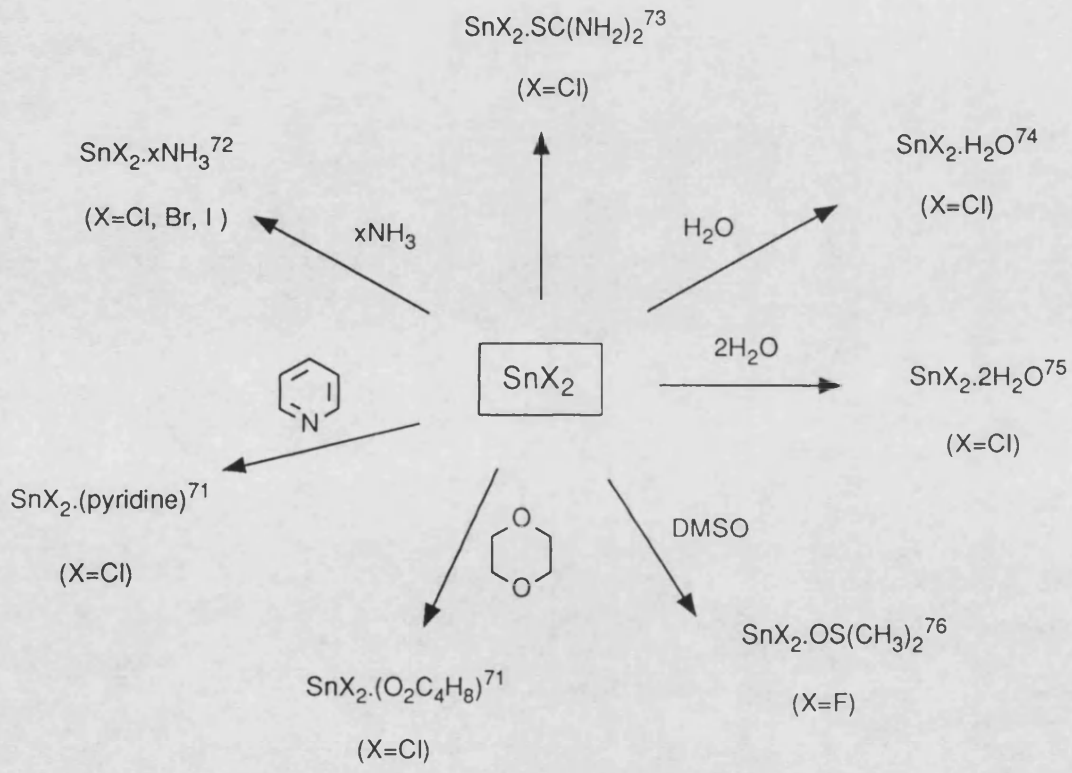

Scheme 1.1 Formation of selected stannous-solvent adducts.

can be accounted for by changes to the hybridisation, charge-distribution and symmetry in the coordination sphere of the tin.

A representative selection of documented ^{119}Sn NMR data of tin(II) compounds is listed in Table 1.3 (all δ values relative to $SnMe_4$). These selected NMR shifts illustrate the wide range over which peaks may be observed for stannous compounds.

Solid-state NMR studies can also be carried out using Magic-Angle Spinning (MAS-NMR) techniques. This typically involves spinning the sample at an angle of 54.73° to the magnetic field at high speeds (in the order of KHz), in order to overcome anisotropic dipole-dipole and quadrupole-field effects. The problems of long spin-lattice relaxation times can usually be effectively overcome by cross-polarisation with a second NMR active nucleus in the system (e.g. ^{1}H, ^{31}P). Like Mössbauer data, it is often possible to correlate solid-state ^{119}Sn NMR data directly with the solid-state structure of compounds as determined by crystallography. Information regarding intermolecular solid-state associations might also be determined. Unfortunately, there is no documented data regarding the application of this technique to inorganic tin(II) compounds and it was unclear as to whether this method might be succesfully applied to the study of such species.

1.8 Tin(II) Compounds of Orally-viable Ligands.

Tin(II) compounds are currently used in many dental formulations as anti-plaque additives (section 1.6). Of particular importance to the use of stannous compounds in this way is to understand the interactions that occur within the formulated product. SnF_2 has been used for many years although the fate of the stannous ion in the toothpaste is unknown. Similarly, the simultaneous use of insoluble stannous pyrophosphate, $Sn_2P_2O_7$, with either fluoride or citrate ions in a

Table 1.3 Selected tin(II) NMR data.

Compound	δ (ppm)	Ref.
SnF_2.nDMSO	-629.0	77
$SnCl_2$.nDMSO	-358.2	77
$SnCl_2$.nDMF	-324.1	77
$SnBr_2$.nDMSO	-319.5	77
$SnBr_2$.nDMF	-202.1	77
SnI_2.nDMF	-152.6	77
$(C_5H_5)_2Sn$	-2199	78
$(MeC_5H_4)_2Sn$	-2172	79
$(Me_5C_5)_2Sn$	-2129	80
$[Sn(OP(C_6H_{11})_3)_2]^{2+}$	-1101[a]	81
$Sn(OCBu^t_3)_2$	-163	48

[a]Originally recorded relative to $Sn(AsF_6)_2$.

paste produces unidentified, soluble tin(II) species. It is known that tin(II) also interacts with sorbitol, a toothpaste humectant (section 1.5), which may simply yield a bulky tin(II) alkoxide. Many of these type of interactions are investigated in the later Chapters of this thesis, and for comparison the documented chemistry of tin(II) fluorides, carboxylates, phosphates and alkoxides is summarised below.

1.8.1 *Tin(II) Fluoride and Complex Fluoro-anions.*

Tin(II) fluoride, SnF_2, has been used as a prime anti-plaque active ingredient of toothpaste and mouthrinse formulations since the 1950's and its chemistry is well established. Solid SnF_2 is known to exist in two crystallographic forms, i.e. monoclinic (α) and orthorhombic (β). The evidence for these structural modifications has been both spectroscopic, using Mössbauer spectroscopy,[82-85] and crystallographic using a combination of single-crystal and powder diffraction X-ray diffraction studies[86,87]. Discrepancies in the earlier Mössbauer data for α- and β-SnF_2 have since been accounted for by the unintentional hydrolysis of the sample of α-SnF_2 during data collection, resulting in the formation of the oxyfluoride, Sn_2OF_2. It is this compound that was mistakenly assumed to be β-SnF_2. The Mössbauer parameters for α and β-SnF_2 and Sn_2OF_2 are listed in table 1.4.

The average value of δ is observed to be significantly higher for the α-modification than it is for the β-phase of SnF_2. This implies that the coordination number about the tin in the α-form is lower than that in β-SnF_2. The value of Δ is significantly greater for the β-form indicating the presence of a higher electric field gradient at the nucleus. This data suggests that β-SnF_2 possesses a more distorted, higher coordination around the tin than that found in the α-form.

The crystallographic data has confirmed the existence of a second modification of SnF_2. In the monoclinic α-form the lattice contains molecular Sn_4F_4 puckered rings with four additional outer fluorine atoms bridging between adjacent

Table 1.4 Mössbauer data for SnF_2 and Sn_2OF_2.[a]

Compound	δ (mms^{-1})	Δ (mms^{-1})	Ref.
α-SnF_2	3.70	1.80	82
	3.47	1.52	85
	3.44	1.54	84
β-SnF_2	3.30	2.20	82
Sn_2OF_2	3.10	3.23	85

[a] All data measured at 78K, relative to SnO_2.

units, i.e. molecular Sn_4F_8 rings (**13**). The tin atoms show SnF_3E coordination (where E represents a stereochemically active lone-pair of electrons) throughout the ring. The four outer fluorine atoms interact with the tin atoms of adjacent rings. The average Sn-F bond lengths within the ring are 2.18Å, while the external Sn-F distances average 2.05Å. The [Sn-F] angles within the ring are 170.4 and 132.1°.

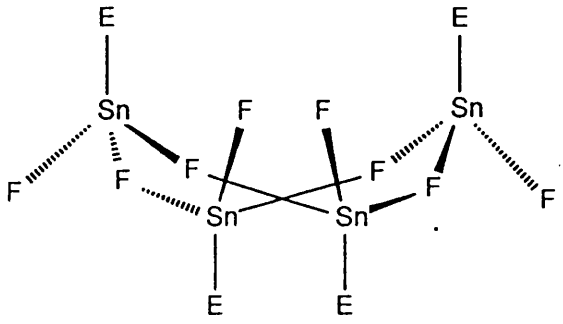

(**13**)

The orthorhombic β-form of SnF_2 has also been described

crystallographically.[86] The structural determination of SnF_2 in this phase modification shows tin atoms to be in a highly distorted octahedral six coordination (SnF_5E) corresponding to covalent sp^3d^2 hybridisation (**14**). The observed increase in coordination number and distortion of the tin environment are consistent with the Mössbauer spectra described above for α- and β-SnF_2.

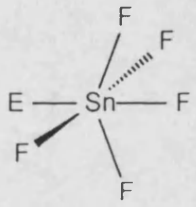

(**14**)

Claims of a third, γ-form, of SnF_2 in the literature appear to be erroneous,[87] and are linked to the fact that the oxyfluoride Sn_2OF_2, already mentioned above, has been mistakenly identified as γ-SnF_2 as a result of earlier work. It is actually at the claimed α-γ phase transition that the hydrolysis occurs. Sn_2OF_2 can also be purposely prepared by the action of heat on a 1:1 solid mixture of $SnF_2$and SnO in a sealed tube heated to 200°C (equation 1.3).[88]

$$SnF_2 + SnO \xrightarrow[\text{(sealed tube)}]{\text{200°C / 24hr}} Sn_2OF_2 \qquad \textbf{(1.3)}$$

The X-ray crystal structure of this compound shows the tin to occupy two distinct environments. Sn(1) has a fourfold coordination, bonded to one oxygen and two flourine atoms with a stereochemically active lone-pair at the apex of the $Sn(1)OF_2E$ unit. Sn(2) is localised at a trigonal bipyramidal $Sn(2)O_2F_2E$ site, the lone-pair being at the corner of the equatorial SnO_2E plane (Fig. 1.13). The Mössbauer spectrum of this compound has been determined (Table 1.4).[85] The bonds corresponding to the Sn(1) site can be assumed to be more covalent, which is consistent with the lower coordination observed for Sn(1). For tin(II) compounds, as a

rule, the lower the value of the isomer shift the more covalent the bond. The large quadrupole splitting, Δ, is consistent with the distorted tin environments found in this compound. The spectral linewidths are also quite broad, which is due to the slightly differing Mössbauer effect for the two sites, Sn(1) and Sn(2).

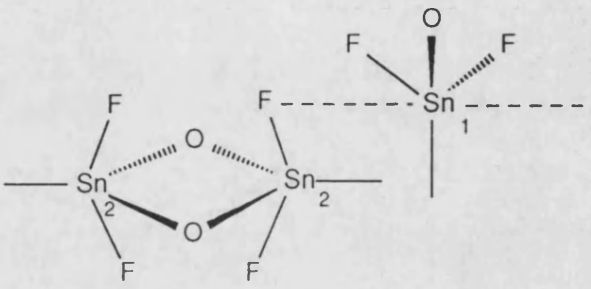

Fig. 1.10 The two tin environments in Sn_2OF_2.

In contrast to the tin(II) fluorides described above crystalline, anhydrous $SnCl_2$ and $SnBr_2$ are reported in the literature to be isostructural with lead(II) chloride, $PbCl_2$.[89-91] The tin atom is surrounded by nine halogen atoms from three different layers in a tri-facially capped trigonal prismatic coordination (section 1.7.2). Crystals of SnI_2 possess a unique layer structure with two distinct tin environments; two-thirds occupying $PbCl_2$-type sites, while the remainder are in $PdCl_2$-type chains. These two tin sites interlock to give almost perfectly regular octahedral coordination.[92]

When SnF_2 is dissolved in solutions containing increasing fluoride ion concentration a series of complex fluorotin(II) species is formed, primarily $[SnF_3]^-$, $[Sn_2F_5]^-$ and $[Sn_3F_{10}]^{4-}$. The strong tendancy to form [Sn-F-Sn] bridging is a predominant factor in the structural chemistry of these complex fluorotin(II) species. Several of these species have been isolated as crystalline solids and their structures determined, although spectral data is not available. The trigonal pyramidal, SnF_3E, and square pyramidal, SnF_4E, coordination units are commonly found in these compounds. Amongst the known fluorotin(II) species ammonium trifluorostannate, $(NH_4)(SnF_3)$, appears to be unique in possessing discreet pyramidal $[SnF_3]^-$ anions with no such F-Sn-F bridging observed.[93] In contrast hydrated potassium

trifluorostannate, $KSnF_3.\frac{1}{2}H_2O$, consists of an infinite $[SnF_3]_\infty^{\infty-}$ chain with two Sn-F bond lengths of 2.27Å within the chain and two stronger bonds of 2.03Å out of the chain, forming distorted SnF_4 pyramids.[94] In salts of $[Sn_2F_5]^-$ the coordination comprises two corner-shared trigonal pyramids (**15**). The Sn-F distances in the [Sn-F-Sn] bridges are 2.22Å, while terminal Sn-F bonds are stronger at around 2.07Å.

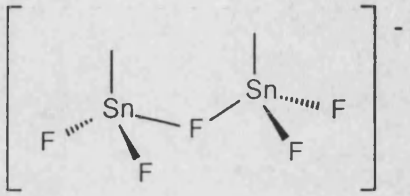

(**15**)

A further fluorotin(II) anion, $[Sn_3F_{10}]^{4-}$, consists of three edge-sharing SnF_4E units (**16**).[95] The Sn-F bonds in the Sn-F-Sn bridges are 2.49Å while the terminal Sn-F bonds are stronger at 2.11Å.

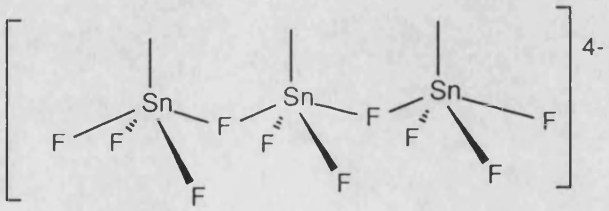

(**16**)

For comparison, the trichlorostannate(II) anion, $[SnCl_3]^-$, has also been isolated in compounds such as $(NH_4)_2[SnCl_3]Cl.H_2O$ (**17**).[96] In this case the tin is coordinated by five covalent chlorine atoms and a chloride ion in a distorted six-coordinate $SnCl_6$ octahedral environment (Fig. 1.11). The actual $SnCl_3$ moiety consists of three Sn-Cl bonds of between 2.54-2.64Å, with the Cl^- ion at a much further distance of 3.22Å from the tin.

The coordination number, Sn-F bond-lengths and Mössbauer data for these documented tin(II) fluoride species is summarised in Table 1.5.

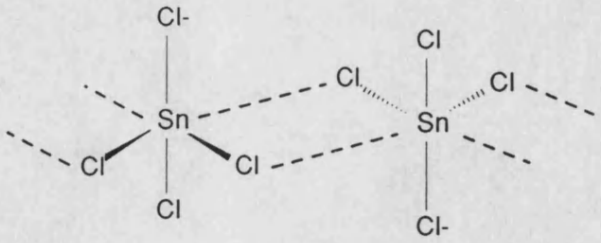

Fig. 1.11 The $SnCl_6$ coordination in $(NH_4)_2[SnCl_3]Cl.H_2O$ (**17**).

Table 1.5 Summary of data for tin(II) fluoride species.

Compound	CN	[Sn-F] / Å	δ (mms^{-1})	Δ (mms^{-1})
α-SnF_2	3	2.07	3.44	1.54
		2.10		
		2.27		
β-SnF_2	5	1.89	3.30	2.20
		2.40		
		2.49		
		2.21		
		2.41		
NH_4SnF_3	3	2.08		
		2.08		
		2.08		
$KSnF_3.\frac{1}{2}H_2O$	4	2.27		
		2.01		
		2.27		
		2.04		
$NaSn_2F_5$	3	2.08		
		2.07		
		2.22		
$Na_4Sn_3F_{10}$	4	2.04		
		2.26		
		2.26		
		2.04		

1.8.2 *Tin(II) Phosphate Compounds.*

Relatively few stannous salts of the mineral oxyacids have been succesfully isolated, with stannous sulphate, $SnSO_4$, being one of the few well characterised compounds of this type.[97] The much quoted stannous nitrate, $Sn(NO_3)_2.20H_2O$ described in the early literature has since been shown to be ice contaminated with traces of water-soluble tin(II) and nitrate species.[98,99] However, a series of stannous salts of the phosphorus oxy-acids have been succesfully identified in the literature, primarily by crystallographic methods, revealing a widely varied and complex range of stoichiometries. Some of the earliest examples of tin(II) orthophosphates described in the literature are stannous phosphate, $Sn_3(PO_4)_2$, stannous hydrogen phosphate, $SnHPO_4$, and stannous dihydrogen phosphate, $Sn(H_2PO_4)_2$.[100] The preparation of stannous phosphite, $SnHPO_3$, and the hypophosphite, $Sn_3(PO_2)_2$ are also quoted.[101,102] Very little spectral data is quoted in the literature for tin(II) phosphate species, although Mössbauer data is available for $Sn_3(PO_4)_2$ and stannous pyrophosphate, $Sn_2P_2O_7$ (Table 1.6).[103]

Table 1.6 Mössbauer data for tin(II) phosphates.[a]

Compound	δ (mms^{-1})	Δ (mms^{-1})
$Sn_3(PO_4)_2$	3.35	1.93
$Sn_2P_2O_7$	3.50	1.60

[a]Recorded at 78K, relative to SnO_2.

This data, although somewhat limited, suggests that the covalent character of the bonding in each of these two compounds is quite similar, with similar

coordination numbers at the tin atoms. The differences in the quadrupole splitting suggests that the orthophosphate possesses a significantly more distorted, or asymmetric, tin coordination than that of the pyrophosphate.

A structural determination of the parent compound, $Sn_3(PO_4)_2$, has been determined, the crystals having been prepared by mixing 1M aqueous solutions of SnF_2 and H_3PO_4 according to equation 1.4.[104]

$$3\,SnF_2 + 2\,H_3PO_4 \longrightarrow Sn_3(PO_4)_2 + 6HF \qquad \textbf{(1.4)}$$

The structure of this compound consists of alternating layers of Sn^{2+} and $[PO_4]^{3-}$ ions arranged parallel to the *ac* plane. Two open channels are formed by the Sn(II) ions, arranged in a helical fashion with each tin at the apex of a pseudo-four coordinate trigonal pyramid with the three nearest oxygen atoms (each from a different phosphate group). The structure shows tin in three environments (Fig. 1.12). Sn(1) is strongly coordinated to three O atoms from three $P(1)O_4$ groups with average Sn-O distances of 2.119Å. The coordination around tin is completed by two weaker Sn-O interactions of average 2.971Å. Sn(2) is similar to Sn(1). There are three strong Sn-O bonds (average 2.100Å) from three different $P(2)O_4$ groups. The only other interaction is a weak Sn-O bond of length 3.054Å. The coordination around Sn(3) is quite different. The basic SnO_3E unit is maintained, but there are three weaker Sn-O bonds (average 2.888Å) and a further very weak bond (3.250Å). This yields an oxygen-bridged Sn(3)-Sn(3) dimer.

A hydrated form of stannous orthophosphate, $Sn_3(PO_4)_2.3H_2O$, has also been reported.[105] A powder-diffraction study of this hydrated compound is distinctly different to that of anhydrous $Sn_3(PO_4)_2$ indicating a substantial disruption of the above structure.[106]

Two further structural determinations of tin(II) salts of phosphorus oxy-acids also incorporate the basic SnO_3E coordination described above for $Sn_3(PO_4)_2$. These are tin(II) hydrogen phosphate, $SnHPO_4$, and tin(II) phosphite, $SnHPO_3$,

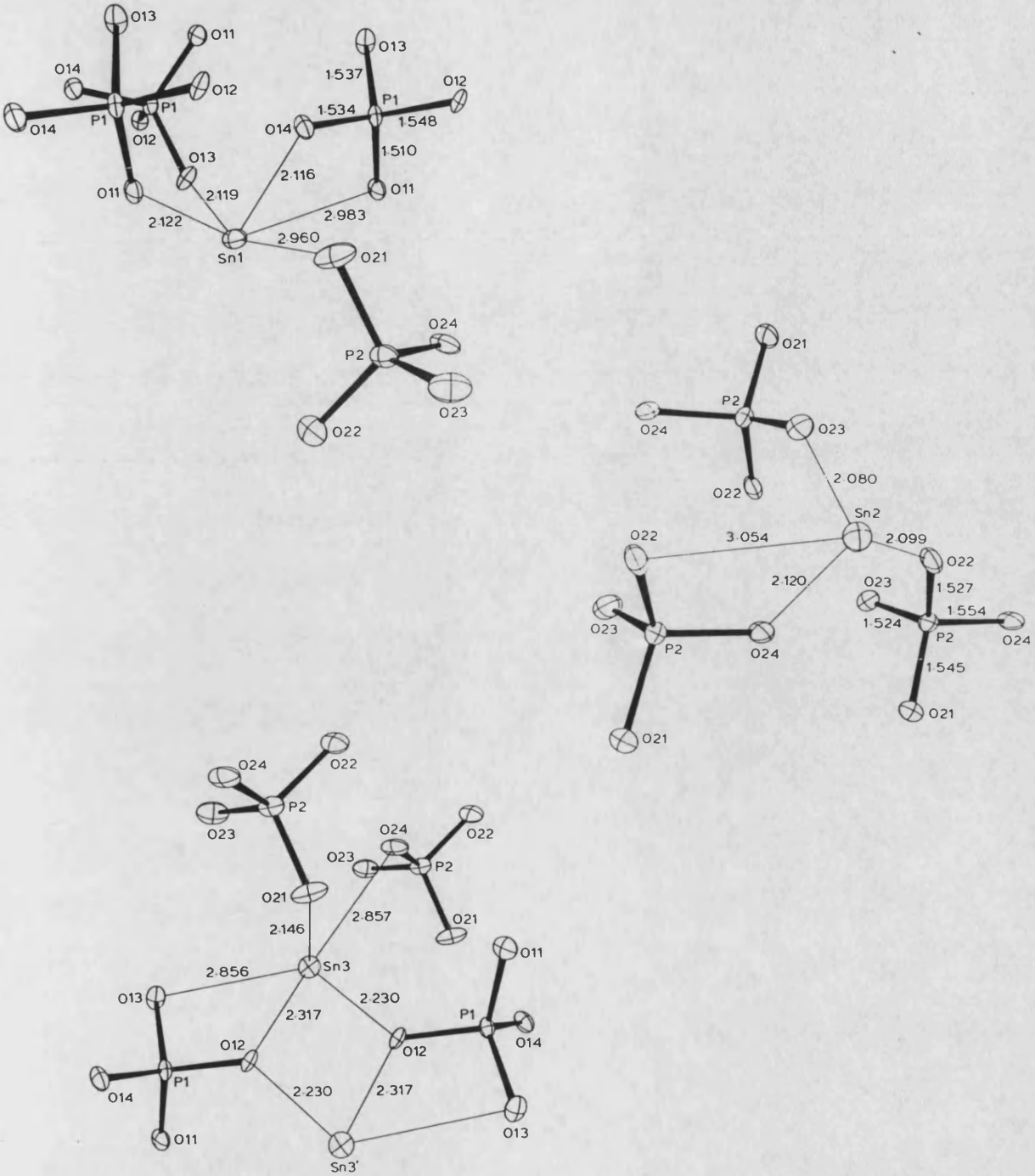

Fig. 1.12 The three tin sites in $Sn_3(PO_4)_2$.

respectively.[107] These two compounds were prepared as shown in equation 1.5 and crystals were formed by slow, carefully controlled crystallisation.

$$\text{(i)}\ Sn + H_3PO_4 \xrightarrow{120^\circ C} SnHPO_4 + H_2$$

$$\text{(ii)}\ SnO + H_3PO_3 \xrightarrow{78^\circ C} SnHPO_3 + H_2O \qquad \textbf{(1.5)}$$

The structure of $SnHPO_3$ consists of both SnO_3E pyramids and $[PO_3]$ units fused together at their bases. The SnO_3E trigonal pyramids have Sn-O bond lengths of 2.18Å, with the next nearest oxygen at a distance of 2.90Å, i.e. outside the first coordination sphere. Each tin atom coordinates to three separate $[PO_3]$ groups forming planar sheets, these extending perpendicular to the *b*-axis (Fig.1.13)

The $SnHPO_4$ structure also consists of a sheet-like framework, formed by the SnO_3E and $[PO_4]$ groups linking together at their corners. The individual sheets are held together by strong hydrogen bonding, which is not present at all in $SnHPO_3$. The nearest-neighbour Sn-O bond lengths are typically 2.32Å in the SnO_3E coordination, while the next nearest O atom lies at 2.61Å. Each tin atom coordinates to three different $[PO_4]$ groups (Fig. 1.13).

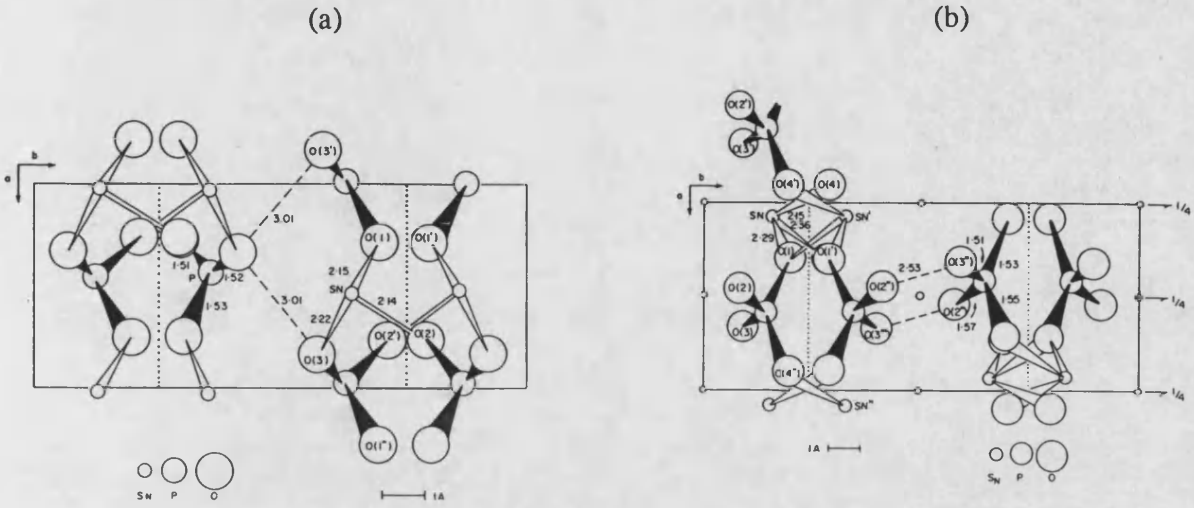

Fig. 1.13 The layer structures of (a) $SnHPO_3$ and (b) $SnHPO_4$.

A structural determination of stannous dihydrogenphosphate, $Sn(H_2PO_4)_2$, prepared according to equation 1.6, has revealed the presence of a different basic tin(II)-oxygen coordination to the SnO_3E geometry most commonly observed.[108] The crystalline product was prepared by the action of phosphoric acid on $SnHP0_4$ at elevated temperatures followed by slow, careful crystallisation.

$$Sn + H_3PO_4 \xrightarrow{140^\circ C} SnHPO_4 + H_2$$

$$SnHPO_4 \xrightarrow[140^\circ C]{H_3PO_4} Sn(H_2PO_4)_2 \qquad \textbf{(1.6)}$$

The tin atoms are each coordinated by four oxygen atoms, all lying on one side of an SnO_4E distorted pseudo-trigonal bypyramid, all four of these O atoms belonging to different $[H_2PO_4]^-$ groups (Fig. 1.14). Two of the bonds are short (2.21Å) while the remaining two are a little longer (2.47Å). On the opposite side of

the tin are four more distant O atoms at 2.92 - 3.18Å. The SnO_4E units share vertices, forming infinite SnO_4 chains of distorted pyramids with a puckered basal plane about tin. These chains are held together through hydrogen-bonding *via* the $[H_2PO_4]^-$ groups.

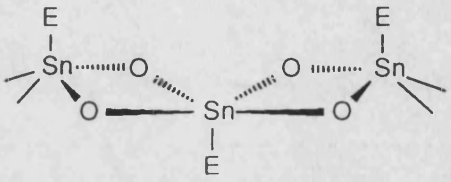

Fig. 1.14 The distorted SnO_4E structure of $Sn(H_2PO_4)_2$.

A reaction of particular importance to dental applications is that between SnF_2 and $Ca_5(PO_4)_3OH$ (HAP). This reaction is complex and at least three stannous phosphate products have been succesfully identified by crystallographic structure determinations. These products include two different stannous hydroxide phosphates $Sn_2(OH)PO_4$ and $Sn_3O(OH)PO_4$.[109,110] Structurally, $Sn_2(OH)PO_4$ contains an asymmetric unit with two Sn atoms, one PO_4 group and an OH group (Fig. 1.15). Each of the tin atoms is coordinated in an SnO_3E pyramidal unit with Sn-O distances of average 2.12Å, with further interactions to more distant O atoms. The two tin environments are found to be crstallographically unique.

Tritin(II) hydroxide oxide phosphate, $Sn_3O(OH)PO_4$, has been isolated as an extremely minor product of the reaction between SnF_2 and HAP. The structure of this compound, as in most tin(II) phosphates, consists of crystallographically unique tin atoms coordinated strongly to three O atoms (Sn-O average 2.15Å) and less strongly to one or more distant O atoms, i.e. the geometry about tin is again pyramidal SnO_3E (Fig.1.16).

A third product of the reaction between SnF_2 and HAP, a tin(II) fluorophosphate, has been implicated in resistance of dental enamel to acid attack (section 1.6).[22] The exact route by which this compound is produced can only be

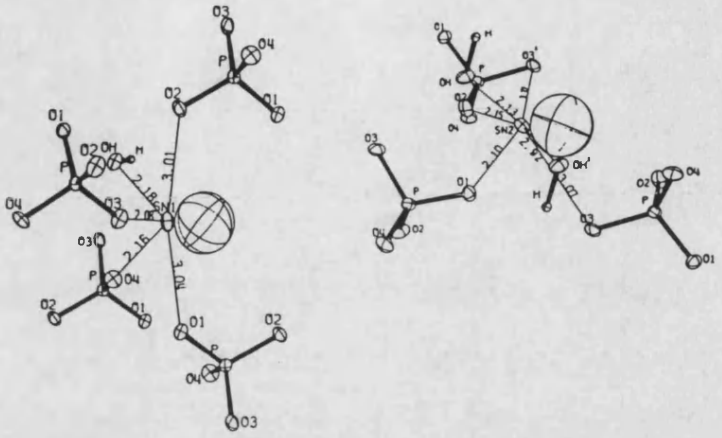

Fig.1.15 The two tin environments in $Sn_2(OH)PO_4$.

guessed at, although the following speculative equation (equation 1.7) has been proposed by Berndt:-

A structural determination of this compound, $Sn_3F_3PO_4$, has revealed the tin atom to exhibit $SnOF_2E$ coordination in a distorted trigonal pyramidal arrangement (Fig. 1.17).[23] This structure can be considered as consisting of phosphate ions bound together through [O-Sn-F-Sn-O] links.

Tin(II) salts of condensed polyphosphoric acids are also known such as the pyrophosphate, $Sn_2P_2O_7$ and tripolyphosphate, $Sn_2P_3(OH)O_9$.[105,111] The tin(II) pyrophosphate salt, like SnF_2, has been applied extensively as an anti-plaque stannous source in dental formulations, although structurally, this material is poorly characterised due to its amorphous nature toward X-rays and its intractable physical properties.

In summary, tin(II) phosphate compounds generally adopt a three coordinate trigonal pyramidal coordination about the tin atom (Table 1.7). Exceptions to this rule are the tin sites in $Sn(H_2PO_4)_2$ which adopt a four coordinate distorted square pyramidal geometry. Typical Sn-O bond lengths in the SnO_3E group range from about 2.08Å to 2.36Å, and in the SnO_4E unit 2.21Å to 2.47Å. This leads to the

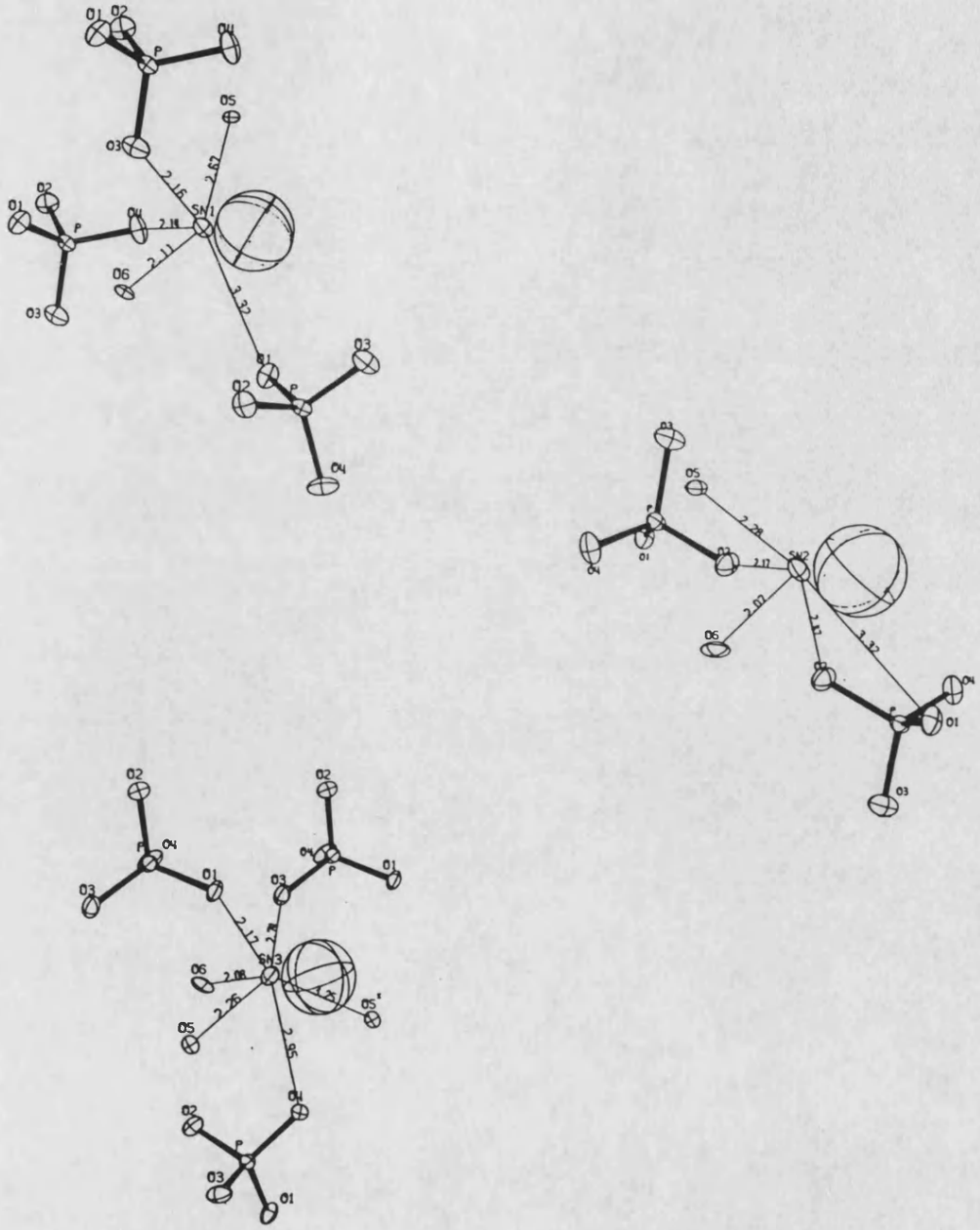

Fig. 1.16 The three tin environments in $Sn_3O(OH)PO_4$.

$$2\,Ca_5(PO_4)_3OH_3 + 19\,Sn^{2+} + 38\,F^- \longrightarrow 6\,Sn_3F_3PO_4 + 10\,CaF_2 + SnO.H_2O \qquad (1.7)$$

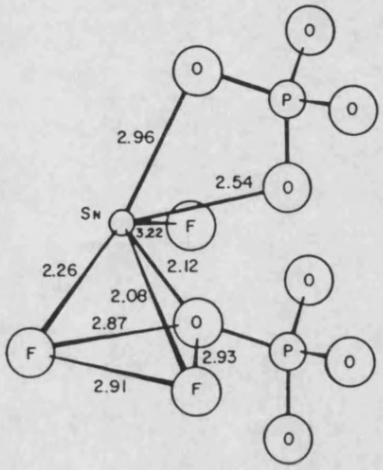

Fig. 1.17 The $SnOF_2E$ tin environment in $Sn_3F_3PO_4$.

prediction of three coordinate tin being most likely in new, uncharacterised tin(II) phosphates and polyphosphates.

Table 1.7 A summary of data for tin(II) oxy-phosphorus compounds.

Compound	CN	[Sn-O] / Å	[Sn-F] / Å	δ (mms^{-1})	Δ (mms^{-1})
$Sn_3(PO_4)_2$	3	Sn(1) 2.12 2.12 2.12 Sn(2) 2.08 2.09 2.12 Sn(3) 2.15 2.23 2.32	-	3.35	1.93
$SnHPO_3$	3	2.15 2.14 2.22	-		
$SnHPO_4$	3	2.15 2.29 2.36	-		
$Sn(H_2PO_4)_2$	4	2.21 2.21 2.47 2.47	-		
$Sn_2(OH)PO_4$	3	Sn(1) 2.08 2.15 2.18 Sn(2) 2.10 2.13 2.15	-		
$Sn_3O(OH)PO_4$	3	Sn(1) 2.12 2.14 2.15 Sn(2) 2.07 2.17 2.28 Sn(3) 2.06 2.16 2.26	-		
$Sn_3F_3PO_4$	3	2.12	2.08 2.26		

1.8.3 *Tin(II) Carboxylates.*

Tin(II) carboxylates are potentially of great importance to formulated dental products: ZCT is used as an anti-plaque additive in conjunction with tin(II) salts such as SnF_2. Their subsequent chemical interaction can be observed experimentally, although the nature of the products formed can only be guessed at. The most probable explanation of such interactions is the formation of a series of stannous carboxylate complexes *in situ*, which may be stable and active themselves. The simplest tin(II) carboxylates, i.e. the formate, $Sn(O_2CH)_2$, and acetate, $Sn(O_2CCH_3)_2$, have been prepared and characterised.[112,57] Other, more complex carboxylates have also been characterised including the oxalate, $Sn(C_2O_4)$, and the dipotassium bis-oxalatostannate(II) monohydrate, $K_2Sn(C_2O_4)_2.H_2O$.[113] Limited spectral data is available for the tin(II) carboxylates and the available Mössbauer data is listed in Table 1.8.

Table 1.8 Mössbauer data for tin(II) carboxylates.[a]

Compound	δ (mms^{-1})	Δ (mms^{-1})	Ref.
$Sn(O_2CH)_2$	3.15	1.56	114
	3.33	1.70	115
$Sn(O_2CCH_3)_2$	3.31	1.77	114
$Sn(C_2O_4)$	3.35	1.65	103

[a]Measured at 78K, relative to SnO_2.

The Mössbauer data for this series of carboxylates shows a marked similarity

for each compound. This implies that in terms of both bond-covalency and coordination geometries the compounds are all quite similar, although one could deduce that the oxalate is a little more regular in its structure due its significantly lower quadrupole splitting.

Synthetically, tin(II) carboxylates are frequently prepared by the esterification of either SnO or $Sn(OMe)_2$ with the appropriate acid.[59,60] This applies to both the simple carboxylates and more complex examples, e.g. salicylic acid forms a tin-oxygen heterocycle (equation 1.8) which has been identified by spectroscopic techniques (due to the infusible nature of the product). Other carboxylates can be prepared in this way and mention is made of a tin(II) poly-hydroxycarboxylate, i.e. stannous D-gluconate. This compound has been patented as an effective and stable anti-plaque stannous source.[116] Although this compound is poorly characterised, it is discussed further in the later chapters.

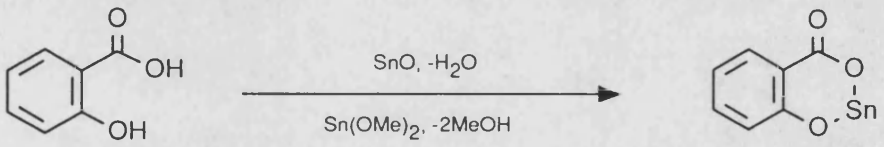

(1.8)

The crystal structure of tin(II) formate shows the tin to have pseudo-trigonal bipyramidal coordination with the lone-pair occupying the equatorial position.[115] Tin forms two short (2.14 and 2.20Å) and two longer (2.36Å) bonds to oxygen atoms from four formate groups. The crystals consist of infinite two-dimensional sheets in which all the formate groups bridge adjacent tin atoms and the structure shows signs of disorder. Half of the formate groups adopt symmetrical chelation, while the remainder are asymmetric. The structure of $Sn(O_2CH)_2$ is illustrated in Fig. 1.18 which shows the formate bridging within the sheets.

The structure of tin(II) oxalate, $Sn(C_2O_4)$, consists of infinite chains where each oxalate group bridges two tin atoms forming five-membered chelate rings, the Sn-Oxalate-Sn fragment being essentially linear.[113] In common with the formate, the

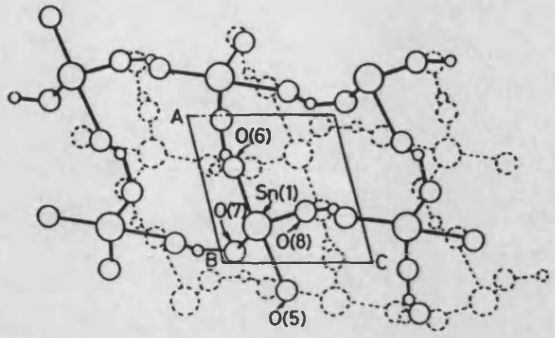

Fig. 1.18 The structure of tin(II) formate, $Sn(O_2CH)_2$.

tin atom has pyramidal four coordination with Sn-O bond lengths of 2.23 and 2.39Å. The resulting $Sn[\text{-}O_2CCO_2\text{-}Sn\text{-}]_\infty$ chains are puckered at the tin with weak Sn-O bonds of 2.87Å connecting adjacent chains (Fig. 1.19(a)). $K_2Sn(C_2O_4)_2.H_2O$ also has pyramidal four coordination at tin, with Sn-O bond lengths ranging from 2.14 to 2.36Å.[113] Infinite chains are also a feature of this structure, although in this case the chains contain discrete bis-oxalatostannate(II) ions interconnected by hydrogen-bound water molecules (Fig. 1.19(b)).

(a) (b)

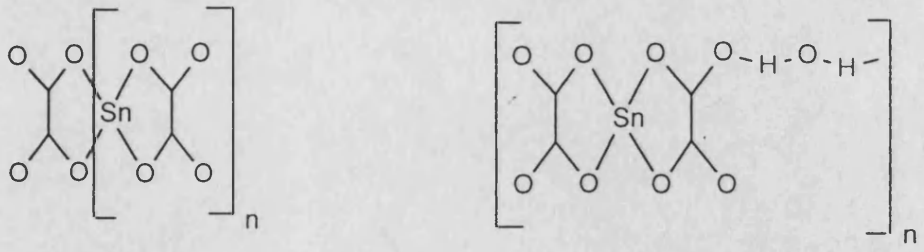

Fig. 1.19 The structures of (a) SnC_2O_4 and (b) $K_2Sn(C_2O_4)_2.H_2O$.

All of these simple carboxylates display four coordinate pyramidal geometry, i.e. SnO_4E. In the case of the complex tricarboxylato anions, $[Sn(O_2CR)_3]^-$ (R = H, CH_3), pyramidal three coordination is observed.[117,118] In these compounds, the three

Sn-O bond distances are all approximately 2.15Å and the three carboxylate functions coordinate to tin in a unidentate manner, i.e. no carboxylate bridging is observed.

As mentioned previously, the characterisation of tin(II) salts of citric acid is of particular importance in understanding the interactions that might occur between Sn^{2+} ions and ZCT in dentifrice formulations. Several pH-titration studies have been performed on the formation of tin(II) salts of both tartaric (**18**) and citric acid (**19**). These studies have indicated that stable SnL_2 species are formed in solution, although other, more complex species are also likely to be present as the ligands are both polyfunctional.[119,120] Upon addition of copper(II) or iron(III) ions to these solutions, a 1:1:1 tin(II): M^{n+}: $(citrate)^{4-}$ species is also claimed to form, with the citrate anion exerting its full tetravalent coordination.[120]

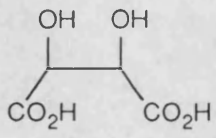

(**18**)

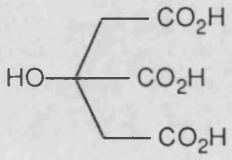

(**19**)

Tin(II) citrate compounds that have been isolated both involve the tetravalent, $(citrate)^{4-}$, anion. These are the di-stannous salt, i.e. $Sn_2(citrate)$, and the di-sodium mono-stannous salt, i.e. $Na_2Sn(citrate)$.[121] The highly water-soluble di-sodium salt has been used as an effective fruit-juice stabiliser. Neither composition has been fully authenticated in the literature and no spectral data is listed.

One of the stannous carboxylates that can be reliably isolated in a pure form is the trifluoroacetate, $Sn(O_2CCF_3)_2$. However, attempted recrystallisation of this compound from dilute trifluoroacetic acid in the presence of traces of atmospheric oxygen has yielded an interesting partial oxidation product: i.e. a mixed valence tin(II)-tin(IV) species, $Sn^{II}_4Sn^{IV}O_2(O_2CCF_3)_8$.[122] A structural determination has revealed a central feature of a $Sn^{II}_2Sn^{IV}_4O_2$ cluster unit containing two μ_3-O atoms bridging one tin(IV) to two tin(II) atoms (Fig.1.20). Each of the tin(II) atom pairs are

further bridged by a $CF_3CO_2^-$ group. In addition, four trifluoroacetate groups bridge the central tin(IV) atom to each of the tin(II) atoms. Overall, the tin(II) atoms are pseudo six-coordinate (SnX_5E) which is quite unusual, the pseudo four-coordinate SnX_3E coordination being much more prevalent in tin(II) compounds.

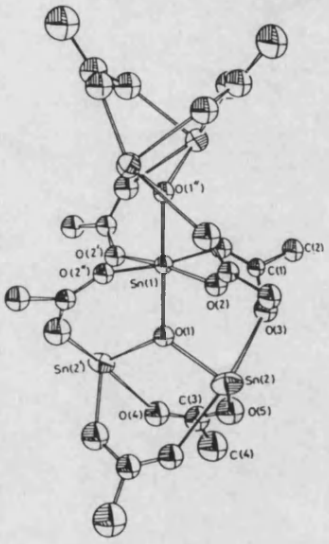

Fig. 1.20 The structure of the mixed valence compound, $Sn^{II}_4Sn^{IV}O_2(O_2CCF_3)_8$.

In summary, simple tin(II) carboxylates generally adopt four coordinate SnO_4E geometry with Sn-O bond lengths in the range 2.13 to 2.36Å. Carboxylate coordination is asymmetrically bridged across two tin atoms forming layer structures. In the case of the complex $Sn(O_2CR)_3^-$ anions, a more typical three coordinate SnO_3E coordination is adopted (Sn-O typically 2.15Å) with three unidentate carboxylate groups surrounding the tin atom. The bond length and spectral data for the series of simple tin(II) carboxylates is summarised in table 1.9. These compounds invariably demonstrate similar [C-O] bond lengths for the RCO_2^- groups, thus indicating the presence of near-symmetrical carboxylate chelation, e.g. $Sn(O_2CH)_2$: [C-O] bond lengths are all between 1.23 and 1.28Å.

Table 1.9 Summary of data for simple tin(II) carboxylates.

Compound	CN	[Sn-O] / Å	δ (mms^{-1})	Δ (mms^{-1})
$Sn(O_2CH)_2$	4	2.36	3.33	1.70
		2.36		
		2.13		
		2.14		
$Sn(C_2O_4)$	4	2 23	3.35	1.65
		2.23		
		2.39		
		2.39		
$K_2Sn(Ox)_2.H_2O$	4	2.14		
		2.20		
		2.36		
		2.30		
$KSn(HO_2C)_3$	3	2.14		
		2.17		
		2.18		
$Sn(O_2CCH_3)_2$	-	-	3.31	1.77

1.8.4 *Tin(II) Alkoxides and Poly-ol Adducts.*

It has been described that the presence of high levels of D-sorbitol (D-glucitol, $C_6H_{14}O_6$ (**20**)) in toothpastes promotes the stability of tin(II) compounds also contained within the formulation to both oxidation and hydrolysis (section 1.6). Consequently, an interaction of interest to dental formulation is the apparent formation of stable chelates between tin(II) compounds and polyhydroxy species such as sorbitol, which is widely used as a dentifrice humectant (section 1.5). Patented claims have been made for 1:1 chelates of stannous salts with ethylene glycol, glycerol, sorbitol, dextrose and sucrose although such documented compounds are poorly characterised.[41] These adducts are likely to be structurally complex due to the polyfunctional nature of these carbohydrates and their structures can only be guessed at. An example of a simple 1:1 Sn(II):sorbitol adduct (**21**) is illustrated, although the actual structure is likely to involve complex bridging to other sorbitol groups.

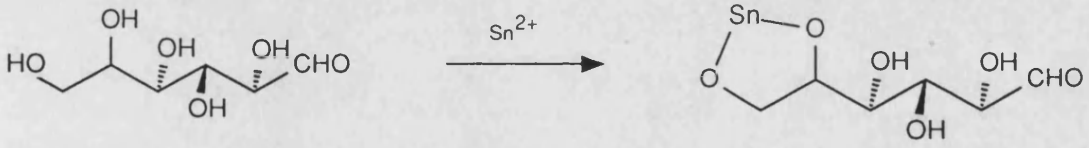

(20) **(21)**

As well as the experimental observations regarding the effect of sorbitol levels upon formulated stannous stability, there is documented electrochemical evidence that the formation of such polyhydroxy-chelates improves the stability of stannous salts to oxidation. For example, in the case of glycerol or sorbitol mixtures with aqueous solutions of $SnCl_2$, a significant increase in the electrochemical redox potential, E°, is observed. This indicates that the resulting tin(II) chelate is a much weaker reducing agent.[123-125] The observed reduction in the ease of oxidation of Sn(II) to Sn(IV) explains why high sorbitol levels are favourable when formulating stable stannous-containing dentifrice products.

The structures of these compounds have not been determined and spectroscopic data is not available, although these poly-ol adducts can be thought of as complex examples of tin(II) alkoxides, $Sn(OR)_2$. The simpler examples of these bis-alkoxides have been widely used as suitably labile tin(II) precursors. The syntheses of tin(II) alkoxides from tin(II) chloride and the corresponding alcohol has been reported according to equation 1.9.[126]

$$SnCl_2 + 2ROH + 2R_3'N \longrightarrow Sn(OR)_2 + 2[R_3'NH]^+Cl^- \qquad (1.9)$$

The simple compounds are actually found to be quite unstable to oxidation and hydrolysis, with particular care required to exclude moisture from the reaction mixture. This requires that the alcohol (ROH) is thoroughly pre-dried by distillation from magnesium metal immediately prior to use. Tin(II) methoxide is a white solid with very limited solubility in polar organic solvents, whereas tin(II) n-butoxide is readily soluble in most common organic solvents, i.e. the solubility increases with the alkoxy-chain length. Infrared data has suggested that tin(II) methoxide has a unique type of polymeric chain structure among the bis-alkoxides (Fig. 1.21(a)) with the higher compounds (e.g. $Sn(OCBu_3^t)_2$) having a simpler dimeric structure (Fig. 1.21(b).[48]

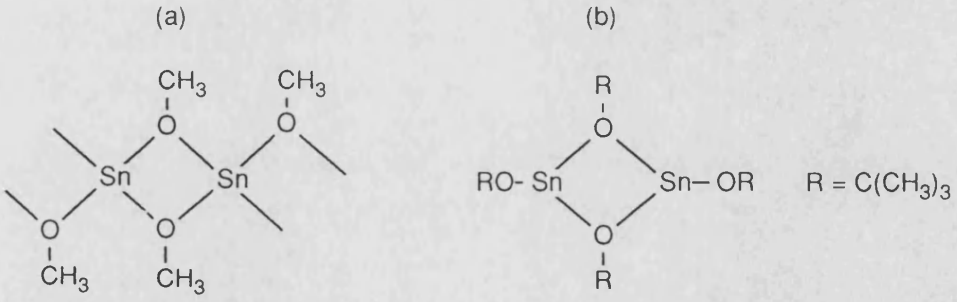

Fig. 1.21 The structures of (a) $Sn(OMe)_2$ and (b) $Sn(OBu^t)_2$.

The simplest tin(II) alkoxides are readily hydrolysed in the presence of an excess of water to give tin(II) oxide, but partial hydrolysis of $Sn(OMe)_2$ has resulted

in the isolation of a crystalline Sn(II) material of composition $Sn_6O_4(OMe)_4$.[127] The X-ray structure of this compound shows it to have an adamantane-type $[Sn_6O_4]^{4+}$ core, around which sit four triply-bridging methoxy groups (Fig. 1.22). The Sn-O bonds in this skeleton are considerably shorter than those typically observed for tin(II) oxygen compounds (2.05 - 2.08Å) but the distances to the methoxy groups are more typical at 2.35 - 2.43Å (*cf.* phosphates and carboxylates). The resulting geometry around the tin is distorted pseudo-trigonal bipyramidal with oxygen atoms of the adamantane cage and methoxy groups occupying equatorial and axial sites respectively. The stereochemically active lone-pair occupies the remaining equatorial position. In spite of the apparently strong bonding in the $[Sn_6O_4]^{4+}$ core, its preservation on further reaction has not been observed.[127] For example, attempts at cleaving the methoxy groups using dilute acetic acid results in the exclusive formation of $Sn(O_2CCH_3)_2$.

In summary, tin(II) chelates of polyhydroxy carbohydrate ligands are observed to be stable compounds to oxidative conditions, whereas the simple alkoxides are relatively unstable to both hydrolysis and oxidation. Very little is known about the structure of the carbohydrate chelates, and structural data is only available for the higher bis-alkoxides.

1.9 Project Objectives.

It is clear from the introduction that the documented chemistry of tin(II) compounds is relatively sparse, particularly if compared to the situation with tin(IV) chemistry. It is well described that stannous fluoride is a particularly effective, but quite unstable anti-plaque dentifrice component However investigation into the possible use of other tin(II) derivatives has been a relatively recent development.

Very little is known about the fate of stannous compounds once they are incorporated into existing toothpaste products. Mössbauer spectroscopic studies have

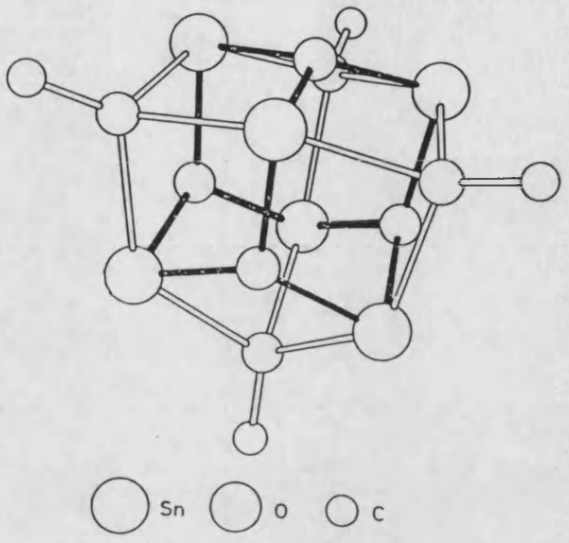

Fig.1.22 The structure of $Sn_6O_4(OMe)_4$, a hydrolysis product of $Sn(OMe)_2$.

qualitatively confirmed that oxidation to tin(IV) species occurs with time and that the parameters of tin(II) species alter considerably once incorporated into a paste.[70]

Questions need to be answered regarding the apparent solubilisation of insoluble tin(II) compounds upon exposure to soluble fluoride ions in a paste. Compounds such as $Sn_2P_2O_7$ - quite insoluble in water - yield high levels of soluble-stannous in a fluoride paste, i.e. a water soluble species of unknown composition is formed. Contact with ZCT also yields high soluble levels of both stannous and citrate ions. This might be due to the formation of soluble tin(II) citrate complex such as those discussed previously (1.8.3). This affords the opportunity to prepare and characterise a range of stannous citrate compounds which may show improved properties and enhanced long-term stability. If insoluble tin(II) citrate species are incorporated into a paste containing fluoride ions, this might also yield soluble stannous species. In addition, there are no reported orally-viable single compounds containing both tin(II) and zinc(II) ions. The preparation of such materials could lead to the synergistic use of both active metal ions in a single

component which might prove to be preferable to using simple mixtures of tin and zinc materials. Mixed-metal polyphosphate and citrate complexes offer themselves as potential candidates for the preparation of such compounds due to their polyfunctional properties. The use of polyhydroxy compounds for the stabilisation of Sn^{2+} also requires further investigation as very little is known about the nature of these interactions.

The net result of these observations is the need to further develop the relevant areas of tin(II) chemistry that might help to enhance the understanding of toothpaste formulation at the molecular level. Of particular importance is the preparation of tin(II) compounds of the types described above that might exhibit improved stability to both hydrolysis and oxidation, coupled to improved solubility and efficacy as potential anti-plaque agents. The study of novel species by X-ray crystallography to gain further structural information is also of great importance in developing structure-activity relationships. Such studies as those outlined above form the basis of this thesis.

2. TIN(II) SALTS OF THE PHOSPHORUS OXY-ACIDS.

It has been described in the introductory Chapter that tin(II) salts have recently found extensive use as potent anti-plaque dentifrice additives alongside zinc salts and organic antibacterials. One of the few primary tin(II) compounds to have been used in this manner is the di-stannous pyrophosphate salt, $Sn_2P_2O_7$, which has proven in use to be highly effective. Several alternative stannous salts of the phosphorus oxy-acids have been described in the literature although none of these have been applied to the anti-plaque application in the quest for improved performance.

It is known that the fate of $Sn_2P_2O_7$, once incorporated into a product, is complex although the exact nature of the species formed remains a matter for speculation. The chemistry of the interaction of Sn(II) with the various excipient components in a product is poorly understood. It is known, for example, that high levels of soluble stannous species can be detected when $Sn_2P_2O_7$ is formulated in the presence of either ionic fluorides or ZCT. In view of the fact that $Sn_2P_2O_7$ is effectively water-insoluble, these observations serve to confirm the formation of novel tin(II) species *in situ*.

In this chapter, the preparation and characterisation of a range of simple tin(II) phosphorus-oxyacid compounds is described. Following this is a detailed investigation of the interaction of $Sn_2P_2O_7$ with fluoride ions, in aqueous solution, in an attempt to identify the soluble species formed. It is anticipated that this might give a further understanding of the interactions taking place in formulated products. Finally, a selection of amorphous tin(II) pyrophosphate salts are further described in terms of EXAFS data obtained at Daresbury SRS in conjunction with Unilever Research Port Sunlight Laboratories (URPSL). The theoretical background to this technique is briefly discussed in Appendix 1. Generally, this technique allows information regarding coordination number and bond lengths to be accurately determined.

2.1 Experimental.

The ease of oxidation of tin(II) compounds has already been described in detail (Section 1.7.3) and for this reason certain precautions have to be observed in the preparation of clean and pure tin(II) species. For all reactions, the apparatus and solvents must first be thoroughly flushed with an inert gas, such as nitrogen, prior to contact with tin(II) materials and the reactions were carried out under an atmosphere of N_2 using standard Schlenk techniques. When the reactions were complete, products were filtered in an inert atmosphere on a Schlenk-stick, whenever suitable, to further prevent contamination of the product with tin(IV) impurities. Where appropriate, organic solvents were dried immediately prior to use by distillation from suitable drying-agents.

The stannous content of these compounds was determined by an iodometric titration according to equation 2.1.[128] During this titration, great care must be taken to exclude atmospheric oxygen from the apparatus, and the solvents must be thoroughly de-oxygenated. The titration is carried out in strongly acidic media (3M HCl) which improves both the solubility and aerobic stability of the inorganic tin(II) compound to be studied.

$$IO_3^- + 2\,Sn^{2+} + 6\,H^+ + Cl^- \xrightarrow{N_2} ICl + 2\,Sn^{4+} + 3\,H_2O \qquad (2.1)$$

Total tin analysis (tin(II), tin(IV)) can be achieved using atomic absorbance spectrophotometry. Sodium and potassium analyses were performed by flame photometry. Analysis for zinc was performed by atomic absorbance spectrophotometry. The infrared spectrum for each compound was obtained as a nujol mull on KBr plates; selected characteristic bands only are quoted. The spectra are assigned according to the documented data in the literature.[129]

^{119}Sn Mössbauer and multinuclear NMR data were also obtained for this

series of compounds where possible. Unfortunately, the majority of these tin(II) phosphates are insufficiently soluble in common solvents to obtain meaningful data from multinuclear NMR spectra, in particular ^{119}Sn NMR data. Whenever possible, solid-state multinuclear MAS-NMR (^{119}Sn, ^{31}P) data is quoted for the highly insoluble compounds, the data was collected in a collaboration with URPSL.[130]

The ^{119}Sn Mössbauer and multinuclear NMR data for this series of tin(II) phosphates are presented in Tables 2.1 and 2.2 respectively. The Mössbauer and NMR data for the series of solubilised tin(II) pyrophosphates are presented in Tables 2.4 and 2.5 respectively. Attempted determination of melting points for this series of compounds proved unsuccessful. It was impossible to distinguish a true melting point due to apparent thermal decomposition of the solid at elevated temperatures (> 200°C).

2.1.1 *Synthesis of stannous phosphite,* $SnHPO_3$ (**22**).[107]

Commercially available blue-black SnO (10.0g, 74.2 mmol) was warmed in 50 ml of thoroughly de-oxygenated water containing H_3PO_3 (6.09g, 74.2 mmol) for 12 hours at around 70-80°C. The near colourless solution was filtered hot, to remove unreacted particles of SnO, and the clear filtrate allowed to slowly cool to room temperature. Careful control of the rate of cooling yielded a colourless, crystalline product. The product was rapidly filtered on a Büchner-funnel, washed with successive aliquots of water, ethanol and ether and thoroughly dried *in vacuo*. Yield: 2.16g (15%). Analysis, found (calc. for HO_3PSn): Sn(II), 57.1 (59.7)%. Selected infrared data: 1075cm^{-1} (*st, br*) υ(P-O); 1020cm^{-1} (*st, br*) υ(P-O); 990cm^{-1} (*st, br*) υ(P-O); 715cm^{-1} (*w, sh*) δ(O-P-O).

2.1.2 *Synthesis of stannous hydrogen phosphate*, $SnHPO_4$ (**23**).[107]

Powdered tin metal (3.0g, 25.3mmol) was allowed to slowly dissolve in 75ml of concentrated H_3PO_4 by carefully warming the mixture to 100°C whilst purging with a constant stream of nitrogen. The hot, viscous solution was rapidly filtered on a Schlenk-stick yielding a clear filtrate to which 5ml of de-oxygenated water was added. Controlled cooling yielded a crop of colourless crystals which were rapidly filtered on a Schlenk-stick and washed successively with water, ethanol and ether. The crystals were thoroughly dried *in vacuo*. Yield: 4.68g (86%). Analysis, found (calc. for HO_4PSn): Sn(II), 51.9 (55.3)%. Selected infrared data: 2395cm^{-1} (*m, br*) υ[(P)O-H]; 1220cm^{-1} (*w, br*) υ(P=O); 900-1100cm^{-1} (*st, mu*) υ(P-O); 700cm^{-1} (*w, sh*) δ(O-P-O).

2.1.3 *Synthesis of stannous orthophosphate*, $Sn_3(PO_4)_2$ (**24**).[104]

1.0M aqueous solutions of SnF_2 and H_3PO_4 were freshly prepared in thoroughly de-oxygenated water. These two solutions were then mixed in the correct stoichiometric ratio (3:2 respectively) in a flask which was continuously purged with nitrogen, e.g. 30ml of 1.0M SnF_2, 20ml of 1.0M H_3PO_4. A milky-white precipitate formed immediately on mixing the two solutions. This precipitate proved difficult to filter satisfactorily on a Büchner-funnel due to fine particle size. Subsequently, a Schlenk-stick was employed with greater success due to the finer porosity of the glass frit. The filtered solid was washed with successive aliquots of water, ethanol and ether and dried *in vacuo* with gentle warming to 70-80°C. Yield: 4.1g (74%). Analysis, found (calc. for $O_8P_2Sn_3$): Sn(II), 63.4 (65.2)%. Selected infrared data: 1210cm^{-1} (*m, sh*) υ(P=O); 940-1140cm^{-1} (*st, mu*) υ(P-O); 710cm^{-1} (*w, sh*) δ(O-P-O);

2.1.4 *Synthesis of stannous phenyl phosphonate*, $C_6H_5P(O)O_2Sn$ (**25**).

Phenylphosphonic acid, $C_6H_5PO(OH)_2$ (5.0g, 31.7mmol) was dissolved in

30ml of thoroughly de-oxygenated water continuously purged with nitrogen. To this solution was added $SnCl_2$ (6.0g, 31.7mmol) with stirring, instantly yielding a white precipitate. The solid product appeared to be quite hydrophobic forming a well-defined layer of solid particles upon the surface of the liquid. The solid was rapidly filtered on a Büchner-funnel, successively washed with water, ethanol and ether and dried *in vacuo*. Yield: 8.0g (92%). Analysis, found (calc. for $C_6H_5O_3PSn$): C, 25.9 (26.2); H, 1.83 (1.82): Sn(II), 42.9 (43.2)%. Selected infrared data: 1312cm^{-1} (*w, br*) υ(P=O); 900-1150cm^{-1} (*st, mu*) υ(P-O); 600-700cm^{-1} (*st, mu*) δ(O-P-O); 455cm^{-1} (*m, sh*) υ(Sn-O).

2.1.5 *Synthesis of stannous phenyl phosphate dihydrate*, $C_6H_5OP(O)O_2Sn.2H_2O$ (**26**).

Disodium phenylphosphate dihydrate, $C_6H_5OP(O)(ONa)_2.2H_2O$ (2.0g, 7.9mmol) was dissolved in 25ml of thoroughly de-oxygenated water while constantly purging with nitrogen. $SnCl_2$ (1.5g, 7.9mmol) was carefully added, with constant stirring, yielding a white precipitate after approximately 10 minutes at room temperature. The precipitate was rapidly filtered on a Büchner-funnel, washed with successive aliquots of water, ethanol and ether and thoroughly dried *in vacuo* with gentle warming to 40-50°C. The product was a fine, white powder which was insoluble in all common solvents. Yield: 2.14g (93%). Analysis, found (calc. for $C_6H_9O_6PSn$): C, 22.2 (22.1); H, 2.14 (2.75); Sn(II), 36.0 (36.3)%. Selected infrared data: 3440cm^{-1} (*m, br*) υ(H-O-H); 1593cm^{-1} (*m, sh*) δ(H-O-H); 1460cm^{-1} (*st, sh*) υ(P=O); 1234cm^{-1} (*st, sh*) υ(P=O); 900-1150cm^{-1} (*st, mu*) υ(P-O); 500-700cm^{-1} (*st, mu*) δ(O-P-O); 417cm^{-1} (*w, sh*) υ(Sn-O).

2.1.6 *Synthesis of di-stannous pyrophosphate*, $Sn_2P_2O_7$ (**27**).

Tetrasodium pyrophosphate, $Na_4P_2O_7$ (10.0g, 37.6mmol) was dissolved in 50ml of thoroughly de-oxygenated water, whilst constantly purging with a stream of

nitrogen. To this solution was added $SnCl_2$ (14.3g, 75.2mmol) with rapid stirring. A dense white precipitate began to form after several minutes, although stirring was continued for 30 minutes at room temperature. The fine particle size of the product made it extremely difficult to filter the solid efficiently. Consequently, a Büchner-funnel fitted with a Whatman 542-grade filter-paper was employed successfully. The solid cake was successively washed with water, ethanol and ether and thoroughly dried *in vacuo* whilst warming to 60°C. Yield: 13.9g (90%). Analysis, found (calc. for $O_7P_2Sn_2$): Sn(II), 58.8 (57.7)%. Selected infrared data: 900-1160cm^{-1} (*st, mu*) υ(P-O); 558cm^{-1} (*st, sh*) δ(O-P-O); 486cm^{-1} (*w, sh*) υ(Sn-O).

2.1.7 *Synthesis of di-sodium mono-stannous pyrophosphate*, $Na_2SnP_2O_7$ (**28**).

Tetrasodium pyrophosphate, $Na_4P_2O_7$ (4.2g, 15.8mmol) was dissolved in 50ml of thoroughly de-oxygenated water while constantly purging with nitrogen. To this solution was added $SnCl_2$ (3.0g, 15.8mmol) with vigorous stirring. After a short while, a dense white precipitate began to form which immediately redissolved on stirring. De-oxygenated ethanol (15ml) was added to the clear solution, with continued stirring, to initiate precipitation of the product. The resulting fine, white precipitate was filtered on a Schlenk-stick, washed successively with a little water, ethanol and ether and thoroughly dried *in vacuo*. Yield: 4.82g (90%). Analysis, found (calc. for $Na_2O_7P_2Sn$): Na, 13.3 (13.6); Sn(II), 34.8 (35.1)%. Selected infrared data: 1302cm^{-1} (*w, sh*) υ(P=O); 890-1180cm^{-1} (*st, mu*) υ(P-O); 500-590cm^{-1} (*st, mu*) δ(O-P-O); 480cm^{-1} (*m, sh*) υ(Sn-O).

2.1.8 *Synthesis of mono-zinc mono-stannous pyrophosphate trihydrate*, $ZnSnP_2O_7.3H_2O$ (**29**).

An aqueous solution of $Na_2SnP_2O_7$ (**28**) was prepared as above, *in situ*, to which one stoichiometric equivalent of anhydrous $ZnCl_2$ (2.15g, 15.8mmol) was

added with rapid stirring. The resultant clear solution was rapidly stirred for 10 minutes, while purging with nitrogen, whereupon a fine, white precipitate began to form. The precipitate was collected on a Büchner-funnel, washed with successive aliquots of water, ethanol and ether and thoroughly dried *in vacuo*. The product proved troublesome to dry effectively and required warming to 90-100°C. Yield: 5.0g (88%). Analysis, found (calc. for $H_6O_{10}P_2SnZn$): Sn(II), 29.9 (28.8); Zn, 14.9 (15.8)%. Selected infrared data: 3400cm^{-1} (*st, br*) υ(H-O-H); 1637cm^{-1} (*st, sh*) δ(H-O-H); 925-115cm^{-1} (*st, mu*) υ(P-O); 723cm^{-1} (*w, br*) υ(Zn-O); 559cm^{-1} (*st, br*) δ(O-P-O); 460cm^{-1} (*w, sh*) υ(Sn-O).

2.1.9 *Synthesis of mono-potassium di-stannous tripolyphosphate,* $KSn_2P_3O_{10}$ **(30).**

Potassium tripolyphosphate, $K_5P_3O_{10}$ (11.6g, 26.4mmol) was dissolved in 75ml of thoroughly de-oxygenated water, continuously purged with nitrogen. $SnCl_2$ (10.0g, 52.7mmol) was added to this solution with stirring, almost immediately yielding a dense white precipitate. The precipitate was collected on a Büchner-funnel fitted with Whatman 542-grade paper, successively washed with water, ethanol and ether and thoroughly dried *in vacuo* with warming to 70-80°C. Yield: 11.8g (85%). Analysis, found (calc. for $KO_{10}P_3Sn_2$): K, 7.0 (7.0); Sn(II), 44.7 (45.0)%. Selected infrared data: 3350cm^{-1} (*w, br*) υ(H-O-H); 1636cm^{-1} (*w, sh*) δ(H-O-H); 1079cm^{-1} (*st, br*) υ(P-O); 913cm^{-1} (*m, sh*) υ(P-O); 552cm^{-1} (*m, br*) δ(O-P-O); 420cm^{-1} (*w, sh*) υ(Sn-O).

2.1.10 *Reaction between* $Sn_2P_2O_7$ *and ionic fluorides (e.g. sodium fluoride)* **(31 - 34).**

In a typical experiment, using sodium fluoride as the fluoride source, $Sn_2P_2O_7$ (5.0g, 12.2mmol) was slurried in 50ml of thoroughly de-oxygenated water with rapid stirring. Solid sodium fluoride was slowly added to this suspension until a clear solution was obtained; it was found that 4 molar equivalents of NaF (2.05g,

48.8mmol) were required to give a reproducibly clear solution. Attempted crystallisation of the soluble species failed, simply yielding a very fine, flock-like precipitate which was unsuitable for filtration. Therefore, in order to obtain spectral data on this water-soluble compound it was necessary to remove the water by suction on a rotary-evaporator. The resulting water-soluble product (**31**) was a colourless, glassy solid which was found to have a high water content and was amorphous to X-rays. Yield: 7.1g (100%). Selected infrared data: 3347cm^{-1} (*st, br*) υ(H-O-H); 1651cm^{-1} (*st, sh*) δ(H-O-H); 1302cm^{-1} (*w, sh*) υ(P=O); 890-1171cm^{-1} (*st, mu*) υ(P-O); 556cm^{-1} (*st, br*) δ(O-P-O); 500cm^{-1} (*m, br*) υ(Sn-F); 468cm^{-1} (*w, sh*) υ(Sn-F); 438cm^{-1} (*m, br*) υ(Sn-O).

Potassium fluoride product (**32**). Selected infrared data: 3351cm^{-1} (*st, br*) υ(H-O-H); 1648cm^{-1} (*st, sh*) δ(H-O-H); 1298cm^{-1} (*w, sh*) υ(P=O); 890-1180cm^{-1} (*st, mu*) υ(P-O); 541cm^{-1} (*st, br*) δ(O-P-O); 495cm^{-1} (*m, br*) υ(Sn-F); 468cm^{-1} (*w, sh*) υ(Sn-F); 438cm^{-1} (*m, br*) υ(Sn-O).

Ammonium fluoride product (**33**). Selected infrared data: 3410cm^{-1} (*st, br*) υ(H-O-H); 1648cm^{-1} (*st, sh*) δ(H-O-H); 1305cm^{-1} (*w, sh*) υ(P=O); 875-1180cm^{-1} (*st, mu*) υ(P-O); 552cm^{-1} (*st, br*) δ(O-P-O); 501cm^{-1} (*m, br*) υ(Sn-F); 470cm^{-1} (*w, sh*) υ(Sn-F); 437cm^{-1} (*m, br*) υ(Sn-O).

Tetra-n-butyl ammonium fluoride product (**34**). Selected infrared data: 3355cm^{-1} (*st, br*) υ(H-O-H); 1631cm^{-1} (*st, sh*) δ(H-O-H); 1300cm^{-1} (*w, sh*) υ(P=O); 860-1200cm^{-1} (*st, mu*) υ(P-O); 556cm^{-1} (*st, br*) δ(O-P-O); 501cm^{-1} (*m, br*) υ(Sn-F); 458cm^{-1} (*w, sh*) υ(Sn-F); 429cm^{-1} (*m, br*) υ(Sn-O).

The remaining reactions with different ionic fluorides were carried out in an identical manner to that described for sodium fluoride yielding very similar observations, i.e. the products with KF (**32**) and NH_4F (**33**) were readily

water-soluble, colourless glasses. The only exception to this rule was the product obtained by reaction of $Sn_2P_2O_7$ with tetra-n-butyl ammonium fluoride. This compound (**34**), which was observed to be extremely hygroscopic, readily formed a colourless, viscous syrup upon exposure to moisture.

2.2 Preparation and Characterisation of Tin(II) Phosphorus Oxy-acid Salts.

A range of tin(II) salts of the phosphorus acids have been prepared and fully characterised. Several of these compounds are documented materials as described in Chapter 1; these were prepared in order to provide access to a wider-ranging body of experimental data, e.g. Mössbauer parameters. It was also anticipated that these materials might be subjected to anti-microbial testing with potentially improved anti-plaque properties. These tests are described fully in Chapter 5.

Stannous phosphite, $SnHPO_3$ (**22**), was prepared according to equation 2.2.

$$SnO + H_3PO_3 \xrightarrow{\Delta,\ 78^\circ C} SnHPO_3 + H_2O \qquad (2.2)$$

The low yield for this reaction is in agreement with the results quoted in the literature. The product is a highly crystalline material with limited solubility in water. Stannous hydrogen phosphate, $SnHPO_4$ (**23**), was prepared according to equation 2.3.

$$Sn + H_3PO_4 \xrightarrow{\Delta,\ 100^\circ C} SnHPO_4 + H_2 \qquad (2.3)$$

This reaction occurs in good yield and the product is also a highly crystalline material although crystallisation took place only after the addition of a small amount of water to the reaction mixture. The infrared data clearly reveals the presence of a broad peak at 2395cm^{-1}. This is characteristic of the υ[(P)O-H] stretching mode.

Stannous orthophosphate, $Sn_3(PO_4)_2$ (**24**), was prepared according to equation 2.4.

$$3\,SnF_2 + H_3PO_4 \longrightarrow Sn_3(PO_4)_2 + 6\,HF \qquad (2.4)$$

This reaction occurs in near-quantitative yield although a good deal of the product was unavoidably lost at the filtration stage. The final product of this reaction,

after thorough drying, was found to be the anhydrous salt, although the initial solid required warming to obtain a suitably dry material. The initial product appeared to be readily hydrated although the dried sample was not observed to be water-sensitive.

Stannous phenyl phosphonate, $C_6H_5P(O)O_2Sn$ (**25**), was prepared according to equation 2.5.

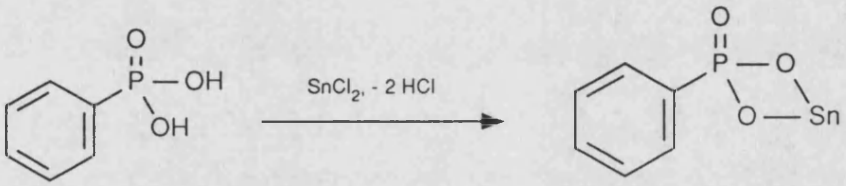

(2.5)

This reaction occurs in a very good yield, the data suggesting that the product is the anhydrous salt. This anhydrous solid is an amorphous white powder with very low solubility in all solvents. The physical properties of this compound suggest that it exists as a polymer in the solid-state. For simplicity, the product is drawn as a monomeric species with two-coordinate tin although intermolecular interactions will increase the coordination around the tin.

The remaining compounds (**26-30**) were all prepared by variations on the same general method. This involves the reaction of stannous chloride with the sodium salt of the corresponding phosphorus oxy-acid in aqueous solution according to equation 2.6. The sodium chloride formed during reaction was removed during filtration and washing.

$$SnCl_2 + ROP(O)(ONa)_2 \xrightarrow{H_2O} ROP(O)O_2Sn + 2\,NaCl \qquad \textbf{(2.6)}$$

R = Ph (**26**), $P(O)O_2Sn$ (**27**), $P(O)(ONa)_2$ (**28**), $P(O)O_2Zn$ (**29**), $P(O)OKP(O)O_2Sn$ (**30**).

Stannous phenyl phosphate dihydrate, $C_6H_5OP(O)O_2Sn.2H_2O$ (**26**) was prepared in good yield by this general method according to equation 2.7.

The product of this reaction appeared to precipitate as the dihydrate, as

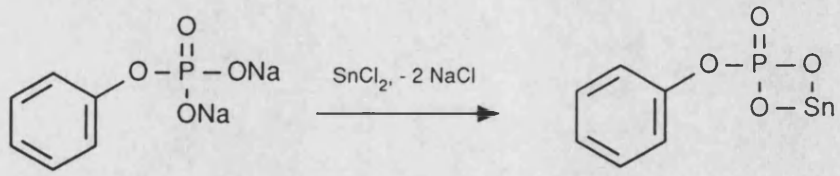

(2.7)

suggested by the analytical data. Characteristic water stretching bands in the infrared spectrum (3440, 1593cm^{-1}) also confirm the presence of water in the lattice. This compound, like the phosphonate (**25**), is extremely insoluble in all common solvents. Similarly, the product is drawn as a simple monomeric compound although the physical properties suggest otherwise. It is likely that various intermolecular interactions will occur in the solid-state.

Di-stannous pyrophosphate, $Sn_2P_2O_7$ (**27**), was also prepared by this general method according to equation 2.8.

$$Na_4P_2O_7 + 2\,SnCl_2 \longrightarrow Sn_2P_2O_7 + 4\,NaCl \qquad (2.8)$$

The product was a very fine, white powder which was found to be virtually insoluble in all solvents. This compound was even insoluble in strongly coordinating solvents such as DMSO. Attempted powder-diffraction studies showed no diffraction pattern, i.e. the material was amorphous to X-rays. The complete absence of a υ(P=O) stretch in the infrared spectrum suggests that a discreet [P=O] bond is no longer present. This characteristic band is normally situated at 1200 - 1500cm^{-1} in the infrared spectrum. The most probable explanation is that all three oxygens attached to one phosphorus are equally bound to tin, i.e. the P=O bond is fully delocalised around the phosphorus atom.

A second tin(II) pyrophosphate, di-sodium mono-stannous pyrophosphate, $Na_2Sn(P_2O_7)$ (**28**), was also prepared as above using a different (1:1) stoichiometry of starting materials. This is illustrated in equation 2.9.

In this preparation, a transitory white precipitate was formed which almost

$$2\,Na_4P_2O_7 + 2\,SnCl_2 \longrightarrow [Sn_2P_2O_7] \xrightarrow{Na_4P_2O_7} Na_2Sn(P_2O_7) + 4\,NaCl \qquad (2.9)$$

immediately redissolved to yield a clear solution. It was assumed that this precipitate was $Sn_2P_2O_7$, as shown, which precipitates before further reacting with a second mole of $Na_4P_2O_7$ to yield the desired product. The analytical and infrared data are consistent with the formation of the anhydrous material, i.e. no υ(H-O-H) bands are observed. This compound is readily water-soluble but only sparingly so in other coordinating solvents.

A novel orally-viable tin(II) pyrophosphate which also contains zinc ions has also been prepared from (**28**). Mono-zinc mono-stannous pyrophosphate trihydrate, $ZnSn(P_2O_7).3H_2O$ (**29**), was prepared according to equation 2.10.

$$Na_2Sn(P_2O_7) + ZnCl_2 \longrightarrow ZnSn(P_2O_7) + 2\,NaCl \qquad (2.10)$$

The mixed-metal pyrophosphate precipitates in good yield as a trihydrate. This is indicated by the analytical and infrared data; the characteristic infrared bands (3400, 1637cm^{-1}) are readily observed. This compound is also amorphous to X-rays and is virtually insoluble in all common coordinating solvents.

A tin(II) tripolyphosphate, $KSn_2(P_3O_{10})$ (**30**), was also prepared in a similar manner. This compound, mono-potassium di-stannous tripolyphosphate was prepared according to equation 2.11.

$$K_5P_3O_{10} + 2\,SnCl_2 \longrightarrow KSn_2(P_3O_{10}) + 4\,KCl \qquad (2.11)$$

Regardless of the initial stoichiometric ratio of the two starting materials used in this reaction, the final product consistently appeared to be the 2:1 (Sn(II): $[P_3O_{10}^{5-}]$) compound as shown in equation 2.11. This observation is consistent with the documented complexation of tin(II) by tripolyphosphates which indicates that this stoichiometry is the favoured composition.[111]

Table 2.1 ^{119}Sn Mössbauer data for the series of tin(II) phosphate compounds.[a].

Compound	δ (mms^{-1})	Δ (mms^{-1})	Γ (mms^{-1})	Γ (mms^{-1})
$SnHPO_3$ (**22**)	3.17	1.71	1.02	1.05
$SnHPO_4$ (**23**)	3.57	1.46	1.29	1.42
$Sn_3(PO_4)_2$ (**24**)	3.55	1.37	1.33	1.29
$PhP(O)O_2Sn$ (**25**)	3.08	1.69	1.37	1.23
$PhOP(O)O_2Sn.2H_2O$ (**26**)	3.20	1.64	1.05	1.04
$Sn_2P_2O_7$ (**27**)	3.27	1.66	1.34	1.31
$Na_2SnP_2O_7$ (**28**)	3.01	1.73	1.21	1.27
$ZnSnP_2O_7.3H_2O$ (**29**)	3.24	1.61	1.18	1.06
$KSn_2P_3O_{10}$ (**30**)	3.14	1.66	1.36	1.22

Note:-

[a]Recorded at 78K, relative to SnO_2.

Table 2.2 ^{119}Sn and ^{31}P multinuclear NMR data for the series of tin(II) phosphate compounds..

Compound	δ (^{119}Sn) / ppm[a]	δ (^{31}P) / ppm[b]	Anisotropy / ppm[c]
$SnHPO_3$ (**22**) [d]	-713.3	1.4	735.9
$SnHPO_4$ (**23**) [d]	-957.9	- 4.7	540.7
$Sn_3(PO_4)_2$ (**24**) [e]	-	- 1.6	-
$Sn_2P_2O_7$ (**27**) [d]	-683.2, -737.9	- 11.6, - 14.7	-
$Na_2SnP_2O_7$ (**28**) [e]	-644.4	- 8.3	-
$ZnSnP_2O_7.3H_2O$ (**29**) [e, f]	-	- 6.7	-
$KSn_2P_3O_{10}$ (**30**) [e, f]	-	- 5.9	-

Notes:-

[a]Referenced to tetramethyltin, $Sn(CH_3)_4$.
[b]Referenced to orthophosphoric acid, H_3PO_4.
[c]Reflects the symmetry of charge distribution about the central tin.
[d]Data collected by MAS-NMR solid-state techniques.
[e]Data collected as a saturated solution in D_2O at ambient temperature.
[f] ^{119}Sn NMR data: Baseline too noisy to readily distinguish genuine peaks (v. low solubility).

The ^{119}Sn Mössbauer data for this series of tin(II) phosphorus-oxyacid compounds (**22-30**) is listed in Table 2.1. As indicated above, the spectra are all recorded on finely-ground, solid samples at liquid nitrogen temperature (78K). The value of the isomer-shift, δ, is quoted with reference to SnO_2 ($\delta = 0.00 mms^{-1}$) and the source is $BaSnO_3$. The presented data clearly indicates that all of the compounds contain tin in its lower +II oxidation state due to the high, positive values for the isomer-shift, δ. Also, the data shows the level of tin(IV) impurities to be undetectable, i.e. the materials are all quite pure in terms of their stannous content with little or no tin(IV) impurities.

The spectrum of each compound is observed to be a doublet. This is indicative that the coordination about the tin atom displays a marked degree of asymmetry.

Considering that the tin atom is coordinated by oxygen atoms in each of these compounds, the variation in δ for this series of compounds can be accounted for by subtle variations in the coordination geometry about the individual tin atoms. In the case of $SnHPO_3$, $SnHPO_4$ and $Sn_3(PO_4)_2$ X-ray crystallographic studies have shown the tin atom to exhibit three coordinate SnO_3E trigonal pyramidal coordination.[104, 107] This type of coordination is prevalent throughout many tin(II) compounds. The values of both δ and Δ for $SnHPO_4$ and $Sn_3(PO_4)_2$ are, in fact, remarkably similar, reflecting the expected similarity in their tin coordination. However, the data for $SnHPO_3$ shows a marked increase in the quadrupole-splitting, Δ, coupled to a significant decrease in the value of δ. Since the coordination number at tin is still nominally three in this compound, the spectral variation in the reduced value of δ might reflect the presence of stronger Sn-O bonding in this compound, resulting in decreased $5s^2$ electron-density at the nucleus. This prediction is in agreement with the observed average [Sn-O] bond lengths within the SnO_3E pyramids for these two compounds, i.e. 2.18Å in $SnHPO_3$, 2.32Å in $SnHPO_4$. The structural bonding in $Sn_3(PO_4)_2$ shows the presence of three tin sites with Sn-O bond-lengths in the range

2.08 - 2.32Å (Table 1.7). Also, $SnHPO_4$ is subject to hydrogen bonding not found in $SnHPO_3$. This bonding has the net effect of bringing adjacent sheets of strongly bound SnO_3 pyramids closer together, thus enabling the existence of weak intermolecular Sn-O interactions beyond the SnO_3 coordination sphere.

The significant increase in the value of Δ in $SnHPO_3$ suggests the presence of a less symmetrical overall coordination about the tin. This is borne-out by the structural data, which shows the Sn-O bonding within the SnO_3 pyramids to be quite unsymmetrical in both compounds. The stronger, additional intermolecular contacts in $SnHPO_4$ might be sufficient to increase the overall charge symmetry about the tin. $Sn_3(PO_4)_2$ also possesses many weak Sn-O interactions which accounts for its relatively low value of Δ.

The Mössbauer data for the majority of the remaining phosphate compounds, for which structural information is unfortunately not available, are remarkably consistent. The data for this series of compounds is very similar to that obtained for $SnHPO_3$ in terms of the values of δ and Δ. This suggests that these compounds (**22, 25-27, 29-30**) all share a broadly similar tin(II) coordination sphere. The most likely explanation of this observation, given the structure of $SnHPO_3$ is that the Sn-O coordination is invariably of the three coordinate pyramidal type, i.e. SnO_3E, and the relatively minor variations in δ and Δ are primarily due to quite subtle changes to Sn-O bond lengths and bond angles.

Perhaps the only exception to this comment is the data for $Na_2SnP_2O_7$ (**28**), which has the lowest isomer-shift and the highest quadrupole-splitting of this series of compounds by a significant margin. Notably, this compound is also the only one of this series to be appreciably water-soluble. These physical observations might imply a different type of coordination about the tin; a strongly-bound, but heavily distorted Sn-O sphere. The overall structure must be less polymeric to account for these physical changes.

The quoted linewidth parameters, Γ_1 and Γ_2, refer to the full-width at

half-height for the two spectral components that make up the doublet. Spectra exhibiting very similar values for both Γ_1 and Γ_2 are generally more symmetrical than those with widely varying parameters. Also, the higher the numerical value of these linewidth parameters, generally, the more distinct tin sites are found within the solid lattice of the compound. An increase in Γ_1 and Γ_2 can be caused by the overlap of the individual spectra corresponding to subtly differing tin environments in the same sample. Physical effects can also cause slight variations to the linewidth parameters and the symmetry of the spectrum, e.g. sample homogeneity, particle-size. Of the compounds with known crystal structures (**22-24**) only $SnHPO_3$ exhibits narrow linewidths (Section 1.8.2). The structure of this compound is quite simple consisting of adjacent sheets of SnO_3 pyramids, all tin sites being equal. $SnHPO_4$ has a similar structure although the adjacent sheets are in much closer proximity due to strong intermolecular hydrogen bonding. The broad linewidths suggest that this must create subtly distinct tin sites within the crystallographic unit-cell. $Sn_3(PO_4)_2$ is known to contain three distinct tin sites as revealed in the crystal structure determination. This feature accounts for the relatively broad linewidths observed in the Mössbauer spectrum for this compound.

Typically, the majority of the remaining tin(II) phosphate compounds exhibit quite broad and asymmetric linewidths. In many such cases (**25, 27-30**) this might simply be a function of the apparently amorphous nature of the solid samples creating slight, local variations in tin coordination. The physical properties of these compounds also suggest that they are quite polymeric. Various modes of [Sn-O-P] cross-linking might also affect the overall range of Sn-O geometries, increasing the linewidth. Compounds such as $SnHPO_3$ (**22**) and $C_6H_5OP(O)O_2Sn.2H_2O$ (**26**) exhibit symmetrical spectra with narrow linewidths (Γ_1, Γ_2 = 1.02-1.05mms^{-1}). The implication is that the Sn-O coordination in these compounds is well-defined throughout the sample. In the case of $Sn_2P_2O_7$, for example, the linewidths are quite broad but also quite symmetric (Γ_1 = 1.34, Γ_2 = 1.31mms^{-1}) suggesting the presence

of multiple tin sites with similar coordinations, i.e. all of similar δ and Δ. However, the spectrum of $KSn_2P_3O_{10}$ (**30**) has broad linewidths of unequal width (Γ_1 = 1.36, Γ_2 = 1.22mms^{-1}) implying the presence of multiple tin sites with quite different, overlapping δ and Δ values.

A limited selection of ^{119}Sn and ^{31}P NMR data is presented in Table 2.2, the majority of compounds being insufficiently soluble in suitable solvents to enable data collection. The only compound for which ^{119}Sn NMR data was obtained in solution (D_2O) was $Na_2SnP_2O_7$ (**28**). The presence of single peaks in both ^{119}Sn and and ^{31}P spectra shows the presence of single tin and phosphorus environments in solution. This implies that the structure of this compound is likely to be relatively simple and symmetrical with regard to the pyrophosphate group as both phosphorus atoms are in the same bonding environment. Alternatively, a rapid dynamic equilibrium might exist in solution at ambient temperature yielding these simple spectra. Unfortunately, the spectra could not be obtained at low temperature in D_2O in order to better resolve the presence of futher spectral components. The negative δ(^{31}P) suggests that the two phosphorus nuclei are heavily shielded, i.e. highly charged. The relatively low δ(^{119}Sn) may be due to a shift in the coordination number around the tin atom when the compound is in solution (i.e. CN > 2). The likely outcome will be the coordination of water molecules around the tin atom, i.e. an increase in coordination number to four or five. One possibility when in solution, which also incorporates a highly favourable six-membered (P_2O_3Sn) ring, is the structure shown below:-

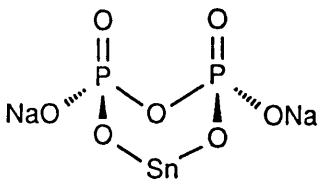

(28)

The remaining tin NMR data was obtained on solid samples using

Magic-Angle Spinning techniques (MAS). Several tin(IV) compounds have been studied by this technique and it has allowed useful information on solid-state structural interactions to be determined. For example, high-resolution ^{119}Sn and ^{31}P solid-state studies have been used to probe the structures of amorphous and microcrystalline tin(IV) hydrogenphosphates and trialkyltin(IV) hydroxides.[131,132] The extension of this technique to study inorganic tin(II) species has not been reported in the literature although this data confirms the possibility.

Where there is more than one peak quoted for a compound, this implies that there is more than one crystallographic site within the asymmetric unit. The anisotropy data reflects the distribution of the electronic charge around the ^{119}Sn nucleus. A perfectly spherical electronic distribution would produce an anisotropy figure of 0.0ppm; the higher figures for tin(II) compounds are primarily due to the influence of the lone-pair.

The data obtained from ^{119}Sn MAS-NMR can be directly correlated with ^{119}Sn Mössbauer spectroscopy, as the two techniques give data relating to tin coordination in the solid-state. The data for $SnHPO_3$ (**22**) and $SnHPO_4$ (**23**) shows single peaks for both ^{119}Sn and ^{31}P spectra. Considering the ^{31}P data, the presence of a single peak implies the presence of only one type of phosphorus environment in each structure; this has already been shown to be the case by crystallography. The very slight shift in $\delta(^{31}P)$ from 1.35ppm (**22**) to -4.49ppm (**23**) is perhaps due to the extra shielding of the phosphorus nucleus brought about by the high electronegativity of the fourth oxygen atom in $SnHPO_4$. Alternatively, it might simply be due to the higher coordination number around the phosphorus atom in $SnHPO_4$. The shift in $\delta(^{119}Sn)$ from -713.3ppm (**22**) to -957.9ppm (**23**) is most likely due in part to the increased shielding effect on the tin nucleus brought about by the increased electronegativity of the ligand in $SnHPO_4$. The most significant factor is the presence of additional intermolecular Sn-O bonding in $SnHPO_4$, i.e. an increase in coordination number beyond the basic SnO_3 unit.

The anisotropy data shows a marked increase in $SnHPO_3$ (735.9ppm compared to 540.7ppm in $SnHPO_4$): This increase in asymmetry about the tin can be linked to the increased quadrupole-splitting, Δ, observed in the Mössbauer spectra.

The ^{31}P MAS-NMR spectrum of $Sn_2P_2O_7$ (**27**) clearly demonstrates that two distinct phosphorus environments are present in this compound. Similarly, the ^{119}Sn data shows that there are also two distinct tin(II) environments in the overall structure. In each case, the two peaks are of approximately equal intensity. Each phosphorus is highly shielded (highly negative δ), and the two tin atoms, although quite similar, also appear to be broadly similar in character to the tin environments in (**22, 28**). The data suggests that the basic coordination in $Sn_2P_2O_7$ is also of the pyramidal SnO_3E type as predicted by the Mössbuer data. The presence of two tin sites, as confirmed by MAS-NMR, is in agreement with the broad linewidths obtained in the Mössbauer spectrum.

Structural data for metal pyrophosphate species is very limited. The structure determination of $Na_4P_2O_7.10H_2O$ showed the $P_2O_7^{4-}$ ion to consist of two tetrahedra joined by a common oxygen atom.[133] The central [P-O-P] angle is 134° and the central P-O bond lengths (1.61Å) are longer than the terminal P-O bonds (1.51Å). A linear configuration for the pyrophosphate ion has also been predicted for the isomorphous cubic series MP_2O_7 (M = Zr, Hf, Si, Ti, Sn, and U).[134]

For stannous pyrophosphate there is a total absence of any documented crystallographic data. Perhaps the most likely explanation of the spectral data for $Sn_2P_2O_7$ is one of a cross-linking polymerisation process involving many ordered [P-O-Sn] intermolecular bridging interactions, thus yielding two distinct crystallographic types of tin and phosphorus environments. This would provide an explanation of the physical properties of this material, e.g. acute insolubilty. This cross-linking would result in the delocalisation of the P=O double bond character as shown overleaf.

This intermolecular bridging provides an explanation for the absence of

υ(P=O) peaks in the infrared spectrum of this compound. These P=O peaks are usually observed in the range 1200 - 1500cm^{-1}. Alternatively, it could simply be that two distinct isomers of $Sn_2P_2O_7$ (e.g. **27a**, **27b**) co-exist in the solid-state. However, if this were the case, it is unclear as to why these species should be so insoluble in comparison with $Na_2SnP_2O_7$.

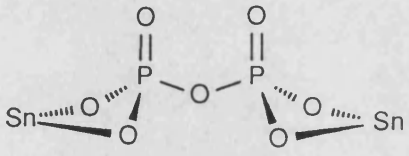

(27a)

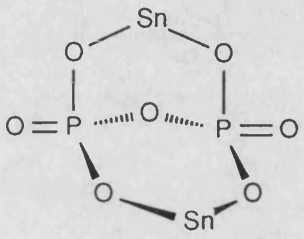

(27b)

These isomers are drawn as discreet monomers for simplicity - this is highly unlikely due to the reactive nature of the P=O bond and the inclination of the tin atoms to increase their coordination number.

In an attempt at further resolving this situation, tin-EXAFS data has been recorded for the two amorphous tin(II) pyrophosphate compounds, i.e. $Sn_2P_2O_7$ (**27**) and $Na_2SnP_2O_7$ (**28**). This technique can provide valuable information concerning the coordination number and bond lengths about the tin atom in the solid-state. The EXAFS data is tabulated in Table 2.3.

Table 2.3 EXAFS data for amorphous tin(II) pyrophosphates.

Compound	Number of atoms	Atom type	Bond length / Å	Error /Å	R value
$Sn_2P_2O_7$	5.82	O	2.18	0.02	15.8
	2.02	P	3.37	0.01	
	1.03	P	3.64	0.01	
$Na_2SnP_2O_7$	5.95	O	2.15	0.02	19.3
	1.84	P	3.33	0.01	
	1.08	P	3.63	0.02	

The EXAFS results show very little difference in the basic coordination sphere of the central tin atom. In both cases, the first shell around the central tin contains six oxygen atoms with average Sn-O bond lengths of 2.18Å ($Sn_2P_2O_7$) and 2.15Å ($Na_2SnP_2O_7$). Beyond this innermost shell of oxygen atoms is a second coordination shell which contains two phosphorus atoms. The average Sn-P distances range from 3.37Å ($Sn_2P_2O_7$) to 3.33Å ($Na_2SnP_2O_7$). A third coordination sphere, comprising a further Sn-P separation is observed for both of these compounds.

Beyond this third shell, the data is much less satisfactory and it is much more difficult to accurately interpret. These results suggest that in each of these two pyrophosphate compounds the tin coordination is very similar with each tin atom coordinating to two distinct PO_3 groups from the pyrophosphate ion. It could simply be that the solid lattice contains two distinct SnO_3E coordination units with the O atoms belonging to two PO_3 units. Alternatively, it might be that an overall SnO_3O_3' coordination is present, i.e. a distorted octahedral arrangement (Section 1.7.2) in which the basic coordination unit is the SnO_3 trigonal pyramid. A further SnO_3' coordination would lie beyond this inner shell yielding a cross-linked polymeric structure.

The fact that the basic SnO_3 unit is predominant in the structural chemistry of tin(II) phosphates (Section 1.8.2) is well established. This three-coordinate geometry is predominant in many other oxygen-bound tin(II) salts although the presence of a second SnO_3' coordination sphere has been identified in a few cases. For example, $SnSO_4$ has an SnO_3O_3' coordination with six Sn-O bond lengths of 2.25, 2.27, 2.27, 2.95, 3.08, 3.08Å.[159,160] However, the Mössbauer parameters of a commercial sample of this compound (δ, 3.90; Δ, 1.21mms^{-1}) are quite different to those of the pyrophosphates. A further example of an approximate SnO_3O_3' coordination is found in (triformato)stannate(II) anions, $Sn(O_2CH)_3^-$. The six Sn-O bond lengths are 2.18, 2.17, 2.14, 2.88, 3.01, 2.97Å.[117] The Mössbauer data for the potassium salt of this anion (δ, 3.05; Δ, 1.85mms^{-1}) is much more similar to that of the tin(II)

pyrophosphates.[161] The latter data confirms that the coordination suggested by EXAFS analysis might be consistent with the Mössbauer data.

The existence of true octahedral six-coordinate tin(II) is relatively rare in documented compounds and is unprecedented for tin(II) phosphates. One six-coordinate tin(II) compound is cubic SnSe which displays an octahedral six-coordinate rock-salt structure (Section 1.7.2). All of the documented tin(II) phosphate species exhibit three-coordination with the exception of $Sn(H_2PO_4)_2$ which is four-coordinate (Table 1.7).

If this compound does exhibit the SnO_3O_3' coordination, a possible arrangement about the central tin atom is proposed in Fig. 2.1. This shows the SnO_3O_3' geometry, with the three phosphorus atoms arranged in two distinct coordination shells. Two of these come from the two terminal PO_3 groups, while the third is from an adjacent P_2O_7 group.

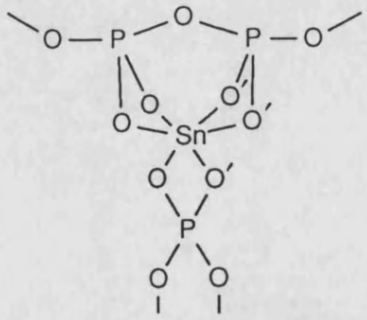

Fig. 2.1 The SnO_3O_3' coordination about tin.

The Sn-O bond lengths in each of these two compounds are comparable with those in other tin(II) phosphate species. These are listed in Table 1.7 and typically range from 2.06 - 2.47Å. The shorter average Sn-O bond lengths in di-sodium mono-stannous pyrophosphate are consistent with the Mössbauer data which shows a significant reduction in the isomer-shift compared with $Sn_2P_2O_7$.

The most likely explanation for the different physical properties between these two materials is a substantial reduction in polymeric cross-linking in the di-sodium salt. This is in agreement with the presence of a strong υ(P=O) band in the infrared spectrum of $Na_2SnP_2O_7$ (890-1180cm^{-1}) which suggests that less cross-linking occurs through the P=O bond. Such a band was absent in the spectrum of $Sn_2P_2O_7$.

The experimental EXAFS fourier transform curves for these two compounds are presented in Figs. 2.2 and 2.3.

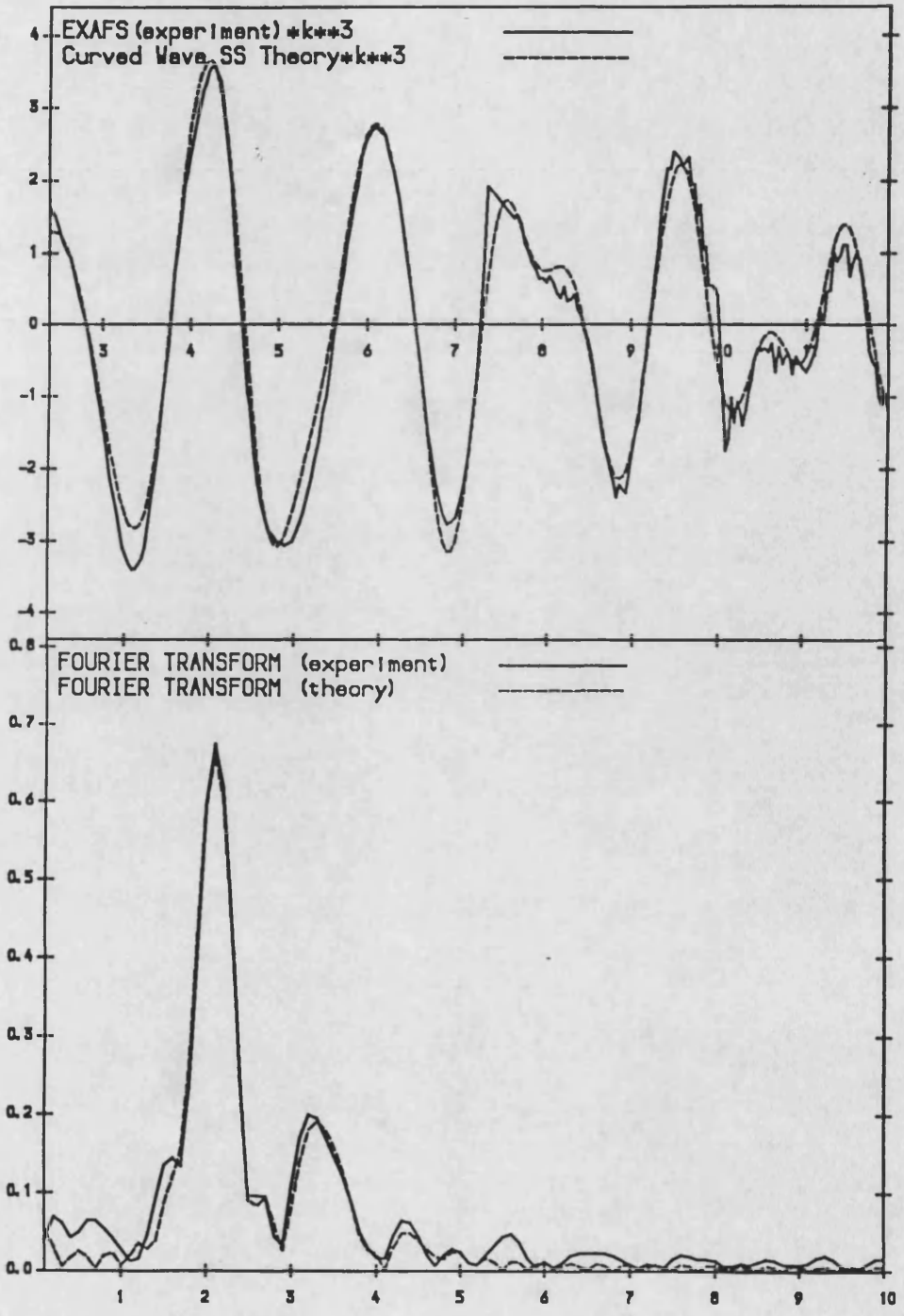

Fig. 2.2 The EXAFS fourier transform curves for $Sn_2P_2O_7$.

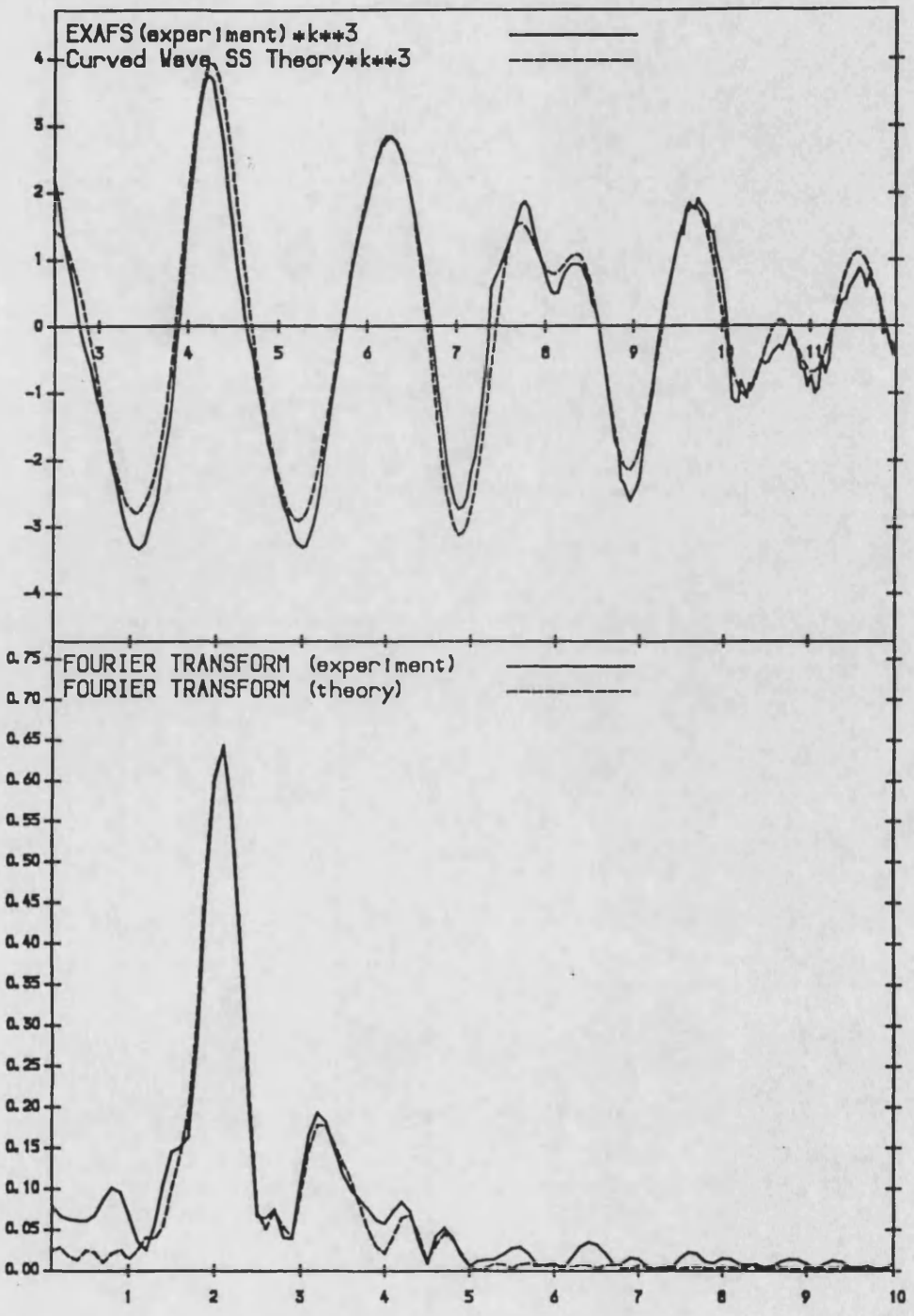

Fig. 2.3 The EXAFS fourier transform curves for $Na_2SnP_2O_7$.

2.3 The Interaction of Stannous Pyrophosphate With Fluoride Ions in Aqueous Solution.

It has previously been described in some detail in the introduction that toothpaste formulations containing $Sn_2P_2O_7$ and an ionic fluoride source are known to yield a water-soluble source of stannous. The identity of the species formed in this interaction is unknown, although the fact that $Sn_2P_2O_7$ is essentially insoluble indicates a dramatic change in the nature of the tin(II) coordination. In this section, the interaction of $Sn_2P_2O_7$ with ionic fluorides is examined in terms of changes to both physical and chemical properties as observed by spectroscopic techniques.

It can be readily observed experimentally that four molar equivalents of an ionic fluoride source are required to completely solubilise one equivalent of $Sn_2P_2O_7$. The product of this reaction is found to be extremely water-soluble, although repeated attempts at crystallisation of the product were unsuccessful.

A range of simple fluoride species with a variety of cations were successfully used to produce a selection of solubilised tin(II) pyrophosphates. The fluorides used include sodium fluoride, potassium fluoride, ammonium fluoride and tetra-n-butylammonium fluoride. The tetra-n-butylammonium fluoride was used in the hope of producing a solubilised tin(II) pyrophosphate that was also soluble in polar organic solvents due to the bulky organic cation. The resulting material was noted to be sparingly soluble in very polar solvents such as tetrahydrofuran and methanol. Slow crystallisation over a prolonged period of a saturated solution of this species in THF yielded a crop of fine needle-like crystals from the reaction flask. Unfortunately, these crystals rapidly lost solvent on filtration yielding a white powder. Mössbauer analysis of this solid revealed that these crystals contained exclusively tin(IV) (δ, -0.22mms^{-1}; Δ, 0.00mms^{-1}), the spectrum appearing as a broad singlet (Γ, 1.21mms^{-1}). The implication of this result is that atmospheric oxygen must have

entered the flask during the crystallisation.

The observed results of these solubilisation experiments are briefly summarised in Scheme 2.1 for this series of reactions.

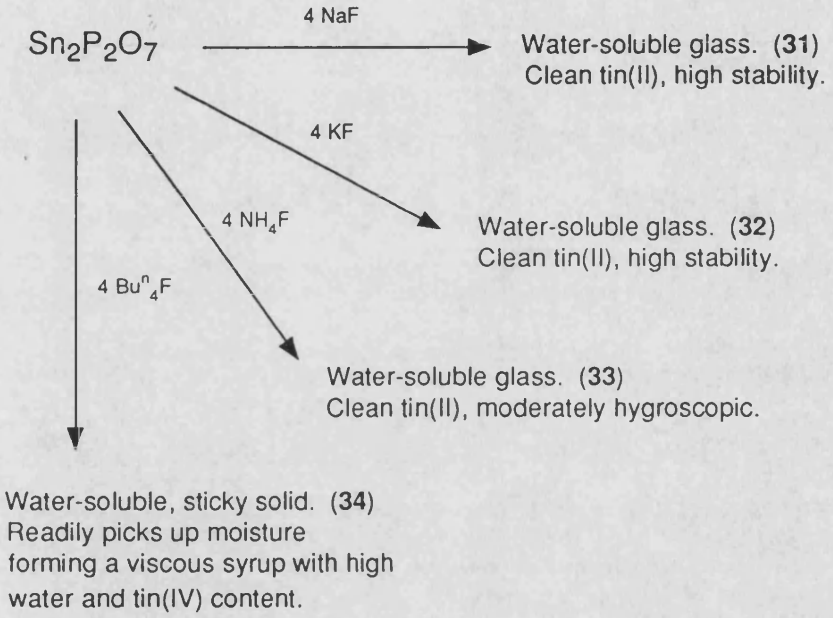

Scheme 2.1

The fact that four molar equivalents of fluoride ions were required to fully, and reproducibly solubilise one mole of $Sn_2P_2O_7$ allows the prediction of three possible reaction routes as described in equation 2.12:-

$$Sn_2P_2O_7 + 4\,MF \xrightarrow[N_2]{H_2O} 2\,SnF_2 + M_4P_2O_7 \quad \text{.....(i)}$$

$$M_2SnP_2O_7 + MSnF_3 + MF \quad \text{.....(ii)} \qquad (2.12)$$

$$M_4[Sn_2F_4(P_2O_7)] \quad \text{.....(iii)}$$

^{119}Sn Mössbauer and the appropriate NMR data for the complete series of

solubilised pyrophosphate compounds is presented in Tables 2.4 and 2.5 respectively. Also included, for comparitive purposes, is the relevant data for $NaSnF_3$ (**35**), SnF_2 (**36**), $Na_4P_2O_7$ and NaF.

For simplicity, the three possible reaction routes are each considered in terms of the interaction of $Sn_2P_2O_7$ with sodium fluoride.The three reaction routes proposed in equation 2.12 will each be considered in turn:-

(i) *Formation of SnF_2 and $Na_4P_2O_7$*: This route, although perhaps the most obvious of the three, can be dismissed quite readily on the grounds of the spectral data quoted above. The Mössbauer parameters for SnF_2 are found to be quite different to those of the solubilised stannous pyrophosphate. Similarly, the ^{119}Sn and ^{19}F NMR values for SnF_2 and the solubilised pyrophosphate are also quite different. The ^{31}P NMR of $Na_4P_2O_7$ is also quite different to the value obtained for the solubilised compound. In conclusion, the spectral data does not appear to support the formation of SnF_2 and $Na_4P_2O_7$ upon reaction of $Sn_2P_2O_7$ with 4 moles of NaF.

(ii) *Formation of $Na_2SnP_2O_7$ and $NaSnF_3$*: This route requires the presence of just three molar equivalents of NaF and not four. However, it might be possible that either an excess of NaF is required for the reaction to occur completely or, alternatively, an [$Na_2SnP_2O_7$.NaF] double-salt might be formed in solution. Such double-salt species have long been known for the alkali-metal orthophosphates [e.g. $2(Na_3PO_4).NaF.19H_2O$] but there are no documented examples for pyrophosphate compounds.[135-137] A further possibility is that the excess NaF might further react with the $NaSnF_3$ to produce the complex fluorotin(II) anion, Na_2SnF_4.

The Mössbauer data does not rule out the possibility that this reaction might occur - the overlap of the two individual spectra of $NaSnF_3$ and $Na_2SnP_2O_7$ would yield a doublet with approximately similar parameters to those of the solubilised pyrophosphate, although one might expect rather broader linewidths if this were so.

Similarly, the ^{119}Sn and ^{31}P NMR data is somewhat inconclusive (the ^{31}P NMR data is effectively identical in both $Na_2SnP_2O_7$ and the solubilised mixture).

Table 2.4 ^{119}Sn Mössbauer data for the series of solubilised tin(II) pyrophosphates.[a]

Compound	δ (mms^{-1})	Δ (mms^{-1})	Γ_1 (mms^{-1})	Γ_2 (mms^{-1})
$Sn_2P_2O_7$ (**27**)	3.27	1.66	1.34	1.31
$Na_2SnP_2O_7$ (**28**)	3.01	1.73	1.21	1.27
$Sn_2P_2O_7$ + 4 NaF (**31**)	3.00	1.81	1.24	1.13
$Sn_2P_2O_7$ + 4 KF (**32**)	3.01	1.84	1.06	1.11
$Sn_2P_2O_7$ + 4 NH_4F (**33**)	3.00	1.83	1.04	1.00
$Sn_2P_2O_7$ + 4 $Bu^n{}_4F$ (**34**)	3.07	1.90	1.21	1.30
$NaSnF_3$ (**35**) [b]	2.96	1.92	1.35	1.44
SnF_2 (**36**) [c]	3.15	1.95	1.36	1.34

Notes:-

[a]Recorded at 78K, referenced to SnO_2.

[b]Prepared by mixing aqueous solutions of SnF_2 and NaF in a 1:1 ratio. The solid $NaSnF_3$ slowly crystallises from solution.

[c]Commercially available sample.

Table 2.5 NMR data for the series of solubilised tin(II) pyrophosphates.

Compound	δ (^{119}Sn) / ppm [a]	δ (^{31}P) / ppm [b]	δ (^{19}F) / ppm [c]	δ (^{1}H) / ppm	δ (^{13}C) / ppm
$Sn_2P_2O_7$ (27) [d]	-683.2, -737.9	-11.6, -14.7	-		
$Na_2SnP_2O_7$ (28)	-644.4	-8.3	-		
$Sn_2P_2O_7$ + 4 NaF (31)	-654.1	-8.3	-99.7		
$Sn_2P_2O_7$ + 4 KF (32)	-655.2	-8.2	-100.1		
$Sn_2P_2O_7$ + 4 NH_4F (33)	-654.2	-8.1	-100.0		
$Sn_2P_2O_7$ + 4 $Bu^n{}_4F$ (34)	-650.9	-8.4	-98.6	0.803 (t) 3H, 1.217 (m) 2H 1.496 (m) 2H, 3.042 (t) 2H	13.91 (C_4), 20.13 (C_3) 24.11 (C_2), 59.06 (C_1)
$NaSnF_3$ (35) [e]	-684.3	-	-89.5		
SnF_2 (36) [f]	-772.6	-	-83.5		
NaF [f]	-	-	-123.2		
$Na_4P_2O_7$ [f]	-	-3.5	-		

Notes:-
[a]Ref to $SnMe_4$: [b]Ref to H_3PO_4: [c]Ref to CF_3CO_2H: All spectra recorded as satutared solutions in D_2O except [d]MAS-NMR data.
[e]Prepared by mixing NaF and SnF_2 in a 1:1 ratio: [f]Commercially available sample.

Consider however the effect on the ^{119}Sn NMR data if a rapid ligand-exchange equilibrium was occurring in solution at room temperature. The time-averaged picture of this situation would be seen as only one tin environment. The resulting spectrum might consist of a single ^{119}Sn peak approximately midway between those of $NaSnF_3$ (-684.3ppm) and $Na_2SnP_2O_7$ (-644.4ppm), i.e. a single peak at -664.4ppm (Fig. 2.4). The actual peak in the solubilised pyrophosphate occurs at -654.1ppm, i.e. a difference of just 10ppm in 650ppm. Unfortunately, it is not possible to perform the NMR experiment at reduced temperature in order to further resolve the individual peaks as the solvent is deuterium oxide. The 'solubilised' pyrophosphate is not sufficiently soluble in organic solvents to perform low-temperature NMR experiments.

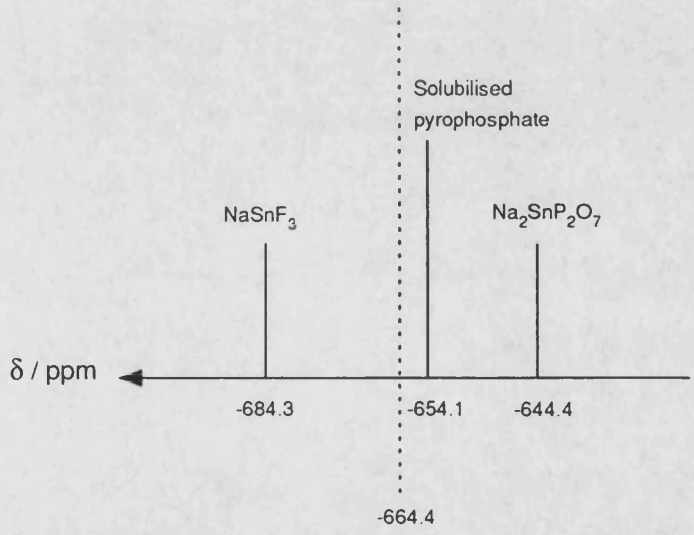

Fig. 2.4 The ^{119}Sn NMR of $NaSnF_3$, $Na_2SnP_2O_7$ and solubilised pyrophosphate.

The ^{19}F NMR data for $NaSnF_3$ and the solubilised pyrophosphate are quite different. In the event that this reaction does occur, one would expect the spectra for these two samples to be effectively identical; unfortunately this is not so. If an excess of NaF is required, this is not visible in the ^{19}F NMR as a free fluoride ion. Similarly, if a pyrophosphate double-salt is present, containing one mole of NaF, the free F^-

cannot be detected by NMR. In conclusion, the ^{19}F NMR data suggests that the reaction between $Sn_2P_2O_7$ and 4 moles of NaF does not result in the formation of $NaSnF_3$ and $Na_2SnP_2O_7$.

(iii) *Formation of $Na_4[Sn_2F_4(P_2O_7)]$*: It is well known that tin is a fluorophilic element, i.e. the Sn-F bond is quite strong and highly favoured. For this reason, it is suggested that the addition of four moles of fluoride to $Sn_2P_2O_7$ produces an ionic tin(II) fluoride-phosphate (**31**) with two F^- ions strongly bound to each tin atom. Such an arrangement is likely to produce a highly water-soluble material. This would arise due to the replacement of [P-O-Sn] cross-linking with Sn-F bonding. The net result would be a breakdown of the polymeric structure of $Sn_2P_2O_7$ which accounts for its intractable nature.

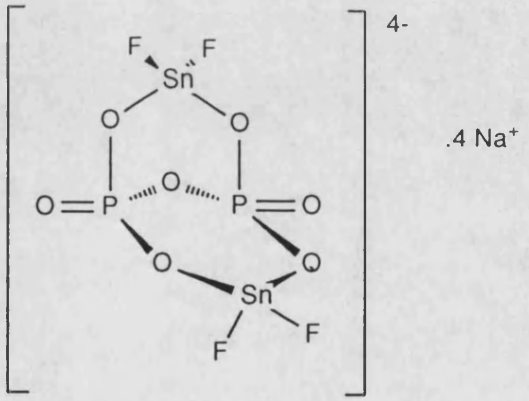

(31)

The example shown is one of the simplest of the many possible variations of this structure. The formation of such a complex is consistent with all of the spectral data, i.e. infrared, Mössbauer and NMR. The observed reduction in the isomer-shift ($0.27 mms^{-1}$) is most likely due to the replacement of O atoms with more electronegative F atoms around the tin. This would cause the withdrawal of more $5s^2$ electron density. Similarly, the increased electric-field asymmetry due to the highly electronegative fluoride ions accounts for the increased quadrupole-splitting

($0.15 mms^{-1}$) in the Mössbauer spectrum of the solubilised pyrophosphate. The single ^{119}Sn NMR peak shows the presence of a single tin environment in the compound when in solution. Assuming the tin coordination is greatly simplified in the solid-state explains the relatively narrow linewidths in the Mössbauer spectrum. The increased electronegativity of the atoms coordinating around the tin is the most likely cause of the substantial downfield chemical shift in the ^{119}Sn NMR.

The infrared data is consistent with the presence of a phosphate group which still has a partial P=O character ($890\text{-}1171 cm^{-1}$). This implies that not all P-O's are equally bound to the tin as in $Sn_2P_2O_7$. Both Sn-O ($438 cm^{-1}$) and Sn-F (468, $500 cm^{-1}$) bonds can also be identified in the spectrum of the sodium fluoride solubilised compound.

The ^{31}P NMR data implies that the phosphorus environment is similar to that in $Na_2SnP_2O_7$ which, as drawn, would appear to be the case. The single ^{19}F NMR peak is consistent with the formation of an Sn-F bonded species (*cf.* SnF_2, $NaSnF_3$) with only one fluorine environment present in the compound when in solution.

Tin EXAFS data has also been obtained for the solubilised form of $Sn_2P_2O_7$. Unfortunately, due to the physical nature of the glassy solid, the data is not of a high quality and rapidly deteriorates at values of $k > 6$ (Appendix 1). However, the data is presented in Table 2.6 and is of sufficient quality for the determination of the first and second coordination shells.

Table 2.6 The EXAFS data for tin(II) pyrophosphate solubilised with 4 NaF.

Compound	Number of atoms	Atom type	Bond length / Å	Error/Å	R value
$Sn_2P_2O_7$ + 4 NaF (**31**)	5.23	F	2.08	0.02	21.32
	1.81	O	2.31	0.02	

The EXAFS data clearly shows the presence of a first coordination shell consisting of Sn-F bonds of average length 2.08Å. A second coordination shell can also be observed which consists of Sn-O bonds of average length 2.31Å. Comparison of this data with the values of Sn-F bonds in the literature for tin(II) fluoride species (Table 1.5) shows typical bond lengths of 1.89 - 2.49Å. Typical Sn-O bond lengths in tin(II) phosphate compounds range from 2.06 - 2.47Å (Table 1.7). These typical bond lengths clearly indicate that it would be expected to find a first coordination sphere that contained Sn-F bonds as opposed to Sn-O bonds.

The first shell coordination number of 5 is the same as that found in β-SnF_2 (Section 1.8.1) in which the tin is found in an SnF_5E distorted octahedral coordination. The documented Mössbauer parameters (δ, 3.30mms^{-1}; Δ, 2.20mms^{-1}) for this compound are significantly different from those of the solubilised pyrophosphate (δ, 3.00mms^{-1}; Δ, 1.81mms^{-1}) which must indicate the presence of substantially dissimilar tin environments. A possible explanation is the inaccuracy of the Sn-F coordination number in the EXAFS data. Mössbauer data for the tin(II) oxyfluoride, Sn_2OF_2 (δ, 3.10mms^{-1}; Δ, 3.23mms^{-1}) (Table 1.4), shows closer agreement for the value of δ although Δ is much too high.

The presence of the two oxygen atoms in the second coordination shell supports the formation of a tin(II) fluoride-phosphate species as proposed. Unfortunately, the data is not of sufficient quality to resolve an Sn-P separation in this material. One explanation is the formation of a more symmetrical environment than those found in Sn_2OF_2 (Section 1.8.1) which has fluoride ions bridging two tin atoms. Multiple [Sn-F-Sn] bridging is known to be a predominant feature of the structural chemistry of tin(II) fluorides and complex fluoro-anions (Section 1.8.1). A proposed structure for the solubilised tin(II) pyrophosphate in the solid-state is shown in Fig. 2.5. This has two central tin atoms, each bridged by four F atoms in the inner coordination shell with each tin further coordinated by a pair of O atoms from a $P(O)O_2$ group.

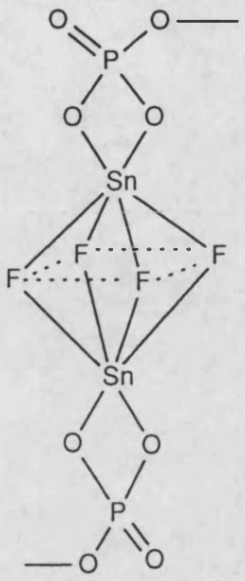

Fig. 2.5 A proposed structure for the solubilised tin(II) pyrophosphate.

The EXAFS fourier transform curves for this compound are illustrated in Fig. 2.5.

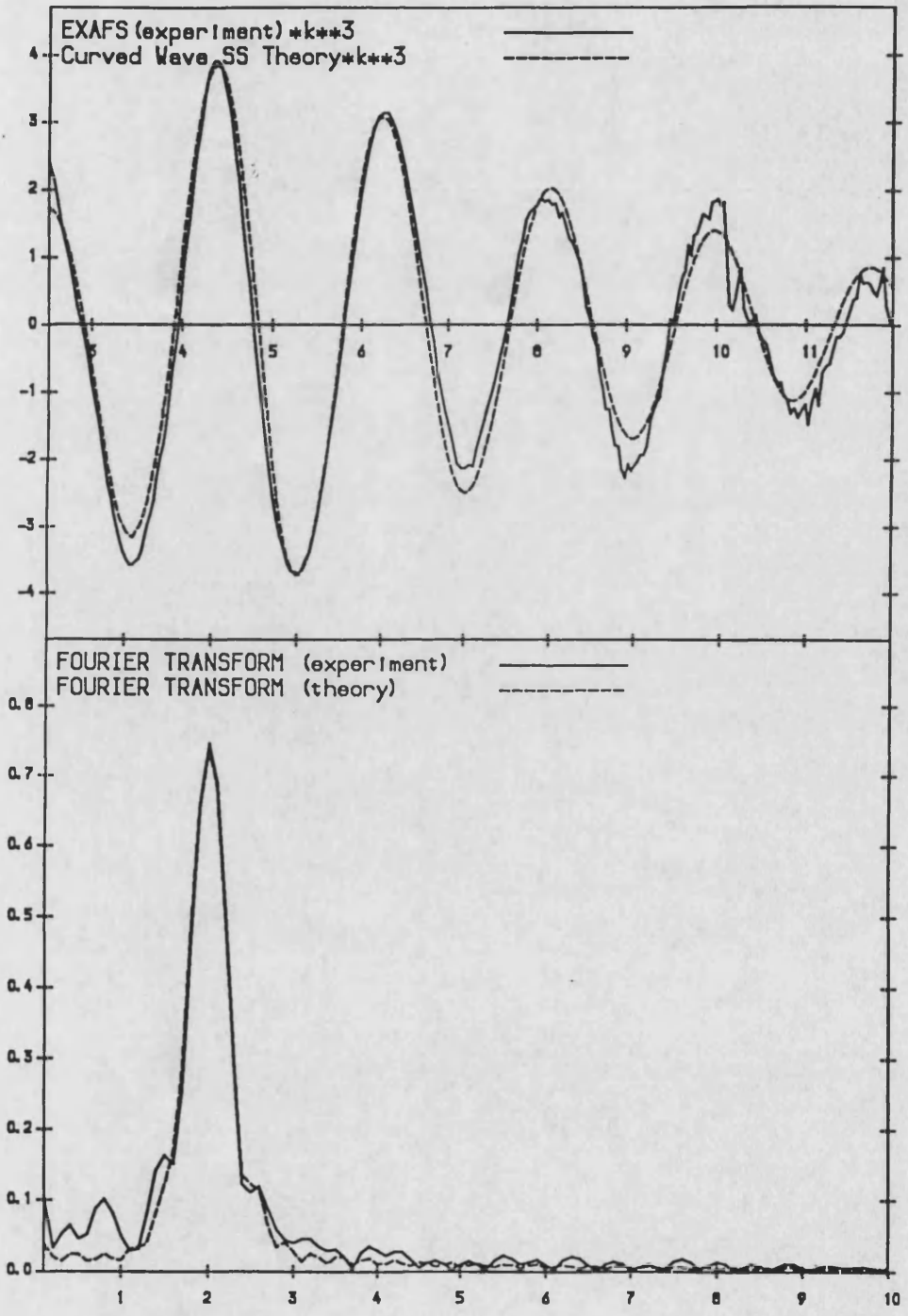

Fig. 2.5 The EXAFS fourier transform curves for $Sn_2P_2O_7$ + 4 NaF.

Conductivity measurements: Conductivity measurements of an aqueous solution of solubilised $Sn_2P_2O_7$ have also been carried out using a pre-calibrated conductivity bridge. In order to compare different solutions, the molar conductivity, Λ_M, must first be determined where:-

$$\Lambda_M = (C \times \text{conductivity}) / \text{molarity}$$

and C is the cell constant.

Measurement of the conductivity of a compound in solution can not only show qualitatively the presence or absence of ions, but will also indicate the number of ions produced by one mole of that compound by comparison with known electrolytes.

For the purposes of this experiment, the conductivity of the solubilised tin(II) pyrophosphate was compared with the conductivities of 1.0 mMolar aqueous solutions of a series of Pt(IV) complexes as shown in Table 2.7.[138]

The conductivity of a 1.0 mMolar solution of the solubilised pyrophosphate appears to contain 4 - 5 moles of ions per mole of compound. This observation is consistent with the prediction that the formation of a complex tin(II) fluoride-phosphate, as described above, is the most likely explanation of the solubilisation of $Sn_2P_2O_7$ with fluoride ions. For the purposes of comparison, the conductivity results obtained for the solubilised pyrophosphate with the remaining fluoride sources (**32-34**) were remarkably similar.

Overall, there is a remarkable consistency in the Mössbauer, NMR, infrared and conductivity data for this simple series of ionic fluoride-solubilised pyrophosphates. This leads to the conclusion that the fate of the tin(II) pyrophosphate is the same regardless of the cation type used in these fluoride-solubilisation experiments. Consequently, the water-soluble stannous species detected in dentifrice formulations containing both insoluble $Sn_2P_2O_7$ and an ionic fluoride source (e.g. NaF, NaMFP) would appear to be complex tin(II) fluoride-phosphates of the type described above. However, in a commercially formulated toothpaste product many complex excipient interactions would be in competition (Section 1.5). Consequently,

Table 2.7 Conductivity measurements for solubilised tin(II) pyrophosphate.

Compound	Λ_M (Sm^2Kmol^{-1})	Number of ions	Formula
$PtCl_4.6NH_3$	52.3	5	$[Pt(NH_3)_6]^{4+} + 4Cl^-$
$PtCl_4.5NH_3$	40.4	4	$[Pt(NH_3)_5Cl]^{3+} + 3Cl^-$
$PtCl_4.4NH_3$	29.9	3	$[Pt(NH_3)_4Cl_2]^{2+} + 2Cl^-$
$PtCl_4.3NH_3$	9.7	2	$[Pt(NH_3)_3Cl_3]^{+} + Cl^-$
$PtCl_4.2NH_3$	0.0	0	$Pt(NH_3)_2Cl_4$
$Sn_2P_2O_7$ + 4 NaF. **(31)**	46.0	5	$[Sn_2F_4(P_2O_7)]^{4-} + 4\ Na^+$
$Sn_2P_2O_7$ + 4 KF. **(32)**	44.8	5	$[Sn_2F_4(P_2O_7)]^{4-} + 4\ K^+$
$Sn_2P_2O_7$ + 4 NH_4F. **(33)**	47.1	5	$[Sn_2F_4(P_2O_7)]^{4-} + 4\ NH_4^+$
$Sn_2P_2O_7$ + 4 Bu_4^nNF. **(34)**	48.2	5	$[Sn_2F_4(P_2O_7)]^{4-}$ + 4 $Bu_4^nNF^+$

the above predictions for the reaction between $Sn_2P_2O_7$ and ionic fluorides can only serve as a simple model of the real situation.

3. TIN(II) SALTS OF SIMPLE SUGAR PHOSPHATES AND RELATED COMPOUNDS.

The preparation and characterisation of a range of simple tin(II) phosphates and polyphosphates has been fully described in the preceeding pages of Chapter 2. The chelation of polyhydroxyl compounds, such as carbohydrates, to tin(II) species has also been mentioned previously (Section 1.8.4). These interactions clearly promote the stability of stannous compounds to oxidation. Such chelating interactions are of great importance in further understanding the fate of stannous species in a formulated dentifrice as these products typically contain 40% sorbitol as a humectant (Section 1.5). Consequently, the preparation of simple tin(II) phosphate compounds might usefully be further extended to include tin(II) phosphate salts of polyolphosphoric acid species such as the sugar phosphates, themselves important molecules in biological processes and mechanisms.

It would be anticipated that under these circumstances the combination of strong [Sn-O-P] bonding to the phosphate group, coupled with chelation from the adjacent polyhydroxyl carbohydrate function would facilitate the preparation of highly air-stable, orally-viable tin(II) species. However, the presence of the phosphate group might not be essential, and for this reason a series of simple tin(II) salts of sugar carboxylates might also show improved stability over simple tin(II) carboxylates. Similarly, the interaction of simple stannous species (e.g. tin(II) halides) with simple sugars might yield a series of highly stable, chelated tin(II) compounds.

In this chapter, the preparation of a range of simple tin(II) sugar phosphates is described. Furthermore, the subsequent interaction of a sparingly soluble tin(II) sugar phosphate with fluoride ions in aqueous solution is also studied in some detail (*cf.* $Sn_2P_2O_7$ in Chapter 2). These compounds are characterised in terms of analytical and spectral data, supplemented with tin EXAFS studies (refer to Appendix 1 for a

discussion of this technique).

Following this discussion, the preparation and characterisation of a range of tin(II) salts of orally-viable sugar carboxylates is described (e.g. D-gluconic acid). Finally, the interaction of tin(II) halides (e.g. SnF_2) with simple, non-functionalised sugars (e.g. α-D-glucose) in aqueous solution is examined and the synthesis of a series of 1:1 tin(II)-sugar compounds from soluble tin(II) alkoxides was attempted.

3.1 Experimental.

Unless indicated otherwise, the preparative and analytical methods follow the same form as described for the inorganic phosphates in the introductory section to Chapter 2, e.g. precautions to prevent oxidation. For all compounds, infrared spectra are recorded as a nujol mull on KBr plates and stannous analyses are determined iodometrically according to equation 2.1. ^{119}Sn Mössbauer and multinuclear NMR data are tabulated in the relevant discussions which follow. Unless described otherwise, all NMR data was recorded on a saturated solution in D_2O at ambient temperature.

3.1.1 *Synthesis of mono-stannous α-D-glucose-1-phosphate monohydrate*, $(C_6H_7O(OH)_4)OP(O)O_2Sn.\ H_2O$ (37).

Di-sodium α-D-glucose-1-phosphate tetrahydrate (2.50g, 8.0mmol) was dissolved in 25ml of thoroughly de-oxygenated water. To this clear solution was carefully added $SnCl_2$ (1.52g, 8.0mmol) with rapid stirring whilst constantly purging with nitrogen. After approximately 10 minutes, a fine, flock-like white precipitate began to form. After stirring for a further 10 minutes, the product was rapidly filtered on a Schlenk-stick, washed with successive aliquots of water, ethanol and ether and thoroughly dried *in vacuo*. Yield: 2.78g (92%). Analysis, found (calc. for

$C_6H_{13}O_{10}PSn$): C, 18.2 (18.2); H, 3.21 (3.29); Sn(II), 32.1 (32.6)%. Selected infrared data: 3401cm^{-1} (*st, br*) υ(H-O-H); 1603cm^{-1} (*st, sh*) δ(H-O-H); 1339cm^{-1} (*m, sh*) υ(P=O); 880-1150cm^{-1} (*st*) υ(P-O); 548cm^{-1} (*st, sh*) δ(O-P-O); 475cm^{-1} (*m, br*) υ(Sn-O). ^{1}H NMR data: 3.34 (*dd,* 1H, J_{aa}=9.7Hz, J_{aa}=9.7Hz) H_3; 3.43 (*dd,* 1H, J_{aa}=9.7Hz, J_{aa}=7.4Hz) H_4; 3.67 (*d,* 2H, *J*=7.4Hz) H_6; 3.80 (*m,* 1H) H_5; 3.85 (*dd,* 1H, J_{aa}=9.1Hz, J_{ea}=3.1Hz) H_2; 5.39ppm (*dd,* 1H, J_{aa}=9.1Hz, J_{ea}=3.1Hz) H_1. ^{13}C NMR data: 64.1 (C_6), 73.1, 74.2, 75.4, 76.2 (C_2-C_5), 97.8ppm (C_1).

3.1.2 *Synthesis of mono-stannous α-D-glucose-6-phosphate trihydrate,* $(C_6H_7O(OH)_4)OP(O)O_2Sn.\ 3H_2O$ (38).

Di-sodium α-D-glucose-6-phosphate hydrate (1.00g, 3.3mmol) was dissolved in the minimum amount of de-oxygenated water (10ml). To this solution, solid $SnCl_2$ (0.62g, 3.3mmol) was added with stirring. After stirring for 30 minutes at room temperature, no precipitate had formed. 20ml of de-oxygenated methanol were added dropwise to this solution yielding a fine, flock-like white precipitate. The solid was rapidly filtered on a Schlenk-stick, washed successively with water, ethanol and ether and thoroughly dried *in vacuo*. Yield: 0.97g (79%). Analysis, found (calc. for $C_6H_{17}O_{12}PSn$): C, 16.9 (16.7); H, 3.28 (3.94); Sn(II), 28.0 (27.6)%. Selected infrared data: 3290cm^{-1} (*st, br*) υ(H-O-H); 1635cm^{-1} (*m, sh*) δ(H-O-H); 1310cm^{-1} (*w, br*) υ(P=O); 870-1100cm^{-1} (*st*) υ(P-O); 500-560cm^{-1} (*m*) δ(O-P-O); 428cm^{-1} (*w, sh*) υ(Sn-O). ^{1}H NMR data: 3.26 (*dd,* 1H, J_{aa}=9.7Hz, J_{aa}=7.9Hz) H_4; 3.39 (*dd,* 1H, J_{aa}=9.7Hz, J_{aa}=9.8Hz) H_3; 3.68 (*dd,* 1H, J_{aa}=9.8Hz, J_{ea}=3.2Hz) H_2; 3.94 (*m,* 1H) H_5; 4.16 (*d,* 2H, *J*=7.9Hz) H_6, 5.21ppm (*d,* 1H, *J*=3.2Hz) H_1. ^{13}C NMR data: 67.5 (*d,* $^2J_{(P\text{-}C)}$=6.7Hz) (C_6), 71.3, 71.9, 72.1, 75.1 (C_2-C_5), 93.2ppm (C_1).

3.1.3 *Synthesis of anhydrous mono-stannous β-D-glucose-6-phosphate,* $(C_6H_7O(OH)_4)OP(O)O_2Sn$ (**39**).

Mono-potassium β-D-glucose-6-phosphate hydrate (1.00g, 3.6mmol) was dissolved in the minimum amount of de-oxygenated water (7.5ml). To this solution, solid $SnCl_2$ (0.68g, 3.6mmol) was added with stirring. After stirring for 30 minutes at room temperature, no precipitate had formed so 15-20ml of de-oxygenated methanol were added dropwise to this solution, rapidly yielding a fine, flock-like white precipitate. The solid was filtered on a Schlenk-stick, washed successively with water, ethanol and ether and thoroughly dried *in vacuo* with warming to 60°C. Yield: 1.04g (77%). Analysis, found (calc. for $C_6H_{11}O_9PSn$): C, 19.1 (19.1); H, 3.85 (3.00); Sn(II), 30.8 (31.5)%. Selected infrared data: 3187cm^{-1} (*w, br*) υ(O-H); 1648cm^{-1} (*w, sh*) υ(O-H); 1305cm^{-1} (*w, br*) υ(P=O); 870-1150cm^{-1} (*st*) υ(P-O); 570cm^{-1} (*m, br*) δ(O-P-O); 458cm^{-1} (*w, br*) υ(Sn-O). ^1H NMR data: 3.24 (*dd*, 1H, J_{aa}=9.6Hz, J_{aa}=7.3Hz) H_4; 3.35 (*dd*, 1H, J_{aa}=9.6Hz, J_{aa}=9.6Hz) H_3; 3.68 (*dd*, 1H, J_{aa}=9.6Hz, J_{aa}=8.6Hz) H_2; 3.90 (*m*, 1H) H_5; 4.18 (*m*, 2H) H_6; 4.65ppm (*d*, 1H, *J*=8.6Hz) H_1. ^{13}C NMR data: 70.0 (C_6), 71.0, 72.2, 74.2, 75.7 (C_2-C_5), 95.6ppm (C_1).

3.1.4 *Synthesis of mono-stannous glycerol-2-phosphate monohydrate,* $(HOCH_2)_2C(H)OP(O)O_2Sn.\ H_2O$ (**40**).

Di-sodium glycerol-2-phosphate (1.00g, 4.6mmol) was dissolved in 25ml of thoroughly de-oxygenated water. Solid $SnCl_2$ (0.88g, 4.6mmol) was added with continuous stirring at room temperature. After several minutes, a fine, white precipitate began to form. The mixture was allowed to stir for 30 minutes and the product was filtered on a Schlenk-stick. The solid-cake was washed with successive aliquots of water, ethanol and ether and dried *in vacuo* with warming to 60-70°C. Yield: 1.28g (96%). Analysis, found (calc. for $C_3H_9O_7PSn$): C, 11.3 (11.7); H, 2.89 (2.90); Sn(II), 40.6 (38.7)%. Selected infrared data: 3250cm^{-1} (*st, br*) υ(H-O-H);

1653cm^{-1} (*st, sh*) δ(H-O-H); 1308cm^{-1} (*m, sh*) υ(P=O); 880-1200cm^{-1} (*st*) υ(P-O); 540-600cm^{-1} (*st*) δ(O-P-O); 465cm^{-1} (*m*) υ(Sn-O). ^{1}H NMR data: 3.72 (*d*, 4H, *J*=7.8Hz) $H_{1,3}$; 4.28ppm (*quint.*, 1H, *J*=7.8Hz) H_2. ^{13}C NMR data: 58.6 [$CH(OPO_3Sn)(CH_2OH)_2$], 84.2ppm [($CH(OPO_3Sn)$].

3.1.5 *Synthesis of hydrated barium D-6-phosphogluconate,* [$BaO_2P(O)CH_2$-$CH(OH)CH(OH)CH(OH)CH(OH)CO_2]_2Ba.\ xH_2O$ (**41**).[139]

Commercially available hydrated barium α-D-glucose-6-phosphate (5.00g, 12.7mmol) was dissolved in 40ml of water with gentle warming. To this turbid solution were added solid $BaCO_3$ (5.90g, 30.0mmol) and 0.75ml of analar-grade Br_2. The mixture was kept at room temperature for 2 hours with frequent shaking after which time the orange colouration had largely disappeared. Excess bromine was removed by aeration, and excess barium carbonate removed by filtration on a Büchner-funnel. The filtrate and washings were adjusted to pH 3.5 by the careful addition of glacial acetic acid.

After the addition of 240ml of ethanol to the solution, a fine, white precipitate was formed. The suspension was cooled to 0°C in an ice-bath for 30 minutes and refiltered. The filtered solid was washed with 100ml of 80% ethanol and dried thoroughly *in vacuo*. A small additional quantity of product can be recovered by treating the clear filtrate with a saturated solution of $Ba(OH)_2$ until the solution is pink to phenolphthalein.

The dried precipitates were combined and dissolved in 200ml of water with the aid of 1.0ml of glacial acetic acid. Saturated $Ba(OH)_2$ was added to a permanent pink end-point with phenophthalein and the product precipitated with 100ml of ethanol. The product was collected on a Büchner-funnel, washed with successive aliqouts of ethanol and ether and dried *in vacuo* with gentle warming to 60°C. The product was quite insoluble and because of this, NMR data was not available. Yield:

6.40g (45%). Analysis, found (calc. for $C_{12}H_{40}Ba_3O_{30}P_2$): C, 10.9 (12.6); H, 2.97 (3.34)%, i.e. x=10 (decahydrate). Selected infrared data: 3409cm^{-1} (*st, br*) υ(H-O-H); 1657cm^{-1} (*st, sh*) δ(H-O-H); 1588cm^{-1} (*m, br*) $\upsilon_{as}(CO_2Ba)$; 1304cm^{-1} (*w, sh*) υ(P=O); 970-1100cm^{-1} (*st*) υ(P-O); 500-565cm^{-1} (*st*) δ(O-P-O); 435cm^{-1} (*m, br*) υ(Ba-O).

3.1.6 *Synthesis of di-stannous mono-barium D-6-phosphogluconate hydrate,* $[SnO_2P(O)OCH_2CH(OH)CH(OH)CH(OH)CH(OH)CO_2]_2Ba.\ xH_2O$ (**42**).

The title compound was prepared from the hydrated barium salt of D-6-phosphogluconate (**41**). This was prepared from the barium salt of α-D-glucose-6-phosphate according to a literature preparation.[139]

Barium D-6-phosphogluconate decahydrate (0.50g, 4.45mmol) was dissolved in 20ml of thoroughly de-oxygenated 80% ethanol/water. Solid $SnCl_2$ (1.70g, 8.9mmol) was added with stirring and the mixture stirred overnight at room temperature. This yielded a flock-like white precipitate which was filtered on a Schlenk-stick, successively washed with water, ethanol and ether and dried *in vacuo* with warming to 70°C. The product was noted to be insoluble in all common solvents. Qualitative tests for barium (e.g. dil. H_2SO_4) proved positive for the presence of barium. The final product was insufficiently soluble to obtain NMR data. Yield: 0.54g (74%). Analysis, found (calc. for $C_{12}H_{40}BaO_{30}P_2Sn_2$): C, 12.5 (13.1); H, 2.65 (3.64); Sn(II), 19.8 (21.6)% (assuming x=10H_2O, i.e. decahydrate). Selected infrared data: 3000-3400cm^{-1} (*st, br*) υ(H-O-H); 1660cm^{-1} (*m, sh*) δ(H-O-H); 1605cm^{-1} (*w, br*) $\upsilon_{as}(CO_2Ba)$; 1250cm^{-1} (*w, sh*) υ(P=O); 920-1100cm^{-1} (*st*) υ(P-O); 510cm^{-1} (*m, br*) δ(O-P-O); 470cm^{-1} (*w, br*) υ(Sn-O).

3.1.7 *Synthesis of mono-stannous D-6-phosphogluconato chlorostannate(II) heptahydrate,* $[SnO_2P(O)OCH_2CH(OH)CH(OH)CH(OH)CH(OH)CO_2]SnCl.\ 7H_2O$ **(43).**

The title compound was prepared from tris-ammonium D-6-phosphogluconate which was prepared from the decahydrated barium salt (**41**) *in situ.*

Barium D-6-phosphogluconate decahydrate (300.0mg, 0.26mmol) was suspended in 25ml of water with stirring. Ammonium sulphate, $(NH_4)_2SO_4$ (105.0mg, 0.79mmol) was added to this suspension and the mixture stirred at room temperature overnight. The suspension was filtered on a Büchner-funnel fitted with a Whatman 42-grade filter-paper to remove barium sulphate produced in the reaction. The clear solution was evaporated to dryness on a rotary-evaporator.

The evaporated solid, assumed to be ammonium D-6-phosphogluconate, was redissolved in 20ml of 50% water/ethanol. An excess of solid $SnCl_2$ (0.16g, 0.84mmol) was added to the solution which instantly yielded a fine, white precipitate. The suspension was stirred for a further 30 minutes and the solid filtered on a Schlenk-stick, washed with ethanol and ether and dried *in vacuo* with warming to 60°C. The product was too insoluble to obtain solution NMR data. Yield: 0.20g, (71%). Analysis, found (calc. for $C_6H_{24}ClO_{17}PSn_2$): C, 10.3 (10.7); H, 3.21 (3.57); Sn(II), 33.2 (35.3)%. Selected infrared data: 3379cm^{-1} (*st, br*) υ(H-O-H); 1622cm^{-1} (*st, sh*) δ(H-O-H); 1572cm^{-1} (*st, sh*) $\upsilon_{as}(CO_2Sn)$; 1305cm^{-1} (*w, br*) υ(P=O); 900-1100cm^{-1} (*st*) υ(P-O); 507-582cm^{-1} (*st*) δ(O-P-O); 455cm^{-1} (*w, br*) υ(Sn-O). N.B. υ(Sn-Cl) bands are not visible when using KBr plates (approx. 350cm^{-1}).

3.1.8 *Interaction of mono-stannous* α*-D-glucose-1-phosphate monohydrate with sodium fluoride in solution* (**44**).

In a typical experiment, using sodium fluoride as the ionic fluoride source,

Sn(II) α-D-G1P (**37**) (1.00g, 2.6mmol) was suspended in 25ml of cold, thoroughly de-oxygenated water. Solid NaF (0.22g, 5.2mmol) was added to this suspension and the mixture stirred at room temperature for 10 minutes under an inert atmosphere. The slurry rapidly dispersed, yielding a clear solution. The solvent volume was reduced by half on a rotary-evaporator and 5ml of de-oxygenated ethanol added to initiate precipitation of the product. The fine, white water-soluble solid was collected on a Schlenk-stick and dried *in vacuo*. Yield: 1.16g (95%). Analysis, found (calc. for $C_6H_{13}F_2Na_2O_{10}PSn$): C, 14.8 (15.1); H, 3.14 (2.72); Sn(II), 23.8 (24.8)%. Selected infrared data: 3300cm^{-1} (*st, br*) υ(H-O-H); 1651cm^{-1} (*m, br*) δ(H-O-H); 1262cm^{-1} (*w, sh*) υ(P=O); 936-1150cm^{-1} (*st*) υ(P-O); 530-563cm^{-1} (*st*) δ(O-P-O); 495cm^{-1} (*m, br*) υ(Sn-F); 441cm^{-1} (*m, br*) υ(Sn-O). ^{1}H NMR data: 3.34 (*dd*, 1H, J_{aa}=9.7Hz, J_{aa}=9.1Hz) H_3; 3.44 (*dd*, 1H, J_{aa}=9.7Hz, J_{aa}=7.3Hz) H_4; 3.67 (*d*, 2H, J=7.4Hz) H_6; 3.80ppm (*m*, 1H) H_5; 3.86 (*dd*, 1H, J_{aa}=9.1Hz, J_{ea}=3.0Hz) H_2; 5.50ppm (*dd*, 1H, J_{ea}=3.0Hz) H_1. ^{13}C NMR data: 63.1 (C_6), 72.1, 73.3, 75.2, 74.8 (C_2-C_5), 98.8ppm (C_1).

3.1.9 *Synthesis of anhydrous stannous bis-D-gluconate,* $[HOCH_2CH(OH)$-$CH(OH)CH(OH)CH(OH)CO_2]_2Sn$ (**45a**).

Sodium D-gluconate (11.50g, 52.7mmol) was dissolved in the minimum quantity of thoroughly de-oxygenated 90% ethanol. $SnCl_2$ (5.00g, 26.4mmol) was added and the mixture stirred at room temperature for 30 minutes. After this time, a small quantity of a fine, white precipitate of NaCl had formed. The suspension was filtered on a Schlenk-stick and the clear filtrate evaporated to dryness *in vacuo* yielding a highly water-soluble white powder. The solid was placed in a Soxhlet thimble and continuously extracted with refluxing 90% ethanol under nitrogen for at least 36 hours in order to remove traces of NaCl from the product. However, the analytical data reveals that the final product probably still contained traces of NaCl

after prolonged soxhlet purification. Yield: 10.9g, (81%). Analysis, found (calc. for $C_{12}H_{22}O_{14}Sn$): C, 25.3 (28.3); H, 3.81 (4.32); Sn(II), 21.1 (23.3)%.

3.1.10 *Alternative synthesis of stannous bis-D-gluconate from trimethylsilyl-D-gluconate* (**45b**).

Trimethylsilyl-D-gluconate was found to be a highly moisture-sensitive oil and was difficult to isolate successfully. For this reason, this material was prepared *in situ* immediately prior to reaction with tin(II) chloride.

Sodium D-gluconate (5.00g, 25.6mmol) was suspended in 75ml of freshly distilled tetrahydrofuran with rapid stirring. Trimethysilyl chloride (2.49g, 25.6mmol) was dissolved in 100ml of distilled tetrahydrofuran and added dropwise to the suspension. The mixture was stirred at room temperature for 6 hours under nitrogen. After this time, a fine, white precipitate of NaCl was observed which was removed by filtration. The solvent volume was reduced by 50% *in vacuo* and the remaining solvent thoroughly de-oxygenated. Solid $SnCl_2$ (2.43g, 12.8mmol) was added to the clear solution and allowed to stir at room temperature for 3 hours. The clear solution was evaporated to dryness *in vacuo* to remove tetrahydrofuran and trimethylsilyl chloride produced as a by-product of the reaction. The product was a fine, white powder. Yield: 5.9g (91%). Analysis, found (calc. for $C_{12}H_{22}O_{14}Sn$): C, 27.9 (28.3); H, 4.50 (4.32); Sn(II), 22.9 (23.3)%. Selected infrared data: 3150, 3308, 3427, 3541cm^{-1} (*st, sh*) υ(O-H); 1599cm^{-1} (*st, br*) $\upsilon_{as}(CO_2Sn)$; 453cm^{-1} (*m, sh*) υ(Sn-O). ^1H NMR data: 3.67 (*d*, 2H, *J*=8.1Hz) H_6; 3.74 (*m*, 2H) $H_{4,5}$; 3.95 (*dd*, 1H, *J*=9.3Hz, *J*=7.3Hz) H_3; 4.30 (*d*, 1H, *J*=7.3Hz) H_2. ^{13}C NMR data: 62.6 (C_6), 70.2 (C_5), 71.5 (C_4), 72.1 (C_3), 72.5 (C_2), 193.0ppm (CO_2Sn).

3.1.11 *Synthesis of stannous bis-D-glucuronate tetrahydrate,* $[(C_5H_9O_5)CO_2]_2Sn.4H_2O$ **(48).**

Sodium D-glucuronate (5.00g, 23.1mmol) was suspended in 100ml of 80% ethanol and the mixture was thoroughly de-oxygenated. Solid $SnCl_2$ (2.20g, 11.6mmol) was added to this suspension and the mixture stirred at room temperature for 24 hours. A dense, white precipitate was produced which was filtered on a Schlenk-stick, washed with water, ethanol and ether and thoroughly dried *in vacuo.* The product was an off-white powder with limited solubility in common solvents. For this reason, no NMR data was available. Yield: 5.8g (87%). Analysis, found (calc. for $C_{12}H_{26}O_{18}Sn$): C, 24.8 (24.9); H, 3.97 (4.51); Sn(II), 18.1 (20.6)%. Selected infrared data: 3100, 3333, 3462, 3601cm^{-1} (*st, sh*) υ(O-H); 3300cm^{-1} (*st, br*) υ(H-O-H); 1595cm^{-1} (*st, br*) $\upsilon_{as}(CO_2Sn)$; 451cm^{-1} (*m, br*) υ(Sn-O).

3.2 Preparation and Characterisation of Tin(II) Sugar Phosphate salts.

The series of simple tin(II) sugar phosphate compounds described below were all prepared according to the general preparative method described earlier in equation 2.6 for the preparation of simple inorganic tin(II) phosphates. This involves the reaction of tin(II) chloride with the alkali metal salt (e.g. Na^+, K^+) of the corresponding sugar phosphate in aqueous solution.

^{119}Sn Mössbauer and multinuclear NMR data for this series of sugar phosphate compounds is presented in Tables 3.1 and 3.2 respectively. The atom labelling scheme for the glucose phosphates is as shown in the example of the parent compound, α-D-glucose.

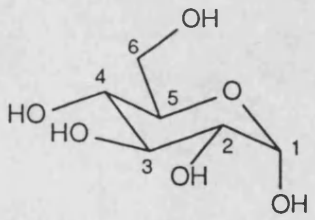

Tin(II) α-D-glucose-1-phosphate monohydrate, Sn(α-G1P) (**37**), was prepared by the reaction of tin(II) chloride with di-sodium α-D-glucose-1-phosphate tetrahydrate in water, according to equation 3.1:-

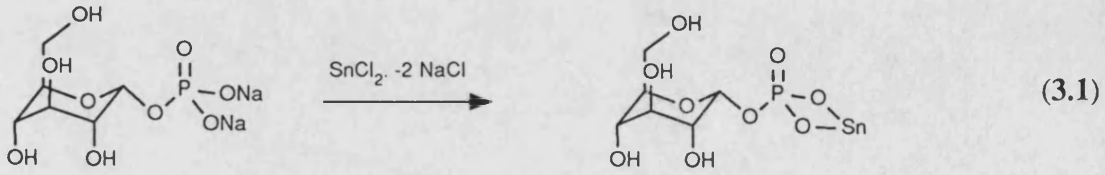

(**3.1**)

(**37**)

The product readily precipitates from an aqueous reaction mixture as a monohydrate and is only sparingly soluble in water at room temperature.

Characteristic broad water stretching bands in the infrared spectrum (3401, 1603cm^{-1}) confirm that the solid is hydrated. Attempted recrystallisation of this compound from suitably polar solvents (e.g. THF, MeOH, EtOH) yielded fine, flock-like precipitates. Slow evaporation of an aqueous solution yielded a colourless, viscous syrup. This observation is symptomatic of sugar species when in solution which have a strong tendancy to form syrups (e.g. honey, molasses). Attempted determination of a melting point for this compound was unsuccessful, decomposition to a brown solid occurring at around 115°C. This is most likely due to caramelisation of the sugar function. The physical properties of this solid suggest that it is polymeric and not monomeric as illustrated.

The tin(II) salts of two anomeric isomers of glucose phosphate, i.e. tin(II) α-D-glucose-6-phosphate trihydrate, Sn(αG6P) (**38**), and tin(II) β-D-glucose-6-phosphate, Sn(βG6P) (**39**), were prepared by the reaction of $SnCl_2$ with the corresponding sugar phosphate as shown in equation 3.2:-

The products of both of these reactions are readily water-soluble white solids which can be precipitated from aqueous solution with the addition of a little alcohol (e.g. MeOH, EtOH). The analytical and infrared data (3290, 1635cm^{-1}) suggests that the α-isomer precipitates as a trihydrate whereas the β-isomer precipitates from solution as the anhydrous salt. No strong, broad water peaks are observed in the infrared spectrum of the β-anomer. Attempted recrystallisation of this material yielded similarly unsuccessful results to those with Sn(αG1P), i.e. flock-like solids or hydrated syrups. The high water-solubility of these compounds suggests that intermolecular attractions are relatively weak. However, the tin atoms will not exhibit the simple two-coordinate bonding illustrated in the solid-state.

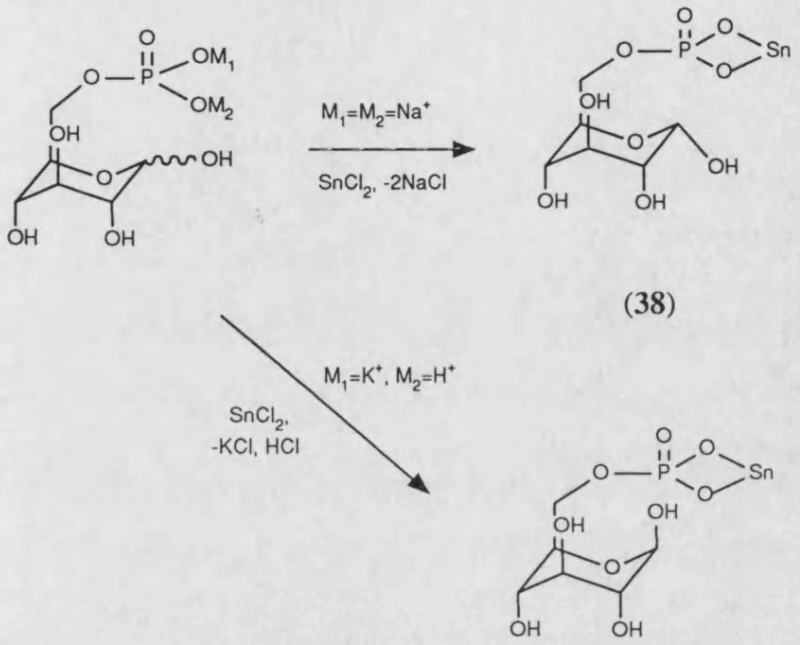

(38)

(3.2)

(39)

Tin(II) glycerol-2-phosphate, $(HOCH_2)_2CHOP(O)O_2Sn.\ H_2O$ (**40**), was prepared from the reaction between tin(II) chloride and di-sodium glycerol-2-phosphate in aqueous solution according to equation 3.3:-

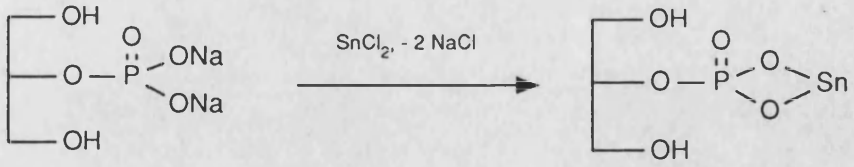

(3.3)

(40)

The product of this reaction readily precipitates from solution as the monohydrate and has quite limited solubility in warm water. Infrared data (3250, 1653cm^{-1}) confirms the presence of water molecules within the solid. Attempted recrystallisation of this compound from boiling water proved unsuccessful - the precipitate was of a very fine, flock-like nature which was difficult to filter

successfully. Similar results were obtained from a saturated aqueous solution which was allowed to evaporate slowly under nitrogen. The solid is effectively insoluble in all common organic solvents suggesting that it is quite polymeric in the solid-state.

Several tin(II) salts of D-6-phosphogluconate have been prepared from the sparingly water-soluble hydrated barium salt of this phosphorylated sugar carboxylate. Barium D-6-phosphogluconate hydrate, $[BaO_2P(O)CH_2CH(OH)$-$CH(OH)CH(OH)CH(OH)CO_2]_2Ba.\ xH_2O$ (**41**), was prepared from barium α-D-glucose-6-phosphate according to equation 3.4:-[139]

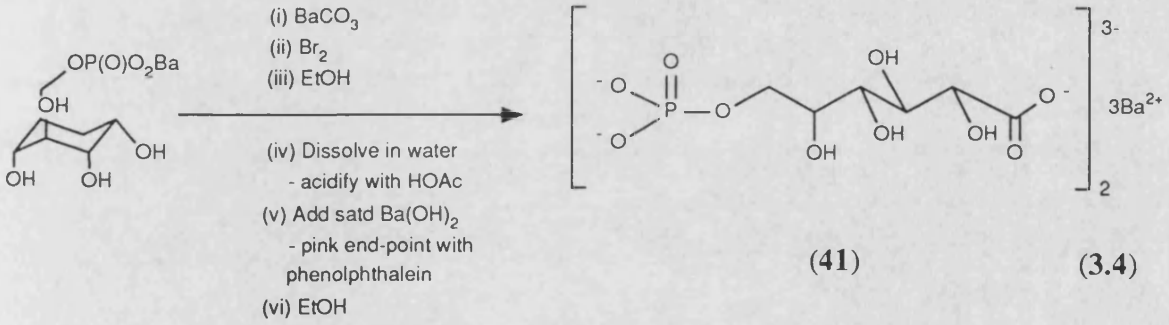

(**41**) (**3.4**)

In this preparation, commercially available barium α-D-glucose-6-phosphate was converted into the open-chain barium salt of 6-phosphogluconic acid. This process is carried out by an oxidation process using bromine. Sugars such as D-glucose are termed reducing sugars because they readily undergo these oxidation reactions under relatively mild conditions. In sugars where the anomeric carbon is protected (e.g. methyl β-D-allopyranoside) the sugar is stable to mild oxidising conditions. Such compounds are called non-reducing sugars. In the aldehyde sugars, or aldoses, the most susceptible group to oxidation is the aldehyde group. The aldehyde group is constantly present in solution due to the equilibrium process shown in equation 3.5. D-glucose is an aldohexose sugar as it contains six carbon atoms. Therefore, D-glucose is susceptible to oxidation to form D-gluconic acid.

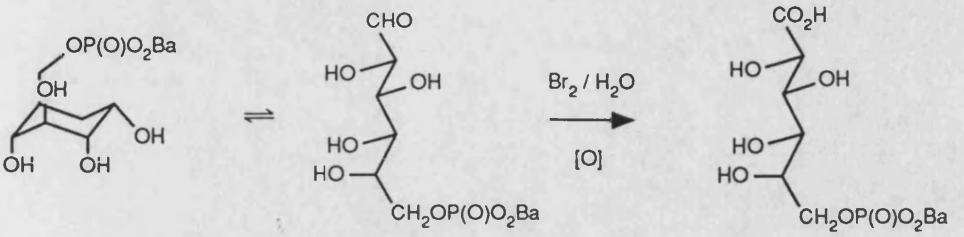

(3.5)

Ba(αG6P) Aldehyde Barium D-6-phosphogluconic acid

For preparative purposes, the oxidation reaction is usually carried out at neutral or slightly acidic pH. With sugars such as D-glucose, the yield of the corresponding aldonic acid (D-gluconic acid) can be as high as 95%.[162] The preparation of D-6-phosphogluconate was carried out in the presence of excess barium ($BaCO_3$) in order to obtain the final product as the barium salt. The product had to be precipitated from solution with ethanol. Subsequently, the solid product was recrystallised from acidified water in the presence of barium at neutral pH. Again, the solid was precipitated with ethanol, yielding an extensively hydrated material. The analytical data suggests that the product is the decahydrate contaminated with traces of inorganic barium salts. Very strong water peaks in the infrared (3409, 1657cm^{-1}) confirm the presence of large quantities of water in the solid.

Hydrated di-stannous mono-barium D-6-phosphogluconate, $[SnO_2P(O)O\text{-}CH_2CH(OH)CH(OH)CH(OH)CH(OH)CO_2]_2Ba.xH_2O$ (**42**), was prepared by reaction of (**41**) with tin(II) chloride in aqueous solution as shown in equation 3.6:-

This reaction yielded a flock-like white precipitate, the analytical data suggesting that the product was a decahydrated (x = 10) di-stannous mono-barium salt. This observtion is consistent with the infrared data which shows very strong bands at 3000-3400 and 1660cm^{-1}. Qualitative analysis confirmed the presence of barium in the product by precipitation of insoluble $BaSO_4$. Attempted replacement of

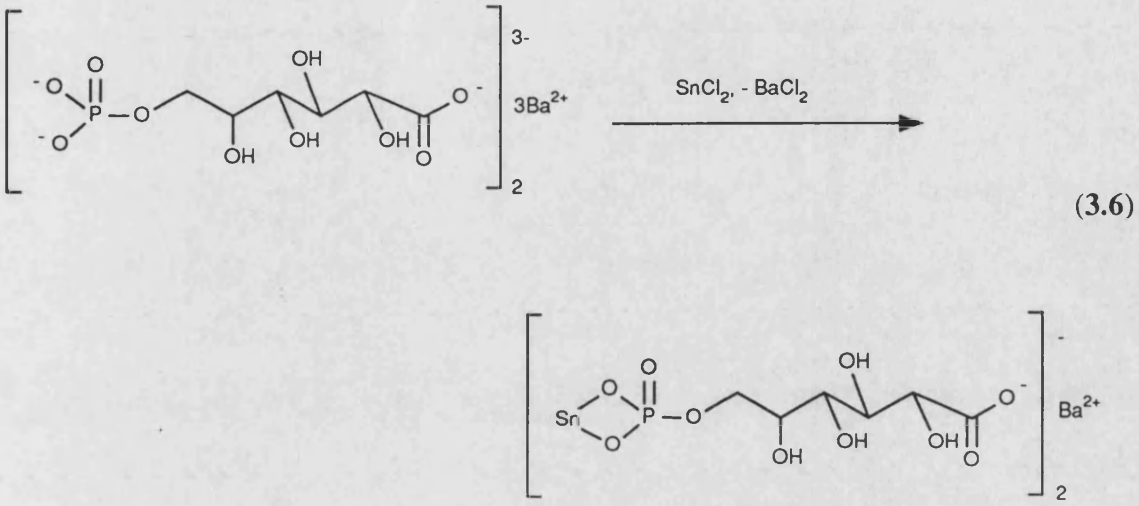

(3.6)

(42)

the third barium ion with a stannous ion by varying the initial stoichiometric ratio of starting materials proved to be unsuccessful. The poor solubility of this compound suggests that it is quite polymeric in the solid-state. Attempted recrystallisation of this solid from boiling water yielded a crop of dendritic crystals that were unsuitable for crystallography.

Spectral data supports the analytical data in suggesting that (**42**) is a di-stannous mono-barium compound. ^{119}Sn Mössbauer data for (**42**) (δ, 3.16mms^{-1}; Δ, 1.77mms^{-1}) suggests that the stannous ion bonds exclusively to the phosphate groups as illustrated. Unfortunately, pK_a data is not available for the phosphoric and carboxylic protons. The Mössbauer data for the inorganic phosphates in Chapter 2 typically show a spectrum with the following parameters: δ, 3.16 (±0.06)mms^{-1}; Δ, 1.69 (±0.05)mms^{-1}. However, the data for a series of inorganic tin(II) carboxylates in Chapter 4 typically have the following parameters: δ, 3.02 (±0.08)mms^{-1}; Δ, 1.94 (±0.10)mms^{-1}. Also, the narrow linewidth parameters for (**42**) (Γ, 1.03mms^{-1}; Γ, 0.94mms^{-1}) suggests that the two tin atoms are in very similar environments. This data strongly suggests that the tin atoms are bound to a phosphate group as opposed to a carboxylate group. Unfortunately, NMR data was not available to further confirm

this statement.

Mono-stannous D-6-phosphogluconato chlorostannate(II) heptahydrate, $[SnO_2P(O)OCH_2CH(OH)CH(OH)CH(OH)CH(OH)CO_2]SnCl.\ 7H_2O$ (**43**), was prepared from the reaction of tin(II) chloride with ammonium D-6-phosphogluconate (Scheme 3.1) which was freshly prepared from (**41**) *in situ*.

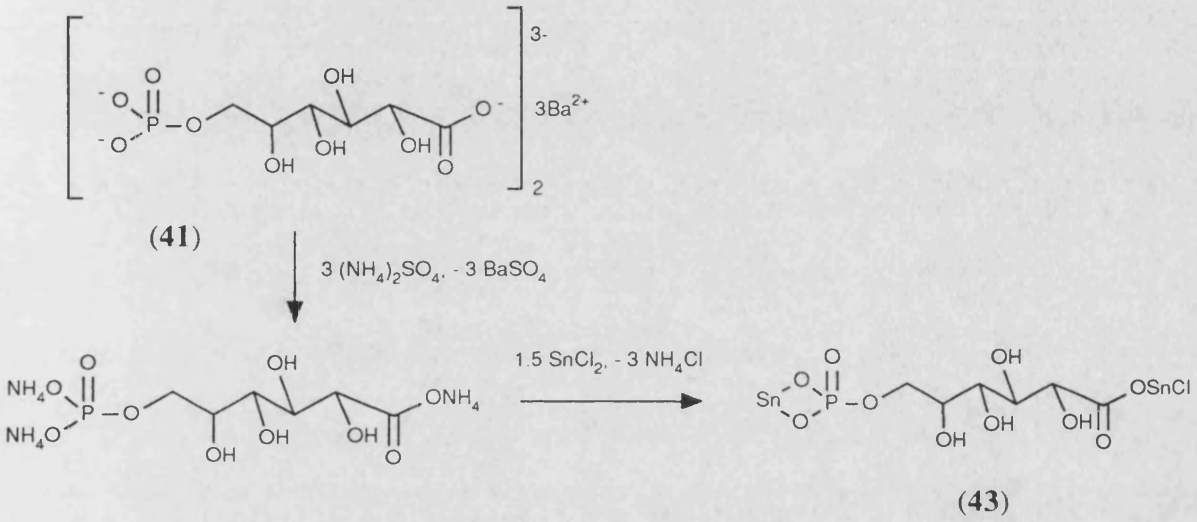

Scheme 3.1 Synthesis of mono-stannous D-6-phosphogluconatochlorostannate(II).

The analytical and infrared spectral data are consistent with the formation of a heptahydrated chlorostannate(II) carboxylate salt, as shown, as opposed to the expected tin(II) phosphogluconate salt, $(RCO_2)_2Sn$ (R = tin(II) phosphogluconate). The infrared data shows strong bands for the water molecules at 3379 and 1622cm^{-1}. The infrared data also contains absorptions due to $\upsilon_{as}(CO_2)$ (1572cm^{-1}) and the phosphate group (υ(P=O) (1305cm^{-1}), υ(P-O) (900-1100cm^{-1}) and δ(O-P-O) (507-582cm^{-1}). Unfortunately, peaks due to υ(Sn-Cl) cannot be observed as these usually occur at around 350cm^{-1}, i.e. below the threshold of KBr plates.[129]

The Mössbauer data for this compound (δ, 3.09mms^{-1}; Δ, 1.73mms^{-1}) is consistent with the formation of a compound containing a tin(II) phosphate and carboxylate site. The overall isomer-shift occurs approximately midway between that

of a typical tin(II) phosphate (3.16mms^{-1}) and a carboxylate (3.02mms^{-1}). The relatively broad linewidths (Γ, 1.22mms^{-1}; Γ, 1.11mms^{-1} also suggests that two slightly dissimilar tin environments are present. Because of the similarity in the electronegativity between oxygen and chlorine, one would not expect to observe a significant shift in the parameters due to the presence of a [-CO_2Sn-Cl] group as opposed to a simple carboxylate. Attempts at fitting this spectrum to two distinct tin sites were not satisfactory. The goodness of fit (κ^2=1.289) was not significantly improved over that above (κ^2=1.269).

This compound is sparingly soluble in hot water and other highly polar solvents (e.g. MeOH) although attempted recrystallisation yields a fine, flock-like precipitate.

Table 3.1 ^{119}Sn Mössbauer data for the series of tin(II) sugar-phosphate compounds.[a]

Compound	δ (mms^{-1})	Δ (mms^{-1})	Γ (mms^{-1})	Γ (mms^{-1})
Sn(αG1P) (**37**)	3.11	1.78	0.89	0.89
Sn(αG6P) (**38**)	3.14	1.67	1.05	0.93
Sn(βG6P) (**39**)	3.12	1.69	1.14	1.05
Sn(Glyc-2-phos) (**40**)	3.17	1.78	1.26	1.07
Sn_2Ba(6-P-Gluc) (**42**)	3.16	1.77	1.03	0.94
Sn_2(6-P-Gluc)SnCl (**43**)	3.09	1.73	1.22	1.11

Note:-

[a]Recorded at 78K, relative to SnO_2.

Table 3.2 ^{119}Sn and ^{31}P NMR data for the series of tin(II) sugar phosphate compounds

Compound	$\delta(^{119}Sn)$ / ppm[a]	$\delta(^{31}P)$ / ppm[b]
Sn(αG1P) (**37**)	-	-0.7
Sn(αG6P) (**38**)	-693.1	-7.9
Sn(βG6P) (**39**)	-718.4	-6.5
Sn(Glyc-2-phos) (**40**)	-	-1.9
Sn_2(6-P-Gluc)SnCl (**43**)	-	-4.3

Note:-

[a]Referenced to tetramethyltin, $Sn(CH_3)_4$.
[b]Referenced to orthophosphoric acid, H_3PO_4.

The ^{119}Sn Mössbauer data for the series of tin(II) sugar-phosphates (**37-40, 42-43**) is listed in Table 3.1. As indicated, the spectra were all recorded on finely-ground solid samples at liquid nitrogen temperature (78K). The value of the isomer-shift, δ, is quoted with reference to SnO_2 (δ = 0.00mms^{-1}). The data clearly shows that all of these compounds contain tin in its lower +II oxidation state due to the high, positive values of δ. The spectra also indicate that the level of tin(IV) impurities is very low, i.e. the materials are quite pure in terms of stannous content. Typically, the levels of Sn(IV) impurities is less than 5% by peak areas. This spectral feature confirms the results obtained in the titrimetric stannous analyses for these compounds (Section 3.1). Typically, the stannous analyses are a little low which suggests that either (a) the compounds contain a trace of tin(IV) impurity or (b) slight oxidative decomposition occurs during the titrimetric analysis.

The spectrum of each of these compounds is a doublet with quite large quadrupole splitting, Δ. This spectral feature indicates that the tin atom in each compound displays a marked asymmetry. In each of these compounds, the central tin atom is primarily coordinated by oxygen atoms. Therefore, the minor variations in the Mössbauer parameters can be accounted for in terms of slight changes to the oxygen coordination sphere.

The values for the isomer shift, δ, for this series of compounds are remarkably similar in each case at δ, 3.13 (±0.04)mms^{-1}. The implication is that the basic tin environment is very similar for each compound. The values of δ compare well with those observed for the series of tin(II) phosphorus oxy-acid salts described previously (Table 2.1). The isomer shift for the inorganic tin(II) phosphates (**22-30**) typically lie in the range δ, 3.16 (±0.06)mms^{-1}. The values for the quadrupole splitting are also quite similar for this group of tin(II) sugar phosphates; typically Δ, 1.74 (±0.05)mms^{-1}. The only slight exceptions to this are the spectra for the anomeric α- and β-G6P tin(II) salts which have a slightly lower value of Δ (Δ, 1.67mms^{-1}, 1.69mms^{-1} resp.). Similarly, the values for Δ are readily comparable with those

obtained for the series of inorganic tin(II) phosphates described previously. Typically, the value of Δ for these inorganic salts lies in the range 1.69 ($\pm$0.05)mms^{-1}. The linewidths for all of these spectra are quite narrow. This suggests that the tin environments are all very similar throughout the individual solid lattices.

The implication of these results is that the tin coordination in the sugar phosphates is very similar to that of the inorganic tin(II) phosphates. Almost without exception, tin is three coordinate in tin(II) phosphates. By inference, in the absence of suitable crystallographic data, the tin environment in the sugar phosphates is also likely to be of the SnO_3E type.

As described above, the spectrum for mono-stannous D-6-phosphogluconato chlorostannate(II) heptahydrate (**43**) is also quite similar even though the coordination sphere of one tin atom will contain both chlorine and oxygen atoms. This is most probably due to the comparable electronegativities of these two elements. The rather broad linewidths reflect the fact that two distinct tin environments are present in this compound.

Typically, the majority of these compounds exhibit slightly asymmetric spectra with differing linewidth parameters, Γ_1 and Γ_2. In many cases, this might simply be a function of the apparently amorphous, polymeric nature of the less-soluble species. This polymerisation process would have the effect of creating subtle local variations in tin coordination. In particular, the spectrum of Sn(glycerol-2-phosphate) (**40**) is quite asymmetric with relatively broad lines. This compound is very insoluble and is likely to be quite polymeric. Similarly, the linewidths in the spectrum of (**43**) are very similar to those of (**40**) suggesting similar structural features, i.e. polymeric or amorphous tin coordination. However, in the case of tin(II) α-G1P (**37**) the linewidths are significantly narrower and quite symmetrical. The implication of this data is that the tin atoms within this solid lattice are in very similar, relatively well-defined crystallographic sites throughout.

Unfortunately, due to the low solubility of many of these compounds, only a

very limited selection of ^{119}Sn and ^{31}P NMR data for this series of tin(II) sugar phosphates is available. This data is presented in Table 3.2. The presence of single peaks in both the ^{119}Sn and ^{31}P spectra indicates the presence of single tin and phosphorus environments for each compound when in solution. Unfortunately, solid-state MAS-NMR techniques were not available for the less soluble compounds of this group.

The phosphorus NMR data shows little variation for each of the compounds for which data is available. However, the slightly negative $\delta(^{31}P)$ values suggest that the phosphorus nuclei are shielded causing a slight shift upfield from H_3PO_4. The variations are a little too small to enable firm conclusions to be drawn.

Tin NMR data is only available for the two most water-soluble of these compounds, i.e. tin(II) α- and β-G6P (**38, 39**). The spectra for each of these two anomeric isomers are typical of those for the inorganic tin(II) phosphates (Tables 2.2, 2.5). Typically, for the inorganic phosphate species, $\delta(^{119}Sn)$ lies in the range -644 to -958ppm. Both of the sugar phosphate spectra show a single peak upfield from $Sn(CH_3)_4$, i.e. highly negative values of $\delta(^{119}Sn)$: -693.1ppm for Sn(αG6P), -718.4ppm for Sn(βG6P). Although the difference is quite small, the spectrum of β-G6P isomer shows the ^{119}Sn peak to be further upfield by 25.3ppm. This is most likely a function of the influence of the hydroxyl group at the anomeric position - this will come into much closer proximity to the tin atom in the β-isomer, as discussed in Section 3.2.1.

3.2.1 *Conformation of the glucose ring in the stannous salts of isomeric glucose phosphates.*

Three isomeric stannous salts of glucose phosphate (**37-39**) have been prepared and characterised. ^{1}H and ^{13}C NMR data are available for all of these compounds which can be used to glean useful information concerning the conformation of the glucose ring. Further information regarding the inter and intramolecular coordination of tin to hydroxyl groups around the ring might also be obtained from the ^{13}C data.

Although spin-spin coupling works through the bonding electrons, the magnitude of the coupling constant *J* is related to the relative orientations of the coupled nuclei in space. For example, the *J* value between adjacent axial hydrogens in cyclohexanes is 10-13Hz, whereas *J* between axial and equatorial or between two equatorial hydrogens is only 3-5Hz as illustrated in the following example.

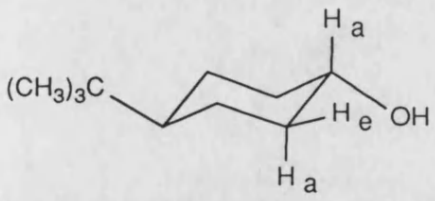

J_{aa} = 11.1Hz
J_{ae} = 4.3Hz

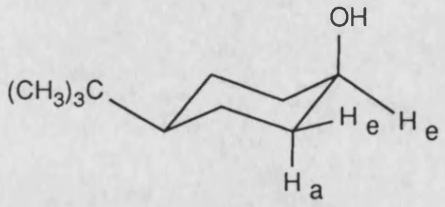

J_{ee} = 2.7Hz
J_{ae} = 3.0Hz

The dihedral angle between two [C-C-H_a] axial planes is 180°, whereas the axial-equatorial and equatorial-equatorial dihedral angles are both 60°. The relation between the coupling constant, *J*, and the dihedral angle between hydrogens has been established theoretically and can be depicted graphically in a form known as the

Karplus curve. The coupling constant between two hydrogens reaches a minimum when the dihedral angle is 90°. With the aid of the Karplus relationship, useful structural information can be garnered from an examination of the *J* values. The effect is most easily seen in conformationally-locked cyclohexanes. In cyclohexanes, $J_{\text{axial-axial}}$ is generally large (10-13Hz), whereas $J_{\text{axial-equatorial}}$ and $J_{\text{equatorial-equatorial}}$ are somewhat smaller at 3-5Hz.

These rules can be further extended to incorporate the carbohydrates such as D-glucose and its substituted derivatives. Although either the five- or six-membered hemiacetal structure is possible, almost all of the simple sugars exist in the six-membered ring form. When the hemiacetal is formed, the former aldehyde becomes a stereocentre, hence the α- and β-anomeric forms of D-glucose. Interconversion of the two cyclic forms is subject to both acid and base catalysis and occurs in solution by the mechanism for acetal formation and hydrolysis.

As in cyclohexanes, two alternative chair forms are possible, and the one that predominates is the one with fewer repulsive interactions. For β-D-glucose, there is a large difference between the two chair forms. In one form, all five substituents are in the equatorial positions, whereas they are all axial in the other. The difference between the two has been estimated at 6 $kcalmol^{-1}$ in favour of the former α-isomer. For most of the aldohexoses, the preferred conformation is found to be the one with the CH_2OH group in the equatorial position. The boat conformation is quite unstable for aldohexoses and is rarely encountered.

Analysis of the ^1H NMR data for the series of tin(II) glucose phosphates can give an indication as to the conformation of the ring. However, the rules established regarding the *J* values for cyclohexanes can only be an approximation in the case of carbohydrates. This is due to the torsional effect of the endocyclic [-C-O-C-] bond within the ring upon the overall conformation.[163] The observed ranges for *J* values of chair forms of carbohydrates are listed in Table 3.3.

The ^1H and $^{13}C\{^1H\}$ NMR data for the series of tin(II) glucose phosphates is

Table 3.3 Coupling constants for carbohydrate rings.

Coupling	Hz
$J_{ax\text{-}ax}$	8.6 - 11.5
$J_{eq\text{-}eq}$	0.3 - 3.5
$J_{eq\text{-}ax}$	1.5 - 5.8

presented in Tables 3.4 and 3.5 respectively. All of the data is recorded in D_2O solution. Consequently, peaks in the proton spectrum due to the exocyclic hydroxyl groups are not observed due to deuterium exchange. The $^{13}C\{^1H\}$ data is compared to the literature data for α-D-glucose, and the alkali metal salts of α-G1P, α-G6P and β-G6P.[164,223,224,225]

Table 3.4 ^{1}H NMR data for the series of isomeric tin(II) glucose phosphates.

Compound	H_1	H_2	H_3	H_4	H_5	$2H_6$
Sn(αG1P) (37)	5.39ppm (dd)	3.85ppm (dd)	3.34ppm (dd)	3.43ppm (dd)	3.80ppm (m)	3.67ppm (d)
	$^{3}J_{P-H}$ 8.4Hz J_{ea} 3.1Hz	J_{aa} 9.1Hz J_{ea} 3.1Hz	J_{aa} 7.4Hz J_{aa} 9.1Hz	J_{aa} 9.7Hz J_{aa} 7.4Hz		J 7.4Hz
Sn(αG6P) (38)	5.21ppm (d)	3.68ppm (dd)	3.39ppm (dd)	3.26ppm (dd)	3.94ppm (m)	4.16ppm (d)
	J_{ea} 3.2Hz	J_{aa} 9.8Hz J_{ea} 3.2Hz	J_{aa} 7.9Hz J_{aa} 9.8Hz	J_{aa} 9.7Hz J_{aa} 7.9Hz		J 7.9Hz
Sn(βG6P) (39)	4.65ppm (d)	3.68ppm (dd)	3.35ppm (dd)	3.24ppm (dd)	3.90ppm (m)	4.18ppm (d)
	J_{aa} 8.6Hz	J_{aa} 9.6Hz J_{aa} 8.6Hz	J_{aa} 7.3Hz J_{aa} 9.6Hz	J_{aa} 9.6Hz J_{aa} 7.3Hz		J 7.4Hz

Table 3.5 $^{13}C\{^{1}H\}$ NMR data for the series of isomeric tin(II) glucose phosphates.

	Chemical shift δ / ppm					
Compound	C_1	C_2	C_3	C_4	C_5	C_6
α-D-glucose	92.9	72.5	73.8	70.6	72.3	61.6
Na_2(αG1P)	96.3	72.9	74.3	70.9	74.1	61.9
Na_2(αG6P)	93.0	72.2	73.3	69.9	71.3	64.8
K_2(βG6P)	96.7	74.8	76.3	69.9	75.6	64.8
	C_1	C_2-C_5				C_6
Sn(αG1P) (**37**)	97.8	75.4	76.2	73.1	74.2	64.1
Sn(αG6P) (**38**)	93.2	74.9	75.1	71.3	72.1	67.5 (d) $^{2}J_{P\text{-}C}$ 6.7Hz
Sn(βG6P) (**39**)	95.6	73.2	74.2	71.0	75.7	70.0

Analysis of the coupling constants in the ^1H NMR data shows that each of the tin(II) salts must contain an aldohexose group in the chair conformation. The type of chair adopted is the same for each compound in which the exocyclic [-CH_2O-] group lies equatorially. This is in agreement with the theoretical predictions above which state that the conformation adopted is that which minimises repulsions between substituents on the ring. Of particular importance is the geometry at the anomeric position, C_1, and the endocyclic [-C_4-C_5O-] bonds. Unfortunately, the ^1H and $^{13}C\{^1H\}$ data for the alkali metal salts were complex and difficult to assign fully (e.g. the $^{13}C\{^1H\}$ spectra typically contain 10-15 peaks). The data quoted in Table 3.5 for the ^{13}C spectra of these tin(II) compounds is thus compared to the literature data for the alkali metal salts. This complexity of the spectra suggests that these salts are fluctional in aqueous solution and a mixture of species are present in equilibrium. However, the tin salts provide notably clearer spectral data suggesting that the equilibria are less complex when a large metal cation is bound to the phosphate group.

In Sn(αG1P), $J_{1,2}$= 3.1Hz which is indicative of an equatorial-axial spatial relationship between the two protons. However, a second coupling, $^3J_{P\text{-}H}$= 8.4Hz is also observed due to the phosphorus on the phosphate group at C_1. This value is quite consistent with that reported in the literature, $^3J_{gauche}$= 3-8Hz.[165] The coupling between H_4 and H_5 is reduced to 7.4Hz which suggests that the protons are not axially aligned at 180° to one another. The implication is that this fragment of the ring is slightly puckered to allow for the endocyclic O atom.

In Sn(αG6P), $J_{1,2}$= 3.2Hz which is also indicative of a equatorial-axial spatial relationship between the two protons. The chemical shift of H_1 is slightly upfield of H_1 in the αG1P isomer due to the loss of the phosphate at C_1. Similarly, the $J_{4,5}$ coupling is only 7.9Hz due to puckering of the ring causing the two protons to be not truly axial to one another.

In Sn(βG6P), $J_{1,2}$ is now increased to 8.6Hz reflecting the fact that both H_1 and H_2 now lie in an axial position. The chemical shift of H_1 is now substantially

reduced over the two α-isomers at 4.65ppm. This observation is consistent with NMR data for other carbohydrates.[166,167] $J_{4,5}$ coupling is only 7.3Hz, again due to puckering of the ring causing the two protons to be not truly axial.

The fate of the rest of the ring appears to be largely unchanged from one isomer to another. Unfortunately, the signals due to H_5 are complex and cannot easily be resolved into individual components. This is due to complex coupling with H_4 and the two protons attached to the exocyclic [-CH_2O-] group, H_6.

The ^{13}C NMR data might be useful in providing information regarding the chelation of exocyclic hydroxyl groups to the tin atom. Comparison with the parent compounds, i.e. α-D-glucose and the alkali metal phosphate salts, should show small but measurable downfield shifts in the corresponding peak positions where chelation to tin is taking place. However, the ^{13}C data for these compounds is very difficult to interpret fully. The signals due to C_2 through to C_5 are all very similar in chemical shift and it is difficult to reliably distinguish the individual peaks. The peaks due to C_1 and C_6 are more readily identified in the spectra as shown in Table 3.5.

Sn(αG1P) shows a small increase in the position of several peaks corresponding to C_2-C_5 indicating that either intermolecular bridging or intramolecular chelation to tin must be taking place. Molecular models suggest that intramolecular chelation to $C(OH)_{3,4}$ is quite possible in this compound although the axial proton at C_3 will provide steric repulsion to the approaching tin atom. Intermolecular bridging to hydroxyl groups of an adjacent glucose ring might also occur in this compound. This mode of bonding is further supported by the physical properties of this material, i.e. poor solublilty.

In contrast, the two isomers of Sn(G6P) exhibit fewer changes overall to the spectra. The peak due to C_6 in Sn(αG6P) shows evidence of $^2J_{P\text{-}C}$ coupling (6.7Hz). This effect is not observed in the spectra of Sn(αG1P) (at C_1) or Sn(βG6P) (C_6) although the coupling might be too small to be reliably and reproducibly detected. The conclusion from molecular models is that the glucose-6-phosphate salts might

primarily exhibit intramolecular chelation between the tin atom and the hydroxyl groups that are in suitably close proximity. For example, in the β-isomer, a particularly favourable arrangement is formed through chelation of the tin atom to the hydroxyl at the anomeric position, C_1. Again, this conclusion is supported by the physical properties, i.e. enhanced water-solubility.

However, these observations are rather incomplete and unsatisfactory due to the difficulties in fully assigning the ^{13}C spectral data. Presenting the NMR data as a 2-D ^1H *vs.* $^{13}C\{^1H\}$ correlation spectrum would enable the complete assignment of the ^1H spectrum as above (Table 3.4) and hence the ^{13}C data. This technique was applied to the α-isomer of tin(II) glucose-6-phosphate. However, the data obtained was complicated by the fact that the peaks in the ^{13}C spectrum were all slightly different to those previously obtained for this compound (Table 3.5). However, ^{13}C peaks for carbohydrates have been found to vary considerably by 1-2ppm depending on the concentration and ambient temperature.[225] The data obtained by this technique is as follows: 93.2 (C_1), 73.4 (C_2), 76.4 (C_3), 74.8 (C_4), 72.1 (C_5), 65.2ppm (C_6). Comparison with the data in Table 3.5 for the alkali metal salt of αG6P shows that the peaks due to C_2 to C_4 have all shifted downfield (1.2, 3.1 and 4.9ppm respectively) while the remaining peaks have all remained effectively unchanged. The indication is that chelation to tin occurs through each of these sites although that to $C(OH)_4$ is the strongest. This prediction is found to be feasible when molecular models are employed. Further studies of this type are required in order to glean further information regarding the role of the exocyclic hydroxyl groups in the other tin(II) glucose phosphate compounds.

The predicted conformations of the parent compound, α-D-glucose and the three tin(II) salts of α-D-glucose-1-phosphate, α-D-glucose-6-phosphate and β-D-glucose-6-phosphate are illustrated in Fig. 3.1. Note the puckering of the ring about the [-C_4-C_5-O-] bonds.

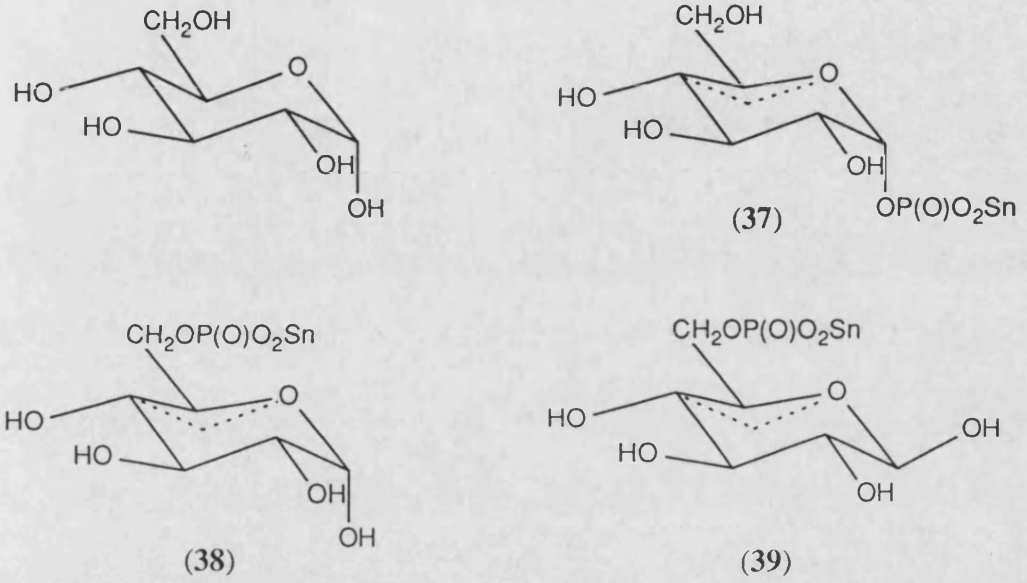

Fig. 3.1 The predicted conformation of the isomeric tin(II) glucose phosphates.

3.2.2 *Tin-EXAFS data for the isomers of glucose phosphate.*

The use of EXAFS data to glean useful structural data has been demonstrated in Chapter 2 for selected amorphous inorganic tin(II) pyrophosphates. Tin-EXAFS data has also been obtained for the isomeric tin(II) glucose phosphate salts in the hope of providing further useful structural information about the tin coordination sphere. This technique can provide valuable information concerning the coordination number and bond lengths about the central tin atom in the solid-state. The EXAFS data is presented in Table 3.6:-

Unfortunately, due to the fine, flocculent nature of these solids, the EXAFS data is not of a very high quality and the best-fit R values range from 17.03 - 24.96 whereas an R value of 15-20 is desirable. Because of this, the accuracy of the data is questionable, particularly the calculated number of atoms within each shell.

The data shows that each of the tin(II) sugar phosphates contain an innermost shell consisting of O atoms about the central tin. The radii of these first shells are all remarkably similar and range from just 2.13-2.14Å. Beyond this first shell, all of these compounds also contain a second shell of O atoms. Again, the radii of these second shells are also quite similar and range from 2.35-2.37Å. A third coordination sphere containing approximately one P atom is also observed for each of these compounds. The radii of these outer shells shows a little more variation for the three compounds and range from 3.26-3.37Å. Beyond this third coordination shell the data is generally much less satisfactory and becomes much more difficult to interpret successfully.

Essentially, the tin coordination is quite similar in each of these three compounds. This observation is in full agreement with the Mössbauer and NMR data discussed previously which also confirms the tin to be in similar environments. The innermost Sn-O bond-lengths in each case compare well with those observed in other,

Table 3.6 EXAFS data for isomeric tin(II) glucose phosphate compounds.

Compound	Number of atoms	Atom type	Bond length / Å	Error / Å	R value
Sn(αG1P) (37)	5.56	O	2.14	0.02	17.03
	1.31	O	2.37	0.02	
	0.85	P	3.34	0.02	
Sn(αG6P) (38)	4.71	O	2.14	0.02	20.70
	2.12	O	2.35	0.03	
	0.83	P	3.32	0.03	
Sn(βG6P) (39)	5.88	O	2 .13	0.02	24.96
	1.01	O	2.37	0.01	
	0.76	P	3.26	0.01	

documented tin(II) phosphates and phosphorus oxy-acid salts (Table 1.7) which typically range from 2.06-2.47Å. Similar values for the innermost Sn-O bond have been observed in tin(II) pyrophosphate compounds using EXAFS results. These are discussed in Section 2.2 and the results are listed in Table 2.3. Similarly, the second-shell Sn-O bond lengths are typical of those observed in compounds of this type. In each case, the third coordination shell containing a single P atom lies at a significantly reduced radius from the central tin atom than that observed for tin(II) pyrophosphate species (Table 2.3). In the pyrophosphates, the P atom is typically at a distance of 3.64Å from the tin.

In the light of the similarities in spectral data between the inorganic tin(II) phosphates and the sugar phosphates, the most likely coordination about the tin atom is also based upon the three coordinate SnO_3E pyramidal type. It also appears that a second coordination sphere exists beyond this leading to an approximate SnO_3O_3' octahedron.

The fact that the basic SnO_3 unit is predominant in the structural chemistry of tin(II) phosphates (Section 1.8.2) is well established. This three-coordinate geometry is also predominant in many other oxygen-bound tin(II) salts although the presence of a second SnO_3' coordination sphere has been identified in just a few cases. For example, $SnSO_4$ has an SnO_3O_3' coordination with six Sn-O bond lengths of 2.25, 2.27, 2.27, 2.95, 3.08, 3.08Å.[159,160] However, the Mössbauer parameters of a commercial sample of this compound (δ, 3.90; Δ, 1.21mms^{-1}) are quite different to those of the pyrophosphates. A further example of an approximate SnO_3O_3' coordination is found in (triformato)stannate(II) anions, $Sn(O_2CH)_3^-$. The six Sn-O bond lengths are 2.18, 2.17, 2.14, 2.88, 3.01, 2.97Å.[117] The Mössbauer data for the potassium salt of this anion (δ, 3.05; Δ, 1.85mms^{-1}) is much more similar to that of the tin(II) phosphates and sugar phosphates.[161] The latter data confirms that the approximate SnO_3O_3' coordination suggested by EXAFS analysis might be consistent with the Mössbauer data.

If the sugar phosphates do exhibit an approximate SnO_3O_3' coordination, a possible arrangement about the central tin atom would be similar to that for the inorganic salts proposed in Fig. 2.1. However, in the case of the sugar phosphates, each tin atom is coordinated by a just a single phosphate group, the additional oxygen atoms are due to the exocyclic hydroxyl chelation discussed above as well as water of hydration.

The data for the α- and β-anomers of glucose-6-phosphate indicate that the β-isomer has an extra oxygen in the inner Sn-O shell. This is most likely to be the hydroxyl at the anomeric C_1 position which is more favourably orientated to come into closer contact with the tin (Fig. 3.1). Essentially, the data for the α-G1P and β-G6P salts are almost indistinguishable. The NMR data suggests that Sn(αG1P) is polymeric with multiple intramolecular chelations. The longer bond might be a weaker intramolecular interaction to the hydroxyl attached to C_4.

The experimental EXAFS fourier transform curves for this series of compounds illustrated in Figs. 3.2 to 3.4.

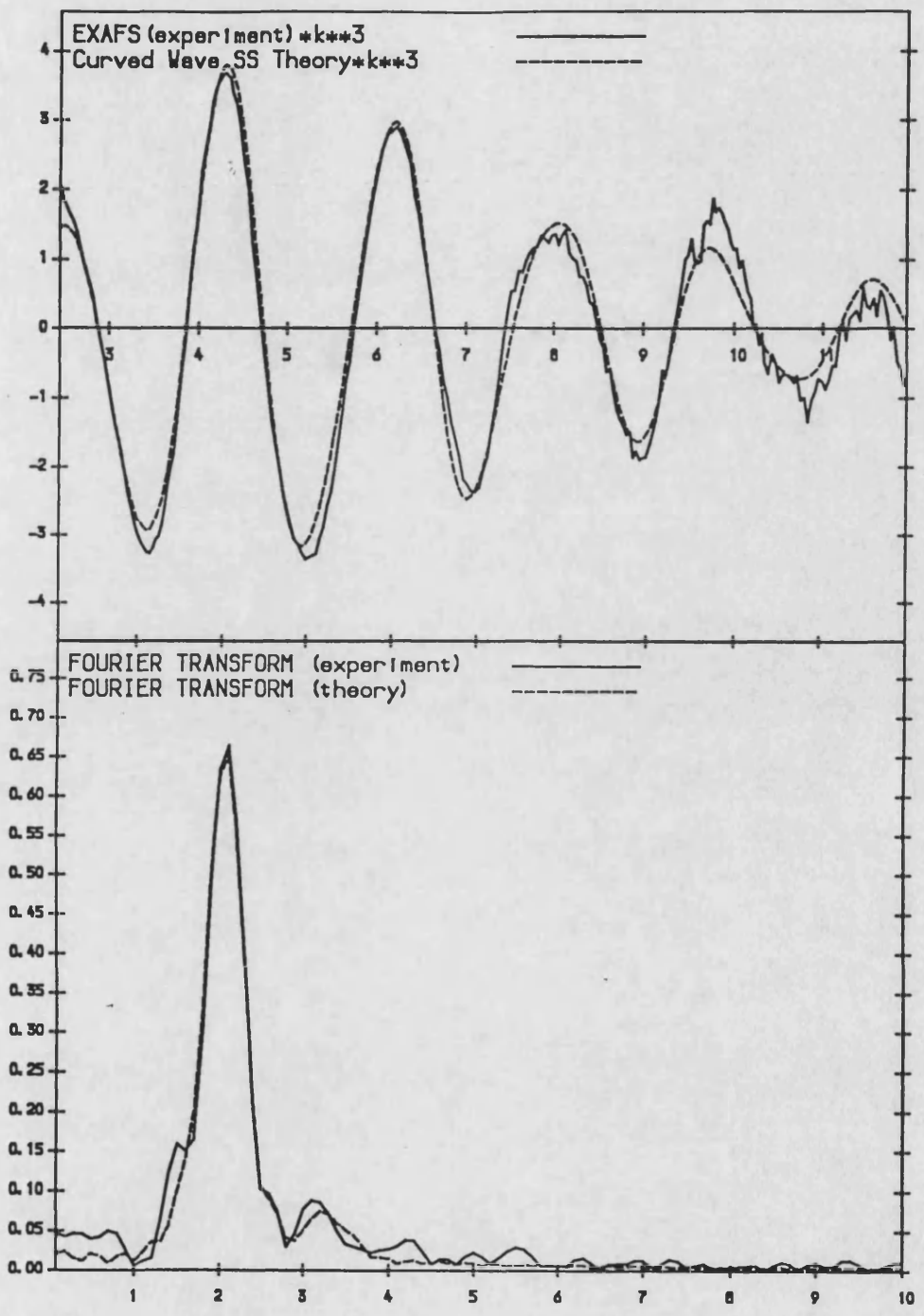

Fig. 3.2 The EXAFS fourier transform curves for Sn(αG1P) (37).

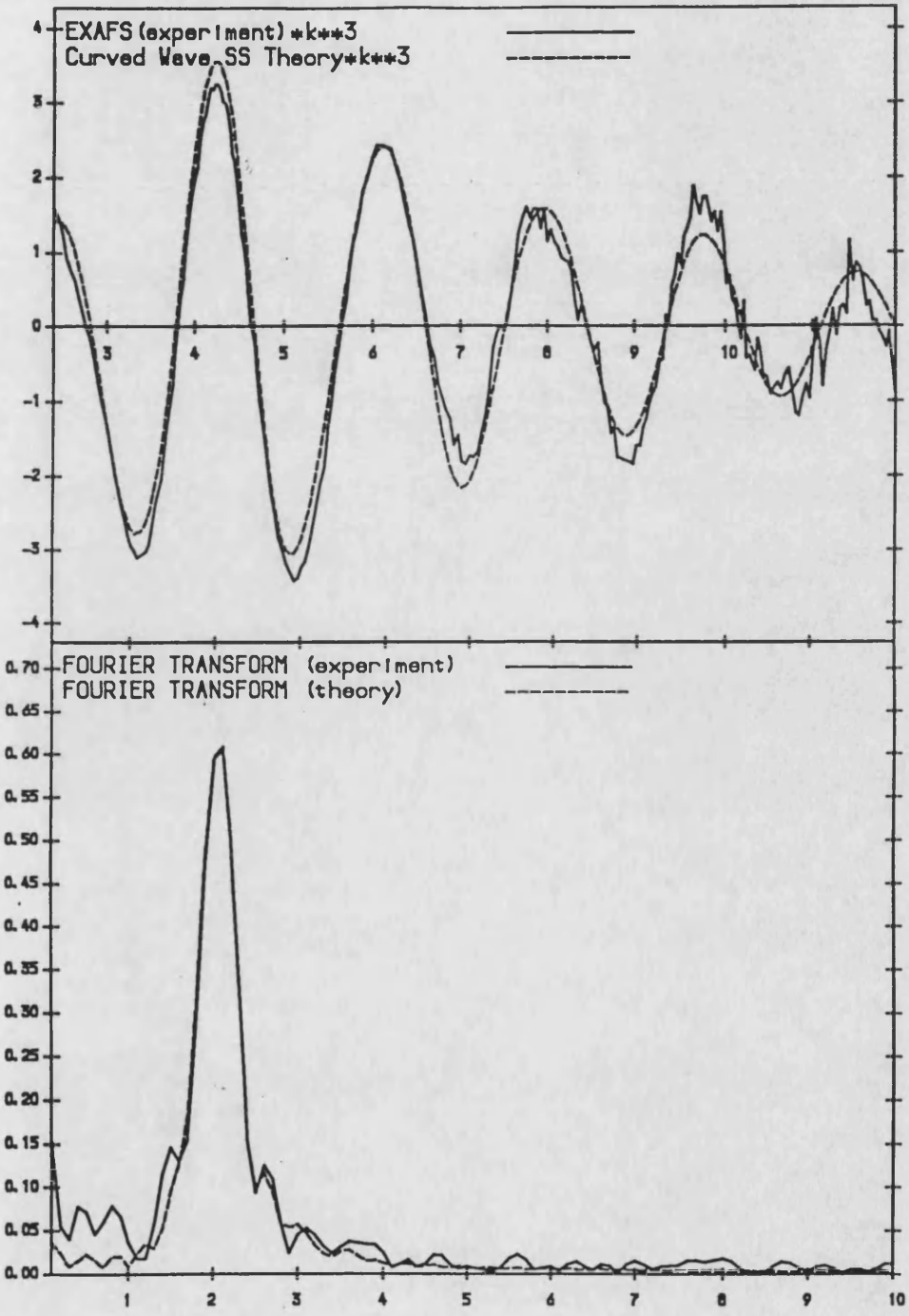

Fig. 3.3 The EXAFS fourier transform curves for Sn(αG6P) (**38**).

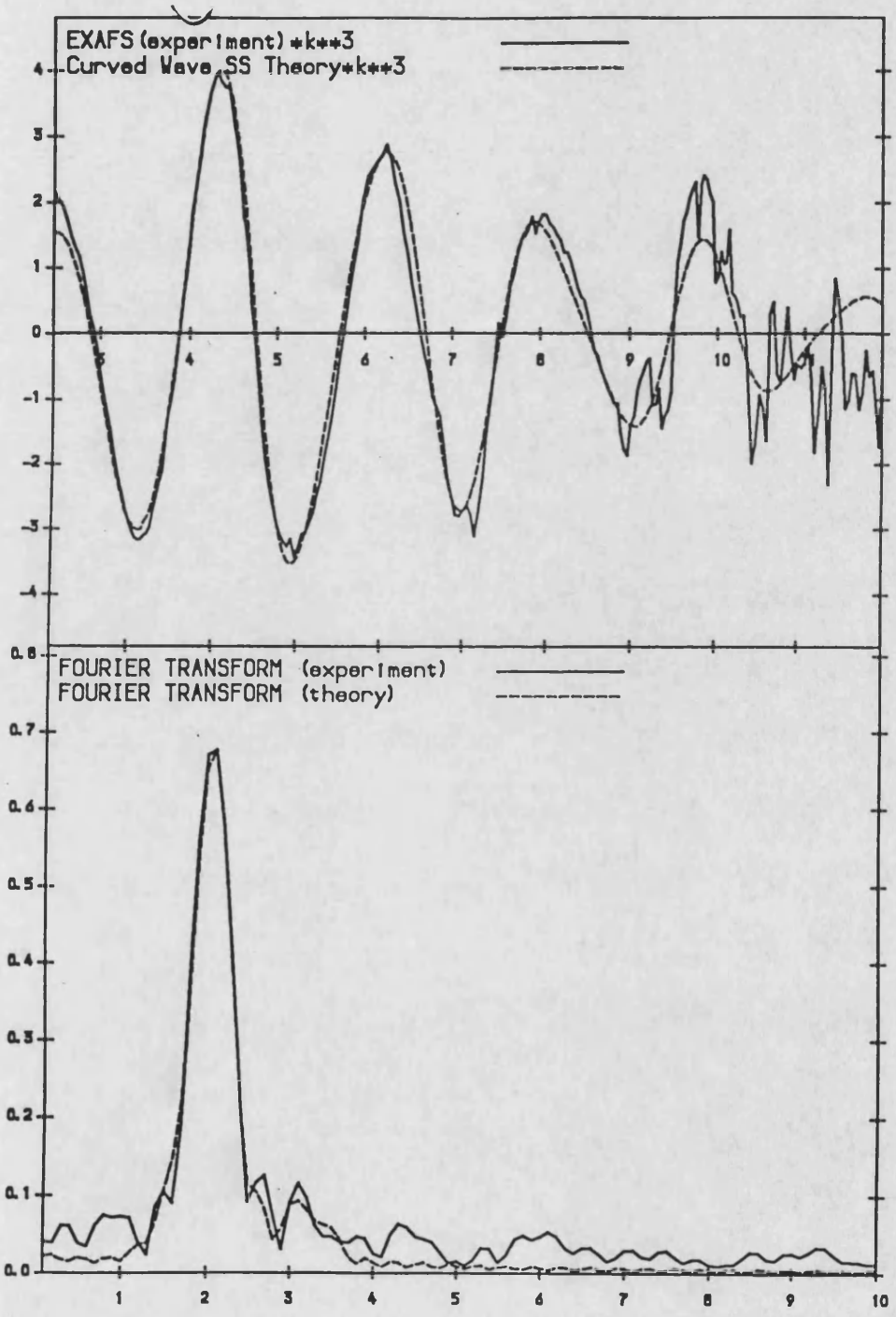

Fig. 3.4 The EXAFS fourier transform curves for Sn(βG6P) (39).

3.4 The Preparation and Characterisation of Related Tin(II) Carbohydrate Compounds.

The preparation and characterisation of a series of sugar phosphates of tin(II) have been described in the preceeding pages. A major drawback of these materials is the requirement for relatively expensive (though commercially-available) starting materials. The preparation of suitably pure glucose-phosphate starting materials is a highly involved procedure with low yields.[139] Similarly, the preparation of other phosphorylated sugars is also highly involved, e.g. sucrose 6′-phosphate.[168,169] For this reason, the preparation of a range of stannous salts of inexpensive, readily available related compounds is described. These compounds include salts of 'sugar carboxylates' (aldonic acids). The synthesis of tin(II) compounds involving unsubstituted, simple sugars was also attempted.

The first such compound, anhydrous tin(II) bis-D-gluconate, $[HOCH_2CH(OH)CH(OH)CH(OH)CH(OH)CO_2]_2Sn$ (**45a,b**), the tin(II) salt of D-gluconic acid, was prepared in good yield using two preparative methods. This compound has been patented by the Procter and Gamble organisation as an effective anti-plaque dentifrice additive (Section 1.6).

Problems arose during the synthesis of this compound from sodium-D-gluconate and tin(II) chloride. The product of this reaction (**45a**) is highly water-soluble which made it extremely difficult to successfully separate the final product from the NaCl produced as a by-product of the reaction. Soxhlet-purification of the crude product in refluxing 90% ethanol/water under nitrogen for 36 hours apparently removed traces of NaCl from the product. However, an inevitable side-effect of this procedure was the partial decomposition of the tin(II) bis-D-gluconate to form minor tin(IV) impurities.

A solution to this problem was to first prepare, *in situ*,

trimethylsilyl-D-gluconate from the sodium salt by reaction with trimethylsilylchloride, $(CH_3)_3SiCl$. This reaction was carried out in a polar organic solvent such as THF and the NaCl produced readily precipitated from solution and could be removed by filtration. Upon reacting the soluble trimethylsilyl-D-gluconate with $SnCl_2$, the by-product of the reaction was trimethylsilylchloride, a volatile liquid that could be readily removed *in vacuo*. The eventual product of this reaction (**45b**) was also a highly water-soluble white powder. Attempted slow crystallisation yields a viscous, pale-yellow oil. These two preparative routes to stannous bis-D-gluconate are illustrated in Scheme 3.2.

The infrared data for this compound confirms the analytical data in suggesting that the solid is anhydrous. The series of strong, sharp υ(OH) peaks in the spectrum (3150-3541cm^{-1}) are due to the OH groups attached to the chain. The spectrum also shows the asymmetric vibration arising from the $-CO_2$ group, i.e. $\upsilon_{as}(CO_2)$ at 1599cm^{-1}. Unfortunately, in the absence of structural data, difficulties arise in deciding between the presence of unidentate, bridging or chelating carboxylates.[170] It has been concluded that if $\upsilon_{as}(CO_2)$ is at a higher frequency, and $\upsilon_s(CO_2)$ at lower frequency than the ionic carboxylate, one can reliably infer unidentate coordination. However, reliable assignment of the symmetric vibration $\upsilon_s(CO_2)$ is very difficult as it generally occurs in the C-C and C-H region which is densely occupied by other strong bands. It has been demonstrated that correlations claimed to establish other coordination modes are not always valid.[171] In the case of the tin(II) carboxylates, the data for tin(II) formate, which is known to contain symmetric and asymmetric bridging carboxylates, shows a multiplicity in the two peaks. These occur at the following frequencies: $\upsilon_{as}(CO_2)$; 1561, 1548cm^{-1}; $\upsilon_s(CO_2)$; 1341, 1330cm^{-1}.[115] In the case of tris-formatostannate(II), which contains only unidentate carboxylates, $\upsilon(CO_2) \leq 1650cm^{-1}$.[172] Unfortunately, structural data for other simple $Sn(O_2CR)_2$ compounds is not available. However, as shown in Chapter 4, $\upsilon_{as}(CO_2)$ for a tin(II) citrate occurs at 1561cm^{-1}. Structural data has confirmed that the carboxylate groups

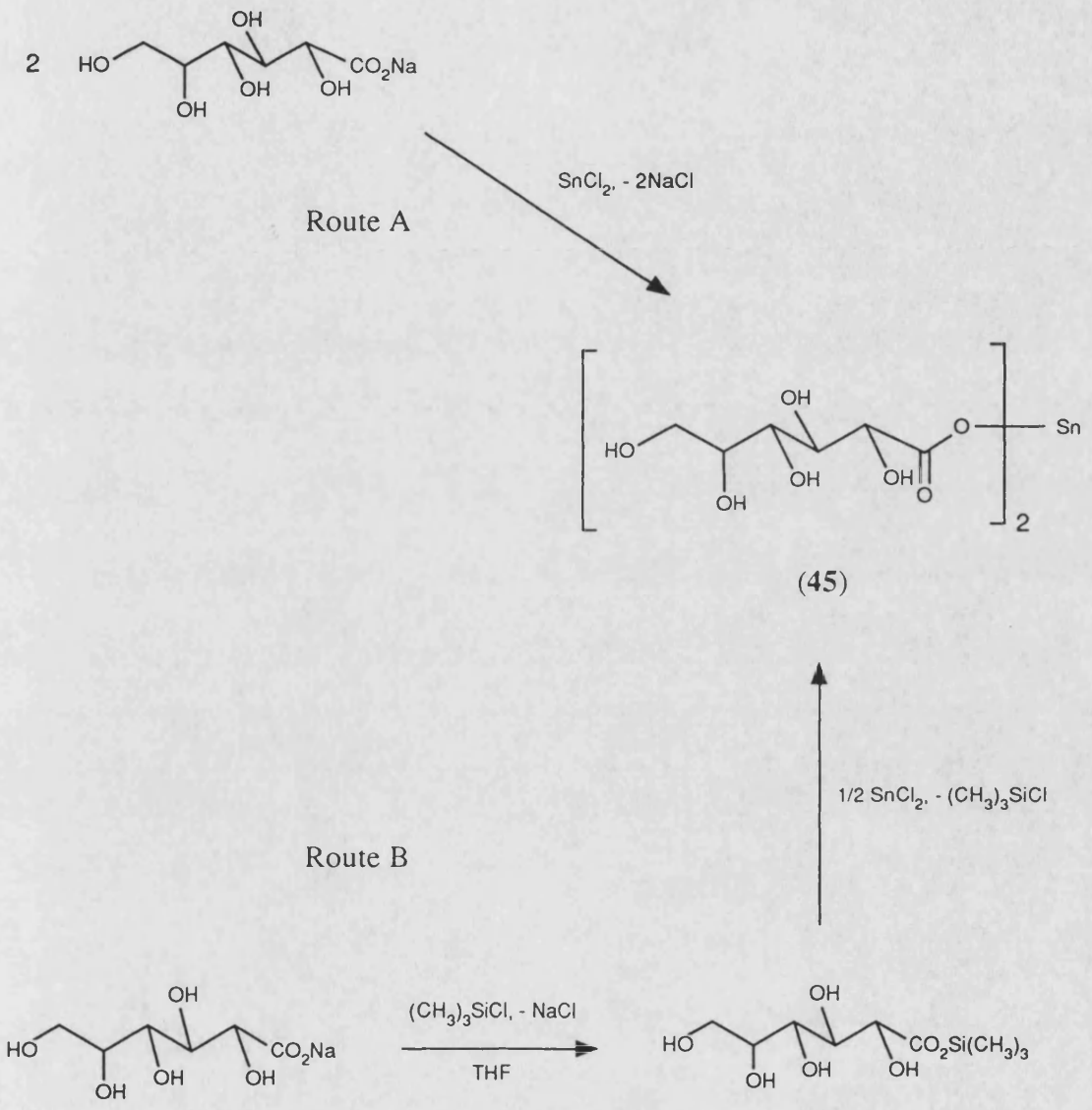

Scheme 3.2 The preparation of tin(II) bis-D-gluconate.

are unidentate although strong hydrogen bonding to the C=O group is responsible for the low frequency of this band. Hence, any interpretation of the carboxylate coordination modes in tin(II) compounds from the infrared data alone is inherently unreliable.

The value of $\upsilon_{as}(CO_s)$ for this compound (1599cm^{-1}) is a little lower than that observed for other metal α-hydroxycarboxylates and appears to be much closer to that of the uncoordinated ionic ligand (1597cm^{-1}).[141] For example, $\upsilon_{as}(CO_2)$ for [Al^{III}(D-gluconate)(OH)$_2$] is observed at 1635cm^{-1}. Using the rule established above, it appears unlikely that the gluconate coordinates in a unidentate fashion to the tin(II) atom. However, since this compound is anhydrous, i.e. the absence of strong hydrogen bonding, it appears that weak bidentate carboxylate character is present. The high water-solubility would suggest that the solid is not polymeric which suggests that the ligand does not bridge adjacent tin atoms as in $Sn(O_2CH)_2$, i.e. the gluconate is most likely weakly bidentate in a chelating fashion.

The ^{1}H NMR data for (**45**) displays a complex spectrum which appears very similar to that of sodium gluconate. However, the peak at 4.30ppm (*d*, *J*=7.3Hz) due to the C_2 bound proton is shifted downfield by 0.13ppm in the stannous salt. The $^{13}C\{^1H\}$ NMR data shows six peaks (62.6, 70.2, 71.5, 72.1, 72.5, 193.0ppm) corresponding to the six carbons in the gluconate chain. The peak due to the C_1 carboxylate (193.0ppm) is shifted far downfield (183.4ppm in D-gluconic acid) due to the influence of the coordinated tin. All other peaks are effectively unchanged from the free ligand suggesting that hydroxyl chelation to tin does not occur in solution.

A second tin(II) sugar carboxylate was also prepared in good yield. α-D-glucuronic acid has a cyclic structure similar to that of αG6P with a carboxylate group in place of the CH_2 group to which the phosphate function was bound. Tin(II) bis-D-glucuronate tetrahydrate, $[(C_5H_9O_5)CO_2]_2Sn.\ 4H_2O$ (**46**), was prepared by the reaction of sodium D-glucuronate with $SnCl_2$ in 80% ethanol according to equation 3.7. The product of this reaction readily precipitated as the tetrahydrate and was a slightly off-white powder with limited solubility in common solvents.

The infrared spectrum supports the analytical data in suggesting that the product is readily hydrated. Broad, intense peaks at 3300 and 1635cm^{-1} are due to the vibrational modes of the water molecules. Sharp, strong bands are also observed at

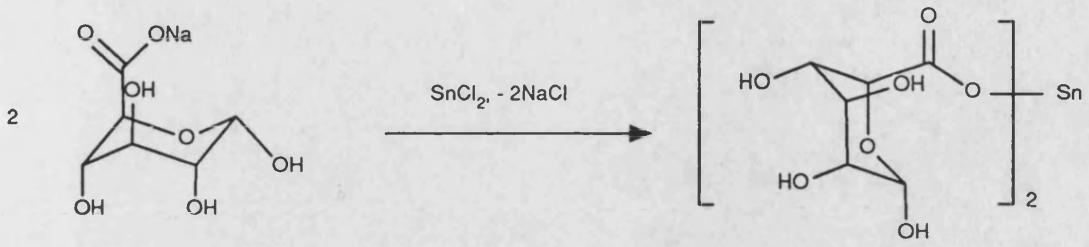

(3.7)

(46)

3100, 3333, 3462, 3601cm^{-1} due to the exocyclic OH's. The carboxylate band is quite similar to that of (**45**), i.e. $\upsilon_{as}(CO_2)$ occurs at 1595cm^{-1}. Again, it is difficult to reliably assign the mode of carboxylate cooordination to the tin(II). $\upsilon_{as}(CO_2)$ for sodium glucuronate is very similar to that in (**46**) and occurs at 1601cm^{-1} suggesting that the coordination is not wholly unidentate. The poor solubility of this compound suggests that the coordination might involve tin-tin bridging as in tin(II) formate. Unfortunately, NMR data was not available due to the limited solubility. This compound was also noted to be quite unstable to atmospheric oxygen.

The ^{119}Sn Mössbauer and ^{119}Sn NMR data for these two compounds are listed in Table 3.7.

The Mössbauer data for this series of carboxylates (**45a,b-46**) is observed to be quite similar for each of the three species. This data is also noted to be comparable to the literature data recorded for several simple tin(II) carboxylates, e.g. $Sn(O_2CH)_2$, $Sn(O_2CCH_3)_2$ (Table 1.8), for which the documented parameters are δ, 3.33 ($\pm$0.02)mms^{-1} and Δ, 1.71 ($\pm$0.06)mms^{-1}. In each case, the simple compounds invariably have polymeric bridged structures with four-coordinate pyramidal tin atoms. The most likely conclusion is that the tin environment in the sugar-carboxylate salts is also of the SnO_4E pyramidal type due to similarity of the data. In the case of the highly soluble D-gluconate, four coordination is most likely achieved through bidentate coordination of the carboxylate. D-glucuronate appears to be polymeric with a similar bridged structure to the formate and oxalate.

Table 3.7 ^{119}Sn Mössbauer[a] and ^{119}Sn NMR data for tin(II) salts of aldonic acids.

Compound	δ (mms^{-1})	Δ (mms^{-1})	Γ (mms^{-1})	Γ (mms^{-1})	δ(^{119}Sn) / ppm[b]
Sn(D-gluconate)$_2$ (**45a**)	3.15	1.75	1.20	1.04	-560.1
Sn(D-gluconate)$_2$ (**45b**)	3.09	1.74	1.14	1.06	-570.9
Sn(D-glucuronate)$_2$ (**46**)	3.22	1.70	1.15	0.95	-

Notes:-

[a]Recorded at 78K, relative to SnO_2.
[b]Recorded in D_2O, relative to external $Sn(CH_3)_4$.

The linewidths of these spectra are also quite narrow which implies the formation of a uniform tin coordination throughout the solid lattice. However, the linewidths Γ_1,Γ_2 are also unequal reflecting the asymmetry of the doublets. This is characteristic of a rather asymmetrically bonded tin.

Tin NMR data is also available for the two samples of tin(II) D-gluconate with the data being typical for tin(II) coordinated by oxygen (*cf.* inorganic tin(II) phosphates in Chapter 2 and sugar phosphates in Chapter 3). Both spectra show only a single peak suggesting a single tin environment. The similarity of the data for each of the two samples ($\Delta\delta$ = 10.8ppm) supports the conclusion that the tin environments are very similar even though the products were formed *via* two different methods. Due to the scarcity of documented NMR data for tin(II) carboxylates, the ^{119}Sn NMR data for a series of freshly-prepared long-chain fatty-acid stannous salts was recorded for comparison with the gluconate. The spectra for tin(II) laurate [$Sn(O_2C(CH_2)_{10}CH_3)_2$], palmitate [$Sn(O_2C(CH_2)_{12}CH_3)_2$] and stearate [$Sn(O_2C(CH_2)_{16}CH_3)_2$] all showed single peaks at -494.1, -489.8 and -480.6ppm respectively (recorded on saturated solutions in d_6-benzene). All of these signals are located downfield of the gluconate. The differences ($\Delta\delta\approx$75ppm) might simply be due to solvent effects as D_2O can coordinate to the gluconate, increasing the coordination at tin. Alternatively, chelation of the OH's (particularly the α-OH) along the chain to the tin atom might exist in the gluconate although evidence for this cannot be detected in the ^{1}H and ^{13}C{^{1}H} NMR data.

The preparation of simple 1:1 tin(II)-sugar compounds was also attempted but was largely unsuccessful. The rationale behind these preparations was to synthesise stable tin(II)-sugars without the need for functionalised starting materials, e.g. sugar phosphates, aldonic acids. In each of the three examples involving α-D-glucose, α-D-fructose and α-D-sucrose (**47-49**), the method involved reacting soluble tin(II) alkoxides with the sugar in an organic solvent. The synthetic routes employed are illustrated in Scheme 3.3 although the products shown are for illustration purposes.

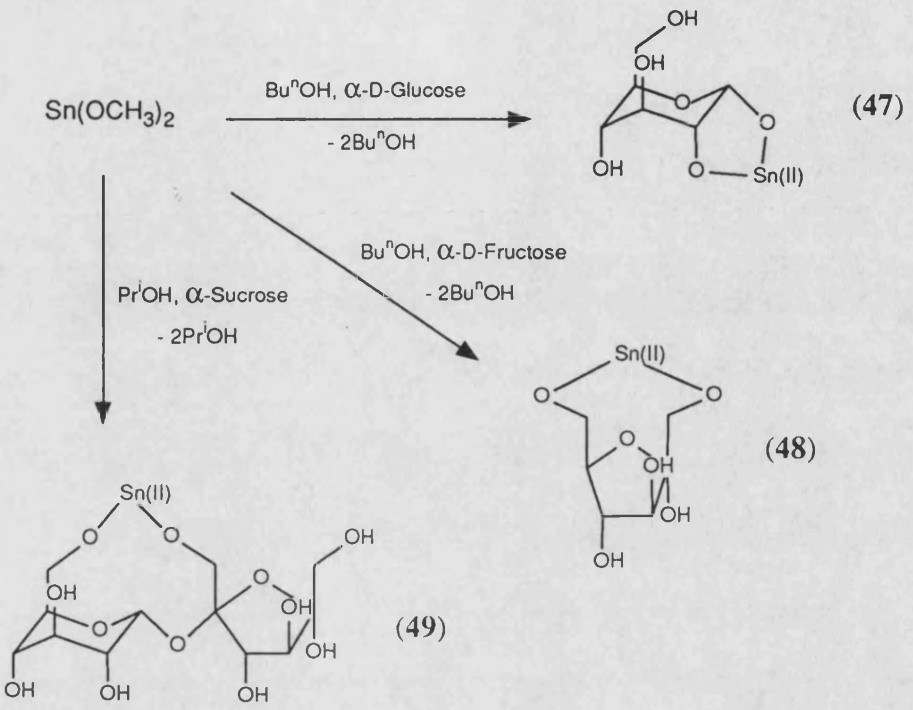

Scheme 3.3 Synthesis of 1:1 tin(II)-sugar compounds.

The glucose product (**47**) was a white, insoluble solid which was fortuitously found to be close to the expected product analytically. However, the Mössbauer spectrum (δ_1, 2.94mms^{-1}, Δ, 1.85mms^{-1}; δ_2, -0.05mms^{-1}) revealed the presence of a strong singlet due to significant amounts of tin(IV) impurity (10-15%).

The fructose product (**48**) was also a white insoluble solid which was also apparently quite pure analytically. However, as above, the Mössbauer spectrum (δ_1, 2.93mms^{-1}, Δ, 1.91mms^{-1}; δ_2, -0.03mms^{-1}) also revealed the presence of a strong singlet due to a tin(IV) impurity.

Finally, the sucrose product (**49**) was the least successful of this series. The product was a pale-yellow powder that was insoluble in all common solvents. The analytical data revealed the solid to contain a negligible quantity of carbon or

hydrogen and the stannous content was also very low. The Mössbauer spectrum (δ_1, 2.74mms^{-1}, Δ, 2.14mms^{-1}; δ_2, -0.04mms^{-1}) also revealed the presence of a strong singlet due to a tin(IV) impurity. No attempts were made to further investigate the identity of these compounds. Essentially however, such compounds would have been bulky alkoxides, $Sn(OR)_2$ (R = sugar residue). It is known that the simple tin(II) alkoxides are particularly susceptible to both oxidation and hydrolysis which might account for the apparent difficulty in the preparation of these sugar compounds. The preparation of the α-D-glucose and α-D-fructose compounds may have been partially successful. However, the preparation of the α-sucrose analogue appears to have simply produced a mixed tin(II)/tin(IV) oxide as the Mössbauer data for orthorhombic SnO is very similar to that of (**49**) (δ, 2.80mms^{-1}, Δ, 2.20mms^{-1}).[173]

Attempts have also been made to produce crystalline adducts of simple tin(II) halides (e.g. SnF_2) with simple monosaccharides (e.g. α-D-glucose) in the hope of gleaning structural information regarding the modes of chelation. Unfortunately, repeated attempts at forming suitable crystalline adducts from both aqueous and alcoholic solutions simply yielded crystals of the uncoordinated tin(II) halide.

A 1:1 molar mixture of SnF_2 and α-D-glucose in D_2O (**50**) was submitted for ^{119}Sn NMR studies in the hope of observing a shift in the peak due to SnF_2 alone (δ, -772.6ppm). The spectrum of the mixture was a sharp singlet at -776.1ppm, i.e. an upfield shift of just 3.5ppm. The result initially suggests that the tin atom does not coordinate to the carbohydrate although it is more likely that SnF_2 is already coordinated by many O atoms when dissolved in D_2O. Further studies are required to clarify this situation (e.g. ^{13}C NMR data).

The rationale behind the carbohydrate adduct formation was to prepare a highly air-stable form of stannous caused by chelation to a poly-ol species (Section 1.8.4). For instance, it has been demonstrated that the presence of D-sorbitol in dental products enhances the stability of tin(II) compounds to both oxidation and hydrolysis although such adducts are poorly characterised. It has been stated in the literature that

the aerial stability of a methanolic solution of $SnCl_2$ is greatly enhanced in the presence of a suitable nucleoside such as that in Fig. 3.5.[142] It is suggested that a 1:1 adduct of the type shown is formed in solution resulting in a thirty-fold increase in stability.

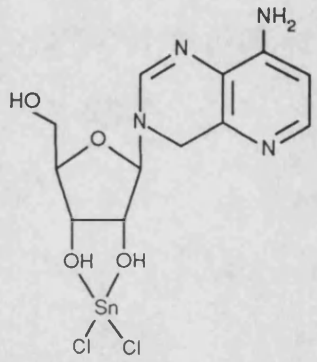

Fig. 3.5 Adduct of $SnCl_2$ with a pentose nucleoside.

3.4 The Interaction of Tin(II) α-D-Glucose-1-phosphate With Fluoride Ions In Aqueous Solution.

A colloidal suspension containing calcium salts of sugar phosphates together with free fluoride ions has recently been patented as an effective and highly stable oral-health fluoride-delivery composition.[140] The Ca^{2+}/sugar phosphate/F^- ratio employed is 1:1:2 which produces colloidal particles which are noted to contain high levels of fluoride which, upon application, is claimed to dramatically increases the fluoride uptake at the enamel surface.. Mention is also made of extending this formulation to incorporate tin(II) salts of suitable sugar phosphates. The patented calcium salts include those of glucose-1-phosphate, glucose-6-phosphate, sucrose sulphate and gluconic acid.

The interaction of tin(II) pyrophosphate, $Sn_2P_2O_7$ (**27**), with fluoride ions in aqueous solution has been discussed in detail in Section 2.3. Briefly, it can be demonstrated that four molar equivalents of a simple ionic fluoride source are required to fully solubilise one mole of $Sn_2P_2O_7$ in water. Physical and spectral data suggests that the product of this interaction is an ionic tin(II) fluoride-pyrophosphate, $Na_4[Sn_2F_4(P_2O_7)]$ (**31**).

This work has also demonstrated that just two molar equivalents of fluoride ions are required to fully solubilise one mole of tin(II) α-D-Glucose-1-phosphate in aqueous solution. Tin(II) α-D-Glucose-1-phosphate (**37**) has quite limited solubility in cold water, however, the addition of two moles of NaF to a suspension in water rapidly yields a highly soluble species (**44**). The net result of these observations is that the overall tin(II): fluoride ratio is the same in each of these solubilisation reactions, i.e. 2 F^- ions per tin atom. As a consequence of these observations, it is possible to speculate that the product of the solubilisation of Sn(αG1P) with 2 NaF might have a similar tin environment to that of the ionic fluoride-pyrophosphate

discussed previously (Equation 3.7).

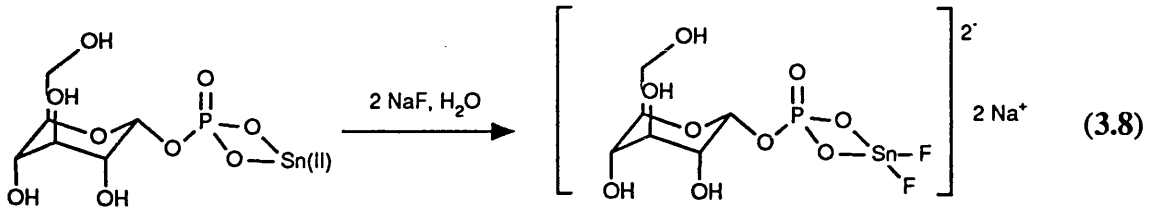

(3.8)

(44)

The infrared data for the solubilised sugar phosphate clearly indicates that the phosphate group is retained. Characteristic peaks due to υ(P=O) (1262cm^{-1}), υ(P-O) (936-1150cm^{-1}) and δ(O-P-O) (530-563cm^{-1}) are all quite strong. The spectrum also shows the presence of peaks due to a fluorotin compound, i.e. υ_1(Sn-F) (495cm^{-1}). This data further supports the formation of a species like that illustrated in equation 3.8.

The ^{1}H and ^{13}C{^{1}H} NMR data confirms the preservation of the cyclic glucose ring within the molecule. The ^{1}H spectrum is virtually indistinguishable from that of (37) which has been discussed previously in Section 3.2.1. This implies that the ring is also in a chair conformation which is slightly puckered about the endocyclic [-C_4-C_5-O-] bonds. Interestingly, the ^{13}C{^{1}H} data shows an additional upfield shift in the positions of several peaks (C_2-C_5) relative to those observed for (37) (Table 3.5). This implies that the extent of intermolecular bonding and intramolecular chelation between the exocyclic hydroxyl groups attached to these carbon atoms and the tin atom are reduced in the solubilised species. This suggests that solubilising (37) causes a partial breakup of the polymeric structure in the solid-state which helps to account for the dramatic change in physical properties.

^{119}Sn Mössbauer and multinuclear NMR data for the products of the two solubilisation reactions are listed in Tables 3.8 and 3.9 respectively together with the Mössbauer data for the two starting materials. For the purposes of comparison, only

the reactions with sodium fluoride are considered, i.e. $Sn_2P_2O_7$ + 4NaF, Sn(αG1P) + 2NaF. Note that the solubilisation of Sn(αG1P) was only performed with NaF as the source of fluoride ion.

Table 3.8 ^{119}Sn Mössbauer data for solubilised tin(II) phosphate compounds.[a]

Compound	δ (mms^{-1})	Δ (mms^{-1})	Γ (mms^{-})^{1}	Γ (mms^{-1})
$Sn_2P_2O_7$ + 4NaF (**31**)	3.00	1.81	1.24	1.13
Sn(αG1P) + 2NaF (**44**)	2.98	1.81	1.04	0.97
$Sn_2P_2O_7$ (**27**)	3.27	1.66	1.34	1.31
Sn(αG1P) (**37**)	3.11	1.78	0.89	0.89

Note:-

[a]Recorded at 78K, relative to SnO_2.

Table 3.9 Multinuclear NMR data for solubilised tin(II) phosphate compounds.

Compound	δ (^{119}Sn) / ppm [a]	δ (^{31}P) / ppm [b]	δ (^{19}F) / ppm [c]
$Sn_2P_2O_7$ + 4NaF (**31**)	-654.1	-8.3	-99.7
Sn(αG1P) + 2NaF (**44**)	-655.1	2.7	-101.4

Notes:-

[a]Referenced to $SnMe_4$: [b]Referenced to H_3PO_4: [c]Referenced to CF_3CO_2H.

In the complete solubilisation of Sn(αG1P), the predicted formation of an ionic fluoride-phosphate complex is consistent with all of the available spectral data, i.e. infrared, Mössbauer, NMR. As predicted, the tin and flourine environments for the pyrophosphate and glucose-1-phosphate species appear identical. The phosphorus NMR data cannot be compared directly.

The reduction in the isomer-shift is due to the increased electronegativity of the fluoride ions bound to tin. The increased electric-field asymmetry brought about by the highly electronegative fluoride ions might also be expected to create an increase in the quadrupole splitting for the solubilised α-D-glucose-1-phosphate. However, in this case, this is not borne out by the experimental data, an insignificant increase of just $0.04 mms^{-1}$ is observed. This suggests that replacing intermolecular Sn-O bonds with Sn-F bonds has little or no overall effect on the charge distribution about tin.

The linewidths in the Mössbauer spectrum for solubilised tin(II) α-D-glucose-1-phosphate are significantly lower than those in the solubilised pyrophosphate. This reflects the presence of only one tin in the molecule, i.e. the likelihood of greater uniformity in the tin coordination. The single peak in the tin NMR shows the presence of just one tin environment when in solution.

Conductivity measurements: The solubilisation of $Sn_2P_2O_7$ with 4 NaF was investigated using conductivity data to determine the number of ions produced by this compound in solution. The results indicated that 4-5 moles of ions were generated by one mole of the tin(II) fluoride-phosphate (Section 2.3). The same experiment was also carried out for the solubilised Sn(αG1P) species, the results of which are presented in Table 3.10.

The conductivity of a 1.0 mMolar solution of the solubilised glucose-1-phosphate indicates that it apparently contains 3 moles of ions per mole of compound. This too is consistent with the formulation predicted for this compound.

Table 3.10 Conductivity measurements for solubilised tin(II) α-D-glucose-1-phosphate.

Compound	Λ_M (Sm^2Kmol^{-1})	Number of ions	Formula
$PtCl_4 . 6NH_3$	52.3	5	$[Pt(NH_3)_6]^{4+} + 4Cl^-$
$PtCl_4 . 5NH_3$	40.4	4	$[Pt(NH_3)_5Cl]^{3+} + 3Cl^-$
$PtCl_4 . 4NH_3$	29.9	3	$[Pt(NH_3)_4Cl_2]^{2+} + 2Cl^-$
$PtCl_4 . 3NH_3$	9.7	2	$[Pt(NH_3)_3Cl_3]^{+} + Cl^-$
$PtCl_4 . 2NH_3$	0.0	0	$Pt(NH_3)_2Cl_4$
Sn(αG1P) + 2 NaF. (44)	25.7	3	$[SnF_2(\alpha G1P)]^{2-} + 2\ Na^+$

Tin EXAFS data has also been obtained for the solubilised form of tin(II) α-D-glucose-1-phosphate (Fig. 3.6). As was the case with the pyrophosphate (Table 2.6), the glass-like nature of the solid does not lend itself to the production of high quality data. However, the experimental data is presented in Table 3.11 and allows interpretation of only the first and second coordination shells. Unfortunately, due to the quality of the data, the predicted coordination numbers might not be very accurate.

Table 3.11 EXAFS data for solubilised tin(II) α-D-glucose-1-phosphate.

Compound	Number of atoms	Atom type	Bond length / Å	Error / Å	R value
Sn(αG1P) + 2NaF (44)	5.12	F	2.07	0.02	20.77
	1.52	O	2.28	0.02	

Like the EXAFS data for solubilised tin(II) pyrophosphate, the data clearly shows the presence of a first coordination shell consisting of Sn-F bonds; these are of average length 2.07Å. A second shell consists of Sn-O bonds of average length 2.28Å. The Sn-F bond lengths of documented tin(II) fluoride species typically range from 1.89 - 2.49Å (Table 1.5), whilst Sn-O bonds are typically 2.06 - 2.47Å in tin(II) phosphate compounds (Table 1.7). The first shell coordination number of 5 is the same as that observed for β-SnF_2 in which the tin exists in an SnF_5E coordination (Section 1.8.1). However, the Mössbauer data for this fluoride (δ, 3.30mms^{-1}; Δ, 2.20mms^{-1}) are very different to the data for the solubilised product (δ, 2.98mms^{-1}; Δ, 1.81mms^{-1}). A very similar situation exists for the EXAFS data for $Sn_2P_2O_7$ + 4NaF.

Mössbauer data for the oxyfluoride, Sn_2OF_2, has been documented (δ, 3.20mms^{-1}; Δ, 3.24mms^{-1}) and shows much closer agreement for δ although Δ is far too high.

The presence of 1-2 O atoms in the second shell supports the formation of a tin(II) fluoride-phosphate. Unfortunately, the data is not sufficiently well resolved to identify a third shell Sn-P separation in this compound. As described previously for the solubilised pyrophosphate (**37**), a solution to this problem lies in the formation of a more symmetrical environment involving multiple [Sn-F-Sn] bridging. A proposed structure is illustrated in Fig. 2.5 which has two central tin atoms, each bridged by four fluorines. Each tin would be further coordinated by the phosphate oxygens of the glucose-1-phosphate.

In conclusion, all of the experimental data indicates that the fate of the tin atoms in $Sn_2P_2O_7$ and Sn(αG1P) is much the same when exposed to fluoride ions. Two moles of ionic fluoride ions are required per tin atom to fully solubilise these otherwise insoluble materials in water. The data indicates that the most likely product of these reactions, in the absence of X-ray structural data, is a complex tin(II) fluoride-phosphate ion.

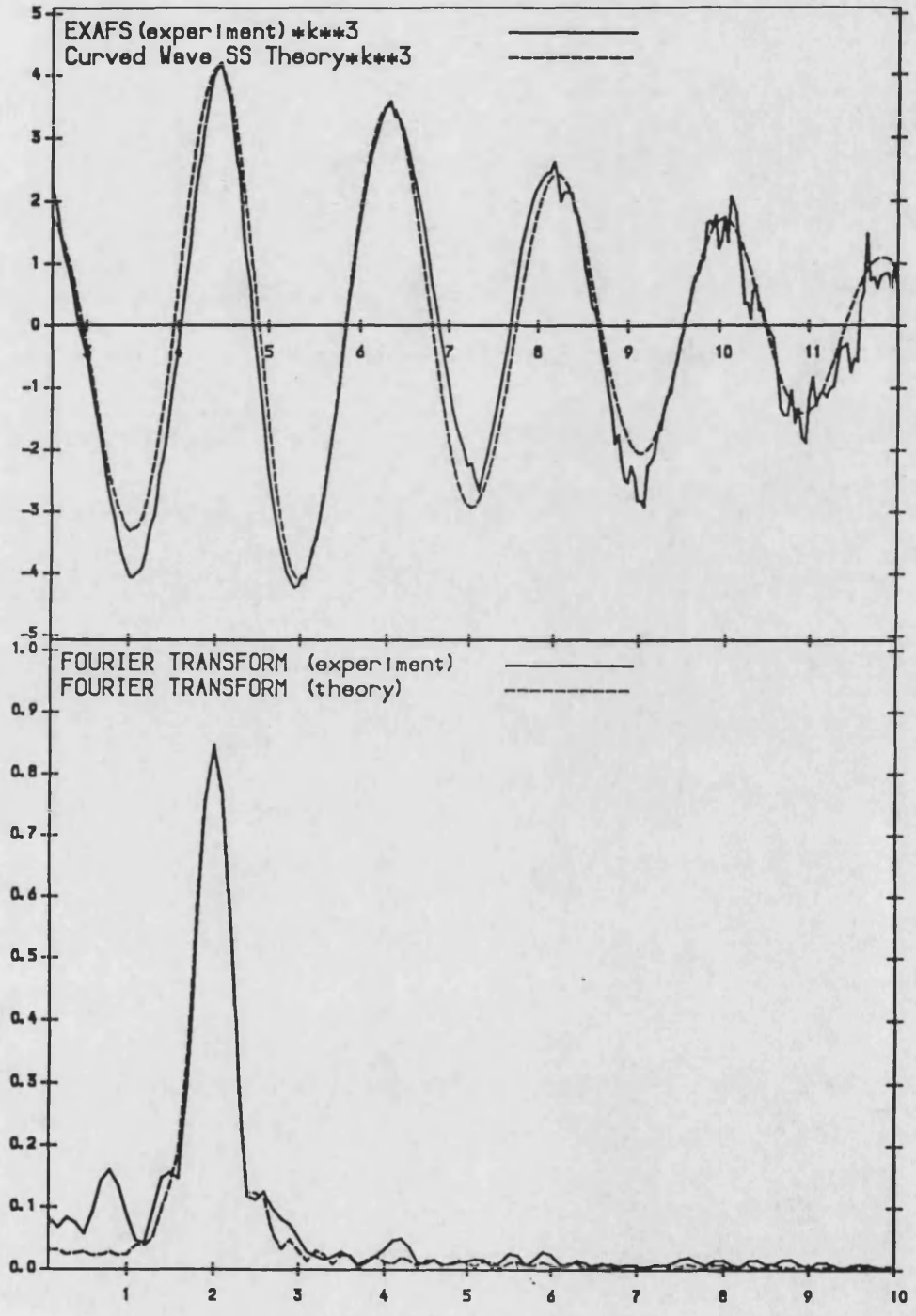

Fig. 3.5 The EXAFS fourier transform curves for Sn(αG1P) + 2 NaF (**44**).

4. TIN(II) SALTS OF CITRIC ACID.

The preceeding two chapters have dealt with the preparation and characterisation of a series of tin(II) phosphate and sugar phosphate compounds. Also, a limited selection of related polyhydroxy-carboxylate salts were discussed in Chapter 3. The chemistry of a further type of tin(II) compound is also of importance in further understanding the interactions occurring within dental formulations, i.e. those compounds formed from tin(II) and the citrate anion. It has previously been described in Section 1.6 that ZCT is a prime anti-plaque active ingredient of a typical commercially available dentifrice. It has been demonstrated at URPSL that the addition of insoluble tin(II) phosphate salts to such ZCT formulations, in order to achieve still greater anti-plaque activity, yields a highly water-soluble tin(II) species. The likelihood is that the interaction between these two active ingredients results in the formation of a soluble tin(II) citrate species *in situ* although this remains unproven.

In this chapter, the preparation and characterisation of a range of simple tin(II) salts of citric acid is discussed. Citric acid (**19**) is an important naturally occurring compound and is found in oranges, lemons, currants, beetroot and many flower and plant seeds. It is also frequently used as a constituent of fruit drinks, pharmaceutical syrups and for adjusting the pH of food products. Citric acid is a tribasic acid [pK_{a1}, 3.13 (R_2CO_2H); pK_{a2}, 4.76 ($-CH_2CO_2H^1$); pK_{a3}, 6.40 ($-CH_2CO_2H^2$) at 25°C] although the hydroxyl proton can also be lost producing a tetravalent $[citrate]^{4-}$ anion although a value for pK_{a4} is not quoted.[174] The deprotonation of the carboxylic acid functions and the α-hydroxyl group in citric acid is illustrated in Scheme 4.1.

There are just two tin(II) compounds of citric acid documented in the literature, i.e. di-stannous citrate, Sn_2(citrate), and di-sodium mono-stannous citrate, Na_2Sn(citrate).[121] The latter, highly water-soluble compound has found use as an effective fruit-juice stabiliser when storing juices in cans. Unfortunately, structural or

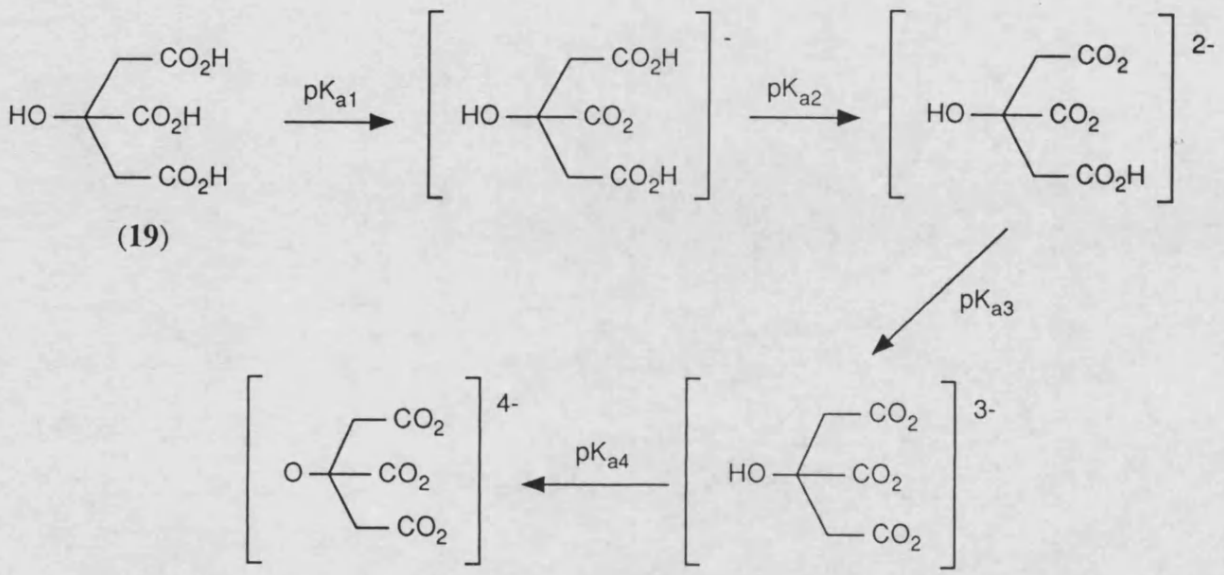

(19)

Scheme 4.1 The successive deprotonation of citric acid (**19**).

spectral data is not quoted in the literature for either of these patented compounds.

Both of these compounds have been prepared according to the literature methods in order to obtain the necessary spectral and analytical data relating to these two formulations. Following these initial preparations a series of analogous tin(II) citrate species were prepared in order to gain further spectral data and to begin to investigate their potential anti-microbial properties (Chapter 5). It was anticipated that suitable examples of tin(II) citrate compounds might prove to be highly effective as anti-plaque agents. It was also hoped that structural studies might also be possible if suitably crystalline samples of these compounds could be isolated.

It was also expected that the polyfunctional nature of citric acid might allow the preparation of a single compound containing both tin(II) and zinc. The di-sodium mono-stannous salt suggests itself as a suitable starting material (*cf.* $ZnSn(P_2O_7)$) for the preparation of mono-zinc mono-stannous citrate, ZnSn(citrate).

In addition to these synthetic studies, the interaction of the insoluble di-stannous salt of citric acid, Sn_2(citrate), with aqueous solutions of fluoride ions was also studied spectroscopically (*cf.* $Sn_2P_2O_7$, Sn(αG1P) in Chapters 2,3 resp.). These interactions were examined using multinuclear NMR and Mössbauer data.

A crystalline tin(IV) citrate was isolated from an aged solution of tetramethyl ammonium mono-stannous citrate. The crystal structure of this compound is reported. Similarly, the crystal structure of a stannous salt of esterified citric acid is also presented, i.e. mono-stannous 1,3-dimethyl citrate.

4.1 Experimental.

Unless indicated otherwise, the preparative and analytical methods follow the same general form as those described for the ionic phosphates in the introduction to Chapter 2, e.g. precautions to prevent oxidation. For all compounds, infrared spectra were recorded as a nujol mull on KBr plates and stannous analyses were determined iodometrically according to equation 2.1.[128] Sodium and potassium analyses were determined by flame-photometry. Zinc analysis was performed by atomic absorbtion spectrophotometry. The ^{119}Sn Mössbauer and multinuclear NMR data are tabulated in the relevant discussions which follow. Unless indicated otherwise, all NMR data was recorded on a saturated solution in D_2O at ambient temperature.

4.1.1 *Synthesis of Anhydrous Di-stannous Citrate,* $Sn_2(C_6H_4O_7)$ (**51**).[121]

Anhydrous citric acid (2.11g, 11.0mmol) was dispersed into 40ml of thoroughly de-oxygenated water with rapid stirring until fully dissolved. To this clear solution solid $SnCl_2$ (4.46g, 23.5mmol) was added and the mixture allowed to stir for 10 minutes until a clear solution was formed. 20ml of 2M NaOH solution was added dropwise to the reaction mixture with stirring whilst also rapidly purging the flask with N_2. As the pH rose to 5.0 and above, a dense white precipitate was formed. The solid product was rapidly filtered on a Büchner-funnel and washed with successive aliquots of water, ethanol and ether. In order to remove the water held within the solid, it was necessary to dry the solid *in vacuo* whilst warming to 70 - 80°C. The product was a fine, white powder. Yield: 4.3g (92%). Analysis, found (calc. for $C_6H_4O_7Sn_2$): C, 16.6 (16.9); H, 1.27 (1.65); Sn(II), 53.8 (55.8)%. Selected infrared data: 1553cm^{-1} (*st, br*) $\upsilon_{as}(CO_2Sn)$; 489cm^{-1} (*m, br*) υ(Sn-O). ^{13}C MAS-NMR data: 48.8 (CH_2); 52.9 (CH_2); 79.9 (tert. *C*); 178.4 (CH_2CO_2Sn); 181.3ppm (R_2CO_2Sn).

4.1.2 *Synthesis of Di-sodium Mono-stannous Citrate Monohydrate,* $Na_2Sn(C_6H_4O_7).H_2O$ (**52**).[121]

Solid $SnCl_2$ (9.50g, 50.1mmol) was dissolved in 25ml of thoroughly de-oxygenated water. To this solution was slowly added 50ml of 2M NaOH solution whilst purging the flask with N_2. A dense white precipitate of hydrous tin(II) oxide was formed. This solid was rapidly filtered, washed with water and immediately re-suspended in 25ml of thoroughly de-oxygenated water. Anhydrous citric acid (9.60g, 50.0mmol) was added to this suspension and the mixture allowed to stir at room temperature for 10 minutes. A further 50ml of 2M NaOH solution were added dropwise to the reaction mixture until the slurry dispersed and a clear solution was formed. This solution was evaporated to dryness on a rotary-evaporator yielding a colourless glass. This solid was dispersed into 20ml of iso-propanol, filtered and thoroughly dried *in vacuo*. Yield: 11.9g (96%). Analysis, found (calc. for $C_6H_6O_8Na_2Sn$): C, 19.9 (19.4); H, 1.90 (1.62); Na, 13.2 (12.4); Sn(II), 27.3 (32.0)%. Selected infrared data: 3393cm^{-1} (*st, br*) υ(H-O-H); 1635cm^{-1} (*m, sh*) δ(H-O-H); 1593cm^{-1} (*st, br*) $\upsilon_{as}(CO_2Sn)$; 500-575cm^{-1} (*br*) υ(Sn-O). ^{1}H NMR data (D_2O): 2.74ppm (*q*, 4H, *J*=15.3Hz) (CH_2). ^{13}C NMR data: 46.7 (CH_2); 76.1 (tert. *C*); 177.2 (CH_2CO_2Sn); 183.7ppm (R_2CO_2Sn).

4.1.3 *Synthesis of Hydrated Di-potassium Mono-stannous Citrate ,* $K_2Sn(C_6H_4O_7).1.5H_2O$ (**53**).

The preparation of (**53**) followed exactly the same procedure as the preparation of (**52**) described in section 4.1.2 above with the exception that 2M KOH solution was used in place of the 2M NaOH. Yield: 18.7g (91%). Analysis, found (calc. for $C_6H_7O_{8.5}SnK_2$): C, 17.6 (17.5); H, 1.73 (1.70); K, 17.9 (19.0); Sn(II), 26.3 (28.8)%. Selected infrared data: 3373cm^{-1} (*st, br*) υ(H-O-H); 1650cm^{-1} (*m, br*) δ(H-O-H); 1599cm^{-1} (*st, br*) $\upsilon_{as}(CO_2Sn)$; 480-500cm^{-1} (*m, br*) υ(Sn-O). ^{1}H NMR

data (D_2O): 2.78ppm (*q*, 4H, *J*=15.3Hz) (CH_2). ^{13}C NMR data: 47.2 (CH_2); 76.6 (tert. *C*); 177.2 (CH_2CO_2Sn); 184.4ppm (R_2CO_2Sn).

4.1.4 *Synthesis of Hydrated Di-ammonium Mono-stannous Citrate,* $(NH_4)_2Sn(C_6H_4O_7)$ (**54**).

The preparation of (**54**) followed exactly the same procedure as the preparation of (**52**) described in section 4.1.2 above with the exception that 2M NH_4OH solution was used in place of the 2M NaOH. Yield: 15.4g (90%). Analysis, found (calc. for $C_6H_{12}O_7N_2Sn$): C, 21.3 (21.0); H, 4.28 (3.50); N, 8.17 (8.27); Sn(II), 26.6 (34.6). Selected infrared data: 3192cm^{-1} (*w, br*) υ(H-O-H); 1684cm^{-1} (*w, br*) δ(H-O-H); 1599cm^{-1} (*st, br*) $\upsilon_{as}(CO_2Sn)$; 500-570cm^{-1} (*br*) υ(Sn-O). ^1H NMR data: 2.72 (*q*, 4H, *J*=15.4Hz) (CH_2); 7.13ppm (*br.s*, 8H) (NH_4). ^{13}C NMR data: 46.3 (CH_2); 75.6 (tert. *C*); 176.7 (CH_2CO_2Sn), 183.0ppm (R_2CO_2Sn).

4.1.5 *Synthesis of Mono-tetramethylammonium Mono-stannous Citrate Di-methanolate,* $[(CH_3)_4N]Sn(C_6H_5O_7).2CH_3OH$ (**55**).

Solid $SnCl_2$ (4.75g, 25.1mmol) was dissolved in 15ml of thoroughly de-oxygenated water. To this clear solution, 25ml of 2M NaOH solution was added dropwise whilst continuously purging the reaction flask with N_2. A dense white precipitate of hydrous tin(II) oxide was formed. This solid was rapidly filtered on a Schlenk-stick, washed with water and immediately re-suspended in 15ml of thoroughly de-oxygenated water. Anhydrous citric acid (4.80g, 25.0mmol) was added to this suspension and the mixture allowed to stir at room temperature for 10 minutes. Tetramethylammonium hydroxide pentahydrate, $(CH_3)_4NOH.5H_2O$ (9.15g, 51.0mmol) was dissolved in 25ml of de-oxygenated water and the fresh solution was added dropwise to the reaction mixture until the slurry had dispersed and a completely clear solution was formed. This solution was evaporated to dryness on a

rotary-evaporator yielding a colourless, hygroscopic oil. This oil was dissolved into 20ml of methanol and allowed to precipitate overnight in the refrigerator. The product was filtered on a Schlenk-stick, washed with cold ether and thoroughly dried *in vacuo*. Yield: 7.4g (66%). Analysis, found (calc. for $C_{12}H_{26}O_9NSn$): C, 32.5 (32.3); H, 5.61 (5.61); N, 3.57 (3.10); Sn(II), 25.4 (26.7)%. Selected infrared data: 1616cm^{-1} (*st, br*) $\upsilon_{as}(CO_2Sn)$; 567cm^{-1} (*w, br*) υ(Sn-O). ^{1}H NMR data (D_2O): 2.73 (*q*, 4H, *J*=15.1Hz) (CH_2); 3.10 (*s*, 12H) [$N(CH_3)_4$]; 3.26ppm (*s*, 6H) (CH_3OH). ^{13}C NMR data: 46.1 (CH_2); 48.4, (CH_3OH); 54.5, 54.7, 54.8, 54.8 [$N(CH_3)_4$]; 76.1 (tert. *C*); 176.0, (CH_2CO_2Sn), 183.4ppm (R_2CO_2Sn).

4.1.6 *Synthesis of Hydrated Mono-zinc Mono-stannous Citrate*, $ZnSn(C_6H_4O_7)$ (**56**).

Di-ammonium mono-stannous citrate (2.50g, 7.3mmol) (**54**) was dissolved in 25ml of thoroughly de-oxygenated water. Solid $ZnCl_2$ (0.99g, 7.3mmol) was added to this solution and the mixture refluxed under N_2 for 12 hours. After this time, a dense white precipitate had formed around the inner surface of the flask. This solid was carefully suspended into the supernatant liquid. The resulting suspension was allowed to cool to room temperature, and 5ml of methanol added to assist the precipitation. The product was filtered on a Schlenk-stick, washed with successive aliquots of water, ethanol and ether and thoroughly dried *in vacuo*. Yield: 2.1g (77%). Analysis, found (calc. for $C_6H_4O_7SnZn$): C, 19.9 (19.4); H, 1.61 (1.08); Sn(II), 28.3 (31.8); Zn, 14.2 (17.6)%. Selected infrared data: 3420cm^{-1} (*w, br*) υ(H-O-H); 1556-1579cm^{-1} (*st*) $\upsilon_{as}(CO_2M)$; 500-557cm^{-1} (*m, br*) υ(M-O) (M = Sn, Zn). NMR data was not available due to the poor solubility of the compound.

4.1.7 *Synthesis of 1,3-dimethyl Citrate Monohydrate*, $(HO)C(CO_2H)$-$(CH_2CO_2CH_3)_2.H_2O$ (**57**).[143]

Anhydrous citric acid (50.00g, 260.4mmol) was dissolved in 250ml of

methanol together with 2.0g of 98% sulphuric acid. The mixture was refluxed together for one hour. The reaction mixture was allowed to cool to room temperature and 250ml of cold water added with stirring. The solution was neutralised with solid calcium carbonate to remove excess citric and sulphuric acid as their insoluble calcium salts. The suspension was filtered yielding a clear solution which was evaporated to dryness *in vacuo*. This yielded a colourless glass which was redissolved in 100ml of cold water. This solution was filtered to remove traces of insoluble salts and the filtrate was acidified to pH 4.5 with conc. hydrochloric acid. This yielded a white precipitate which was filtered and twice recrystallised from water. The crystalline product was filtered on a Büchner-funnel and air-dried. Yield: 18.0g (29%). Analysis, found (calc. for $C_8H_{14}O_8$): C, 40.6 (40.3); H, 5.97 (5.88). Melting point: 122°C (Lit. 125°C).[143] Selected infrared data: 3420cm^{-1} (*st, sh*) υ(H-O-H); 1742cm^{-1} (*st, sh*) $\upsilon_{as}(CO_2H)$; 1717cm^{-1} (*st, sh*) $\upsilon_{as}(CO_2Me)$; 1638cm^{-1} (*m, br*) υ(H-O-H); 1232cm^{-1} (*m, sh*) $\upsilon_s(CO_2Me)$. ^{1}H NMR data ($CDCl_3$): 2.87 (*q*, 4H, *J*=15.4Hz) (CH_2); 3.66 (*s*, 6H) (OCH_3); 5.00ppm (*br.s*, 2H) (H_2O). ^{13}C NMR data: 43.9, 44.2 (CH_2); 52.2, 53.2 (OCH_3); 74.2 (tert. *C*); 171.7, 171.8 ($CH_2CO_2CH_3$); 176.4ppm (R_2CO_2H).

4.1.8 *Synthesis of Anhydrous 1,3-dimethyl-2-^{t}butyl Citrate,* (HO)C[CO_2-($C(CH_3)_3$)]($CH_2CO_2CH_3$)$_2$ (**58**).[144]

1,3-dimethyl citrate (6.00g, 25.2mmol) (**57**) was suspended in 50ml of tertiary-butyl acetate. 1.0ml of 60% perchloric acid solution was carefully added to this suspension and the mixture stirred at room temperature for 72 hours. After this time, the reaction mixture was slowly poured into 100ml of saturated sodium hydrogen carbonate solution and extracted with ether. This procedure was repeated twice (2 x 150ml) and the combined ether extracts evaporated to dryness on a rotary-evaporator. 150ml of 60/80° petrol were added to the residue and the oil

dissolved with rapid stirring. The by-product of the reaction, i.e. trimethyl citrate, readily crystallises from this solution and can be efficiently removed by filtration. The clear filtrate was subsequently evaporated to yield the desired product as a a colourless viscous oil. Yield: 5.4g (78%). Analysis, found (calc. for $C_{12}H_{20}O_7$): C, 53.8 (52.2); H, 7.92 (7.30)%. Selected infrared data (Liq. film): 3489cm^{-1} (*st, sh*) υ(C-O-H); 1757cm^{-1} (*st, sh*) $\upsilon_{as}(CO_2Bu^t)$; 1728cm^{-1} (*st, sh*) $\upsilon_{as}(CO_2Me)$. ^{1}H NMR data ($CDCl_3$): 1.51 (*s*, 9H) [$(CH_3)_3C$]; 2.82 (*q*, 4H, *J*=15.4Hz) (CH_2); 3.69ppm (*s*, 6H) (OCH_3). ^{13}C NMR data: 27.5 [$(CH_3)_3C$]; 43.2 (CH_2); 51.6 (OCH_3); 72.9 (tert. *C*); 83.1 [$(CH_3)_3C$]; 169.9 ($CH_2CO_2CH_3$); 172.1ppm ($R_2CO_2u^t$).

4.1.9 *Synthesis of Anhydrous 2-^{t}butyl Citrate,* $(HO)C[CO_2(C(CH_3)_3)](CH_2CO_2H)_2$ (**59**).[144]

1,2-dimethyl-2-^{t}butyl citrate (5.00g, 18.1mmol) (**58**) was dissolved in 20ml of methanol. 20ml of 2M NaOH solution were slowly added to this solution and the mixture stirred at room temperature for 3 hours. The solvent volume was then reduced by 50% on a rotary-evaporator and the resulting aqueous solution acidified to pH 3.0 with conc. hydrochloric acid. The product was extracted with 3 x 100ml of ethyl acetate and the extracts combined. The ethyl acetate was removed *in vacuo* yielding a white solid product. The crude material was recrystallised from boiling ethyl acetate / hexane yielding a white, crystalline solid. Yield: 1.8g (41%). Analysis, found (calc. for $C_{10}H_{16}O_7$): C, 48.2 (48.4); H, 6.50 (6.57). Melting point: 124°C (Lit. 124°C).[144] Selected infrared data: 3485cm^{-1} (*m, sh*) υ(O-H); 1755cm^{-1} (*st, sh*) $\upsilon_{as}(CO_2Bu^t)$; 1705cm^{-1} (*st, sh*) $\upsilon_{as}(CO_2H)$; 1260-1311cm^{-1} (*m*) υ_s(CO). ^{1}H NMR data ($CDCl_3$): 1.41 (*s*, 9H) (CH_3); 2.84ppm (*q*, 4H, *J*=15.1Hz) (CH_2). ^{13}C NMR data: 26.5 [$(CH_3)_3C$]; 43.0 (CH_2); 73.0 (tert. *C*); 84.0 [$(CH_3)C$]; 172.9 ($R_2CO_2Bu^t$); 173.1ppm (CH_2CO_2H).

4.1.10 *Synthesis of Mono-stannous 1,3-Dimethyl Citrate Mono-methanolate,* $C[(O)CO_2Sn](CH_2CO_2CH_3)_2.CH_3OH$ (**60**).

1,3-dimethyl citrate (250.0mg, 1.1mmol) (**57**) was dissolved in 25ml of thoroughly de-oxygenated, dry, distilled methanol. Commercially available tin(II) acetate (249.0mg, 1.1mmol) was carefully added to this solution taking great care to exlude atmospheric oxygen. The reaction mixture was refluxed for 2 hours under an inert N_2 atmosphere. After this time, a turbid off-white suspension remained which was filtered hot on a Schlenk-stick. The clear filtrate was allowed to cool slowly to room temperature where, upon standing, a mass of small colourless crystals were precipitated. The crystals were filtered on a Schlenk-stick and washed with a little ice-cold ether. Yield: 0.36g (89%). Analysis, found (calc. for $C_9H_{14}O_8Sn$): C, 27.6 (29.2); H, 3.53 (3.79). Selected infrared data: 1734cm^{-1} (*st, sh*) $\upsilon_{as}(CO_2Me)$; 1561cm^{-1} (*st, br*) $\upsilon_{as}(CO_2Sn)$; 1270-1377cm^{-1} (*m*) $\upsilon_s(CO)$; 569cm^{-1} (*m, sh*) υ(Sn-O). ^{1}H NMR data (d_6-DMSO): 2.74 (*q*, 4H, *J*=15.3Hz) (CH_2); 3.38 (*s*, 3H) (CH_3OH); 3.55ppm (*s*, 6H) (OCH_3). ^{13}C NMR data: 45.2 (CH_2); 48.9 (CH_3OH); 51.3 (OCH_3); 75.7 (tert. *C*); 172.0 (CH_2CO_2Me); 182.0ppm (R_2CO_2Sn).

4.1.11 *Attempted Synthesis of Mono-stannous Bis-1,3-dimethyl-2-^{t}butyl Citrate,* $Sn[OC(CO_2Bu^t)(CH_2CO_2CH_3)_2]_2$ (**61**).

1,3-dimethyl-2-^{t}butyl citrate (0.71g, 2.6mmol) was dissolved in 10ml of freshly distilled toluene which was thoroughly de-oxygenated. Freshly-prepared tin(II) bis-methoxide (0.23g, 1.3mmol) was carefully added to this solution taking care to exclude atmospheric oxygen and water. The resulting suspension was gently refluxed for 2 hours yielding a slightly turbid solution. This solution was filtered hot on a Schlenk-stick and the clear filtrate allowed to stand overnight at room temperature. A mass of small, colourless crystals were formed which were collected by filtration and washed with a little ice-cold ethanol and ether. Yield: 0.11g

(12.7%). Contrary to the expected stannous citrate ester compound, the product appeared to be an adamantane [Sn-O] cage compound. Analysis, found (calc. for $C_4H_{12}O_8Sn_6$): C, 3.7 (5.3); H, 1.04 (1.33)%. Clearly, the analysis does not fit to the expected compound (calc. for $C_{24}H_{38}O_{14}Sn$): C, 43.1; H, 5.68%. Selected infrared data: 547cm^{-1} (*st, br*) υ(Sn-O).

4.1.12 *Attempted Synthesis of Mono-stannous 2-^{t}butyl Citrate,* Sn[$(O_2CCH_2)_2$-C(OH)(CO_2Bu^t)] (**62**).

Tin(II) methoxide (0.15g, 0.83mmol) was dissolved in 25ml of thoroughly de-oxygenated n-butanol with gentle warming. Solid 2-^{t}butyl citrate (0.21g, 0.83mmol) (**59**) was added to this solution with stirring and the reaction mixture refluxed for 30 minutes. Initially, a colourless, gelatinous precipitate was formed. However, upon refluxing, a fine white precipitate was produced. The suspension was allowed to cool to room temperature and the solid collected by filtration on a Schlenk-stick. The solid-cake was washed with successive aliquots of ethanol and ether and the insoluble white powder thoroughly dried *in vacuo*. Yield: 0.09g (44%). The analysis for this compound suggests that the ester group is lost resulting in the formation of Sn_2(citrate) (**51**). Analysis, found (calc. for $C_6H_4O_7Sn_2$): C, 16.9 (16.9); H, 1.24 (1.65)%. Clearly, the data does not fit to that of the expected compound (calc. for $C_{10}H_{14}O_7Sn$): C, 32.9; H, 3.84%. Selected infrared data: 1541cm^{-1} (*st, br*) $\upsilon_{as}(CO_2Sn)$; 494cm^{-1} (*m, br*) υ(Sn-O).

4.1.13 *Synthesis of Anhydrous Mono-stannous 1,3-di-^{n}butyl Citrate,* C[(O)(CO_2)Sn][$CH_2CO_2(CH_2)_3CH_3$] (**63**).

Tin(II) methoxide (0.38g, 2.1mmol) was dissolved in 25ml of thoroughly de-oxygenated n-butanol with gentle warming. 1,3-dimethyl citrate (0.50g, 2.1mmol) (**57**) was carefully added to the solution of soluble tin(II) ^{n}butoxide and the reaction

mixture gently refluxed for 30 minutes under an atmosphere of N_2. The resulting colourless solution was allowed to cool slowly to room temperature whereupon a fine, white precipitate was formed. The product was filtered on a Schlenk-stick and washed with ice-cold ether. Yield: 0.64g (72%). Analysis, found (calc. for $C_{14}H_{22}O_7Sn$): C, 38.8 (39.9); H, 5.16 (5.23)%. Selected infrared data: 1740cm^{-1} (*st, sh*) $\upsilon_{as}(CO_2{}^nBu)$; 1543cm^{-1} (*st, br*) $\upsilon_{as}(CO_2Sn)$; 1365-1377cm^{-1} (*m*) $\upsilon_s(CO)$; 523cm^{-1} (*m, br*) υ(Sn-O). ^{1}H NMR data ($CDCl_3$): 0.91 (*t*, 6H, *J*=6.7Hz) (CH_3); 1.36, 1.58 (*m*, 8H) [$CH_3(CH_2)_2$); 2.88 (*q*, 4H, *J*=15.3Hz) (CH_2); 4.10ppm (*t*, 4H, *J*=6.7Hz) (OCH_2). ^{13}C NMR data: 13.1 (CH_3); 19.0 (CH_2); 30.5 (CH_2); 43.6 (CH_2CO_2); 65.5 (OCH_2); 75.7 (tert. *C*); 173.0 ($CH_2CO_2{}^nBu$); 180.6ppm (R_2CO_2Sn).

4.1.14 *Synthesis of Bis-citrato Di-tetramethylammonium Tin(IV) Heptahydrate,* $\{Sn[C(O)(CO_2)(CH_2CO_2)(CH_2CO_2H)]\}^{2-}.2[(CH_3)_4N^+].7H_2O$ (**64**).

A dilute aqueous solution of mono-tetramethylammonium mono-stannous citrate di-methanolate, $Sn(C_6H_4O_7)(N(CH_3)_4).2CH_3OH$ (**55**), was allowed to stand in an open conical flask. After several weeks, the clear solution had evaporated to a colourless, viscous oil from which a crop of crystals formed on further prolonged standing. These crystals could not be separated from the supernatant oil by filtration. A small number of crystals were removed by hand and carefully washed with a little ether. Analysis, found (calc. for $C_{20}H_{48}O_{21}N_2Sn$): C, 33.8 (33.9); H, 6.02 (5.80); N, 4.0 (4.0)%. Selected infrared data: 1727cm^{-1} (*m, sh*) $\upsilon_{as}(CO_2H)$; 1644cm^{-1} (*st, br*) $\upsilon_{as}(CO_2Sn)$. ^{1}H NMR data (CD_3OD): 2.80 (*m*, 4H) (CH_2); 3.19ppm (*s*, 12H) [$NCH_3)_4$]. ^{13}C NMR data: 56.5 [$N(CH_3)_4$]; 47.1, 48.8 (CH_2); 76.4 (tert. *C*); 176.0 (CH_2CO_2H); 178.2 (CH_2CO_2Sn); 183.8ppm (R_2CO_2Sn).

4.1.15 *The Interaction of Di-stannous Citrate With Ionic Fluorides in Aqueous Solution* (**65 - 68**).

In a typical experiment, using sodium fluoride as the fluoride source, Sn_2(citrate) (**51**) (1.0g, 2.4mmol) was slurried into 40ml of thoroughly de-oxygenated water with rapid stirring. Solid sodium fluoride was slowly added to this suspension until a clear solution was obtained; it was found that at least 4 molar equivalents of NaF (0.39g, 9.6mmol) were required to give a reproducibly clear solution. Attempted crystallisation of the soluble species failed, simply yielding a very fine, flock-like precipitate which was unsuitable for filtration. Similar results were obtained upon the addition of solvents to the solution, e.g. ethanol. Therefore, in order to obtain spectral data on this water-soluble compound it was necessary to remove the solvent by evaporation at reduced pressure. The resulting product (**65**) was a colourless, glassy solid which was found to have a moderately high water content and was amorphous to X-rays. Analytical data is not quoted due to the method of obtaining a solid product (i.e. total evaporation of solvent). Yield: 1.35g (98%). The additional solubilisation reactions with different ionic fluorides were carried out in an identical manner to that above with NaF, yielding very similar results, i.e. the products with the simple ionic fluorides KF (**66**) and NH_4F (**67**) were also readily water-soluble, colourless glasses. The only exception was the product obtained by reaction of Sn_2(citrate) with tetra-n-butyl ammonium fluoride. This compound (**68**), which was observed to be quite hygroscopic, readily formed a colourless, viscous oil upon exposure to atmospheric moisture (*cf.* $Sn_2P_2O_7$ + $4Bu^n_4NF$) and was difficult to handle. In each case, the product had a high water content (*vide infra*) and spectral data was very similar.

Sodium fluoride product (**65**): Selected infrared data: 3337cm^{-1} (*st, br*) υ(H-O-H); 1651cm^{-1} (*st, sh*) δ(H-O-H); 1594cm^{-1} (*st, br*) $\upsilon_{as}(CO_2Sn)$; 518cm^{-1} (*m, br*) υ_1(Sn-F); 448cm^{-1} (*w, sh*) υ_3(Sn-F); 438cm^{-1} (*m, br*) υ(Sn-O). ^{1}H NMR data

(D_2O): 2.74ppm (*q*, 4H, *J*=15.3Hz) (CH_2). ^{13}C NMR data: 46.6 (CH_2); 76.1 (tert. *C*); 177.4 (CH_2CO_2Sn); 183.9ppm (R_2CO_2).

Potassium fluoride product (**66**): Selected infrared data: 3347cm^{-1} (*st, br*) υ(H-O-H); 1648cm^{-1} (*st, sh*) δ(H-O-H); 1588cm^{-1} (*st, br*) $\upsilon_{as}(CO_2Sn)$; 518cm^{-1} (*m, br*) υ_1(Sn-F); 447cm^{-1} (*w, sh*) υ_3(Sn-F); 436cm^{-1} (*m, br*) υ(Sn-O). ^1H NMR data (D_2O): 2.78ppm (*q*, 4H, *J*=15.3Hz) (CH_2). ^{13}C NMR data: 47.2 (CH_2); 76.6 (tert. *C*); 177.2 (CH_2CO_2Sn); 184.4ppm (R_2CO_2Sn).

Ammonium fluoride product (**67**): Selected infrared data: 3328cm^{-1} (*st, br*) υ(H-O-H); 1648cm^{-1} (*st, sh*) δ(H-O-H); 1594cm^{-1} (*st, br*) $\upsilon_{as}(CO_2Sn)$; 518cm^{-1} (*m, br*) υ_1(Sn-F); 445cm^{-1} (*w, sh*) υ_3(Sn-F); 434cm^{-1} (*m, br*) υ(Sn-O). ^1H NMR data: 2.73ppm (*q*, 4H, *J*=15.1Hz) (CH_2); 7.20ppm (*br.s*, 8H) (NH_4). ^{13}C NMR data: 46.3 (CH_2); 75.7 (tert. *C*); 176.8 (CH_2CO_2Sn); 182.7ppm (R_2CO_2Sn).

Tetra-n-butylammonium product (**68**): Selected infrared data: 3346cm^{-1} (*st, br*) υ(H-O-H); 1648cm^{-1} (*st, sh*) δ(H-O-H); 1578cm^{-1} (*st, br*) $\upsilon_{as}(CO_2Sn)$; 518cm^{-1} (*m, br*) υ_1(Sn-F); 450cm^{-1} (*w, sh*) υ_3(Sn-F); 438cm^{-1} (*m, br*) υ(Sn-O). ^1H NMR data ($CDCl_3$): 0.91 (*t*, 6H, *J*=6.7Hz) (CH_3); 1.36, 1.58 (*m*, 8H) [$CH_3(CH_2)_2$]; 2.88 (*q*, 4H, *J*=15.4Hz) (CH_2CO_2); 4.03ppm (*t*, 4H, *J*=6.7Hz) (NCH_2). ^{13}C NMR data: 13.1 (CH_3); 19.0 (CH_3CH_2); 30.5 ($CH_3CH_2CH_2$); 43.6 (CH_2CO_2); 65.5 (CH_2N); 75.7 (tert. *C*); 173.0 (CH_2CO_2Sn), 180.6ppm (R_2CO_2Sn).

4.2 Preparation and Characterisation of Tin(II) Citrate Compounds.

A range of tin(II) salts of citric acid have been prepared and characterised. Two of these compounds have been previously been patented, i.e. di-stannous citrate and di-sodium mono-stannous citrate.[121] Unfortunately, very little data is quoted in support of these two formulations. These compounds have been re-prepared in order to gain access to a wider body of experimental data, e.g. Mössbauer parameters. A range of analogous species have also been prepared, e.g. di-potassium mono-stannous citrate.

Di-stannous citrate, $Sn_2(C_6H_4O_7)$ (**51**), was prepared from a 2:1 mixture of Sn^{2+} and citric acid according to equation 4.1.

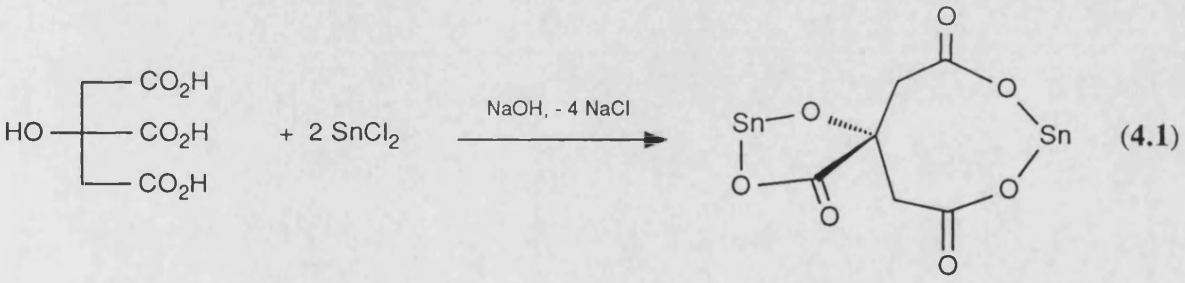

(**4.1**)

(**51**)

This reaction occurred in very good yield in accordance with results quoted in the the literature. The initial precipitate appeared to be quite freely hydrated and lost a great deal of water whilst drying *in vacuo*. The final dried product was a fine white powder with very limited solubility in polar solvents. The absence of characteristic water peaks in the infrared spectrum [e.g. υ(HOH), 3000-3400cm^{-1}] is in agreement with the analytical data in suggesting that the final product is the anhydrous di-stannous salt. The physical properties of this solid suggest that the compound has a polymeric structure in the solid-state. The product is illustrated as a simple monomeric species with two coordinate tin atoms. It is likely that intermolecular

interactions will increase the coordination around the tin atoms. MAS-NMR data (^{13}C, ^{119}Sn) was collected for this compound in a collaboration with URPSL. The ^{13}C NMR spectrum has two distinct peaks relating to the -CH_2- groups at 48.8, 52.9ppm. This suggests that either (a) two symmetrical isomers are present or (b) the citrate group is coordinated asymmetrically in the solid-state. The former is less likely, as this would give rise to the 'doubling' of all peaks in the ^{13}C spectrum. However, only a single peak (79.9ppm) for the tertiary carbon atom is detected. Two carboxylate peaks are also observed (178.4, 181.3ppm) for the terminal and central carboxylates respectively. The presence of two peaks is surprising, indicating that only two carboxylate environments are present. This tends to support the prediction that the citrate molecule coordinates in a symmetrical fashion, i.e. the terminal carboxylates are equivalent which contradicts the presence of two -CH_2- groups. The most likely explanation is that the two terminal [CH_2CO_2Sn] groups are insufficiently different to be distinguished by ^{13}C NMR.

Hydrated di-sodium mono-stannous citrate, $Na_2Sn(C_6H_4O_7).H_2O$ (**52**), di-potassium mono-stannous citrate, $K_2Sn(C_6H_4O_7).1.5H_2O$ (**53**) and di-ammonium mono-stannous citrate $(NH_4)_2Sn(C_6H_4O_7).xH_2O$ (**54**) were prepared according to equation 4.2.

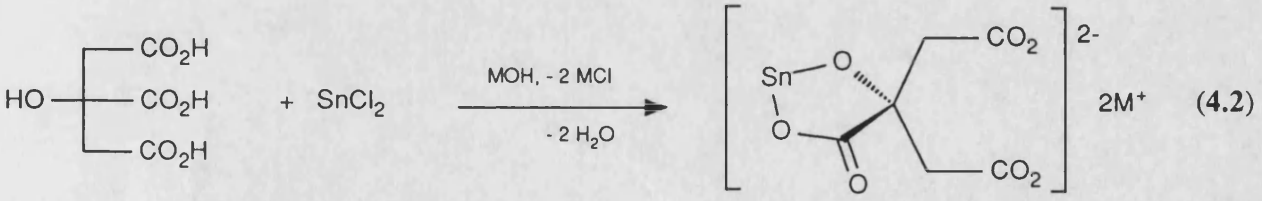

(**4.2**)

M = Na^+ (**52**), K^+ (**53**), NH_4^+ (**54**)

These reactions are effectively the same as that for the preparation of (**51**) with a change in the (Sn^{2+}):citrate ratio to an equimolar stoichiometry. These reactions

also occur in very good yield as in the literature preparation of (**52**).

The presence of strong υ(HOH) bands in the infrared data of (**52**) (3393, 1635cm^{-1}) is in agreement with the analytical data in suggesting that the di-sodium product is hydrated. The product of this first reaction was a glassy white solid which was readily soluble in water but insoluble in all other coordinating solvents. The high water-solubility suggests that this compound is quite ionic and that covalent intermolecular interactions are relatively weak. However, in the solid-state, the coordination number of the tin atom as drawn above will be increased above two due to weaker Sn-O interactions. This compound is amorphous to X-rays and produces no discernable diffraction pattern for a powdered sample.

The ^{1}H NMR spectrum of (**52**) produces an AB pseudo quartet (2.74ppm) which can be assigned to the presence of a pair of diastereotopic CH_2 groups, i.e. CH_aH_b. This characteristic pattern is actually caused by the convergence of a pair of doublets, each of very similar chemical shift, δ_1 and δ_2. This characteristic pattern has been observed in both citric acid and other similar metal citrate compounds, e.g. $Al_2(cit)_2(H_2O)_6$.[141,175,186] The coupling constant, ^2J(H-H), for this compound (15.3Hz) is comparable to that in the parent ligand, citric acid, where the coupling is only slightly greater at 15.5Hz.[226] The position of this CH_2 signal has also been found to be quite independant of external factors such as pH.

The $^{13}C\{^1H\}$ spectrum of (**52**) shows just a single peak for the pair of CH_2 groups (46.7ppm) indicating that the two methylene carbon groups are magnetically equivalent. Two carboxylate peaks are also observed for this compound at 177.2 and 183.7ppm in a 2:1 ratio respectively. The central, tertiary C(OH) signal (76.1ppm) is shifted downfield slightly (74.2ppm in citric acid). This data suggests that the citrate is symmetrically coordinated to tin through the central carboxylate and the α-hydroxyl oxygen as shown.

The preparation of hydrated di-potassium mono-stannous citrate, $K_2Sn(C_6H_4O_7).1.5H_2O$ (**53**) also occurs in very good yield as in the preparation of the

di-sodium salt (**52**). The presence of characteristic υ(HOH) bands in the infrared data (3373, 1650cm^{-1}) is in agreement with the analytical data in suggesting that this product is also hydrated. The white, glassy product was extremely water-soluble at all temperatures but effectively insoluble in other coordinating solvents. The implication is that this solid is also quite ionic although it is likely that the tin atom will exhibit a higher coordination number than that shown in the illustration above. Similarly, as for (**52**), this solid is amorphous to X-rays and shows no powder-diffraction pattern.

The ^{1}H and ^{13}C{^{1}H} NMR data is almost identical to that for (**52**). The ^{1}H spectrum also comprises of a pseudo quartet centred at 2.78ppm (^{2}J=15.3Hz). The ^{13}C{^{1}H} data has a single peak at 47.2ppm corresponding to the pair of equivalent methylene CH_2's and a pair of carboxylate peaks (177.2, 184.4ppm), also in a 2:1 ratio. The C(OH) peak (76.6ppm) is also shifted downfield relative to citric acid suggesting that the α-hydroxyl oxygen is involved in coordination to tin.

Finally, di-ammonium mono-stannous citrate, $(NH_4)_2Sn(C_6H_4O_7)$ (**54**), was also prepared in good yield by a further variation of the same synthetic route to produce a third highly water-soluble white glassy solid. Similarly, this compound is essentially insoluble in all other polar solvents. The presence of only very weak characteristic υ(HOH) bands in the infrared spectrum (e.g. 3000-3400cm^{-1}) correlates with the analytical data in suggesting that the product is essentially anhydrous. This material, like (**52-53**) is also amorphous to X-rays.

The ^{1}H NMR data again has a pseudo quartet at 2.72ppm (^{2}J=15.4Hz), however, a broad singlet at 7.13ppm due to the ammonium protons is also present. The ^{13}C{^{1}H} data (46.3, 75.6, 176.7, 183.0ppm) is very similar to that of (**52,53**), i.e. the citrate group is symmetrically coordinated in solution through the central carboxylate and the α-hydroxyl group.

In each of the above three cases, the terminal methylene carboxylate groups must be fully deprotonated, the negative charges being counterbalanced by the M^{+}

cations.

In contrast, mono-tetramethylammonium mono-stannous citrate di-methanolate, $((CH_3)_4N)Sn(C_6H_5O_7).2CH_3OH$ (**55**), was prepared by a modification of this preparative method using an organic base (Me_4NOH) according to equation 4.3.

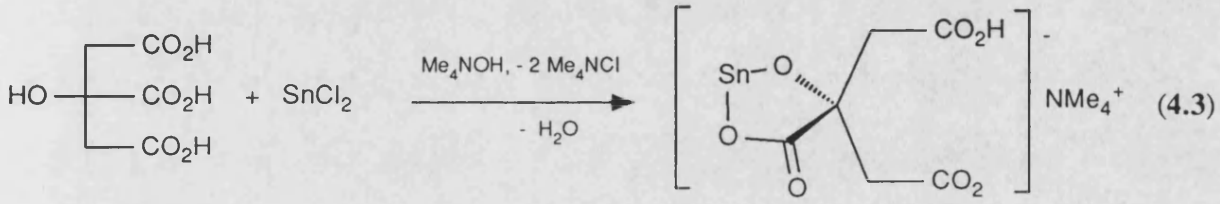

(4.3)

(55)

This compound was prepared using an organic base in the hope that the product might exhibit organic solubility. The initial product of this reaction was a colourless, viscous oil which was readily soluble in methanol. Subsequent recrystallisation from methanol yielded the title compound shown above as a crystalline white solid. Although the stoichiometry of the reaction was the same as used previously (**52-54**), the final product appeared to contain a trivalent $[citrate]^{3-}$ anion. In each of the previous preparations, the citrate group was fully ionised, i.e tetravalent $[citrate]^{4-}$. One mole of $[(CH_3)_4N]^+$ per citrate can be identified by the analytical data and NMR integrals. Similarly, analytical and NMR data suggests that the solid contains two moles of methanol within the solid lattice [i.e. ^1H NMR: 3.26ppm (*s*, 6H), ^{13}C NMR: 48.4ppm]. The ^1H spectrum still contains the characteristic pseudo quartet (2.73ppm) and the $^{13}C\{^1H\}$ spectrum shows a single signal corresponding to the pair of citrate CH_2's (46.1ppm) together with two carboxylates (176.0, 183.4ppm) in a 2:1 ratio. The fact that the two terminal carboxylates cannot be readily distinguished by NMR suggests that a rapid exchange equilibrium is taking place in solution. The C(OH) signal is also shifted downfield

(76.1ppm) suggesting that the hydroxyl group coordinates to tin as for the three ionic solids (**52-54**). The infrared data suggests that the product does not contain water of crystallisation, i.e. no chracteristic strong υ(HOH) peaks are observed although a very broad, weak peak centred at 3300cm^{-1} could be due to the methanol, i.e. υ(C-OH). Surprisingly, a free acid vibration is not observed at 1700-1720cm^{-1} although the $\upsilon(CO_2Sn)$ peak is quite broad and located at quite high frequency, 1616cm^{-1}. The free acid function is most likely involved in hydrogen bonding which results in the lowering of its vibrational frequency due to the partial delocalisation of the [C=O] character. The net effect is to distort the peak assigned as $\upsilon(CO_2Sn)$ causing it to appear at an unusually high frequency.

A possible explantion of this somewhat anomolous result is that $(CH_3)_4NOH$ is an insufficiently strong organic base to ionise the tertiary hydroxyl group. The pK_b of 1.0M aqueous Me_4NOH is 6.75, whereas the pK_b of NH_4OH is 4.75 at 25°C, i.e. ammonium hydroxide is the stronger base. Steric factors might also play a part in the apparent inability of this base to fully ionise the citrate although this is less likely.

Prolonged exposure of an aqueous solution of (**55**) to atmospheric conditions (oxygen, moisture) produced a viscous, colourless oil. Upon further standing, a crop of small transparent crystals of (**64**) were formed after 6-8 weeks. ^{119}Sn Mössbauer and ^{119}Sn NMR data revealed these crystals to contain tin exclusively in its higher (+IV) oxidation state. Analytical and NMR data suggest the composition $(NMe_4)_2Sn(Hcit)_2.7H_2O$. The ^{1}H NMR data has a complex multiplet signal centred at 2.80ppm which is due to the citrate CH_2's. The complexity of the signal indicates that the pair of CH_2 groups are no longer equivalent. A singlet at 3.19ppm integrates to 12 methylammonium protons, i.e. a single $(CH_3)_4N^+$ group for each citrate. The $^{13}C\{^1H\}$ data contained a single peak due to $(CH_3)_4N^+$ at 56.5ppm. Again, two peaks (47.1, 48.8ppm) due to the citrate CH_2's are clearly visible. Three carboxylate peaks are observed, assigned to a free terminal acid group (176.0ppm) and two coordinated carboxylates (178.2, 183.8ppm) in a 1:1:1 ratio. The peak at 178.2ppm is due to the

terminal carboxylate whereas the peak at 183.8ppm can be assigned to the central R_2CO_2Sn group. Infrared data confirmed the presence of a free-acid function as well as coordinated carboxylates ($\upsilon_{as}(CO_2H)$ 1727cm^{-1}; $\upsilon_{as}(CO_2Sn)$ 1644cm^{-1}). These two peaks have an approximate 1:2 ratio respectively. The X-ray crystal structure of (**64**) has been determined and it is discussed fully in Section 4.3.1. This structure determination reveals the free acid to be extensively involved in complex hydrogen bonding and it is somewhat surprising to find that this has little effect upon the position of the $\upsilon(CO_2H)$ vibration.

Anhydrous mono-zinc mono-stannous citrate, $ZnSn(C_6H_4O_7)$ (**56**), was formed from the reaction between di-ammonium mono-stannous citrate (**54**) and zinc chloride according to equation 4.4.

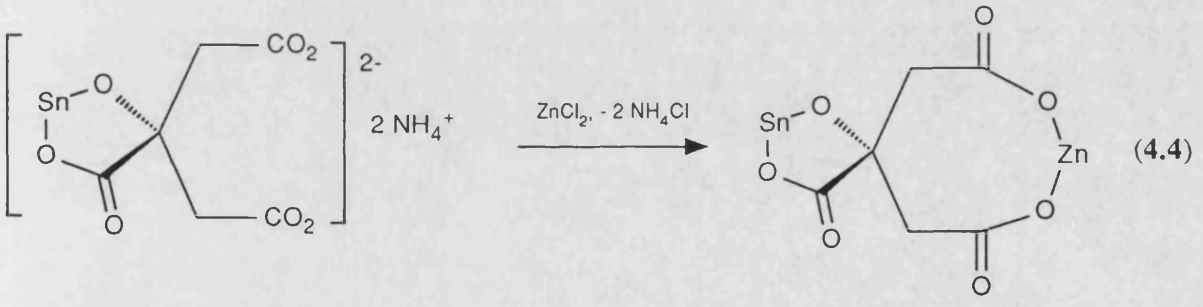

(4.4)

(**54**) (**56**)

This reaction occurs in good yield after refluxing for a short period. Although slightly soluble in boiling water, the product is effectively insoluble in all common solvents at ambient temperature and has similar physical properties to the di-stannous citrate salt (**51**). The implication of this observation is that the mono-zinc mono-stannous salt is also quite polymeric in the solid-state and not monomeric as drawn. Although a peak is observed at 3420cm^{-1} in the infrared spectrum, its intensity is very weak suggesting that very little water of hydration is present in the solid lattice. The asymmetric carboxylate $\upsilon_{as}(CO_2)$ band in the infrared data is quite broad (1556-1579cm^{-1}) which is most likely due to the presence of two metals of

quite different atomic mass bonding to the three carboxylate groups.

The analytical data for stannous and zinc are both a little low for this compound although it is clear that the overall Sn^{2+}:Zn^{2+} ratio is close to 1:1 (actually 1.05:1.0 respectively). It might simply be that the solid is slightly hygroscopic and slowly forms a hydrate upon standing. Unfortunately, NMR data was not available for this compound due to its poor solubility. It is unclear whether the tin binds to the citrate through the central carboxylate and the α-hydroxyl group as shown although this appears to be the preferred mode of coordination in the mono-stannous starting material. If this were the case, the zinc must bind to the citrate through the two terminal -CH_2CO_2 groups.

The selection of tin(II) citrate compounds described above, with the exception of the tetramethylammonium salt (55) all exhibit little or no solubility in organic solvents. The most likely explanation of this low solubility is the prevalence of intermolecular bonding leading to strongly bound polymeric or ionic structures. The scope for covalent Sn-O interactions is wide, due in part to the polyfunctional nature of citric acid. The difficulties encountered with structurally characterising these compounds can be compared with the range of tin(II) pyrophosphates described in Chapter 2. The poor solubility, coupled to the complex polymerisation in the solid-state accounts for the apparent inability of these compounds to crystallise from solution in a form suitable for X-ray structural studies.

Reduction in the degree of intermolecular bonding and/or ionic character should cause these compounds to be more soluble in solvents other than water. The solid-state structure should also become less polymeric. These two properties, combined, should enable the growth of crystals suitable for X-ray diffraction studies. The determination of tin(II) citrate structures would greatly help clarify the coordination of citric acid to tin(II) for which no structural data exists.

Consequently, a series of aliphatic esters of citric acid were synthesised according to literature preparations.[143,144] The three chosen compounds selectively

esterified one, two and finally three of the citrato carboxylate functional groups. Subsequent syntheses of stannous salts of these three mono, di and tri-esters of citric acid were then attempted in the hope of simplifying the degree of possible inter- and intramolecular bonding modes due to the 'elimination' of the esterified sites from the tin coordination sphere.

The three aliphatic citrate esters were prepared from citric acid as shown in Scheme 4.2.

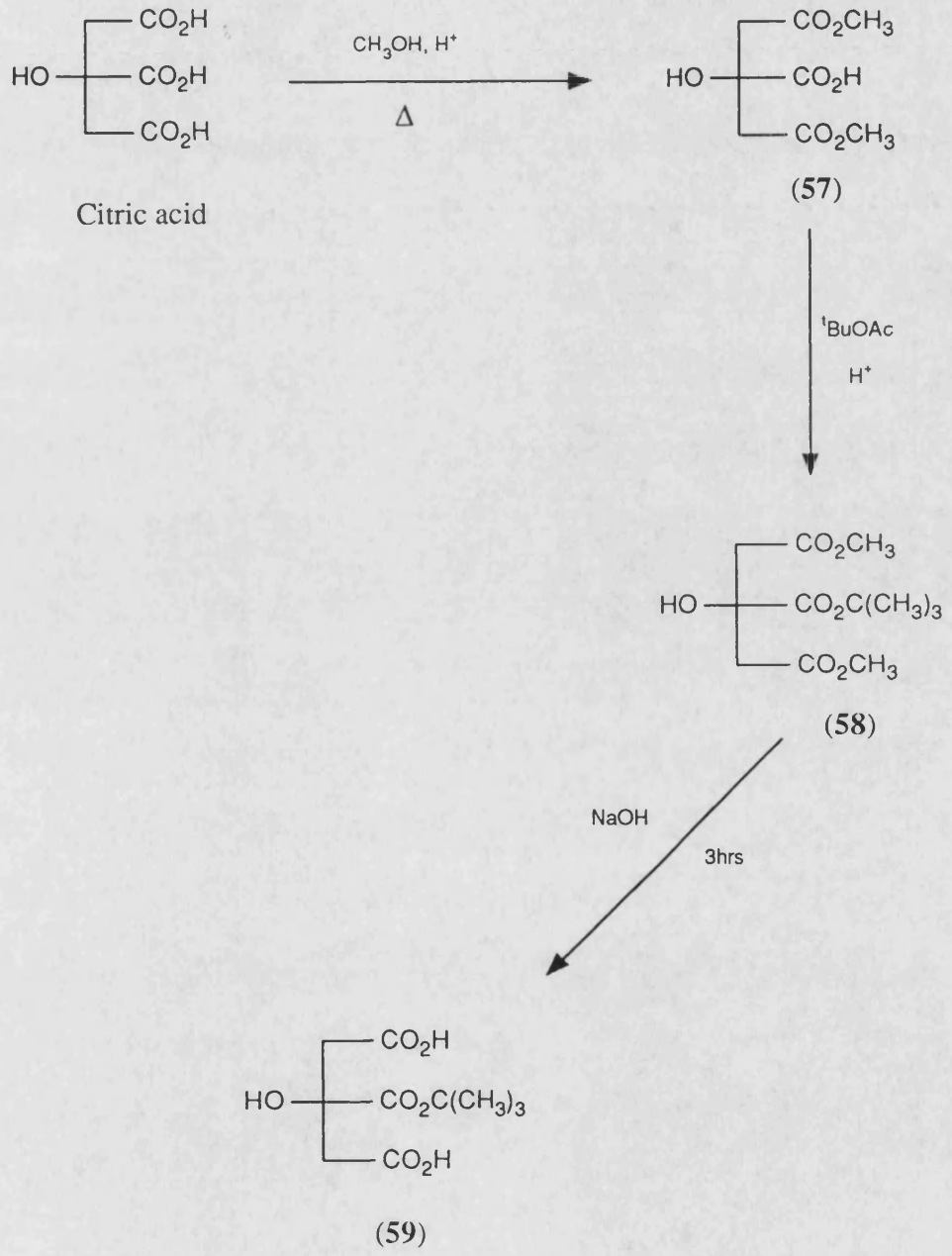

Scheme 4.2 The synthesis of three aliphatic esters of citric acid.

The 1,3-dimethyl citrate ester (**57**) crystallises from water in good yield as the monohydrate. This hydrated compound is a white, highly crystalline solid and it is readily soluble in polar organic solvents (e.g. MeOH, $CHCl_3$). The ^1H NMR spectrum still has the characteristic pseudo quartet (2.87ppm) due to the pair of citrate CH_2's together with a singlet due to the methyl esters (3.66ppm, 6H). An additional broad peak (5.00ppm, 2H) which can be attributed to the water of crystallisation is also observed. $^{13}C\{^1H\}$ data shows a pair of CH_2 peaks (43.9, 44.2ppm) and a pair of $-OCH_3$ ester peaks (52.2, 53.2ppm). Three carboxylate peaks due to the esters (171.7, 171.8ppm) and the free acid (176.4ppm) correlate with the ^1H data in suggesting that the molecule is slightly asymmetric. The asymmetry in the molecule is most likely due to hydrogen bonding between the single water of crystallisation and one of the methyl ester carboxyl oxygens. Intramolecular hydrogen bonding might also occur between the esters and the central acid or the α-hydroxyl group.

Subsequent preparation of the 1,3-dimethyl-2-^{t}butyl citrate ester (**58**) from the reaction between (**57**) and ^{t}butyl acetate yielded a colourless viscous oil in moderate yield. A less-soluble by-product of this reaction, produced by a trans esterification, was claimed in the literature to be the trimethyl citrate ester which was not isolated and identified further. Analytical data for the product suggests that this compound is anhydrous. The ^1H NMR spectrum has the characteristic CH_2 pseudo quartet (2.82ppm) as well as peaks due to the methyl (3.69ppm, 6H) and ^{t}butyl esters (1.51ppm, 9H). The $^{13}C\{^1H\}$ data has a single peak due to the citrate CH_2's (43.2ppm) indicating that the molecule has a greater degree of symmetry than (**57**). The methyl (51.6ppm, 6H) and ^{t}butyl [27.5ppm ($-CH_3$), 83.1ppm ($-CR_3$)] peaks are also readily assigned. The tertiary C(OH) carbon in the citrate group (72.9ppm) is quite distinct from these peaks. The carboxylate peaks occur at 169.9ppm (CH_2CO_2Me) and 172.1ppm ($R_2CO_2Bu^t$). In this molecule, hydrogen bonding is less likely than the dimethyl ester, with only the α-hydroxyl group being freely available for bonding.

Finally, dilute alkaline hydrolysis of (**58**) resulted in the formation of the mono-ester, 2-^{t}butyl citrate (**59**), i.e. selective cleavage of the methyl ester functions. This selectivity is perhaps best accounted for by steric factors, i.e. the bulky ^{t}butyl group prevents the approach of the base to the C=O function. This compound is formed in only moderate yield as the anhydrous crystalline solid. Once again, the ^{1}H NMR spectrum contains the characteristic CH_2 pseudo quartet (2.84ppm) as well as the peak due to the ^{t}butyl ester (1.41ppm, 9H). The $^{13}C\{^1H\}$ data has a single peak due to the citrate CH_2's (43.0ppm) as well as the ^{t}butyl [26.5ppm ($-CH_3$), 84.0ppm ($-CR_3$)] peaks. The tertiary carbon, C(OH) from the citrate group (73.0ppm) is distinct from the aliphatic ester peaks. The carboxylate peaks are observed at 172.9ppm ($R_2CO_2Bu^t$) and 173.1ppm (CH_2CO_2H). As observed for the tri-ester, hydrogen bonding does not appear to be an important feature of the chemistry of this compound.

A useful tool for studying aliphatic esters is the position of the asymmetric carboxyl stretch, $\upsilon_{as}(CO_2)$, in the infrared spectrum. Typically, the [C=O] stretching vibration for normal saturated esters is observed as a strong band at 1735-1750cm^{-1}.[145] The position of this band is higher than that observed for simple carboxylic acids due to influence of the inductive effect provided by the aliphatic ester chain. In general, the larger the alkyl ester group, the greater the inductive effect and the greater the observed shift in $\upsilon_{as}(CO_2)$, $\Delta\upsilon_{as}$. The [C=O] vibration for simple saturated carboxylic acids is normally observed as a strong band at 1700-1725cm^{-1}.[146] Polyfunctional acid species, such as citric acid, commonly exhibit an interaction effect between the different acid groups which significantly affects the position of the $\upsilon_{as}(CO_2)$ bands, e.g. the simplest dicarboxylic acid, malonic acid [$CH_2(CO_2H)_2$] displays two peaks at 1710 and 1740cm^{-1}.[147] The values of $\upsilon_{as}(CO_2)$ for the three citrate esters are tabulated in Table 4.1. The bands for citric acid can be readily assigned by their relative intensities.

Table 4.1 Asymmetric [CO_2] stretching vibrations for the series of aliphatic citrate esters.

Compound	$\upsilon_{as}(CO_2)$ /cm^{-1}	Assignment
Citric acid (**19**)	1744	CO_2H (central)
	1696	CO_2H (terminal)
1,3-dimethylcitrate (**57**)	1742	CO_2H (central)
	1717	CO_2CH_3
1,3-dimethyl-2-^{t}butyl citrate (**58**)	1757	$CO_2C(CH_3)_3$
	1728	CO_2CH_3
2-^{t}butyl citrate (**59**)	1755	$CO_2C(CH_3)_3$
	1705	CO_2H (terminal)

Mono-stannous 1,3-dimethyl citrate (**60**) was subsequently prepared from the corresponding di-ester (**57**) according to equation 4.5.

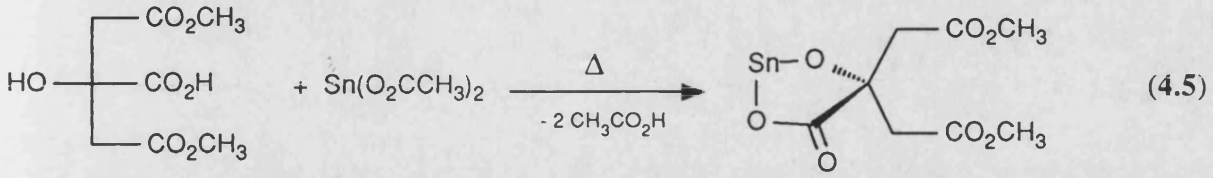

(4.5)

(**57**) (**60**)

The reaction was carried out in freshly dried methanol to avoid hydrolysis of the tin(II) acetate. The methanol was dried immediately prior to use by distilling over magnesium turnings activated with a little iodine. Analytical and NMR data suggested that the final product is a methanol adduct with a methanol:citrate ester ratio of 1:1. The ^{1}H spectrum had the characteristic CH_2 pseudo quartet (2.74ppm, 4H) together with a singlet due to methanol (3.38ppm, 3H) and the methyl esters (3.55ppm, 6H). The $^{13}C\{^{1}H\}$ spectrum showed a single peak due to the citrate CH_2's (45.2ppm), the methanol (48.9ppm) and the citrato methyl esters (51.3ppm). The downfield position of the *C*(OH) peak (75.7ppm) relative to the starting material confirms that the α-hydroxyl group is coordinated to tin. Peaks due to the ester carbonyl group, $CH_2\mathit{C}O_2CH_3$ (172.0ppm), and the coordinated carboxylate, $R_2\mathit{C}O_2Sn$ (182.0ppm), were present in the expected approximate 2:1 ratio. The infrared spectrum shows two carboxylate bands due to both the aliphatic ester, $\upsilon_{as}(CO_2CH_3)$ ($1734cm^{-1}$) and the coordinated carboxylate $\upsilon_{as}(CO_2Sn)$ ($1561cm^{-1}$).

As anticipated, the product was quite soluble in hot organic solvents such as methanol and careful control of the rate of cooling of a saturated methanolic solution yielded a crop of good quality, small cubic, transparent crystals. The single-crystal X-ray structure of this compound has been determined and is discussed fully in Section 4.3.2.

An alternative preparative route to mono-stannous 1,3-dimethyl citrate (**60**) from $Sn(OBu^n)_2$ (prepared *in situ*) was also attempted according to equation 4.6. However, during the course of this preparation a trans-esterification reaction occurred yielding mono-stannous di-n-butylcitrate.

(4.6)

(**57**) (**63**)

This reaction was carried out in neat n-butanol with gentle warming in order to allow the citrate ester to fully dissolve. The product of the reaction precipitated as a fine white solid upon cooling. Analytical and NMR data clearly confirmed that a trans-esterification reaction had occurred between the methyl esters and the excess n-butanol. The net result of this reaction was the unintentional formation of anhydrous mono-stannous 1,3-di-n-butylcitrate (**63**) in good yield. Infrared data showed the presence of a $\upsilon_{as}(CO_2{}^nBu)$ stretch at 1740cm^{-1} which is too high for a methyl ester. The increased inductive effect of the longer n-butyl chain would account for the significant shift in the position of the ester C=O peak (*cf.* 2-^{t}butyl citrate). The ^{1}H NMR spectrum retained the pseudo quartet at 2.88ppm due to the citrate CH_2's. Peaks due to the n-butyl ester are also present (0.91ppm (*t*) 6H, 1.58ppm (*m*) 8H, 4.10ppm (*t*) 4H). Likewise, the $^{13}C\{^1H\}$ spectrum contains four peaks due to the esters, i.e. 65.5, 30.5, 19.0, 13.1ppm (Bu^n C_1-C_4). The citrate peaks include those due to the CH_2's (43.6ppm), the esterified carboxylates, $CH_2CO_2Bu^n$ (173.0ppm) and the metal-coordinated carboxylate, R_2CO_2Sn (180.6ppm). As for (**60**), the *C*(OH) peak is shifted downfield indicating that the α-hydroxyl group is involved in metal coordination.

Unfortunately, repeated attempts at recrystallisation of this compound from a

variety of polar solvents yielded fine, flock-like precipitates that were unsuitable for X-ray crystallography. The eventual product had the formula shown.

The attempted synthesis of mono-stannous bis-1,3-dimethyl 2-^{t}butyl citrate (**61**) was performed according to equation 4.7.

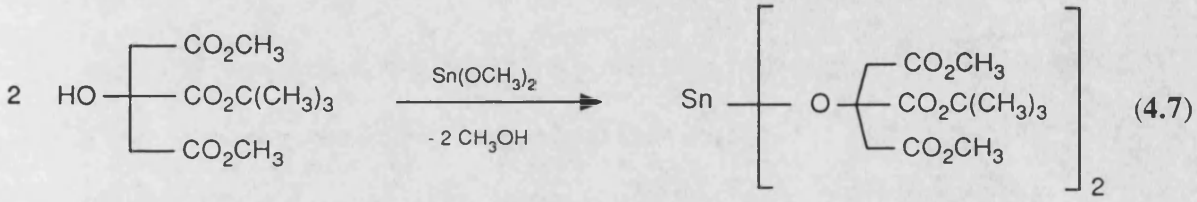

(4.7)

(**58**) (**61**)

This reaction was performed in refluxing toluene and the final product was readily precipitated as a mass of small cubic crystals upon slowly cooling the reaction mixture under an inert atmosphere. Analysis of the product of this reaction showed it to contain very little carbon or hydrogen (3.7, 1.04% respectively) and the infrared spectrum showed very few bands. A single strong, broad band at 547cm^{-1} was assigned as an Sn-O stretch. This result was reproducible over three separate attempts. It was hoped that the citrate tri-ester might have behaved as a 'bulky' alcohol causing the displacement of methanol from $Sn(OCH_3)_2$ to yield the compound illustrated above (**61**). Unfortunately, the experimental results suggest that this compound, if formed, is extremely susceptible to hydrolysis giving rise to the final product described above. Although the identity of this compound was not investigated further, the crystalline solid might have a similar structure to the partial hydrolysis product of $Sn(OCH_3)_2$, i.e. $Sn_6O_4(OCH_3)_4$.[127] This species possesses an adamantane cage structure as shown in Section 1.8.4. The infrared spectrum of this documented compound also shows a strong band at 570cm^{-1}, assigned as an υ(Sn-O) stretch. The slight difference in the Sn-O stretching frequencies suggests a slightly different structure for this unknown species, i.e. it is not $Sn_6O_4(OCH_3)_4$.

The attempted synthesis of mono-stannous 2-^{t}butyl citrate (**62**) was performed

according to equation 4.8.

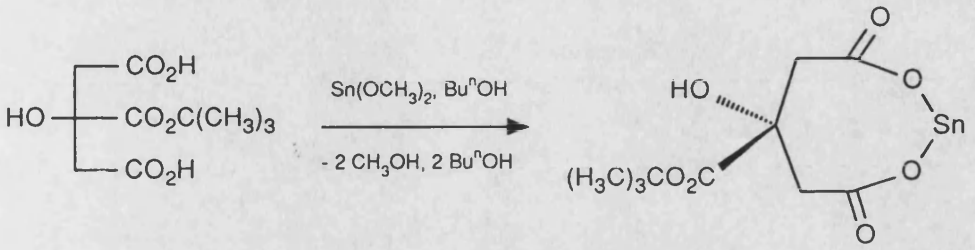

(4.8)

(59) (62)

This reaction was carried out in neat n-butanol as the solvent with gentle warming (i.e. soluble $Sn(OBu^n)_2$ was formed *in situ*). Upon reaction of the soluble tin(II) alkoxide with the mono-ester, a dense white precipitate formed in moderate yield. Analytical and infrared data suggested that the product did not contain an ester function as anticipated (e.g. no $\upsilon_{as}(CO_2R)$ bands at 1735-1750cm^{-1}). The product appeared to be the anhydrous di-stannous salt of citric acid, i.e. Sn_2(citrate) (**51**). The implication of this result is that the ^{t}butyl ester group is cleaved during this reaction although the reason why this should occur under relatively mild reaction conditions is unclear.

Lecomte and his co-workers have made an extensive study of the infrared spectra of organic carboxylic acids and have studied over a thousand such compounds.[152-155] When ionisation occurs, producing the $[CO_2]^-$ group, resonance is possible between the two C-O bonds. In consequence, the characteristic carbonyl absorption disappears and is replaced by two bands. These correspond to the anti-symmetrical and the symmetrical vibrations of the CO_2^- structure. Typically, these bands lie between 1550-1610cm^{-1} and 1300-1400cm^{-1} respectively.

Of these two bands, the former is far more characteristic, as it is generally far more constant in frequency whilst many more skeletal vibrations occur in the wide-range 1300-1400cm^{-1} (e.g. C-H). Typically, the intensity of the asymmetric vibration is much greater than that of the symmetric mode. Lecomte's general

findings have been confirmed by later workers such as those engaged on the penicillin project.[156] Penicillin is an important broad-spectrum antibiotic which contains the crucial tetrahydrothiazole group as well as the carboxylic acid function as shown in Fig. 4.1.

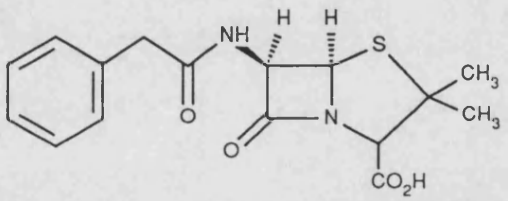

Fig. 4.1 The structure of benzylpenicillin.

The position of the asymmetric vibration, $\upsilon_{as}(CO_2)$ for the series of tin(II) and tin(IV) citrate salts are tabulated in Table 4.2.

The infrared spectrum for each of this series of compounds clearly shows the presence of a carboxyl [CO_2] group. There are three main modes of carboxylate bonding which are likely to be found in compounds of this type, i.e. (a) unidentate, (b) bidentate (bridging or chelating) and (c) unidentate/hydrogen bonded (Fig. 4.2).

All of the simple metal citrate salts (**51-56, 62**) show a single, broad peak corresponding to the $\upsilon_{as}(CO_2)$ vibrations of the three deprotonated carboxylate functions. The peak observed for ZnSn(citrate) (**56**) is particularly broad, spanning a frequency range of 20-30cm^{-1}. The peak positions of the three analogous mono-stannous compounds (**52-54**) are very similar. This suggests that each of these three compounds has a similar structure as suggested by the similarities in the NMR data. Similarly, the peak positions of Sn_2(citrate) and ZnSn(citrate) are also very similar, suggesting a similar structure for this pair of analogous compounds.

In the case of the 1,3-dimethyl (**60**) and 1,3-di-^{n}butyl citrate (**63**) salts of tin(II), two distinct bands are clearly observed. These correspond to the $\upsilon_{as}(CO_2)$ of

Table 4.2 Carboxylate stretching frequencies for the series of tin(II) citrates.[a]

Compound	$\upsilon_{as}(CO)$ / cm^{-1}	Assignment
Sn_2(citrate) (**51**)	1553	$-CO_2Sn$
Na_2Sn(citrate) (**52**)	1593	$-CO_2Sn$
K_2Sn(citrate) (**53**)	1599	$-CO_2Sn$
$(NH_4)_2Sn$(citrate) (**54**)	1599	$-CO_2Sn$
$(Me_4N)Sn$(citrate) (**55**)	1616	$-CO_2Sn$
ZnSn(citrate) (**56**)	1567	$-CO_2M$
Sn 1,3-dimethyl citrate (**60**)	1734 1561	$-CO_2CH_3$ $-CO_2Sn$
Sn 1,3-di-^{n}butyl citrate (**63**)	1740 1543	$-CO_2{}^nBu$ $-CO_2Sn$
$Sn^{IV}(Hcit)_2(NMe_4)_2$ (**64**)	1727 1644	$-CO_2H$ $-CO_2Sn$
$Sn(O_2CH)_2$	1561	$-CO_2Sn$
$Sn[O_2C(CH_2)_{10}CH_3]_2$	1561	$-CO_2Sn$
$Sn[O_2C(CH_2)_{12}CH_3]_2$	1553	$-CO_2Sn$
$Sn(O_2CCF_3)_4$	1600	$-CO_2Sn$
Na_3(Hcitrate)	1660, 1590	$-CO_2^-Na^+$
Sn(oxalate)	1568	$-CO_2Sn$
K_2Sn(oxalate)	1552	$-CO_2Sn$

Note:-

[a]Spectra recorded as a nujol mull.

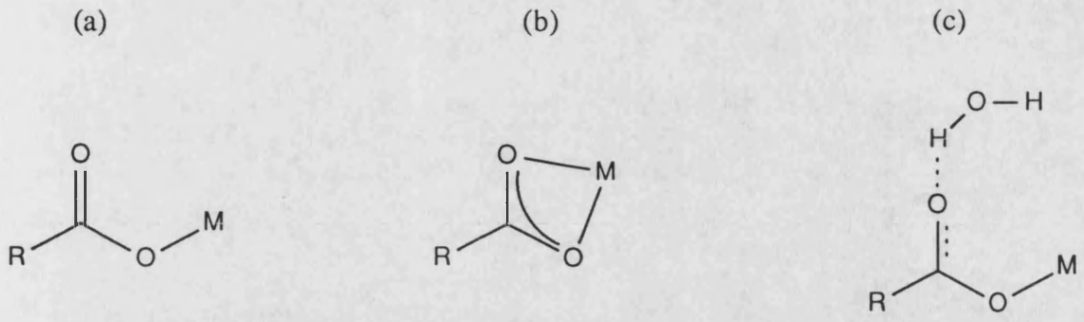

Fig. 4.2 Bonding modes of carboxylate groups to a metal centre.

the R_2CO_2Sn and the $\upsilon_{as}(CO_2)$ vibration of the aliphatic CO_2R group.

It has already been stated in the discussion of the tin(II) salts of aldonic acids, i.e. gluconate and glucuronate in Chapter 3 (Section 3.3) that it is very difficult to accurately predict the mode of coordination of the carboxylate to tin(II) from infrared data alone in the absence of structural data. In the case of tin(II) citrates, the problem is further compounded by the presence of three $-CO_2M$ groups which tends to create one, broad $\upsilon_{as}(CO_2)$ band. Furthermore, many of these compounds are extensively solvated which implies that hydrogen bonding might also play an important part in the position of the $\upsilon_{as}(CO_2Sn)$ band.

For example, both of the tin citrates (**60, 64**) examined by X-ray crystallography contain exclusively unidentate carboxylate groups. In these two cases the values of $\upsilon_{as}(CO_2Sn)$ are, however, quite different, i.e. $1561cm^{-1}$ and $1644cm^{-1}$ respectively. Closer inspection of the structural data reveals that the former compound has a hydrogen bound network involving the C=O of the central carboxylate and the methanol (CH_3OH) of solvation. This would have the effect of delocalising and lowering the C=O double bond character [Fig. 4.2(c)] and reducing the frequency of the $\upsilon_{as}(CO_2Sn)$ band. In the latter case, hydrogen bonding does occur but the majority of the carboxylate groups are unaffected, i.e. the 'net' position

of the broad $\upsilon_{as}(CO_2Sn)$ band is at relatively high frequency due to the greater double bond character.

Comparison with the limited selection of structurally characterised literature examples reveals similar conclusions. Tin(II) formate involves symmetrically and asymmetrically bridging carboxylates and $\upsilon_{as}(CO_2Sn)$ is at relatively low frequency, 1561cm^{-1}.[115] This value is consistent with the delocalisation of the C=O character due to the bidentate bridging mode, i.e. all C-O bonds are essentially equivalent (Fig. 1.18). Similarly, in the case of tin(II) oxalate, each oxalate group bridges to two tin atoms and the $\upsilon_{as}(CO_2Sn)$ band is located at 1568cm^{-1}, i.e. similar to the formate [Fig. 1.19(a)].[113] In the case of di-potassium oxalatostannate(II) monohydrate, the oxalate group involves both bridging to tin and hydrogen bonding to the water of crystallisation and $\upsilon_{as}(CO_2Sn)$ is broad and at very low frequency, i.e. 1552cm^{-1} [Fig. 1.19(b)].

The $\upsilon_{as}(CO_2Sn)$ bands for the series of tin(II) citrates all occur at quite low frequency suggesting that simple unidentate coordination is not present in any of the species. Anhydrous Sn_2(citrate) and ZnSn(citrate) are quite similar (1553, 1567cm^{-1}) suggesting that the carboxylate groups bind to the metals through either bidentate chelation or bridging modes. The latter is more consistent with their physical properties, i.e. poor solubility, suggesting a highly polymeric structure in the solid-state. The infrared spectra of the ionic mono-stannous compounds (**52-55**) are also very similar [$\upsilon_{as}(CO_2Sn)$ 1593-1616cm^{-1}] and the NMR data suggests that the central carboxylate and the α-hydroxyl chelate to tin. The infrared data suggests that either (a) the C=O bond retains some of its double bond character or (b) the carboxylate is truly unidentate and water of hydration hydrogen bonds to the central C=O group (*cf.* methanol in stannous 1,3-dimethylcitrate. MeOH). Two anhydrous long-chain fatty acid salts, $Sn[O_2C(CH_2)_{10}CH_3]_2$ and $Sn[O_2C(CH_2)_{12}CH_3]_2$ were also examined for the purposes of comparison. The two compounds are quite insoluble and show similar spectral features [$\upsilon_{as}(CO_2Sn)$ 1561, 1553cm^{-1} respectively]

suggesting that the carboxylate groups bridge adjacent tin atoms and are not unidentate [*cf.* $Sn(O_2CH)_2$]. There are no simple tin(II) carboxylates which have been found to exhibit bidentate chelating ligands.

The proposed simplification of the bonding within tin(II) citrates by preparation of esters is somewhat analogous to the situation encountered with zinc citrates. Zinc citrate trihydrate (ZCT) is a prime anti-plaque agent for which no structural data exists. However, the recent preparation of zinc (RS)-1-isopropyl citrate tetrahydrate has allowed the crystal structure of a zinc citrate species to be determined.[148] In this structure, each 1-isopropyl citrate chelates to a diaquazinc ion through the end carboxyl, the central carboxyl and the hydroxyl group. Bridging to a second diaquazinc ion occurs through the end carboxyl O atom. The net effect is the formation of extended chelated strips which are packed through van der Waals forces. Each zinc atom is octahedrally coordinated by six oxygen atoms (Fig. 4.3).

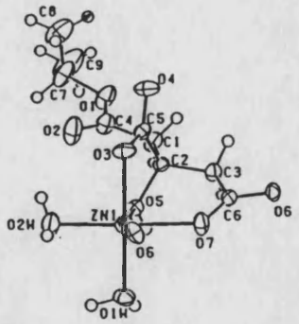

Fig. 4.3 The structure of zinc (RS)-1-isopropyl citrate tetrahydrate.

(RS)-1-isopropyl citrate has been found to be the major component of isopropyl citrate, a synergistic antioxidant food additive.[149] Isopropyl citrate is a complex mixture containing citric acid, 1-isopropyl, 2-isopropyl, 1,2-isopropyl,

1,3-isopropyl and 1,2,3-isopropyl citrate esters as determined by gas chromatographic separation.[150] The identity and structure of each isomer has been determined by ^{1}H and ^{13}C NMR spectroscopy.[151]

The ^{119}Sn Mössbauer and ^{119}Sn NMR data for the series of tin(II) citrate compounds are presented in Tables 4.3 and 4.4 respectively together with a representative selection of data for other tin carboxylates.

The ^{119}Sn Mössbauer spectrum for each of the tin(II) citrate salts (**51-56, 60-63**) were all recorded on finely ground solid samples at liquid nitrogen temperature (78K). The value of the isomer-shift, δ, is quoted with reference to SnO_2 (δ = 0.00mms^{-1}). The presented data clearly indicates that all of these compounds contain tin in its lower +II valence state due to the highly positive value for the isomer-shift, δ. Conversely, the very low, positive value of δ for (**64**) indicates that this compound contains tin in its higher +IV oxidation state.

The values for the quadrupole splitting, Δ, indicate that the spectrum for each of these compounds is a doublet. As a consequence of this data, it can be stated that the coordination about the tin atoms in each compound displays a marked degree of asymmetry.

The data for the series of tin(II) compounds is remarkably consistent, allowing for experimental errors. The variation in δ is only approximately 3.05 ($\pm$0.10)mms^{-1}. The quadrupole splitting, Δ, is equally consistent across the series of citrates, the variation across the series being approximately 1.90 ($\pm$0.10)mms^{-1}.

The only exception to this statement is the data for the product of the reaction between the tri-ester of citric acid and $Sn(OCH_3)_2$ (**61**) (δ, 2.66; Δ, 2.26mms^{-1}). It has already been established that this species is most likely a hydrolysis product of $Sn(OCH_3)_2$ and not a tin(II) carboxylate at all. This theory is further supported by this Mössbauer data, the isomer-shift of the partial hydrolysis product $Sn_6O_4(OCH_3)_4$ is quoted in the literature as δ, 2.78 ($\pm$0.06)mms^{-1} whilst δ for this unknown compound is very similar at 2.66mms^{-1}.[127] A literature value for the quadrupole

Table 4.3 ^{119}Sn Mössbauer data for the series of tin(II) and tin(IV) citrates.[a]

Compound	δ (mms^{-1})	Δ (mms^{-1})	Γ (mms^{-1})	Γ (mms^{-1})
Sn_2(citrate) (**51**)	3.07	1.90	1.08	1.06
Na_2Sn(citrate) (**52**)	3.06	1.85	1.27	1.09
K_2Sn(citrate) (**53**)	2.97	1.81	1.21	1.16
$(NH_4)_2Sn$(citrate) (**54**)	2.99	1.84	1.14	1.09
$(Me_4N)Sn$(citrate) (**55**)	2.80	1.91	0.92	0.90
ZnSn(citrate) (**56**)	3.17	1.92	1.20	1.05
Sn 1,3-dimethyl citrate (**60**)	3.11	2.01	1.02	0.93
Sn 1,3-di-^{n}butyl citrate (**63**)	3.13	1.98	0.84	0.85
$Sn^{IV}(Hcit)_2(NMe_4)_2$ (**64**)	0.16	1.36	0.79	1.03
Sn(D-gluconate)$_2$ (**45**)	3.15	1.75	1.20	1.04
$Sn(O_2CH)_2$	3.33	1.70	1.02	1.11
$Sn(C_2O_4)$	3.35	1.65	-	-
$Sn[O_2C(CH_2)_{10}CH_3]_2$	3.17	1.93	0.90	0.92
$Sn(O_2CCH_3)_2$	3.31	1.77	-	-
$Sn(O_2CCH_3)_4$	0.08	-	1.45	-

Note:-

[a]Spectra recorded at 78K, relative to SnO_2.

Table 4.4 ^{119}Sn NMR data for the series of tin(II) and tin(IV) citrates.

Compound	δ / ppm[a]
Sn_2(citrate) (**51**)[b]	-724.9
Na_2Sn(citrate) (**52**)[c]	-579.9
K_2Sn(citrate) (**53**)[c]	-578.3
$(NH_4)_2Sn$(citrate) (**54**) [c]	-579.6
$(Me_4N)Sn$(citrate) (**55**) [c]	-582.9
Sn 1,3-dimethyl citrate (**60**) [d]	-482.0
Sn 1,3-di-^{n}butyl citrate (**63**) [e]	-497.0
$Sn^{IV}(Hcit)_2(NMe_4)_2$ (**64**) [f]	-54.2, -55.3
$Sn(D\text{-gluconate})_2$ (**45**)[c]	-570.9
$Sn[O_2C(CH_2)_{10}CH_3]_2$[g]	-494.1
$Sn[O_2C(CH_2)_{14}CH_3]_2$[g]	-489.8
$Sn[O_2C(CH_2)_{16}CH_3]_2$[g]	-480.6

Notes:-

[a]Spectra recorded at ambient temp., relative to $SnMe_4$.
[b]Spectrum recorded using MAS-NMR techniques.
[c]Spectrum recorded in D_2O.
[d]Spectrum recorded in d_6-DMSO.
[e]Spectrum recorded in $CDCl_3$.
[f]Spectrum recorded in CD_3OD.
[g]Spectrum recorded in C_6D_6 at 60°C.

splitting, Δ, has not been quoted.

The crystal structure of the 1,3-dimethyl ester salt (**60**) has established that the tin atom is surrounded by four oxygen atoms in an SnO_4E pseudo-trigonal pyramidal arrangement (Section 4.3.2). Four coordination about tin is achieved through combined dimerisation and methanol solvation. The structures of other simple tin(II) carboxylate species also show the tin atom to be four coordinate (Section 1.8.3). In the limited cases where structural data is available, four coordination is generally achieved through divalent carboxylate bridging to form polymeric layer structures. However, the literature Mössbauer data for tin(II) formate, acetate and oxalate have slightly higher δ values of 3.31-3.35mms^{-1}.[103,114,115] These literature values are significantly higher than any of those obtained for this series of tin(II) citrates although a lower δ value of tin(II) formate has also been quoted as 3.15mms^{-1}.[114] This latter value of δ is much more similar to those values recorded for the citrates. However, the data for the citrate compounds compares well with that of the long-chain carboxylates and the aldonic acid salt, Sn(D-gluconate)$_2$ (**45**) with similar values for both δ and Δ. Quite possibly, some of the tin(II) citrates [e.g. (Me_4N)Sn(Hcit) δ, 2.80mms^{-1}] might have a higher coordination in the solid-state which would account for their lower isomer shift parameters. Additional weak, longer-range Sn-O contacts beyond the SnO_4 coordination sphere might produce a pseudo-octahedral $SnO_4O'E$ geometry. However, a crucial factor in the Mössbauer data for the citrates which has not been considerd is the influence of the α-hydroxyl group. The NMR spectral data strongly suggests that this group is coordinated to tin together with the central carboxylate. Therefore, the net spectrum might be considered to be a hybrid between that of a tin(II) carboxylate and an alkoxide. For comparison, the spectrum of $Sn(OCH_3)_2$ has been quoted (δ, 2.80; Δ, 2.02mms^{-1}).[126] The effect of these spectral parameters when combined with the data for a simple $Sn(O_2CR)_2$ [e.g. tin(II) formate] species should produce a compound with the following parameters: δ, 3.07; Δ, 1.86mms^{-1}. These values are remarkably close to

those observed for the series of tin(II) citrates, further supporting the involvement of the α-hydroxyl group in the tin coordination.

The most probable interpretation of the Mössbauer and crystallographic data is that the tin atom in each of these tin(II) citrate salts also exhibits SnO_4E four coordination similar to that in the 1,3-dimethyl citrate salt. The tin atoms would most likely achieve four coordination through chelation or intermolecular bridging to adjacent carboxylate groups. The result of this bridging in the case of (**51,56**) would be extended polymerisation forming chains or sheets of molecules which is consistent with the low values for $\upsilon_{as}(CO_2Sn)$ (Table 4.2). This would account for the low solubility of these two compounds in organic, non-polar solvents. The remaining compounds, with the exception of (**55**) are also insoluble in organic solvents due to their ionic character

In general, the linewidth parameters for the tin(II) citrates are quite broad with a marked asymmetry. The implication of the linewidths is that the tin coordination throughout the lattice is relatively non-uniform. The asymmetry of the lines is often observed in cases where the tin coordination is asymmetric. However, the data for the three water-soluble glasses (**52-54**) shows the linewidths to be considerably broader. This is consistent with the fact these compounds are amorphous to X-rays implying a wholly non-uniform structural distribution throughout the solid lattice. The resulting variation in local tin geometries would account for the broad linewidths.

The tin(IV) citrate (**64**) has been examined by X-ray crystallography and the tin is found to be octahedrally bound to six oxygens (Section 4.3.1). The SnO_6 bonding is quite distorted which accounts for the observed value of Δ ($1.36 mms^{-1}$). The isomer shift is substantially lower than that of the tin(II) carboxylates (δ, $0.16 mms^{-1}$) due to the higher oxidation-state of the tin, i.e. loss of the $5s^2$ lone-pair. The data for tin(IV) acetate quoted in Table 4.3 is a singlet (δ, $0.08 mms^{-1}$) with a very broad linewidth.[220] This spectrum is consistent with the partial structural determination of $Sn(O_2CCH_3)_4$ which has a quite regular eight coordinate

dodecahedral tin geometry.[183] The broad linewidth suggests that significant local structural variations occur in the solid-state.

The ^{119}Sn MAS-NMR data for the di-stannous salt (**51**) shows the presence of a single broad peak quite far upfield of $SnMe_4$ (-724.9ppm). This data can be correlated directly with the Mössbauer data as the two techniques both relate to tin coordination in the solid-state. The broad NMR peak is consistent with the fairly broad linewidths in the Mössbauer spectrum (Γ_1, 1.08; Γ_2, 1.06mms^{-1}). This data suggests that more than one tin environment is present in the solid lattice although the sites are not greatly dissimilar.

Also, $\upsilon_{as}(CO_2Sn)$ is quite low for (**51**) (1553cm^{-1}) relative to (**52-55**) which implies stronger bonding of the tin to the carboxylate groups. Consequently, the increased Sn-O bond strength accounts for the upfield shift of δ in the tin NMR relative to the other citrates.

The solution-state tin NMR for the series (**52-55**) is remarkably consistent, each spectrum recorded in D_2O. The data for each of these compounds appears as a single peak implying that, in solution, a single tin environment is present on the NMR timescale. As implied above, the peaks are downfield of (**51**) suggesting that the Sn-O bonding is relatively weak, as borne out by the shift in $\upsilon_{as}(CO_2Sn)$ (Table 4.2). The implication is that the tin coordination for each of these mono-stannous compounds is very similar when in solution, i.e. similar coordination number, ligand geometry etc.

The ^{119}Sn NMR data for the two citrate esters (**60, 63**) is also very similar. Both compounds also show a single ^{119}Sn peak implying that a single tin environment is present whilst in solution, the peak positions for both occurring slightly downfield of those for the ionic salts. This could simply be due to these spectra being run in solvents other than D_2O, i.e. solvent coordination effects. Alternatively, the differences could be a reflection of different Sn-O bond strengths and geometric distortions around the tin atom. In the solid-state, the two esters show a relatively

high value for the Mössbauer quadrupole-splitting which is indicative of a highly distorted tin coordination. It appears that 'blocking' the two terminal methylene carboxylates in this way has a marked influence upon the symmetry of the tin coordination sphere.

Finally, the tin NMR data for the ionic tin(IV) citrate (**64**) shows the presence of two peaks when in CD_3OD solution. The implication is that two slightly dissimilar tin environments co-exist in solution. The peak positions are only slightly upfield from $SnMe_4$ due primarily to the higher oxidation state of the tin atom in this compound. The crystallographic data clearly shows the presence of two distinct six-coordinate SnO_6 tin sites when in the solid-state which accounts for the marked asymmetry in the Mössbauer linewidths.

4.3 Structural Determinations of Tin Citrate Compounds.

It has been stated previously that the crystal structures of two tin citrate compounds have been determined. These compounds are bis-citrato di-tetramethylammonium tin(IV) heptahydrate **(64)** and mono-stannous 1,3-dimethylcitrate mono-methanolate **(60)**. In the following section, these two structures are each described in detail and compared to structures of a similar type. Selected structural data are included in the discussion, however, the crystal data and additional supplementary structural data is included in Appendices 2 and 3 for **(64)** and **(60)** respectively.

4.3.1 *The Crystal Structure of Bis-citrato Di-tetramethylammonium Tin(IV) Heptahydrate* (64).

A crystal of approximate dimensions 0.5 x 0.5 x 0.2mm was used for data collection.

The asymmetric unit is shown in Fig. 4.4, along with the atom labelling scheme used. The lattice packing arrangement, with water atoms omitted for clarity, is also illustrated in Fig. 4.5. Full tables of anisotropic temperature factors, bond lengths, bond angles and non-bonded interatomic distances are presented in Appendix 2.

Despite a reasonably healthy *R* factor, this structure did not converge well. Attempted anisotropic refinement resulted in unsatisfactory thermal parameters for many of the atoms. Similarly, efforts to apply a weighting scheme either before or after an empirical absorption correction proved fruitless and shift/esd values remained high throughout the refinement. Sample quality may account for some of the above but the very large error on α of 0.19° may have also introduced some systematic

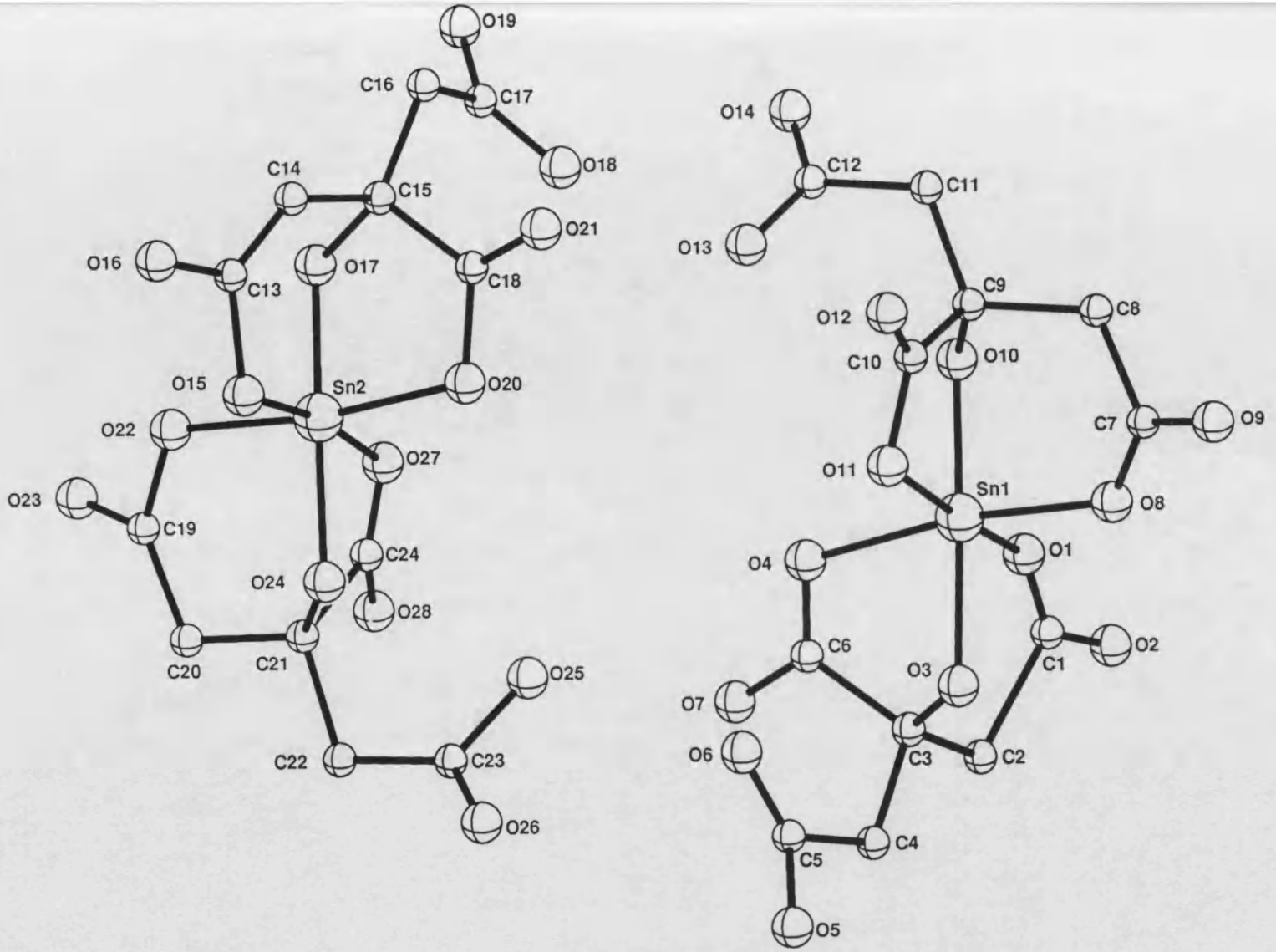

Fig. 4.4 The asymmetric unit cell of bis-citrato bis-tetramethylammonium tin(IV) heptahydrate (**64**), water molecules ommitted.

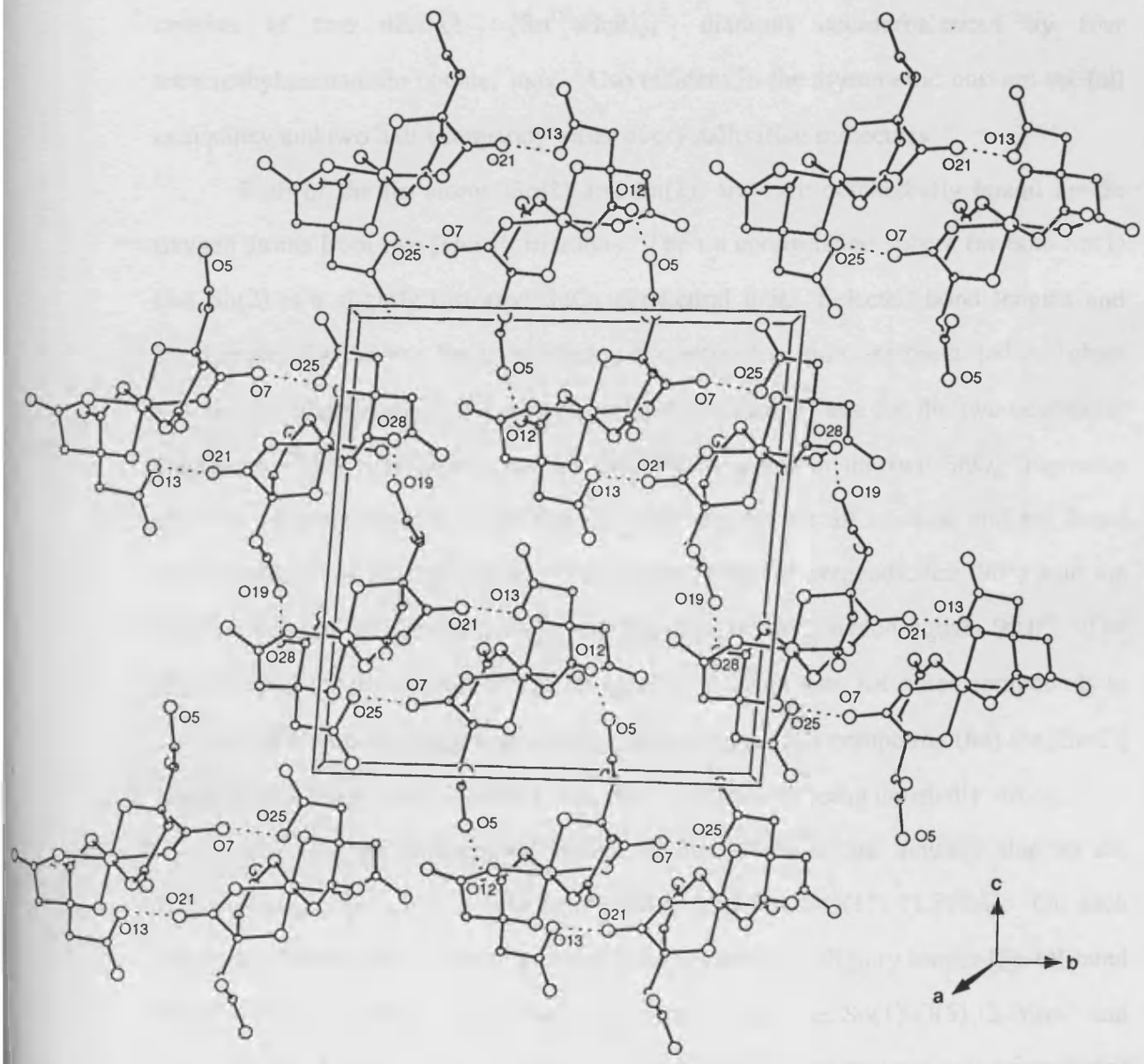

Fig. 4.5 The lattice packing arrangement for bis-citrato di-tetramethylammonium tin(IV) heptahydrate (**64**), water molecules ommitted.

errors into the data set.

However, these difficulties were partially offset by the interesting nature of the structure, both at the molecular and macromolecular level. The asymmetric unit consists of two distinct $[Sn^{IV}(Hcit)_2]^{2-}$ dianions counterbalanced by four tetramethylammonium counter ions. Also resident in the asymmetric unit are six full occupancy and two half occupancy water of crystallisation molecules.

Both of the tin atoms, Sn(1) and Sn(2), are each octahedrally bound by six oxygen atoms from two $[Hcit]^{3-}$ trianions. The tin coordination sphere for both Sn(1) and Sn(2) is a slightly distorted SnO_6 octahedral unit. Selected bond lengths and bond angles for the two SnO_6 octahedral cooordination units are presented in Tables 4.5 and 4.6 respectively. The data is presented as like *vs.* like for the two octahedral fragments. This data clearly reveals the distortion within the two SnO_6 fragments from an ideal octahedron. The [Sn-O] bond lengths are all unequal and the listed bond angles all deviate from being truly linear (180°) or perpendicular (90°) with the single exception of the bond angle $O(10)_{ax}$-Sn(1)-$O(8)_{eq}$ which equals 90.0°. The [Sn-O] bond length data compares favourably with the data for other compounds in which tin(IV) is bound by oxygen atoms. However, in this compound (**64**) the [Sn-O] bond lengths range from 1.892-2.125Å, the shorter bonds being unusually strong.

The two shortest [Sn-O] bonds in this structure are actually due to the α-hydroxyl groups, i.e. Sn(1)-O(10) (1.958Å) and Sn(2)-O(17) (1.892Å). On each fragment, the second citrate α-hydroxyl group produces a slightly longer [Sn-O] bond more in line with those due to the carboxylate groups, i.e. Sn(1)-O(3) (2.066Å) and Sn(2)-O(24) (2.028Å). The shortest of these bonds are unusually strong compared to those observed for other tin(IV) oxygen compounds.

For comparison, in Sn(EDTA).H_2O the [Sn-O] distances are significantly longer and range from 2.074-2.093Å, similarly in $Sn(NO_3)_4$ the [Sn-O] distances range from 2.145-2.195Å and in $K_6Sn_2(C_2O_4)_7.4H_2O$ the Sn-O distances range from 2.073-2.142Å.[176-178] Single crystal structural data for the simple tin(IV) carboxylates

is not available, e.g. structural data for $Sn(O_2CCH_3)_4$ has been determined from powder samples and is reliant upon comparisons with other isostructural compounds such as $Pb(O_2CCH_3)_4$.[183] However, in the simple tin(II) carboxylates, [Sn-O] bond lengths are typically somewhat longer than those in the tin(IV) species. For example, in $Sn(O_2CH)_2$, [Sn-O] bond lengths range from 2.14-2.36Å and in $Sn(C_2O_4)$ the [Sn-O] bond lengths range from 2.23-2.39Å.[115,113] A tin(II) cage compound, $Sn_6O_4(OMe)_4$, has been shown to have unusually strong [Sn-O] bonds within the cage (2.05-2.08Å) but these are still significantly longer than those to the α-hydroxyl groups in the tin(IV) citrate (**64**).

The distorted six-coordinate octahedral coordination observed in this compound is not observed in other simple tin(IV) carboxylates or oxy-acid salts. However, a similar six-coordinate tin coordination has been observed for the central tin(IV) site in $Sn^{II}_4Sn^{IV}O_2(O_2CCF_3)_8$, a mixed-valence compound whose structure has been determined crystallographically (Fig. 1.20).[122] The central tin(IV) atom is in a slightly distorted octahedral environment with the axial [Sn-O] distance (2.07Å) being slightly shorter than the equatorial [Sn-O] distance (2.12Å). Like those in (**64**) the [Sn-O] distances in this tin(IV) coordination are at the lower end of the range usually shown by tin(IV) oxy-acid salts. The SnO_6 unit in this case is not as distorted as that in (**64**). The [O_{eq}-Sn-O_{eq}] bond angle is 171.3° and the [O_{ax}-Sn-O_{eq}] angles range from 85.6° to 94.4°. In (**64**), the [O_{ax}-Sn-O_{eq}] angles range from 79.4° [O(3)-Sn(1)-O(4)] to 98.4° [O(11)-Sn(1)-O(3)] and [O_{eq}-Sn-O_{eq}] range from 171.0° [O(8)-Sn(1)-O4)] to 173.8° [O(1)-Sn(1)-O(11)]. The [O_{ax}-Sn-O_{ax}] bond angles also both deviate slighty from truly linear and range from 175.7° [O(17)-Sn(2)-O(24)] to 178.4° [O(3)-Sn(1)-O(10)].

Six coordinate tin(IV) is also found in other compounds. For example, two dithiocarbamate salts of general composition $Sn(S_2CNR_2)_4$ (R_1=C_2H_5, R_2=CH_3) have been structurally characterised and have been found to have distorted octahedral SnS_6 geometry about tin. This arises due to two bidentate and two monodentate ligands

with average [Sn-S] distances being quite different for the chelated (2.545, 2.583Å) and monodentate (2.504, 2.518Å) ligands due to strain in the chelate ring.[179,180]

In general, six coordination is very common for organotin(IV) species, although inorganic compounds such as the carboxylates often exhibit a higher coordination about the tin. Three examples of coordination number seven for an inorganic tin(IV) species have been investigated.[176,181] In $Sn(EDTA).H_2O$, the tin is coordinated by the two nitrogens and four carboxylate oxygens of the hexadentate EDTA ligand as well as the oxygen atom of the water molecule to form an unusual seven-coordinated molecule. The large deviations from planarity for any set of four or five donor atoms exclude descriptions of the molecule interms of pentagonal bipyramidal or capped trigonal prismatic geometries.

The unusual geometry of tin(IV) oxalato species, $K_6Sn_2(C_2O_4)_7.4H_2O$, consists of discrete dimeric units, $[Sn_2(C_2O_4)_7]^{6-}$, in which each tin is also seven coordinated, bonding to three terminal chelating oxalate groups and one 1,2-*trans*-bridging oxalate ligand. The geometry about tin is highly distorted and can best be described as tetragonal base-trigonal base.[178]

The tropolonato complexes of tin(IV), e.g. $Sn(C_7H_5O_2)_3(Cl).CHCl_3$, also display seven coordination. The coordination geometry is distorted pentagonal bipyramidal, oxygen atoms from the bidentate tropolonato groups occupying the five basal and one axial positions and the Cl^- ion occupying the final axial position. The axial bond to the oxygen is quite short (2.050Å) relative to that for the basal oxygens (2.130-2.168Å).

Eight coordination is quite rare in simple inorganic tin(IV) compounds. It has been confirmed for the structure of $Sn(NO_3)_4$ in which tin exhibits a regular dodecahedral coordination. The preference for dodecahedral coordination for tightly coordinated chelating ligands such as the nitrate may be explained in terms of the minimisation of ligand-ligand repulsions in this arrangement.[177] Crystal data for $Sn(O_2CCH_3)_4$ and $Pb(O_2CCH_3)_4$ show very close values for the unit cell parameters

and have the same space-group extinctions. The implication is that the two compounds are isomorphous.[182] It is known that lead(IV) acetate is eight coordinate which implies that tin(IV) acetate is also eight coordinate.[183]

Table 4.5 [Sn-O] bond lengths for the two SnO_6 octahedra in bis-citrato di-tetramethylammonium tin(IV) heptahydrate (**64**).

Bond	Length / Å	Bond	Length / Å
Sn(1)-O(1)	2.095(1)	Sn(2)-O(15)	2.040(2)
Sn(1)-O(3)	2.066(2)	Sn(2)-O(17)	1.892(2)
Sn(1)-O(4)	2.125(1)	Sn(2)-O(20)	2.041(2)
Sn(1)-O(8)	2.067(1)	Sn(2)-O(22)	2.062(3)
Sn(1)-O(10)	1.958(2)	Sn(2)-O(24)	2.028(3)
Sn(1)-O(11)	2.105(2)	Sn(2)-O(27)	2.111(2)

Note:-

E.s.d.'s are shown in parentheses.

Table 4.6 [O-Sn-O] bond angles for the two SnO_6 octahedra in bis-citrato di-tetramethylammonium tin(IV) heptahydrate.

Bond	Angle / °	Bond	Angle / °
O(1)-Sn(1)-O(11)	173.8(5)	O(15)-Sn(2)-O(27)	171.5(9)
O(3)-Sn(1)-O(10)	178.4(5)	O(17)-Sn(2)-O(24)	175.7(8)
O(8)-Sn(1)-O(4)	171.0(6)	O(20)-Sn(2)-O(22)	172.0(0)
O(1)-Sn(1)-O(3)	87.1(6)	O(15)-Sn(2)-O(17)	92.8(9)
O(1)-Sn(1)-O(4)	86.3(5)	O(15)-Sn(2)-O(20)	89.5(8)
O(1)-Sn(1)-O(8)	93.8(5)	O(15)-Sn(2)-O(22)	92.2(0)
O(1)-Sn(1)-O(10)	92.5(7)	O(15)-Sn(2)-O(24)	91.4(0)
O(10)-Sn(1)-O(4)	99.0(7)	O(20)-Sn(2)-O(24)	96.3(9)
O(10)-Sn(1)-O(11)	81.9(7)	O(24)-Sn(2)-O(27)	81.7(0)
O(10)-Sn(1)-O(8)	90.0(7)	O(24)-Sn(2)-O(22)	91.8(0)
O(11)-Sn(1)-O(8)	89.0(6)	O(27)-Sn(2)-O(22)	83.7(0)
O(11)-Sn(1)-O(4)	91.9(6)	O(27)-Sn(2)-O(20)	95.8(9)
O(11)-Sn(1)-O(3)	98.4(6)	O(27)-Sn(2)-O(17)	94.2(9)
O(3)-Sn(1)-O(8)	91.6(6)	O(17)-Sn(2)-O(22)	87.1(0)
O(3)-Sn(1)-O(4)	79.4(6)	O(17)-Sn(2)-O(20)	84.9(9)

Note:-

E.s.d.'s are shown in parentheses.

Two trivalent citrate ligands, $(Hcit)^{3-}$, coordinate in a similar fashion to each tin atom [Sn(1), Sn(2)] through the central carboxylate, one of the terminal methylene carboxylates and the hydroxyl group which is α- to the central carboxylate giving rise to a distorted octahedral arrangement. The two deprotonated carboxylate groups from each citrate coordinate to the tin atom through one oxygen in a unidentate fashion as suggested by the [C-O] bond lengths.

The [C-O] bond lengths for the coordinated carboxylates are presented in a like *vs.* like format in Table 4.7. Each citrate group has a free acid function, CH_2CO_2H. Comparing the [C-O] bond length data for these acid groups shows that each of the two fragments has a true CO_2H group while the second citrate appears to have a highly delocalised CO_2H group. The two free acids which have a strong [C=O] bond, O(5)-C(5)-O(6) and O(25)-C(23)-O(26), have [C-O] bonds which differ by 0.150 and 0.182Å respectively. The bond angles for these two groups are 123.3° and 116.8° respectively, i.e. close to the ideal sp^2 angle of 120°. The remaining free acid groups, O(13)-C(12)-O(14) and O(18)-C(17)-O(19) have [C-O] bond lengths which differ by just 0.029 and 0.024Å respectively, i.e. the [C=O] character is lost through delocalisation. The bond angles for these two groups are 126.9° and 123.7° which are still quite close to the ideal for a CO_2H group. The free CH_2CO_2H groups in which a strong [C=O] bond is observed can be compared with the additional $[CH_2CO_2]^-$ groups which are bound to tin. In these groups, O(1)-C(1)-O(2), O(8)-C(7)-O(8), O(15)-C(13)-O(16) and O(22)-C(19)-O(23) the difference in the two [C-O] bond lengths ranges from 0.083Å [C(19)] to 0.330Å [C(13)]. The bond angles range from 104.0° [C(19)] to 128.8° [C(7)]. These figures serve to illustrate the diversity of [C=O] bond character within the terminal CH_2CO_2Sn bonding.

For both fragments, Sn(1) and Sn(2), the two citrate anions chelate to tin with facial (*fac*) isomerism as opposed to the meridional (*mer*) form. Each tridentate citrate group is bound to the tin through three oxygen atoms which lie at the three vertices of a common face of the octahedral unit.

Interestingly, in each of the two units, $Sn(1)(Hcit)_2$ and $Sn(2)(Hcit)_2$, the two citrate groups appear to bond to the central tin in a different way based on the crystallographic bond length data. In the Sn(1) fragment, one trivalent citrate ligand appears to chelate to tin exclusively through the longer [C-O] bonds of the CO_2^- groups [C(7)-O(8), 1.291Å; C(10)-O(11), 1.382Å]. However, the second citrate chelates to Sn(1) through the shorter [C=O] bonds *via* the oxygen lone pairs as shown in Fig. 4.6(a) [C(1)-O(1), 1.101Å; C(6)-O(4), 1.192Å]. In this SnO_6 unit, the negative charge is localised on one of the citrate ligands.

In contrast, for the Sn(2) fragment, all of the chelating carboxylates bind to tin through the longer [C-O] bond with the exception of the C(24) carboxylate which coordinates through the shorter C(24)-O(27) bond (1.151Å) as shown in Fig. 4.6(b). Overall, each of the bis-citrato tin(IV) moeities have a -2 charge which is countered by the $N(CH_3)_4^+$ ions.

In both fragments, the two α-hydroxyl groups from each of the two citrates $(Hcit)_a$ and $(Hcit)_b$ both lie in the axial positions, i.e. they are located *trans* to each other. Around the equatorial positions, the bound carboxylate groups from the two citrates are not configured in a like *vs.* like *trans* arrangement. The methylene CH_2CO_2 group from $(Hcit)_a$ lies *trans* to the central R_2CO_2 group from the $(Hcit)_b$ group.

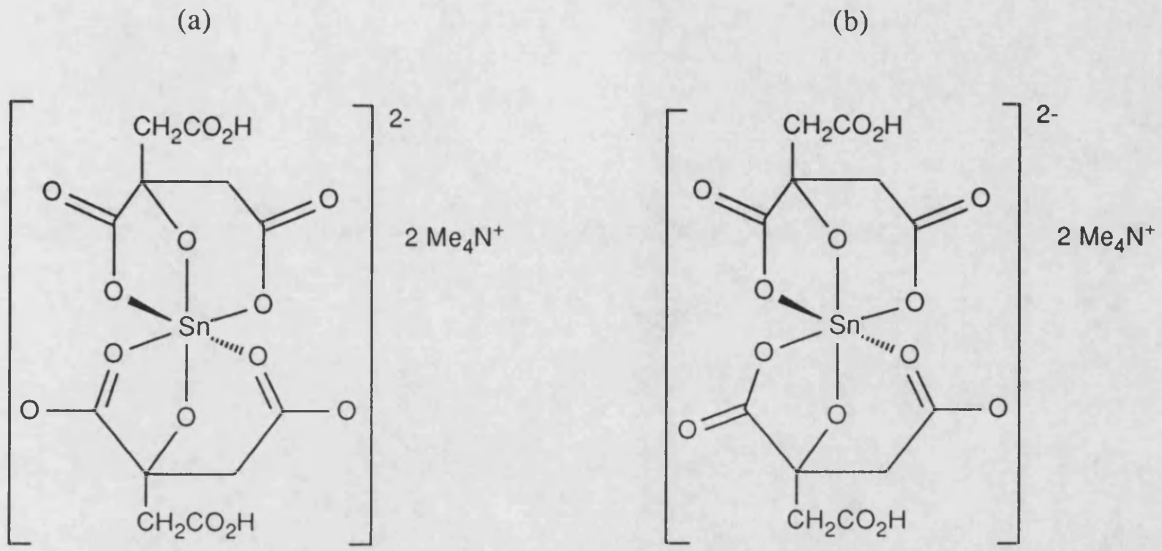

Fig. 4.6 The coordination of two citrate dianions to (a) Sn(1) and (b) Sn(2) in (**64**) based upon crystallographic bond length data.

Table 4.7 [C-O] bond lengths for the citrate ligands in bis-citrato di-tetramethylammonium tin(IV) heptahydrate (**64**).

Bond	Length / Å	Bond	Length / Å
Sn(1)		**Sn(2)**	
C(1)-O(1)	1.101(2)	C(13)-O(15)	1.563(3)
C(1)-O(2)	1.214(2)	C(13)-O(16)	1.233(2)
C(3)-O(3)	1.323(3)	C(15)-O(17)	1.582(4)
C(5)-O(5)	1.348(3)	C(17)-O(18)	1.271(4)
C(5)-O(6)	1.198(3)	C(17)-O(19)	1.295(4)
C(6)-O(7)	1.278(2)	C(18)-O(20)	1.457(4)
C(6)-O(4)	1.192(3)	C(18)-O(21)	1.190(3)
C(7)-O(8)	1.291(2)	C(19)-O(22)	1.406(5)
C(7)-O(9)	1.204(2)	C(19)-O(23)	1.323(4)
C(9)-O(10)	1.409(3)	C(21)-O(24)	1.464(4)
C(12)-O(13)	1.225(3)	C(23)-O(25)	1.450(3)
C(12)-O(14)	1.196(3)	C(23)-O(26)	1.268(3)
C(10)-O(11)	1.382(2)	C(24)-O(27)	1.151(4)
C(10)-O(12)	1.187(2)	C(24)-O(28)	1.332(3)

Note:-

E.s.d.'s are shown in parentheses.

The interaction between the citrate group and a wide range of metal ions has been extensively studied. Many such metal-citrate complexation studies have been performed using formation and stability constants and multinuclear NMR data.[184-193] However, very little information is contained within the literature about the chelation of citric acid to tin(IV). A recent study of a platinum-tin complex with citrate ligands has proposed the complex dimeric structure $[(SnHcit)_4Pt(\mu\text{-}SnHcit)_2Pt(SnHcit)_4]^{6-}$ (Hcit = citrate^{3-}). The central feature of this structure is claimed to a complex anion, $[Pt_2(SnHcit)_{10}]^{6-}$ as illustrated in Fig. 4.7. However, this structure has been determined by the method of radial distribution functions of atoms in powder samples and in solution and not X-ray crystallography.[194]

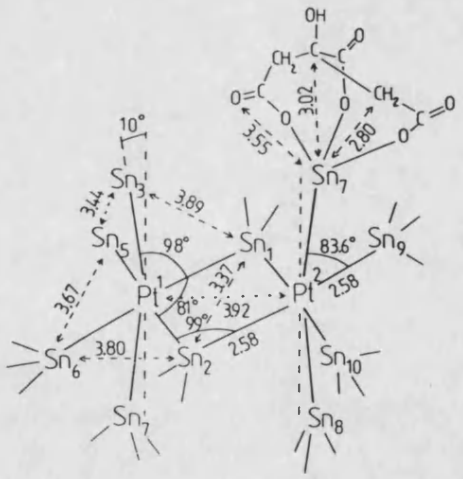

Fig. 4.7 The proposed structure of the complex anion $[Pt_2(SnHcit)_{10}]^{6-}$.

In addition to the potentiometric and spectroscopic studies above, an extensive range of structural data is also available for the complexes of citric acid with a variety of main-group and transition metals. Accordingly, there is a wide variety in the mode of chelation with the citrate anion occurring in the mono-, di-, tri- and tetravalent form. Selected examples of metal-citrate modes of chelation, as determined

crystallographically, are briefly summarised in Table 4.8.

This tabulated data serves to illustrate the diversity and the complexity of citrate chelation to metal ions. Although it has been predicted that the citrate ligand deprotonates in the order central carboxylate (pK_{a1}), followed by the two terminal carboxylates ($pK_{a2,3}$), followed by the α-hydroxyl group, the structural data for this series of compounds shows that this is clearly not always the case.[205] The particular mode of $(Hcit)^{3-}$ tridentate chelation observed for (**64**) has also been observed in other compounds such as $[Mn(H_2O)_6]^{2+}[Mn(Hcit)(H_2O)]_2^{-}.2H_2O$, $[Mg(H_2O)_6]^{2+}$-$[Mg(Hcit)(H_2O)]_2^{-}.2H_2O$ and the trivalent $(Hcit)^{3-}$ citrate ligands in $K_2Sb_4(H_3cit)_2(H_2cit)_4(Hcit)_2(H_2O)_2$. However, equally common in other species is the predicted trivalent state involving chelation of the three carboxylates. These different modes of chelation for trivalent citrate have been ascribed to the influence of the ionised central carboxylate upon the α-hydroxyl group. In certain circumstances, ionisation of the hydroxyl is preferred over the second terminal carboxylate.

The lattice structure of (**64**) is largely determined by the interactions between the non-bound oxygens of the central carboxylate groups on each metal [O(7), O(12) on Sn(1); O(21), O(28) on Sn(2)] and one oxygen from each of the non-bonded terminal methylene carboxylate moieties [O(5), O(13) on Sn(1); O(19), O(25) on Sn(2)]. Each of these four oxygens belong to the longer [C-O] bond as opposed to the shorter bond with greater [C=O] character. Thus it is likely that the residual citrate proton lies in the vicinity of these two types of centres.

Typically, O(7) and O(13) hydrogen bond with O(25) and O(21) respectively to form dimers [O(7)-O(25), 2.66Å; O(13)-O(21), 2.61Å]. In addition, O(12) interacts with O(5) of the molecule generated *via* the operator 1-*x*, 1-*y*, -*z*, [O(12)-O(5), 2.57Å], and in tandem, O(28) interacts with O(19) of the molecule generated *via* the operator 1-*x*, -*y*, 1-*z* [O(28)-O(19), 2.67Å]. This effectvely results in the formation of stair-like linear chains of molecules running diagonally through the lattice, held together by pairs of hydrogen bonds.

Table 4.8 The citrate chelating modes in documented metal-citrate compounds.

		Mode of chelation[a]				
Compound		$-[CO_2]^-$	$-CH_2[CO_2]^-$	$-CH_2[CO_2]^-$	$-C[O]^-$	Ref.
$K_2(H_2cit)$		1	1	0	0	195
$LiK_2(H_3cit)(H_2cit)$	(i)[b]	1	0	0	0	195
	(ii)	0	1	1	0	
$Sr_3(Hcit)_2.5H_2O$		1	1	1	0	196
$K_2Sb_4(H_3cit)_2(H_2cit)_4(Hcit)_2(H_2O)_2$	(i)	1	0	0	0	197
	(ii)	1	0	0	1	
	(iii)	1	1	0	1	
$[LiSb(H_2cit)_2(H_2O)].2H_2O$	(i)	1	0	0	1	197
	(ii)	1	0	0	1	
$Sb_2Ag_2(H_2cit)_4$		1	0	0	1	198
$[SbNa(H_2cit)(H_2O)_2].H_2O$		1	0	0	1	198
$NH_4[Ag_2(Hcit)H_2O]_n$		1	1	1	0	199
$[Mn(H_2O)_6][Mn(Hcit)(H_2O)_2]_2.H_2O$		1	1	0	1	200
$[Mg(H_2O)_6][Mg(Hcit)(H_2O)_2]_2.H_2O$		1	1	0	1	201
$[Al_3(cit)_3(OH)(H_2O)]^{4-}$		1	1	1	1	202
$K_{5-x}(NH_4)_x[Bi_2(cit)_2(Hcit)].(H_2O)_y$	(i)	1	1	1	1	203
(x=0.25, y=13)	(ii)	1	1	1	0	
$(NH_4)_8[Bi_2(cit)_2(Hcit)_2(H_2O)_4](H_2O)_2$	(i)	1	1	1	1	203
	(ii)	1	1	1	0	
$[Fe(H_2O)_6][Fe(Hcit)H_2O].2H_2O$		1	1	1	0	204
$(Me_4N)_5[Ni(cit)_3(OH)H_2O)].18H_2O$		1	1	1	1	204

Note:-
[a]0, Group not deprotonated; 1, Group deprotonated.
[b]Denotes citrate type where more than one is present, e.g. Hcit, H_2cit.

Location and refinement of the water molecules [O(1′)-O(8′)] was extrememly difficult due to the complex nature of the water bonding. The bonding which surrounds the water molecules is both complex and multiple and it is indeed a fair assessment to say that these solvent molecules effectvely 'cement' the entire lattice together. Two of the water sites [O(5′), O(8′)] have half-site occupancies as a result of disorder ranging between two symmetry related positions, proximate to each other in both cases. The hydrogen bonding which surrounds the water molecules [O(1′)-O(8′)] in this compound is complex. The way that the water molecules are incorporated into the lattice is illustrated in Fig. 4.8, two of the water sites having half-occupancy [O(5′), O(8′)] as stated above. The water molecules interact through hydrogen bonding in a complex manner, both with other adjacent water molecules and the citrate groups although none are bound directly to either tin atom, Sn(1) or Sn(2). These hydrogen bonded interactions are graphically illustrated in the figure as broken lines. The (non-bonded) distances between oxygen atoms range from 1.765 to 3.087Å as follows:-

O(1′) interacts with a second water molecule O(3′) (2.554Å) and a citrate residue bound to Sn(1), i.e. O(9′) (3.048Å). O(2′) interacts with O(4′) (2.927Å) and two citrate residues, one bound to Sn(1), i.e. O(6) (2.874Å), and the other bound to Sn(2), i.e. O(23) (2.682Å). As well as the interaction with O(1′) and O(3′) also interacts with a second O(3′) water molecule (2.723Å). Similarly, O(4′) interacts with a second O(4′) (2.699Å) and O(17) (2.778Å) from a citrate group attached to Sn(2) as well as O(2′). O(5′) interacts with two water molecules, i.e a second O(5′) (1.765Å) and O(6′) (3.087Å). A further interaction with O(10) (2.878Å) from one of the citrates bound to Sn(1) is also observed. O(6′) interacts with O(2) (3.040Å) as well as with O(2′) and O(5′). Finally, O(8′) interacts strongly with a second O(8′) (1.787Å), and two citrate oxygens from different citrate groups, i.e. O(7) (2.214Å) and O(24) (2.804Å).

The net result of these complex water-water and water-citrate interactions is a

highly symmetrical 'puckered sheet' of water molecules [O(2'), O(4'), O(5'), O(6')] running through the middle of the unit-cell parallel to the *a*-axis as shown in Fig. 4.8. A second symmetrical plane of water molecules [O(1'), O(3')] is observed both at the top and bottom of the unit-cell. Finally, water molecules [O(8')] effectively fill-in the vacant spaces in the corners of the unit-cell. Essentially, the water molecules are found to fill the void space within the unit-cell and it is a fair assessment to say that the water molecules effectively 'cement' the entire lattice together.

The fact that the carboxylate groups bind to tin in a unidentate manner is consistent with the fact that $\upsilon_{as}(CO_2Sn)$ occurs as a broad band at 1644cm^{-1}. The lattice packing diagram shows that many of the tin-bound carboxylates do not come into proximity of water molecules, i.e. hydrogen bonding does not occur to non-bonding oxygens [e.g. O(12), O(21)]. Therefore, the infrared data is consistent with the presence of primarily unidentate coordination. The fact that a band is also observed at 1727cm^{-1} also suggest the presence of non-hydrogen bound free acid groups with a strong [C=O] bond character. The packing diagram shows that the free acid groups do not exhibit hydrogen bonding to water molecules which would significantly lower the frequency of this band. However, these groups are involved in inter- and intramolecular bonding to form the dimeric Sn(1)-Sn(2) units which suggests that these bonds must be relatively weak. As stated above, these bond lengths range from 2.57-2.66Å which must be sufficiently weak to have little effect upon the position of the $\upsilon(CO_2H)$ band.

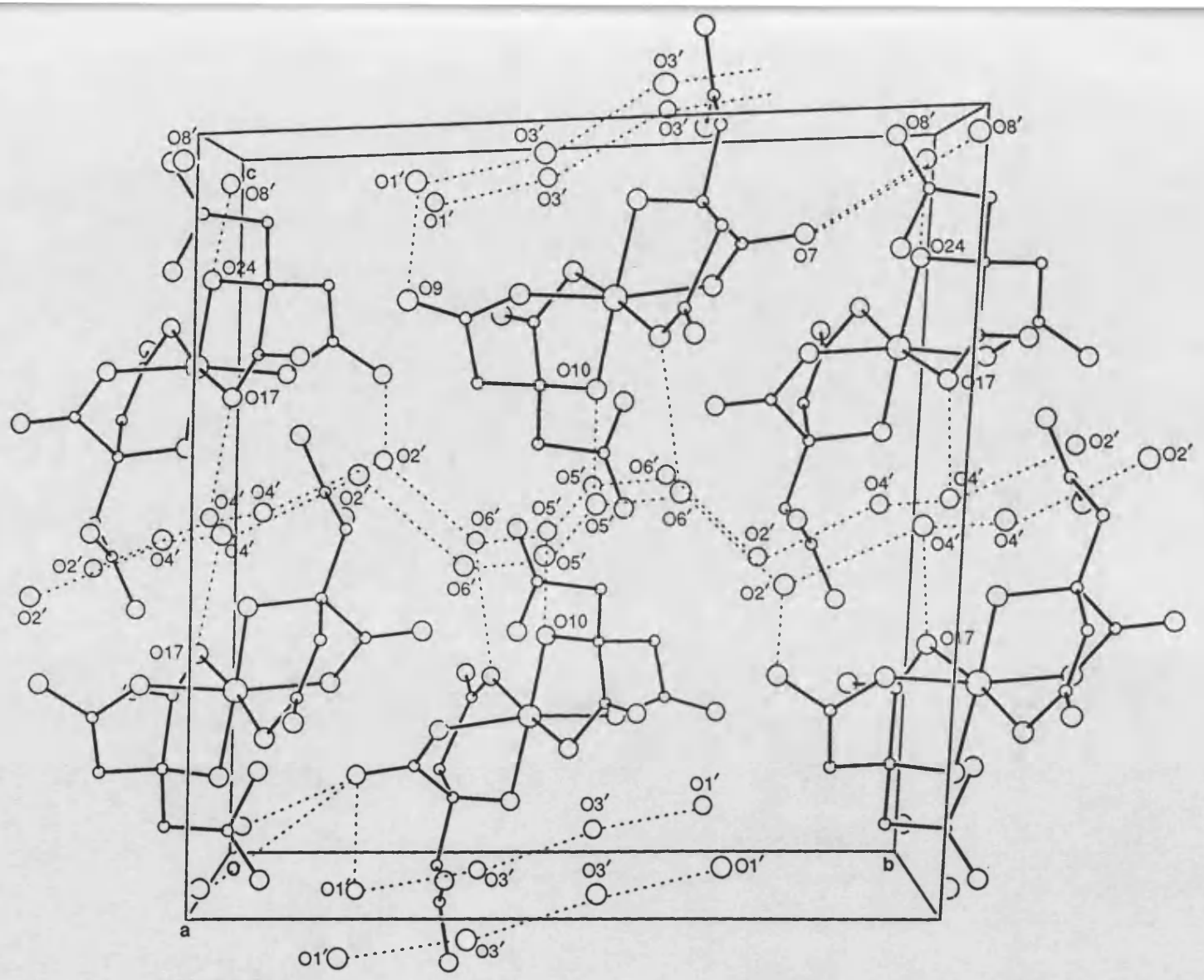

Fig. 4.8 The hydrogen bonding interactions of the water molecules within the lattice of (**64**).

4.3.2 *The Crystal Structure of Mono-stannous 1,3-dimethylcitrate Mono-methanolate* **(60).**

A crystal of approximate dimensions 0.2 x 0.2 x 0.2mm was mounted in a Lindemann capillary tube with a little supernatant methanol and used for data collection.

The asymmetric unit and the mode of dimerisation is illustrated in Fig. 4.9. Crystal data, full tables of final fractional atomic coordinates, isotropic thermal parameters, bond distances and angles are presented in full in Appendix 3.

The tin atom in this compound is found to be distorted ψ-trigonal bypyramidal four coordinate, SnO_4E. Three of the four oxygens around the tin are due to the central carboxylate O(2) and the α-hydroxyl group O(1) from one dimethylcitrate ligand together with the oxygen from the coordinated methanol molecule O(8). The fourth oxygen is due to the α-hydroxyl oxygen of an adjacent molecule O(1′), i.e. this compound exists as discrete dimeric units in the solid-state. The two halves of the dimeric unit are linked by an inversion centre, *i*. Although the 1,3-dimethylcitrate ester was deliberately prepared in order to exclude the terminal CH_2CO_2H carboxylate groups from coordinating to the tin, this type of citrate chelation has been observed elsewhere in non-esterified citrate compounds. For example, the antimony citrate compounds $Sb_2Ag_2(H_2cit)_4$ and $[SbNa(H_2cit)(H_2O)_2].H_2O$ have been found to contain divalent citrate anions which coordinate exclusively through the central carboxylate and the α-hydroxyl group (Table 4.8).[198]

The central feature of this dimeric unit is a four-membered [Sn(1)-O(1′)-Sn(1′)-O(1)] ring. The [Sn-O] bond lengths and [O-Sn-O] bond angles relkating to this unit are presented in Tables 4.9 and 4.10 respectively.

The [Sn-O] bond lengths range from 2.094-2.393Å which is significantly longer than those in the tin(IV) citrate (**64**) described above (Section 4.2.1). In this

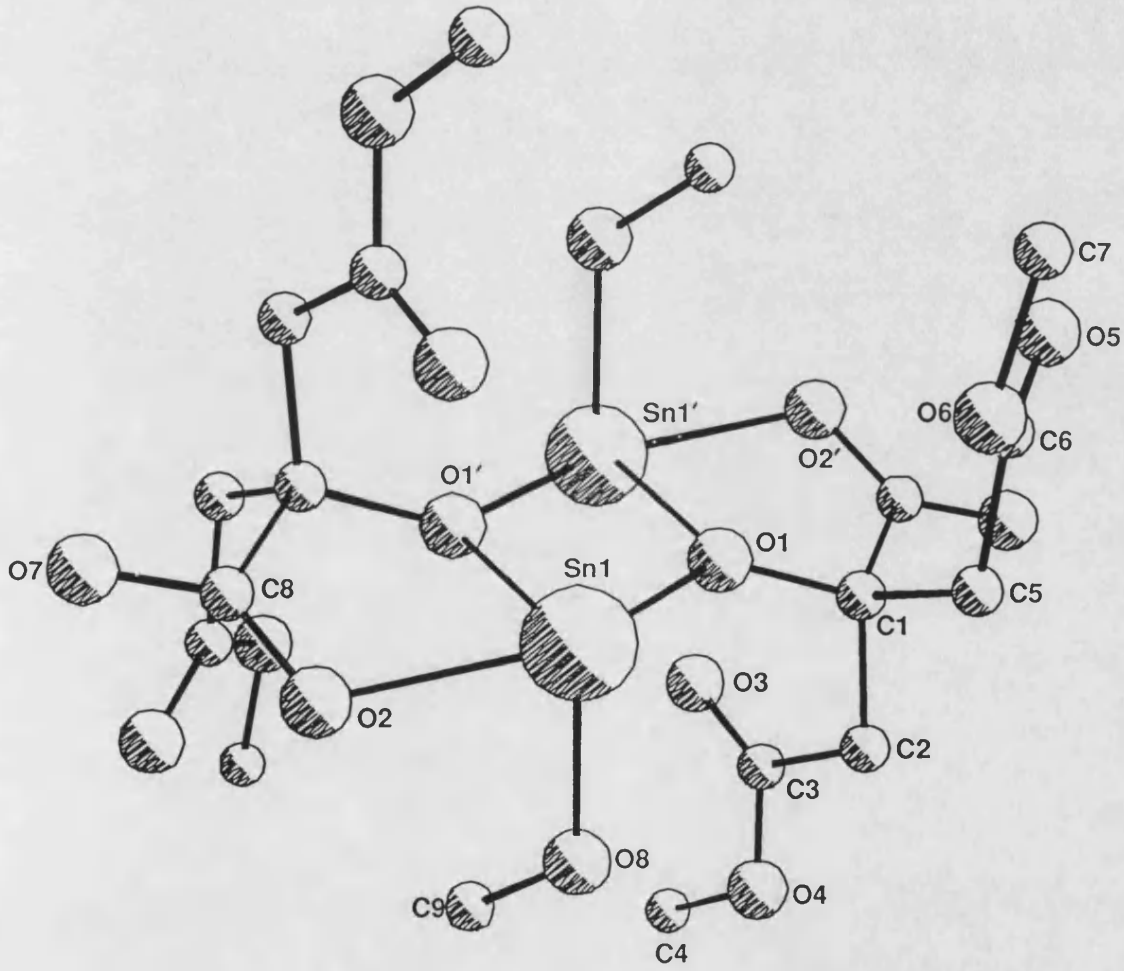

Fig. 4.9 The dimeric structural unit for mono-stannous 1,3-dimethylcitrate mono-methanolate (**60**).

Table 4.9 [Sn-O] bond lengths for stannous 1,3-dimethylcitrate mono-methanolate (**60**).

Bond	Length / Å
Intramolecular	
Sn(1)-O(1)	2.393(5)
Sn(1)-O(2)	2.266(5)
Sn(1)-O(8)	2.272(6)
Intermolecular	
Sn(1)-O(1′)	2.094

Note:-

E.s.d.'s are shown in parentheses.

Table 4.10 [O-Sn-O] bond angles for stannous 1.3-dimethylcitrate mono-methanolate (**60**).

Bond	Angle / °
O(1)-Sn(1)-O(2)	137.4(1)
O(1)-Sn(1)-O(8)	83.7(2)
O(2)-Sn(1)-O(8)	84.4(2)

Note:-

E.s.d.'s are shown in parentheses.

stannic citrate compound the [Sn-O] bond lengths range from 1.892-2.125Å, the shorter bonds in this compound being unusually strong for a tin carboxylate. The shortest of the bonds in the tin(IV) species actually relate to the coordination of the α-hydroxyl groups to tin. The tin(IV) citrate also has a higher coordination number about tin, i.e. a distorted octahedral SnO_6 arrangement.

Comparison of the structure of the tin(II) citrate (**60**) with other simple tin(II) carboxylates shows that the four coordinate ψ-trigonal pyramidal geometry is prevalent. In the simplest case of tin(II) formate, $Sn(O_2CH)_2$, tin forms two short equatorial (2.14, 2.20Å) and two longer axial bonds (2.36Å) to oxygen atoms from four formate groups.[115] However, this situation is not replicated in the citrate compound in which there is one very short intermolecular [Sn(1)-O(1′)] bond (2.094Å) to the α-hydroxyl oxygen from an adjacent molecule, two short [Sn(1)-O(2); Sn(1)-O(8)] bonds (2.266, 2.272Å) to the central carboxylate and the methanol and one significantly longer intramolecular bond (2.392Å). The longer of these [Sn-O] bonds [Sn(1)-O(1)] bond arises due to the α-hydroxyl group [C(1)-O(1)] on the first dimethylcitrate anion. This latter tin(II) alkoxide [Sn-O] bond is significantly longer than [Sn-O] bonds in other tin(II) alkoxide compounds. However, the former intermolecular [Sn-O] alkoxide bond is more typical of the bond lenghts in this type of compound. For example, the [Sn-O] bond lengths in the dimeric $[Sn(OBu^t)_2]_2$ range from 1.97(2)Å for the terminal bonds to 2.16Å within the O-Sn-O bridge.[48] The [Sn-O] distances in $Sn_6O_4(OMe)_4$, a partial hydrolysis product of $Sn(OMe)_2$, are also very short at 2.05(1)-2.08(1)Å within the adamantane cage. The bonds outside of the $[Sn_6O_4]^{4+}$ cage to the methoxy groups are more typical of those found in other tin(II) compounds [2.35(1)-2.43(1)Å].[127] Finally, in the THF adduct of the tin(II) catechol complex $[Sn(1,2\text{-}O_2C_6H_3NO_2\text{-}4)(C_4H_8O)_n]$ the [Sn-O] distances to the ligand are 2.112(4) and 2.208(4)Å.[221]

Simple tin(II) compounds such as tin(II) formate show a vacancy in the coordination sphere at the equatorial position due to the stereochemically active

lone-pair, E. The tin(II) citrate also has an equatorial vacancy at the tin atom due to the lone-pair of electrons. Careful examination of the structural data for (**60**) reveals a fifth oxygen atom in close proximity to the tin atom. The intermolecular distance [Sn(1′)-O(3)] is just 2.787Å which could be indicative of a weak [Sn-O] bond, i.e. the tin atoms would exhibit ψ-octahedral SnO_5E coordination. O(3) approaches Sn(1′) from below the plane of the dimeric [Sn(1)-O(1)-Sn(1′)-O(1′)] four-membered ring. However, the C(3)-O(3) bond is very short (1.198Å) which, in turn, would suggest that the [C=O] bond is very strong. This would suggest that the above interaction is not relevant in the coordination sphere around tin and the tin atoms are truly four coordinate.

The [O-Sn-O] bond angles are quite different for the formate and the citrate although the basic ψ-trigonal pyramidal geometry is apparently maintained, as illustrated in Fig. 4.10. The biggest difference in the bond angles for these two compounds lies in the [O(1)-Sn(1)-O(2)] angle. In the citrate compound, this angle is substantially reduced to 137.4° most probably due to ring strain in the five-membered ring [Sn(1)-O(2)-C(8)-C(1)-O(1′)].

The structures of tin(II) oxalate, $Sn(C_2O_4)$, and dipotassium bis-oxalatostannate(II) monohydrate, $K_2Sn(C_2O_4)_2.H_2O$ also show the tin atoms to have ψ-trigonal pyramidal SnO_4E coordination.[113] In common with both the formate and the citrate, the [Sn-O] bond lengths consist of two short (2.13-2.23Å) and two long (2.36-2.39Å) bonds although the oxalate ligand bridges adjacent tin atoms.

In summary, the stannous salt of 1,3-dimethylcitrate achieves a four-coordinate SnO_4E tin environment through a combination of dimerisation and methanol solvation. Other simple tin(II) carboxylates for which structural data is available achieve the four coordinate state through bridging to form infinite chains (Section 1.8.3). Note that in the case of the complex tricarboxylato anions, $[Sn(O_2CR)_3]^-$ (R=H, CH_3), pyramidal three coordination is observed.[117,118] In these compounds the three [Sn-O] bond lengths are all approximately 2.15Å with each

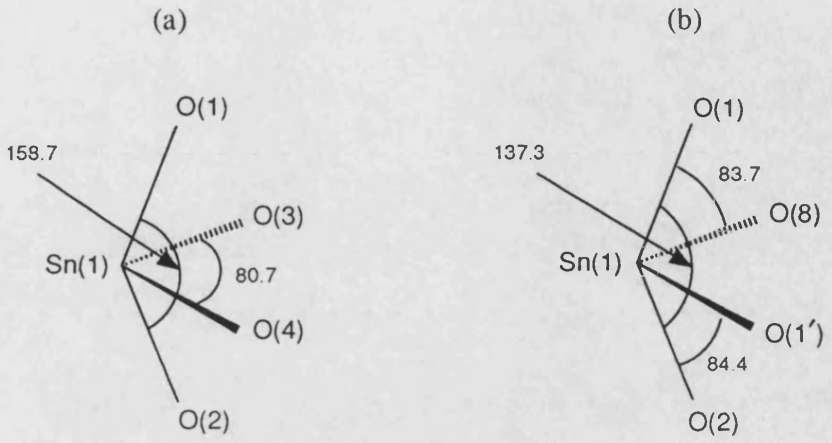

Fig. 4.10 The ψ-trigonal pyramidal geometry of (a) $Sn(O_2CH)_2$ and (b) Sn(1,3-dimethylcitrate).MeOH.

carboxylate bonding in a unidentate manner.

The [C-O] bond lengths for stannous 1,3-dimethylcitrate are presented in Table 4.11. Examination of these bond lengths clearly shows that although the central carboxylate coordinates to the tin atom in a unidentate manner [C(8)-O(7)] (1.234Å) is only marginally shorter than [C(8)-O(2)] (1.265Å). However, the esterified carboxylates [C(3), C(6)] clearly show the presence of a strong [C=O] carbonyl bond which is 0.125-0.139Å shorter than the [C-O-(CH_3)] bond. The hydroxyl C(1)-O(1) bond is significantly longer (1.419Å) than those of the carboxylates as expected.

The lattice structure is built up from a series of the discreet dimeric tin(II) citrate units. Although a methanol molecule is coordinated directly to the tin atom, there is no evidence for the presence of further solvent molecules in the lattice. The individual dimers are bound together through a series of hydrogen bonds which results in the formation of infinite two-dimensional molecular sheets running parallel to the *bc* plane. The hydrogen bonding involves the proton H(8) attached to O(8) from the coordinated methanol and the non-bonded oxygen from the central carboxylate, O(7) as shown in Fig. 4.12. Typically, H(8) of the asymmetric unit

Table 4.11 [C-O] bond lengths for stannous 1,3-dimethyl-citrate mono-methanolate (**60**).

Bond	Length / Å
C(3)-O(3)	1.198(7)
C(3)-O(4)	1.337(7)
C(6)-O(5)	1.194(7)
C(6)-O(6)	1.339(7)
C(8)-O(2)	1.265(7)
C(8)-O(7)	1.237(7)
C(1)-O(1)	1.416(6)
C(4)-O(4)	1.457(7)
C(7)-O(6)	1.450(8)

Note:-

E.s.d.'s are shown in parentheses.

interacts with O(7) of the lattice neighbour *via* the operator -*x*, 0.5+*y*, 0.5-*z*. H(8) was located in the close proximity of O(8) [O(8)-H(8), 0.960(2)Å]. The length of the hydrogen bonds [H(8)-O(7)] are 1.63Å and the angle [O(8)-H(8)-O(7)] equals 166.8°. The fact that this hydrogen bond is quite linear is an indication that it is quite a strong interaction. The non-bonded distance O(7)-O(8) is 2.577Å.

The fact that the central carboxylate is involved in extensive hydrogen bonding accounts for the unexpected similarity of the [C-O] bond lengths, i.e. [C(8)-O(2), 1.265Å; C(8)-O(7), 1.237Å]. The double bond character of the [C(8)-O(7)] bond is effectively reduced through delocalisation throughout the hydrogen bonded network as shown in Fig. 4.2(c). In turn, this loss of double bond character accounts for the infrared data in which the $\upsilon_{as}(CO_2Sn)$ band occurs at

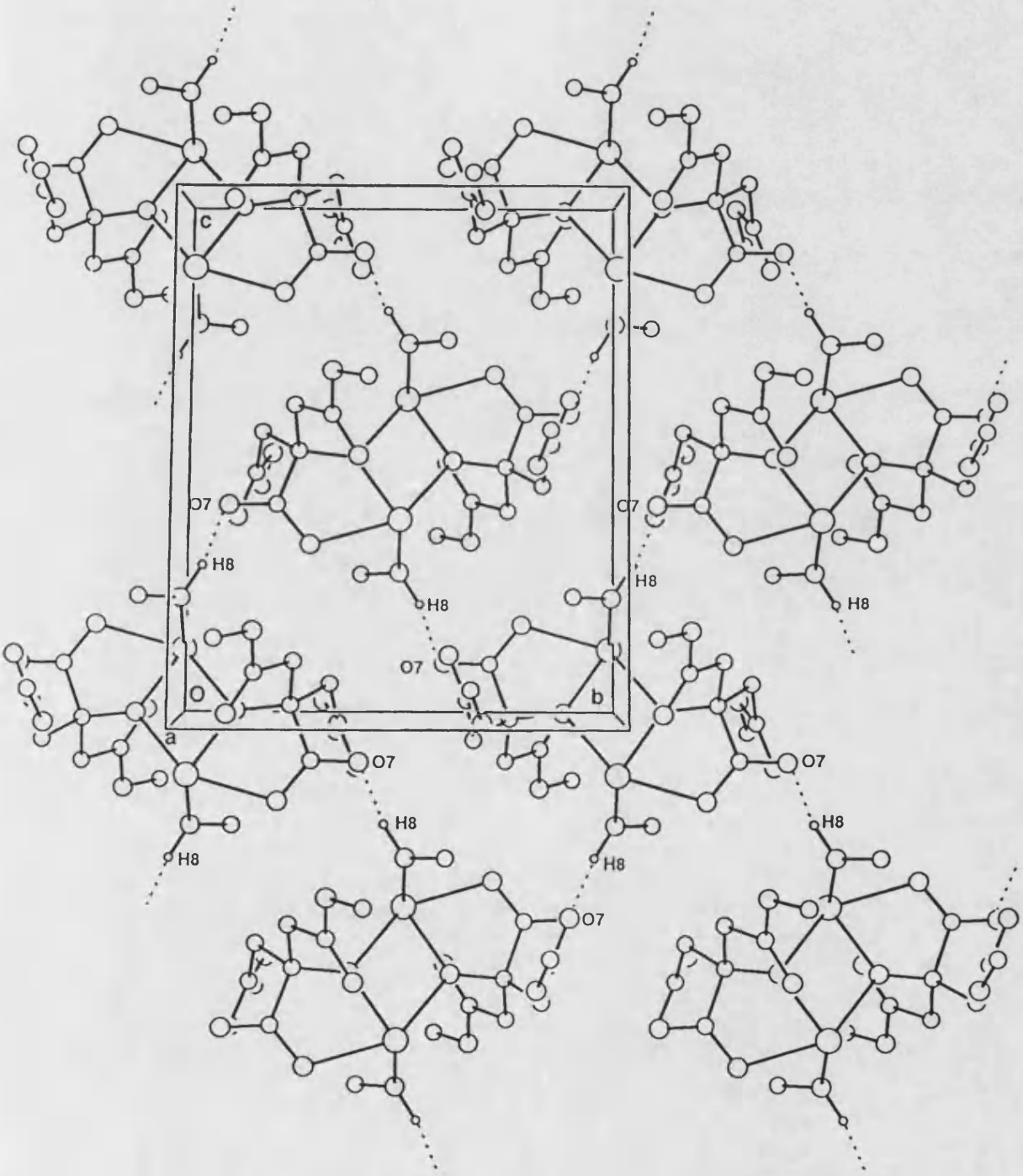

Fig. 4.12 The lattice packing diagram for stannous 1,3-dimethylcitrate mono-methanolate (**60**) showing the hydrogen bonding.

unexpectedly low frequency (1561cm^{-1}) in spite of the fact that the central carboxylate has been identified to bond in a unidentate manner. The fact that $\upsilon(CO_2Sn)$ in the tin(IV) citrate occurs as a broad band at 1644cm^{-1} suggests that the hydrogen bonding must be more extensive in the tin(II) citrate compound. The [C=O] bond length data does not truly reflect this fact however, the C(8)-O(7) bond in (**60**) (1.237Å) is very similar to the average [C=O] bond length in (**64**) (1.220Å). However, the tin(IV) compound shows a wide spread of [C=O] bond lengths (1.101-1.332Å) which accounts for the broad band in the infrared.

4.4 The Interaction of Di-stannous Citrate With Fluoride Ions in Aqueous Solution.

The interaction of ionic fluorides (e.g. NaF, NH_4F) with insoluble stannous compounds has already been described in detail for stannous pyrophosphate (Chapter 2) and stannous α-D-glucose-1-phosphate (Chapter 3). In both cases, the insoluble material is rapidly solubilised upon exposure to two molar equivalents of an ionic fluoride per tin atom. Spectral and physical data suggests that the fate of the tin is very similar in both cases, i.e. formation of a complex tin(II) fluorophosphate.

It is also observed experimentally that four molar equivalents of fluoride (i.e. two per tin) are required to fully solubilise di-stannous citrate (**51**). Although the product of this reaction is readily water soluble, attempted crystallisation of a solid product from solution was not successful. A selection of ionic fluoride sources were used to solubilise the citrate in order to understand the fate of the tin atoms. The fluorides used included sodium fluoride, potassium fluoride, ammonium fluoride and tetra-n-butylammonium fluoride, i.e. a large, bulky organic cation in the hope of obtaining an organic-soluble product.

^{119}Sn Mössbauer and the ^{119}Sn and ^{19}F NMR data for this series of solubilised citrates is presented in Tables 4.12 and 4.13 respectively. Also included is the data for the series of soluble citrates, $Na_2Sn(cit)$ (**52**), $K_2Sn(cit)$ (**53**) and $(NH_4)_2Sn(cit)$ (**54**) as well as $NaSnF_3$ (**35**) and NaF. Unfortunately, the attempted preparation of $(Bu^n_4N)_2Sn(cit)$ was not successful. The oily product was highly unstable and contaminated with tin(IV) impurities.

In contrast to the solubilised phosphates, the ^{119}Sn Mössbauer data for the series of solubilised citrates are remarkably similar to that of the starting material, $Sn_2(cit)$ (**51**). The Mössbauer data for the series of water-soluble citrates (**52-54**) is also very similar to the data for the solubilised species. The implication of this data is

Table 4.12 ^{119}Sn Mössbauer data for the solubilised tin(II) citrates.[a]

Compound	δ (mms^{-1})	Δ (mms^{-1})	Γ (mms^{-1})	Γ (mms^{-1})
Sn_2(citrate) (**51**)	3.07	1.90	1.08	1.06
Sn_2(cit) + 4NaF (**65**)	3.10	1.90	0.96	1.01
Sn_2(cit) + 4KF (**66**)	3.00	1.97	1.01	1.03
Sn_2(cit) + 4NH_4F (**67**)	3.06	1.81	1.04	1.06
Sn_2(cit) + 4$Bu^n{}_4NF$ (**68**)	2.96	1.81	1.10	1.04
Na_2Sn(cit) (**52**)	3.06	1.85	1.27	1.19
K_2Sn(cit) (**53**)	2.99	1.84	1.14	1.09
$(NH_4)_2Sn$(cit) (**54**)	2.97	1.81	1.21	1.16
$NaSnF_3$ (**35**)	2.96	1.92	1.35	1.44

Notes:-

[a]Recorded at 78K, relative to SnO_2.

Table 4.13 ^{119}Sn and ^{19}F NMR data for the solubilised citrates.

Compound	δ (^{119}Sn) / ppm[a]	δ (^{19}F) / ppm[b]
Sn_2(citrate) (**51**)[c]	-724.9	-
Sn_2(cit) + 4NaF (**65**)	-579.7, -698.3	-94.3
Sn_2(cit) + 4KF (**66**)	-574.4, -691.6	-93.8
Sn_2(cit) + 4NH_4F (**67**)	-576.6, -694.3	-96.4
Sn_2(cit) + 4Bu^n_4NF (**68**)	-566.3, -646.3	-97.1
Na_2Sn(cit) (**52**)	-579.9	-
K_2Sn(cit) (**53**)	-578.3	-
$(NH_4)_2Sn$(cit) (**54**)	-579.6	-
$NaSnF_3$ (**35**)	-684.3	-89.5
NaF		-123.2

Notes:-

[a]Ref. to $SnMe_4$; [b]Ref. to CF_3CO_2H; [c]Recorded using MAS-NMR techniques.

that the tin environment in Sn_2(cit), Na_2Sn(cit) and [Sn_2(cit) + 4NaF] is very similar, likewise for the remaining fluoride-solubilised species (**66-68**).

The ^{119}Sn NMR data contains two peaks for each of the solubilised citrates unlike the solubilised phosphates in which only one peak was observed. The peak farthest downfield (-566.3 to -579.7ppm) is noted to be very similar to the peak in the corresponding mono-stannous salt. For example, the peak due to Na_2Sn(cit) (**52**) (-579.9ppm) is replicated in the NaF-solubilised compound (**65**) (-579.7ppm). Assuming that one product of the reaction is the mono-stannous citrate, this does not account for the fate of the fluoride ions.

The second ^{119}Sn peak which occurs further upfield (-646.3 to -698.3ppm) is most likely due to a complex fluorotin(II) species. The ^{119}Sn Mössbauer spectrum for $NaSnF_3$ (**35**) (δ, 2.96; Δ, 1.92mms^{-1}) is very similar to that of Na_2Sn(cit) (**52**) (δ, 3.06; Δ, 1.85mms^{-1}) which suggests that the spectrum of the solubilised compound (**65**) (δ, 3.10; Δ, 1.90mms^{-1}) might be due to the overlying spectra of these two species. Similarly, $\delta(^{119}Sn)$ for $NaSnF_3$ (-684.3ppm) is very similar to the second peak in the NaF-solubilised product (-698.3ppm). However, the formation of $NaSnF_3$ only accounts for three F- ions although the formation of more complex species (e.g. Na_2SnF_4) cannot be ruled out on the basis of the spectral data. Alternatively, it might simply be that an excess of F^- is required to fully solubilise Sn_2(cit), i.e. only three MF are actually used in the reaction. The ^{19}F NMR data suggests that the former is the more likely as there is no free fluoride peak in the spectrum of (**65**). The ^{19}F peak for (**65**) (-94.3ppm) is not unlike that of (**35**) (-89.5ppm) which further supports the formation of a complex fluorotin(II).

The ^{1}H and ^{13}C NMR data is also consistent with the formation of a mono-stannous citrate and a complex fluorotin(II) anion. For example, in the NaF-solubilised species (**65**), the ^{1}H data (2.74ppm, *q*, *J*=15.3Hz) is identical to that of Na_2Sn(cit) (**52**) (2.74ppm, *q*, *J*=15.3Hz). Similarly, the ^{13}C data for (**65**) [46.6 (CH_2's), 76.1 (tert. C), 177.4, 183.9ppm (3 CO_2's)] is almost indistinguishable from

that for (**52**) [46.7 (CH_2's), 76.1 (tert. C), 177.2, 183.7ppm (3 CO_2's)].

Similarly, the infrared data for the NaF-solubilised product (**65**) supports the formation of a mono-stannous citrate [e.g. Na_2Sn(citrate), 1593cm^{-1}] and a stannous fluoride species, i.e. peaks due to $\upsilon_{as}(CO_2Sn)$ (1594cm^{-1}) can be assigned. Also, peaks due to υ(Sn-F) (448, 518cm^{-1}) are also present in the spectrum of (**65**).

Although most of the comments above relate to the reaction between Sn_2(cit) and 4NaF, the same arguments hold for the other fluoride species, KF, NH_4F and Bu^n_4NF. This suggests that the role of the cation is largely passive in the solubilisation process as it was in the case of the stannous pyrophosphate. The solubilisation of Sn_2(cit) is summarised in Scheme 4.3.

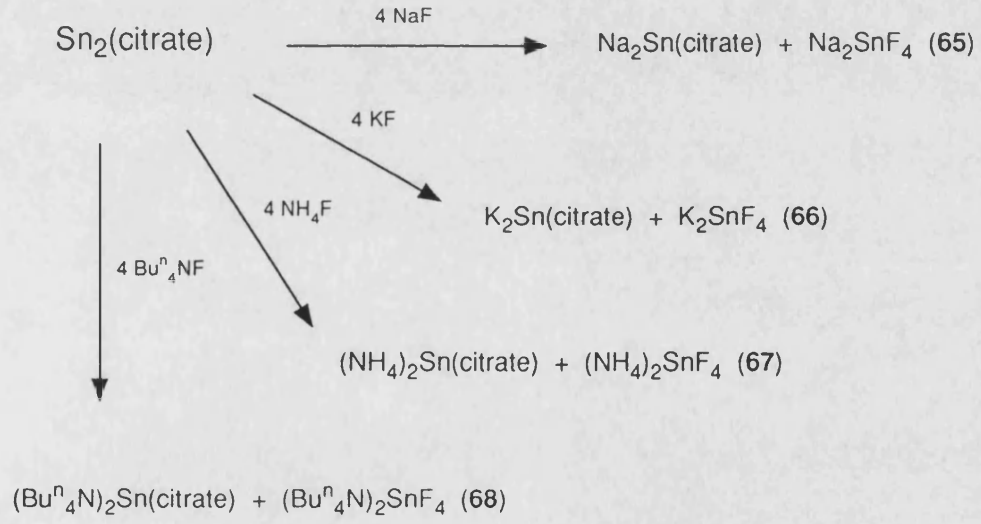

Scheme 4.3 Proposed products of di-stannous citrate solubilisation.

5. THE MICROBIOLOGICAL ACTIVITY OF STANNOUS COMPOUNDS AGAINST ORAL BACTERIA.

The previous Chapters have described in detail the synthesis and characterisation of a series of novel stannous compounds. These stannous compounds include examples of phosphorus oxy-acid salts (Chapter 2), sugar phosphate salts (Chapter 3) and citrate salts (Chapter 4). This Chapter explores aspects of the microbiological activity of selected examples from each of these three main types of stannous compound.

A simple model-system has been developed at Unilever Research Port Sunlight Laboratories (URPSL) for studying the acid-inhibition properties of a particular compound under investigation. This property relates to the degree of inhibition of lactic acid production brought about by the disruption of the anaerobic metabolism of α-D-glucose by oral bacteria. The process by which the lactic acid is generated is referred to as glycolysis and occurs through the glycolytic pathway. For the purposes of this experiment, the particular strain of bacteria used was *Streptococcus Mutans* (NCTC 10449), an important oral organism present in the human oral cavity as a component of plaque.

Following this, *Streptococcus Mutans* suspensions were also exposed to a selection of compounds as aqueous solutions (1.0mMol) and the individual cells subsequently examined by transmission electron microscopy (TEM) in order to establish whether or not tin is retained within the cellular membrane.

However, as well as being an effective anti-microbial agent, a stannous compound must also be partially retained within the oral cavity if it is to be effective in a formulated product. The most potent of anti-bacterial compounds will show poor anti-plaque activity *in vitro* if it is lost immediately after application through rinsing and/or expectoration. For this reason, selected soluble compounds were tested for their adhesion properties upon freshly pellicle-coated synthetic hydroxyapatite.

5.1 The acid-inhibition of selected stannous salts.

The acid-inhibition experiment was carried out using a 'pH-stat' automatic titration apparatus. This equipment automatically, and instantaneously, titrates the lactic acid produced during the bacterial metabolism of α-D-glucose with dilute (*ca.* 0.01N) potassium hydroxide to a constant neutral end-point of pH 7.00 (±0.10). The test solutions were constantly agitated with a mechanical stirrer paddle and the temperature was maintained at 37°C (±0.5°C) by immersion of the sample vessel in a thermostatically controlled water-jacket.

The bacteria used for the test were *Streptococcus Mutans*, a suitable suspension of which was prepared and cultivated as follows:-

A swab of *Streptococcus Mutans* was taken from a pure culture and placed in a bottle containing 20ml of brain/heart infusion (BHI) broth. Two such bottles were prepared and these were then incubated in a CO_2 incubator at 37°C for 5-6 hours. After the period of incubation, the broths containing the cells were each carefully poured into 500ml of BHI broth contained in 1000ml conical flasks. 20ml of sterile 20% (w/v) α-D-glucose solution was also added to both of the flasks. The two 1000ml flasks were then placed in an orbital incubator (at 37°C) overnight at 80-100rpm. The following morning, the broths were poured into six 250ml sorval bottles and balanced with millipore water to the nearest gram. The bottles were then centrifuged at 10,000rpm (in a rotor) at 4°C for 15 minutes. After centrifuging, the waste media was poured into a 2 litre plastic beaker containing 100ml of lysol.

In the bottom of each sorval tube was an off-white pellet of cells. To this pellet was added 25-30ml of 135mM KCl solution. The contents of the sorval tube were shaken to suspend the cells and remove as many lumps as possible. All six suspensions were then combined into one flask and re-centrifuged as before.

All supernatant fluid was discarded into lysol. Approximately 10mls of

135mM KCl were added to the cell pellet and the cells carefully resuspended using a cotton wool swab. The total volume was made up to 200ml with KCl and the suspension centrifuged once more.

The supernatant was discarded into lysol and the cells resuspended with a cotton swab into 5ml of 135mM KCl. The suspension was subsequently poured into a 30ml sterilin flask. The cells were made up to 10ml with KCl yielding a milky-white suspension of viable cells. The flask was stored in ice and shaken frequently during the course of the experiment.

Each of the stannous compounds under investigation was tested over a range of concentrations, nominally 0.05 - 1.00mM stannous in order to establish the concentration dependance of the inhibitory process. For this reason, an accurate determination of the stannous content is required for each of the compounds to be tested. The stannous content for each of the compounds had already been determined using the iodometric titration technique described in Chapter 2 (equation 2.1). Each test solution was of 5.00ml total volume and consisted of the following five components, each of which was carefully added with an automatic pipette:-

(i) 4.00ml 135mM KCl.

(ii) 0.50ml *Streptococcus Mutans* cell suspension.

(iii) 0.10ml 20% sterile glucose solution.

(iv) 0.30ml millipore water

(v) 0.10ml stannous test solution.

The complete list of compounds tested, together with their stannous content is presented in Table 5.1. The basic requirements for testing were (a) access to a suitable quantity of compound and (b) the chosen compound must be sufficiently soluble at pH 7. The majority of the sparingly soluble compounds (e.g. $Sn_2P_2O_7$) formed weakly acidic slurries (pH 3-4) and required the addition of a little dilute KOH in order to form a neutral solution.

The experimental method for determination of percent acid-inhibition is as

Table 5.1 The stannous content of compounds for acid-inhibition testing.

Compound	Sn(II) / Found (% w/w)	Sn(II) / Calc. (% w/w)
$SnHPO_4$ **(23)**	51.9	55.3
$Sn_3(PO_4)_2$ **(24)**	63.4	65.2
$Sn_2P_2O_7$ **(27)**	58.8	57.7
$ZnSn(P_2O_7)$ **(29)**	29.9	28.8
$Sn_2K(P_3O_{10})$ **(30)**	44.7	45.0
$Sn_2P_2O_7$ + 4 NaF **(31)**	38.8	40.9
Sn(αG1P) **(37)**	32.1	32.6
Sn(αG6P) **(38)**	28.0	27.6
Sn(βG6P) **(39)**	30.8	31.5
Sn(glyc-2-phos) **(40)**	40.6	38.7
$BaSn_2$(6-PO_4-gluc) **(42)**	19.8	21.6
Sn(αG1P) + 2 NaF **(44)**	23.8	24.8
Sn(αG6P) + 2 NaF **(65)**[1]	23.6	24.8
$Sn(gluconate)_2$ **(45b)**	22.9	23.3
$Sn(glucuronate)_2$ **(46)**	18.1	20.6
$Sn(lactobionate)_2$ **(66)**[1]	8.2	14.3
Sn_2(citrate) **(51)**	53.8	55.8
Na_2Sn(citrate) **(52)**	27.3	32.0
K_2Sn(citrate) **(53)**	26.3	28.0
$(NH_4)_2Sn$(citrate) **(54)**	26.6	34.6
ZnSn(citrate) **(56)**	28.3	31.8
Sn(malate) **(67)**[1]	46.9	47.0
Sn(maleate) **(68)**[1]	48.0	51.0

Note:- [1]Prepared at Unilever Research Port Sunlight Laboratories.

follows:-

The KCl solution (4.00ml), *S. Mutans* cell suspension (0.50ml) and the millipore water (0.40ml) were placed in a titration vessel and the vessel immersed in the water-jacket. No stannous solution was added to the flask in order to obtain a background control value. The mechanical stirrer and the pH-stat were engaged and the volume of KOH added was noted at two minute intervals. After 10 minutes, the pH had stabilised at pH 7.00 and 0.10ml of glucose solution was added, noting the volume of KOH added. The pH immediately began to fall as the *S. Mutans* metabolised the glucose prompting the rapid addition of KOH solution. After 2 minutes, the final volume of KOH added was recorded.

$$X = (\text{vol. KOH @ 10 min.}) - (\text{vol. KOH @ 8 min.})$$

$$Y = (\text{vol. KOH @ 12 min.}) - (\text{vol. KOH @ 10 min.})$$

The control value = (Y - X) when no stannous solution was added to the *S. Mutans*.

The above procedure was repeated with the addition of the de-oxygenated stannous stock solution. 0.10ml of stannous solution is used together with 0.30ml of millipore water. Therefore, the stock solution of the compound undergoing test should have a concentration fifty-fold that required in the final titrimetric test suspension [e.g. for a final Sn(II) conc. of 1.00mM, a 0.05M stock solution was required]. Upon addition of the glucose, the pH tends to fall much less rapidly due to the inhibitory effect of the stannous species.

The percent acid-inhibition can be determined from equation 5.1.

$$\% \text{ acid-inhibition} = 100 - 100\left[\frac{(Y_{sample} - X_{sample})}{(Y_{control} - X_{control})}\right] \qquad \textbf{(5.1)}$$

For convenience, the results are represented graphically as %-inhibition *vs.* stannous concentration. The following series of graphs illustrate the data for stannous

phosphate (**23**), stannous orthophosphate (**24**) and mono-potassium di-stannous tripolyphosphate (**30**) [Fig. 5.1]; mono-zinc mono-stannous pyrophosphate (**29**), mono-stannous glycerol-2-phosphate (**40**) and mono-barium di-stannous D-6-phosphogluconate (**42**) [Fig. 5.2]; stannous pyrophosphate solubilised with 4NaF (**31**) [Fig. 5.3]; mono-stannous α-D-glucose-1-phosphate (**37**), mono-stannous α-D-glucose-1-phosphate solubilised with 2NaF (**44**) [Fig. 5.4]; mono-stannous α-D-glucose-6-phosphate (**38**), mono-stannous α-D-glucose-6-phosphate plus 2NaF (**65**) [Fig. 5.5]; mono-stannous α-D-glucose-6-phosphate (**38**), mono-stannous β-D-glucose-6-phosphate (**39**) [Fig. 5.6]; mono-stannous bis-D-gluconate (**45b**), mono-stannous bis-D-glucuronate (**46**) and mono-stannous bis-lactobionate (**66**) [Fig. 5.7]; di-stannous citrate (**51**) and mono-zinc mono-stannous citrate (**56**) [Fig. 5.8]; di-sodium mono-stannous citrate (**52**), di-potassium mono-stannous citrate (**53**) and di-ammonium mono-stannous citrate (**54**) [Fig. 5.9]; mono-stannous malate (**67**) and mono-stannous maleate (**68**) [Fig. 5.10]; commercial-grade stannous fluoride (**36**) [Fig. 5.11].

To date, stannous pyrophosphate (**27**) has proven to be one of the more effective materials in this test and has also been employed in dentifrice formulations. For these reasons, $Sn_2P_2O_7$ was chosen as an arbitrary reference for comparative purposes. The acid-inhibition data for this compound is plotted on all of the graphs for the compounds listed above (Figs. 5.1-5.11) for the purpose of comparison.

Acid-inhibition of Streptococcus Mutans.

In 135mM KCl at 37C, to pH 7.00

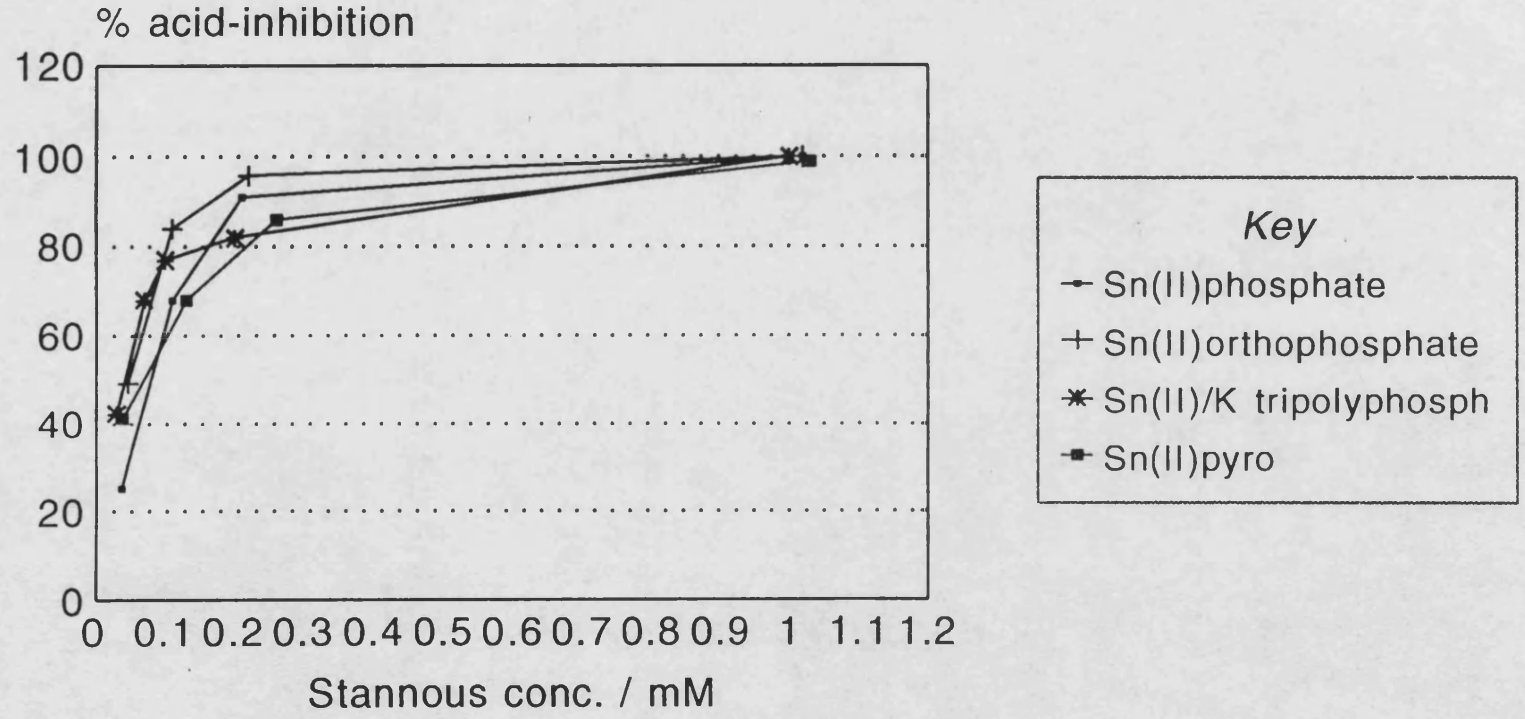

Fig. 5.1

Acid-inhibition of Streptococcus Mutans.

In 135mM KCl at 37C, to pH 7.00

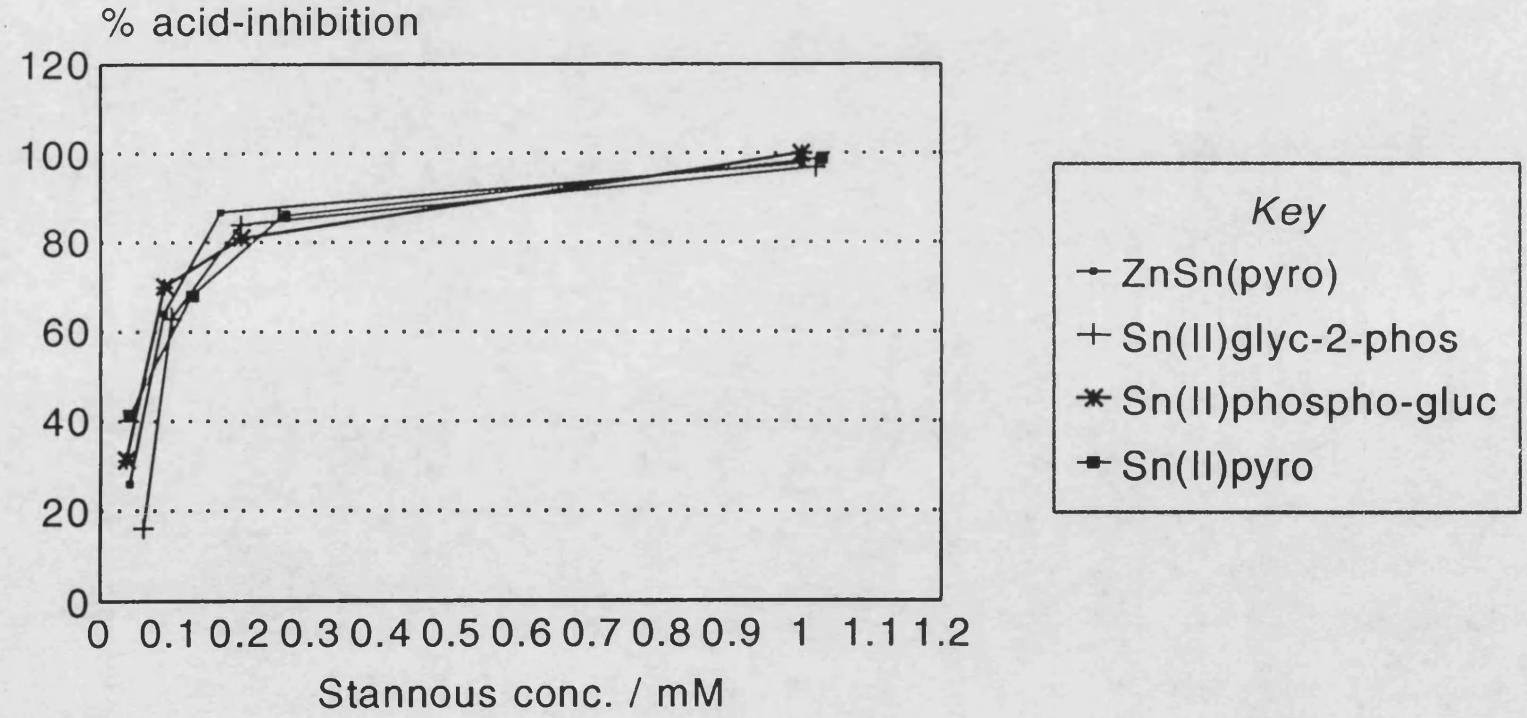

Fig. 5.2

Acid-inhibition of Streptococcus Mutans.

In 135mM KCl at 37C, to pH 7.00

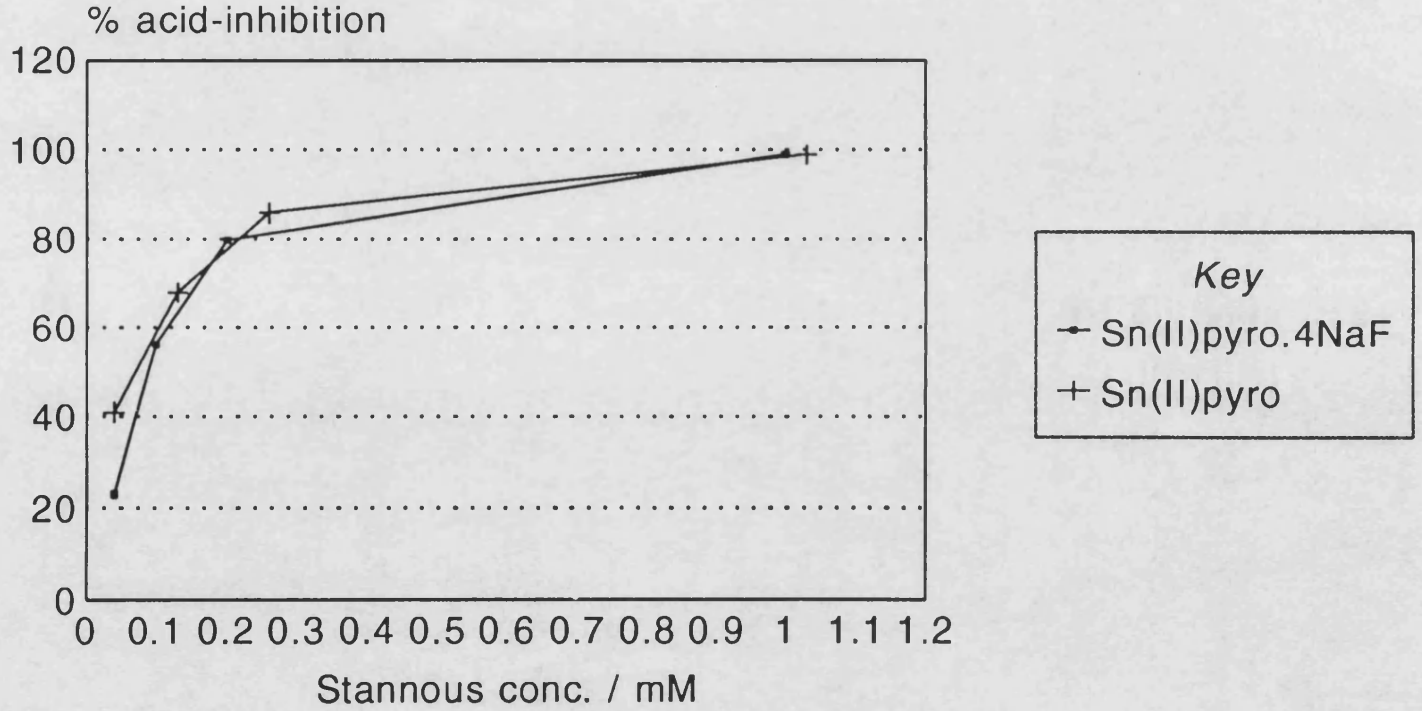

Fig. 5.3

Acid-inhibition of Streptococcus Mutans.

In 135mM KCl at 37C, to pH 7.00

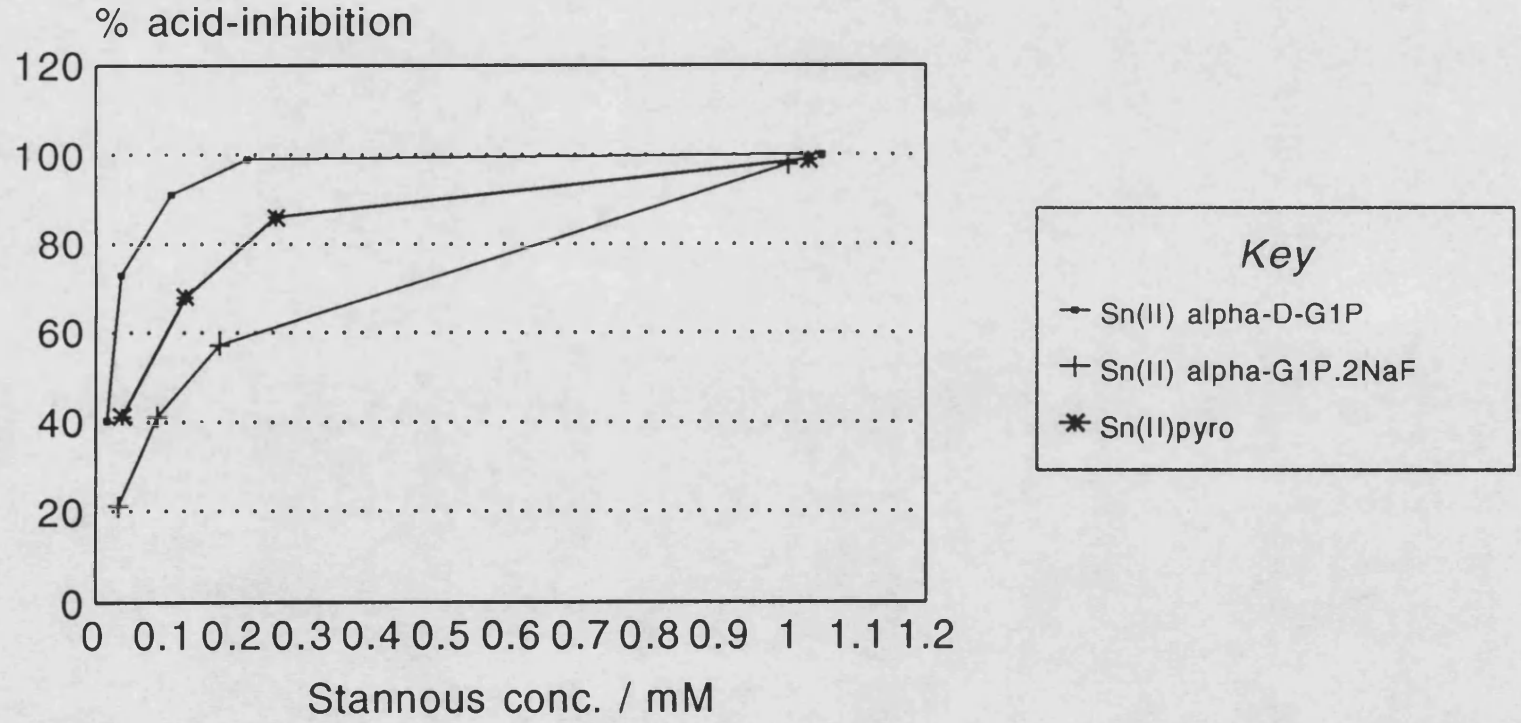

Fig. 5.4

Acid-inhibition of Streptococcus Mutans.

In 135mM KCl at 37C, to pH 7.00

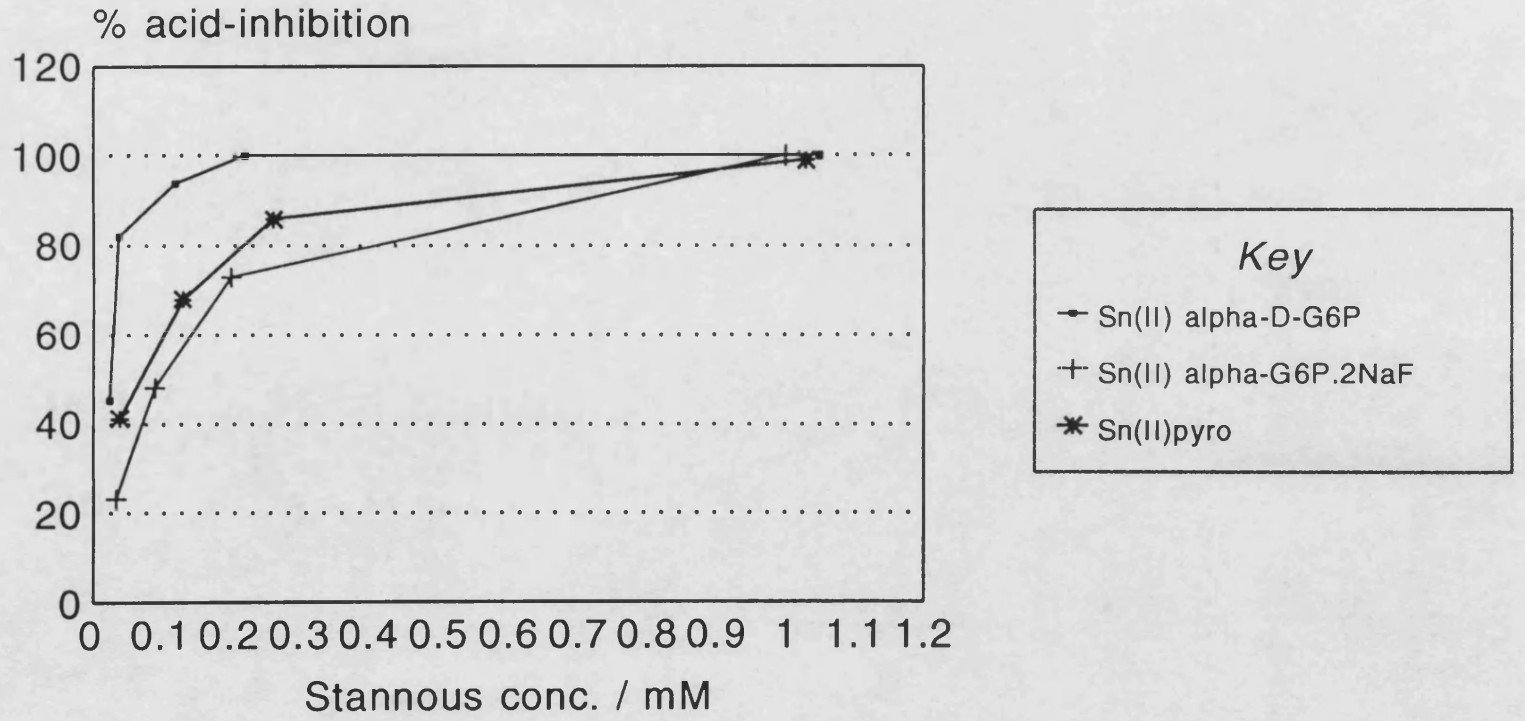

Fig. 5.5

Acid-inhibition of Streptococcus Mutans.

In 135mM KCl at 37C, to pH 7.00

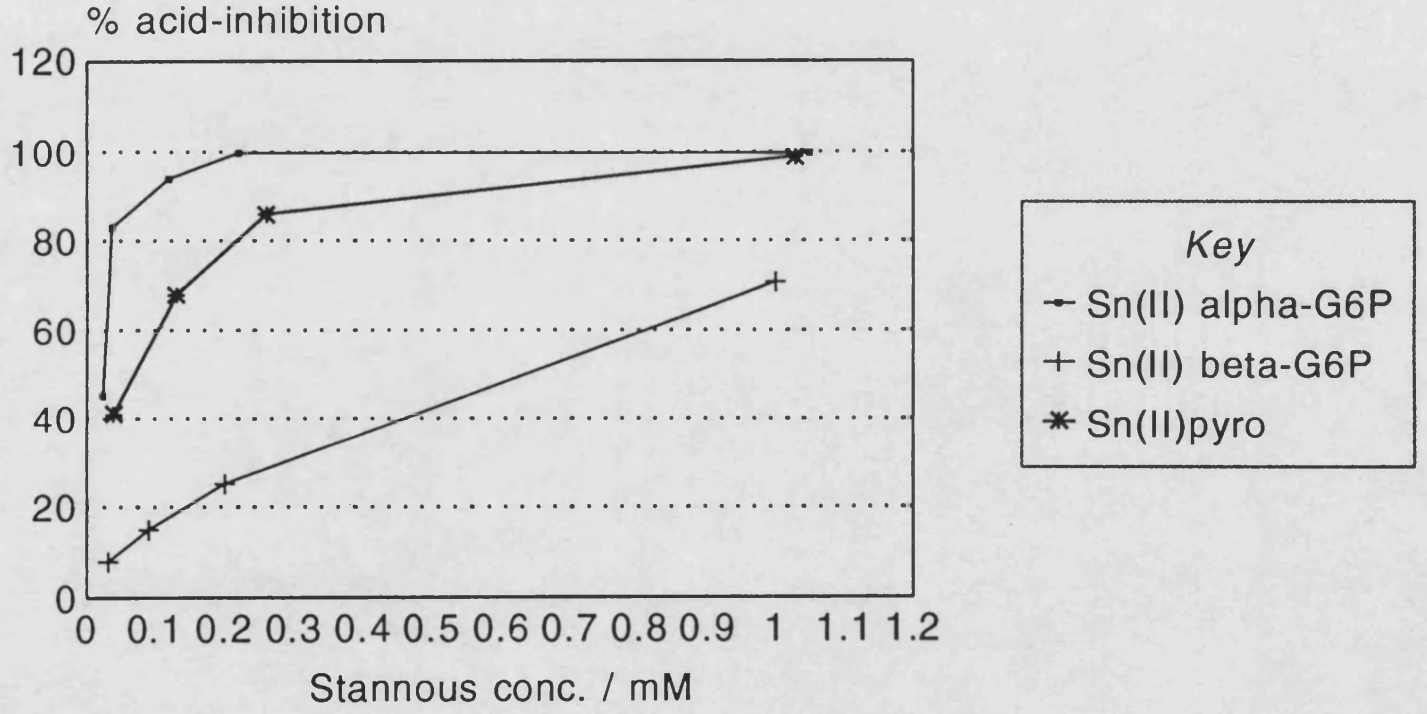

Fig. 5.6

Acid-inhibition of Streptococcus Mutans.

In 135mM KCl at 37C, to pH 7.00

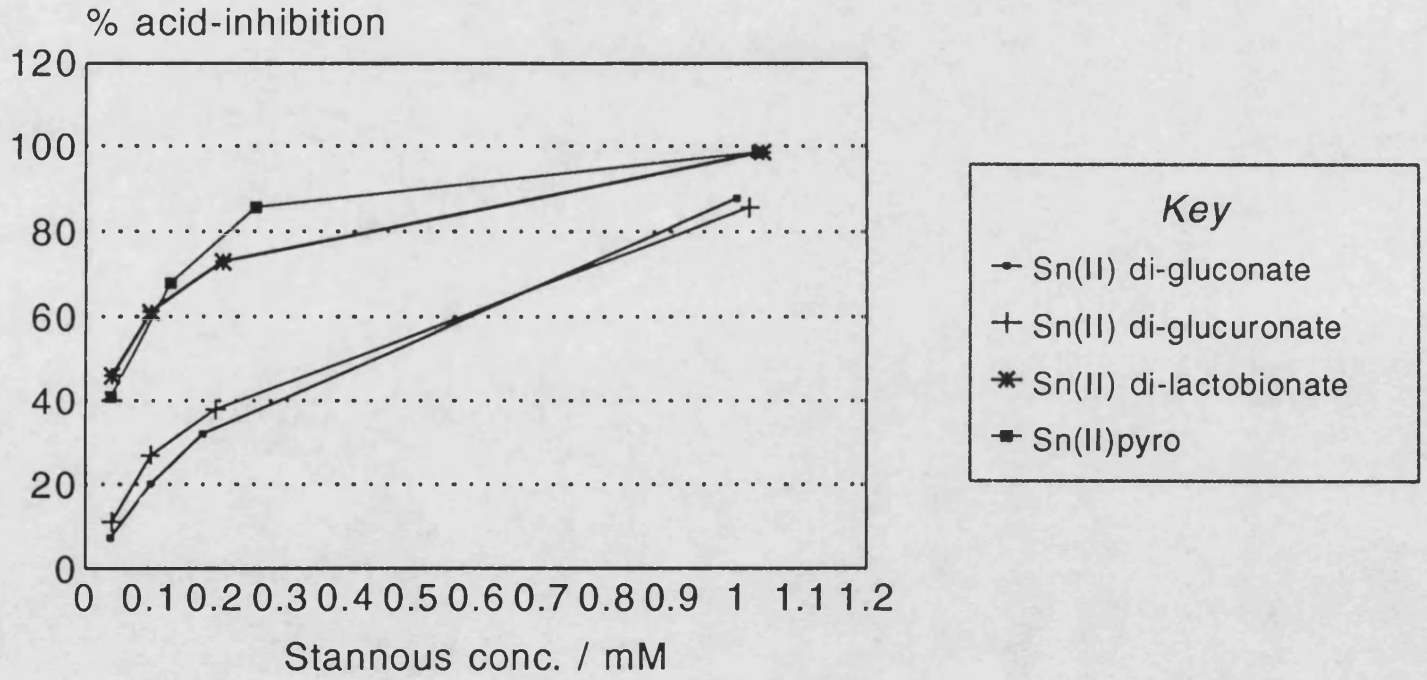

Fig. 5.7

Acid-inhibition of Streptococcus Mutans.

In 135mM KCl at 37C, to pH 7.00

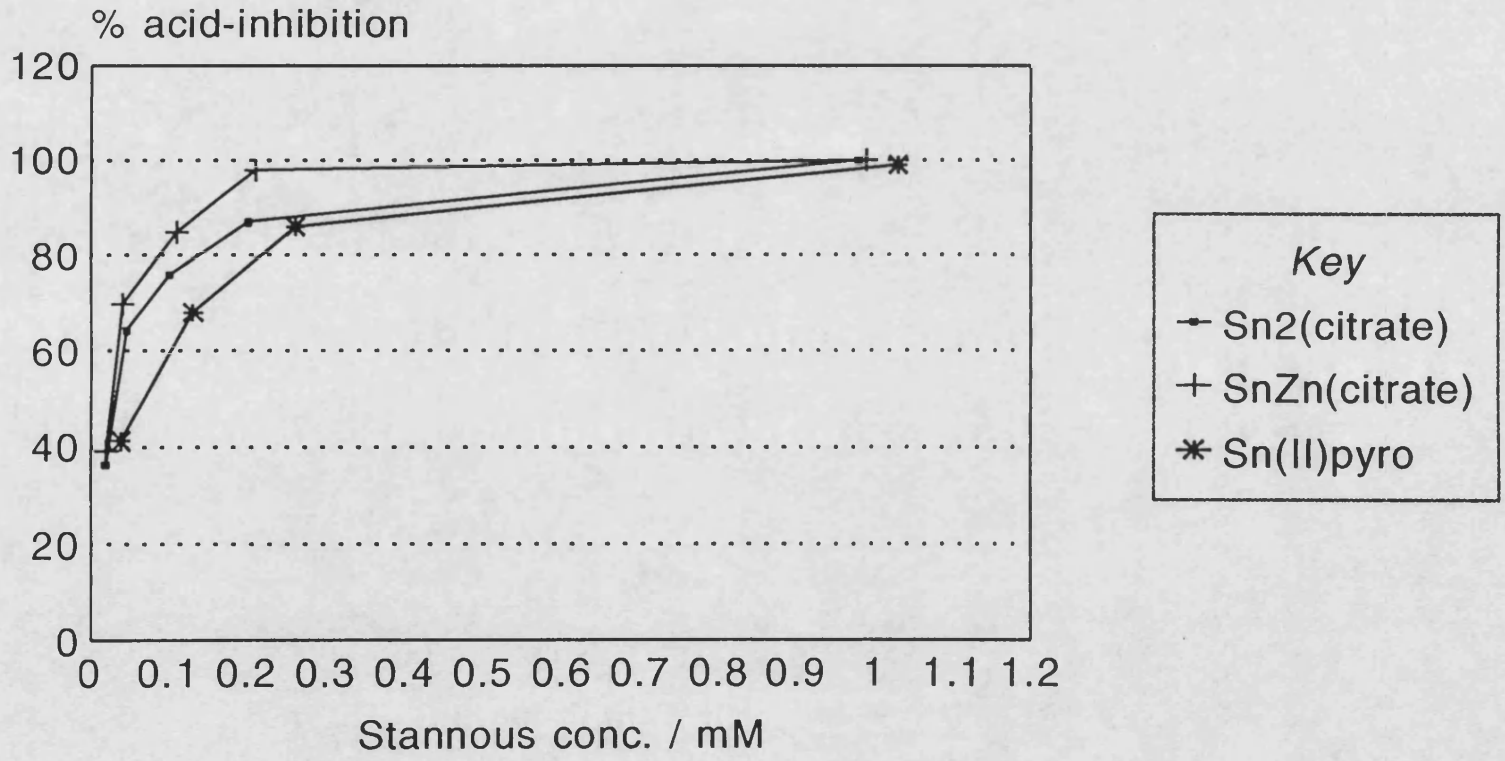

Fig. 5.8

Acid-inhibition of Streptococcus Mutans.

In 135mM KCl at 37C, to pH 7.00

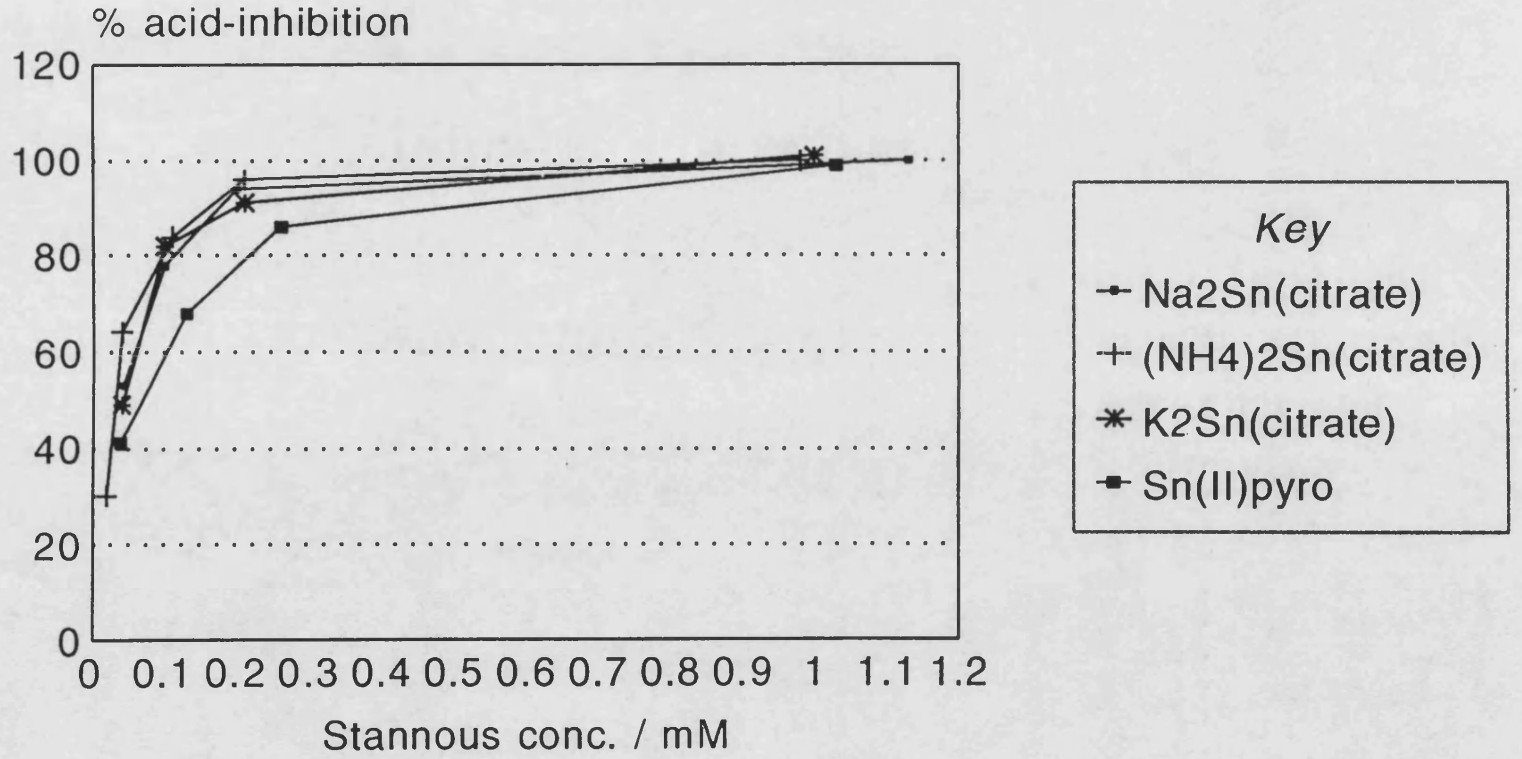

Fig. 5.9

Acid-inhibition of Streptococcus Mutans.

In 135mM KCl at 37C, to pH 7.00

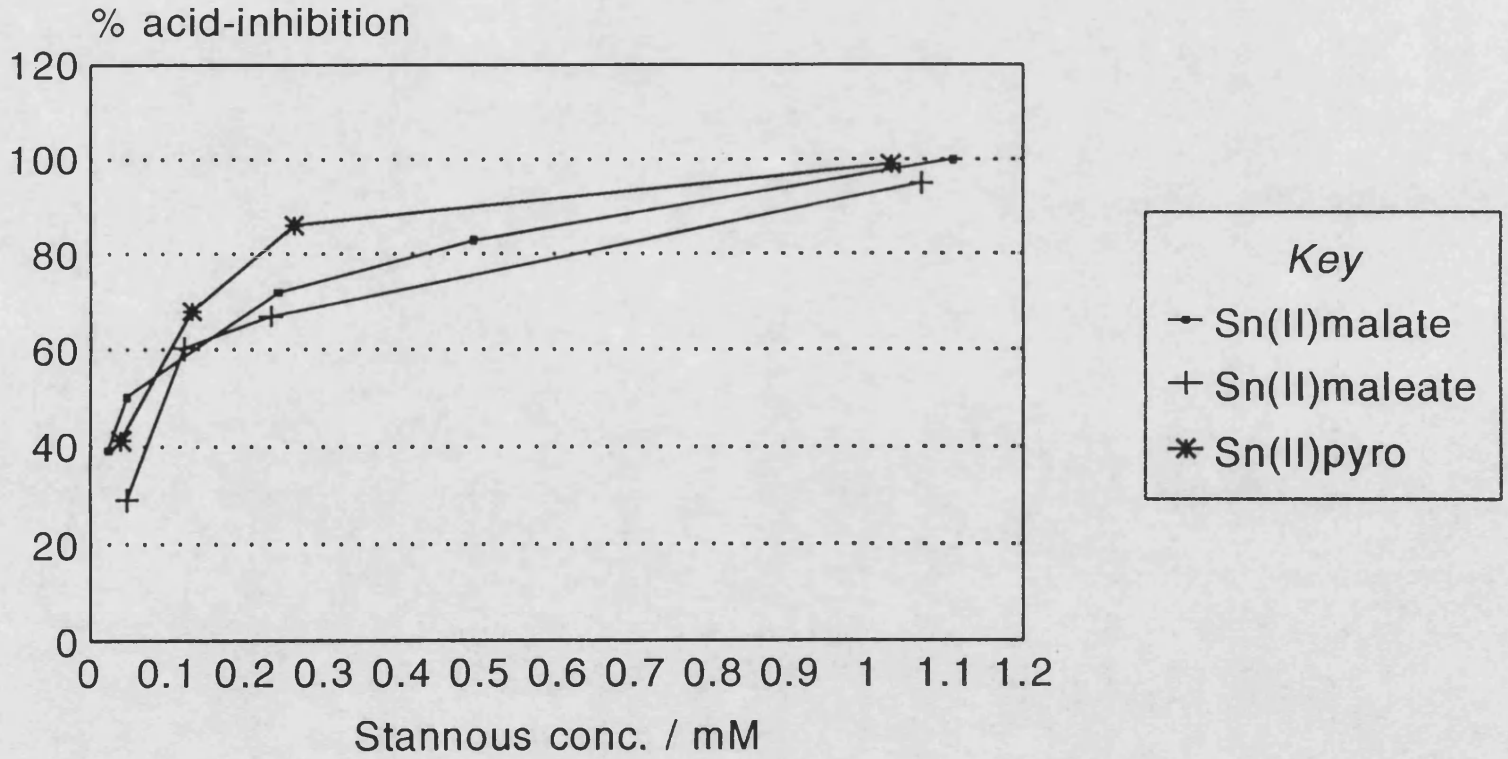

Fig. 5.10

Acid-inhibition of Streptococcus Mutans.

In 135mM KCl at 37C, to pH 7.00

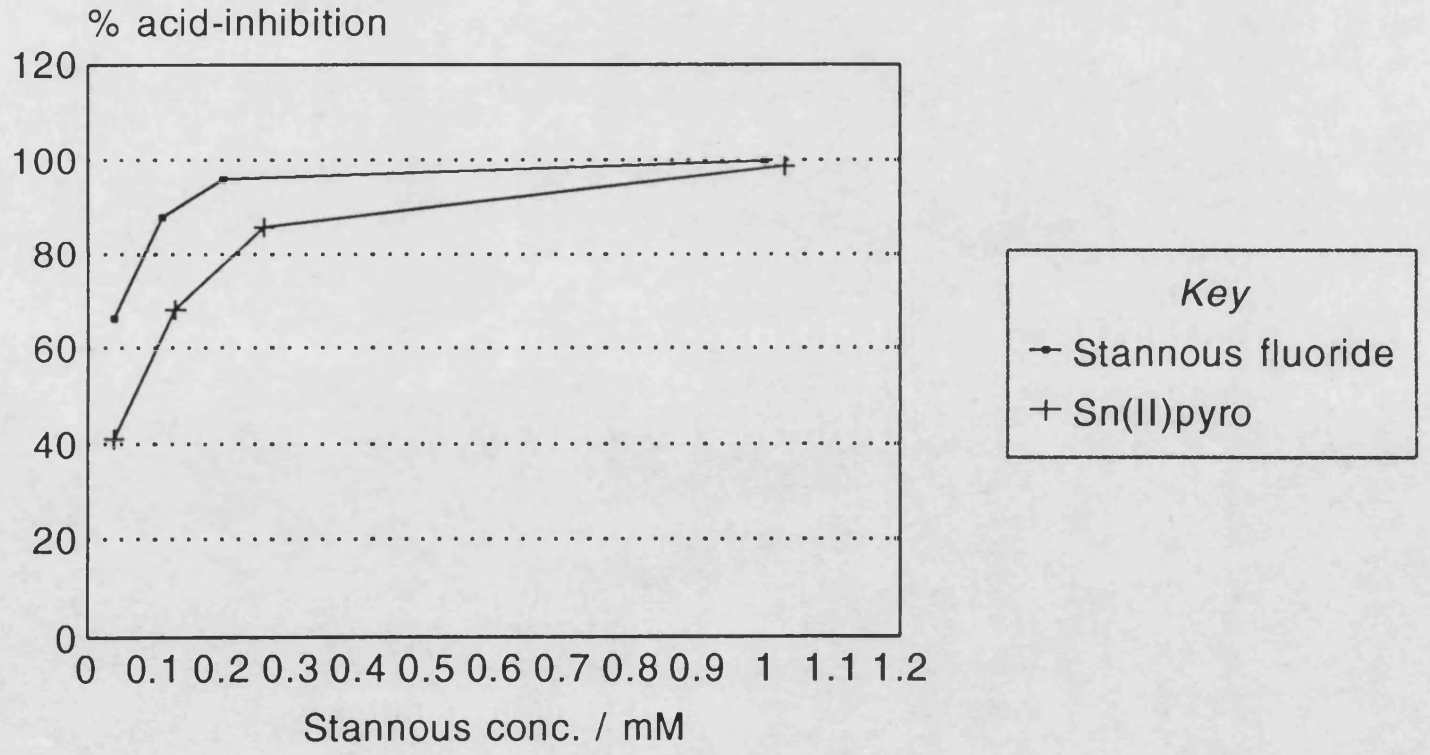

Fig. 5.11

The basic shape of all of the curves is essentially the same for the entire series of stannous compounds tested. Perhaps surprisingly, the increase in acid-inhibition is not found to be directly proportional to the concentration of the stannous solution. In each case, the inhibition effect rises sharply with concentration at very dilute stannous concentrations. However, as the concentration rises beyond about 0.2mM the increase of acid-inhibition gradually becomes much less pronounced. Almost without exception, the inhibitory process was complete (i.e. 100% inhibition) with stannous concentrations of approximately 1.0mM. Interestingly, the curves have a very similar general appearance to those observed for the level of uptake of intracellular tin into *S. Mutans* cells (Fig. 1.1).[38] This suggests that there might be a link between the uptake of tin and the anti-microbial effect.

The inorganic tin(II) phosphate compounds (Figs. 5.1, 5.2) all have very similar inhibitory properties to those of $Sn_2P_2O_7$ (**27**). The experimental curves for (**23**),(**24**),(**29**),(**30**),(**40**) and (**42**) are all remarkably consistent. Perhaps the only slight exception is the glycerol-2-phosphate (**40**) which shows an unusually dramatic decrease in inhibition at low stannous levels. Interestingly, $ZnSn(P_2O_7)$ (**29**) shows similar activity to $Sn_2P_2O_7$ confirming the anti-microbial role of the two metal cations. The effect of the zinc provides a positive anti-microbial effect although it is unclear as to whether or not the two metal ions act through a synergic or an independant, additive mechanism. The sodium fluoride solubilised $Sn_2P_2O_7$ (**31**) (Fig. 5.3) shows that the presence of fluoride exhibits little effect upon the acid-inhibition of (**27**). It might have been expected that the presence of such high fluoride levels would have dramatically improved the efficacy of this material as F^- ions have been shown to exhibit potent anti-microbial properties.[206,207] The absence of this effect further supports the theory that a complex stannous fluorophosphate is present in solution and not a free fluoride.

The sugar phosphates Sn(αG1P) (**37**) and Sn(αG6P) (**38**) (Figs. 5.4, 5.5) both show dramatically improved activity over $Sn_2P_2O_7$. The improvements, particularly

in the latter case, are particularly significant at low stannous levels (i.e. less than 0.20mM). Surprisingly, the anomeric isomer of Sn(G6P), i.e. Sn(βG6P) (**39**) (Fig. 5.6), has a dramatically reduced activity at all concentrations compared to the α-isomer. In fact, the increase of inhibition with concentration is so dramatically reduced at low concentrations as to be virtually linear, full inhibition not being achieved even at high stannous levels. Interestingly, the addition of two moles of NaF to the two α-glucose phosphates, Sn(αG1P)/2NaF (**44**) and Sn(αG6P)/2NaF (**65**), causes a dramatic decrease in the activity of these species at low concentrations. The data for these fluoride salts more closely resembles that of other inorganic tin(II) compounds.

The tin(II) salts of the aldonic acids, tin(II) bis-D-gluconate (**45b**) and bis-D-glucuronate (**46**) (Fig. 5.7), show relatively poor activity over the entire concentration range in a similar fashion to that of Sn(βG6P). Both of these simple sugar carboxylate compounds exhibit remarkably similar inhibitory properties. An aged sample of tin(II) bis-D-lactobionate (**66**) supplied by URPSL was found to contain substantial levels of stannic impurities, hence the low stannous analysis (Table 5.1). Mössbauer analysis of this compound (δ, -0.04mms^{-1}; δ, 3.10; Δ, 1.71mms^{-1}) showed a tin(IV) peak of intensity 10-15% total peak area. Essentially a β-galactose-substituted gluconic acid salt, the inhibitory activity of this species was greatly enhanced over the simple aldonates.

The tin(II) citrates, Sn_2(citrate) (**51**) and ZnSn(citrate) (**56**) (Fig. 5.8) have broadly similar activities, both species showing a slight improvement over $Sn_2P_2O_7$ at all concentrations. However, the mixed-metal citrate has slightly improved inhibitory properties over the di-stannous citrate. As in the $ZnSn(P_2O_7)$ example, the encouraging levels of activity of a Sn(II) and Zn(II) combination is clearly exhibited by the mixed-metal citrate.

The series of mono-stannous citrates, Na_2Sn(citrate) (**52**), K_2Sn(citrate) (**53**) and $(NH_4)_2$Sn(citrate) (**54**) (Fig.5.9) are almost indistinguishable with regard to their

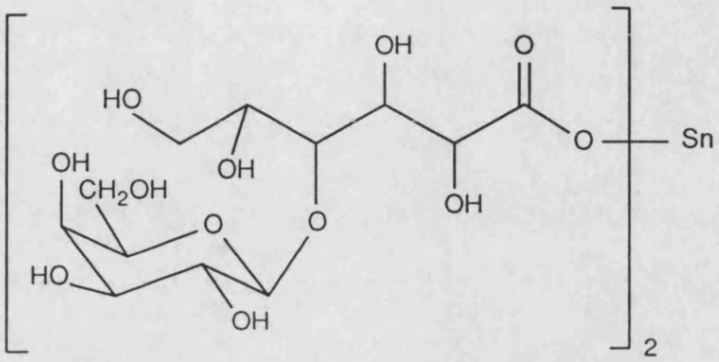

(**66**)

acid-inhibition properties. The three compounds all show a significant improvement upon $Sn_2P_2O_7$ at all stannous concentrations, the di-ammonium salt particularly so at very low levels. Overall, the inhibitory data for all of the tin(II) citrates studied (**51-54**),(**56**) is actually remarkably consistent.

Finally, two simple, air-stable tin(II) carboxylates were prepared and tested at URPSL, i.e. the malate (**67**) and maleate (**68**) (Fig. 5.10).

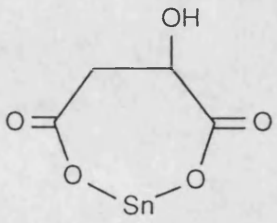

(**67**)

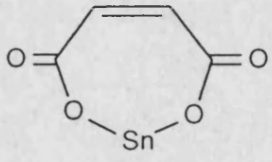

(**68**)

The activity of these dibasic carboxylates is significantly reduced over that of the citrates. Both species exhibit substantially reduced activity over the reference, $Sn_2P_2O_7$, although the malate appears to better maintain its inhibitory properties at

very dilute levels.

The data for commercially-available SnF_2 (**36**) (Fig.5.11) is included for comparitive purposes as the fluoride was the earliest stannous salt to be employed as an anti-plaque agent (Section 1.6). The activity of SnF_2 is greatly enhanced over the pyrophosphate at all concentrations. This might be attributable to the anti-microbial effect of fluoride as SnF_2 is known to yield free F^- ions in aqueous solution.[207] Unfortunately, as described in Chapter 1, solutions of SnF_2 are inherently unstable whereas the pyrophosphate can be readily stabilised in the presence of high sorbitol levels.

On the whole, the acid-inhibition assays for this series of stannous compounds shows extremely encouraging results. Almost without exception, the results are a significant improvement on those obtained for stannous pyrophosphate. This series of results emphatically shows that the anti-microbial activity of stannous salts is partly dependant on other factors besides concentration. For example, the D-gluconate *vs* D-lactobionate situation described above cannot easily be rationalised solely in terms of the stannous environment. Both of these compounds contain stannous in nominally the same environment, i.e. bound to a D-gluconic acid residue, yet the D-lactobionate is dramatically more effective at inhibiting lactic acid-production. Lactobionic acid (4′-O-β-galactopyranosyl D-gluconic acid) is known to behave as a lectin-binding sugar which can readily bind to the lectins contained within cell walls. The dramatic improvement in the anti-bacterial efficacy of (**66**) relative to tin bis-D-gluconate might be attributable to this property. The lactobionate residue would bind strongly to the surface of *S. Mutans*, thus producing a highly effective delivery vehicle of the active stannous directly to the bacterial cells.

In a similar fashion, the activity of the two α-isomers of tin(II) glucose phosphates, and in particular the α-G6P isomer, show greatly enhanced activity over the inorganic tin(II) phosphates. Conversely, the β-anomeric isomer of glucose-6-phosphate exhibits extremely poor activity. Previous studies (Chapters 2,3)

have shown that the basic tin environment in the sugar phosphates is essentially the same as that found in the inorganic phosphates and yet these dramatic differences in their anti-microbial properties are observed. The sugar phosphates are a class of carbohydrates known to be particularly important within living systems. In particular, the α-glucose phosphates (αG1P, αG6P) are intermediates in many metabolic processes such as the degradation of glycogen to lactic acid in the glycolytic pathway. It is possible that the addition of soluble stannous glucose phosphates introduces a foreign metal ion (i.e. Sn^{2+}) into the *S. Mutans* metabolic pathway, effectively disabling the glycolytic metabolism of α-D-glucose. Conversely, the β-anomer of G6P is not 'recognised' in the same way as the α-anomer and is not incorporated into the glycolytic cycle to the same extent. Unfortunately, very little is known about the mechanism of stannous salts as anti-microbial agents. In order to further clarify this situation, a great deal of further work is required.

The technique employed for determining the acid-inhibition of metal ions is a simple, but rather crude, model system utilising one of many oral bacteria. In order to better establish the anti-plaque potential for a particularly promising compound it is necessary to perform an *in vitro* plaque assay. At the time of writing, Sn(αG6P) was being screened using these microbiological techniques at URPSL as a result of the highly encouraging results with *Streptococcus Mutans*.

5.2 The use of transmission electron microscopy to study the effect of stannous compounds upon *Streptococcus Mutans.*

Examples where *Streptococcus Mutans* cells exposed to stannous fluoride solutions have been examined by transmission electron microscopy (TEM) are documented in the literature.[40] Typically, the reported results show that substantial quantities of tin-containing material are retained by the cells as multiple intracellular granules. The granular aggregates of tin species are readily observed as electron-dense dark patches on the TEM micrographs. For the purposes of comparison, suspensions of *S. Mutans* were exposed to aqueous solutions of a representative selection of the novel stannous salts described in this thesis. The limited selection of compounds used include examples of tin(II) sugar phosphates and citrates that showed promising results in the acid-inhibition assay. The effect of the mixed-metal ZnSn(citrate) was also examined in this way.

After exposure to the stannous solutions (1.0mM) for at least 10 minutes, the cell suspensions were then centrifuged at 10,000rpm for 5 minutes, and washed with copious amounts of millipore water. A copper TEM grid was dipped into the cells and examined at magnifications of 30-50,000.

Mono-stannous α-glucose-1-phosphate (**37**) (Fig. 5.12): Although the micrograph for Sn(αG1P) is rather unclear, intracellular granules of tin are visible suggesting that tin is actually transported within the cell where it becomes firmly bound. Typically, these granules are quite large (200-250nm diameter) and concentrated at the two poles of the cells. A very similar situation has been observed for SnF_2 and it has been claimed that the condensation of tin into granules is an attempt at minimising the effect of this foreign invader.[40]

Mono-stannous α-glucose-6-phosphate (**38**) (Fig. 5.13): The micrograph for this compound is much clearer and it reveals the presence of many smaller granules of

intracellular tin-containing material (typically 100nm diameter). The granules also appear much more regularly formed than those in Sn(αG1P) and are more evenly distributed throughout the cells. The presence of small (<50nm diameter) extracellular deposits can also be clearly seen on the outer surface of the cell walls. The extraordinary anti-microbial efficacy of this compound might be attributable to the presence of these small intracellular particles. In this way, maximum disruption to the cellular metabolism is possible.

Di-sodium mono-stannous citrate (**52**) (Fig. 5.14): The micrograph for this compound clearly shows that a different mechanism occurs. There are no visible intracellular granular particles but the outer surfaces of the cell walls are covered in a quite uniform coating of tin species to a depth of 75-100nm.

Di-ammonium mono-stannous citrate (**54**) (Fig. 5.15): Unfortunately, the micrograph for this compound is also rather unclear although it appears that the cells coagulate together around large extracellular deposits of tin-containing material. These deposits appear to 'cement' the individual cells together, filling in the gaps between them.

Mono-zinc mono-stannous citrate (**56**) (Fig. 5.16): In this case, the individual cells appear to be trapped within an extracellular matrix of electron-dense material. This matrix is quite thick and has a depth of 250-600nm. Interestingly, electronlucent holes are clearly visible in the walls of many of the cells.

The observed anti-bacterial properties of stannous fluoride has traditionally been associated with the observed intracellular retention of a tin compound.[39] However, in the citrate examples above, the tin is bound exclusively in an extracellular manner. Electron micrographs of *S. Mutans* exposed to solutions of lead(II) fluoride, PbF_2, also showed the electron-dense material to be located only on the outer surface of the cell walls. However, the binding of lead to cell membranes is not accompanied by significant anti-microbial effects.[208] Zinc fluoride, ZnF_2, also shows little or no anti-bacterial effects but, in contrast to PbF_2, no zinc binding on or

near the bacteria was observed.

In summary, *Streptococcus Mutans* cells retain significant amounts of tin upon exposure to aqueous solutions of stannous compounds either internally or externally. However, in contrast to the previously held belief, anti-microbial effects such as acid-inhibition are not always accompanied by the intracellular retention of tin.

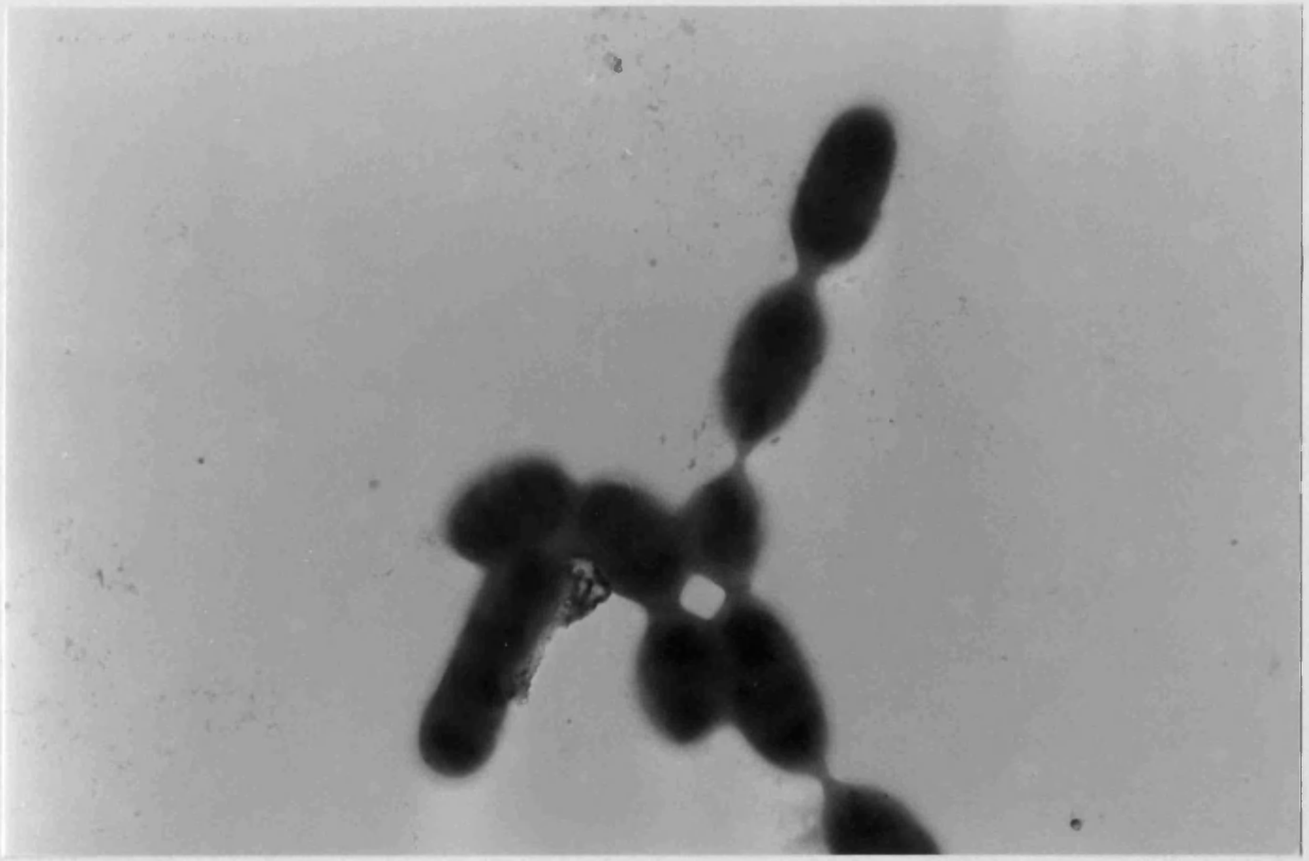

Fig. 5.12 TEM micrograph of *Streptococcus Mutans* cells exposed to Sn(αG1P) (**37**).

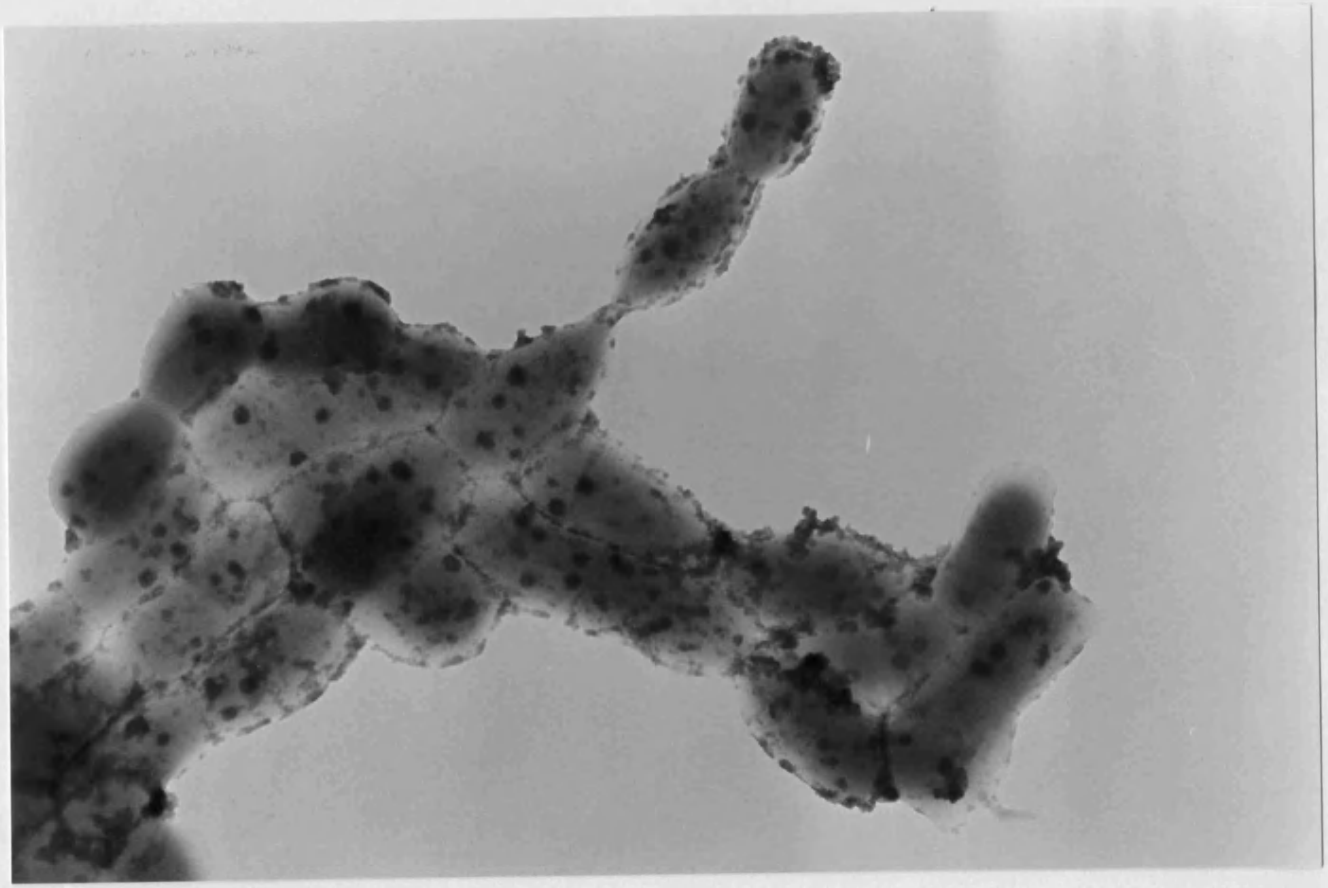

Fig. 5.13 TEM micrograph of *Streptococcus Mutans* cells exposed to Sn(αG6P) (**38**).

Fig. 5.14 TEM micrograph of *Streptococcus Mutans* cells exposed to Na_2Sn(citrate) (**52**).

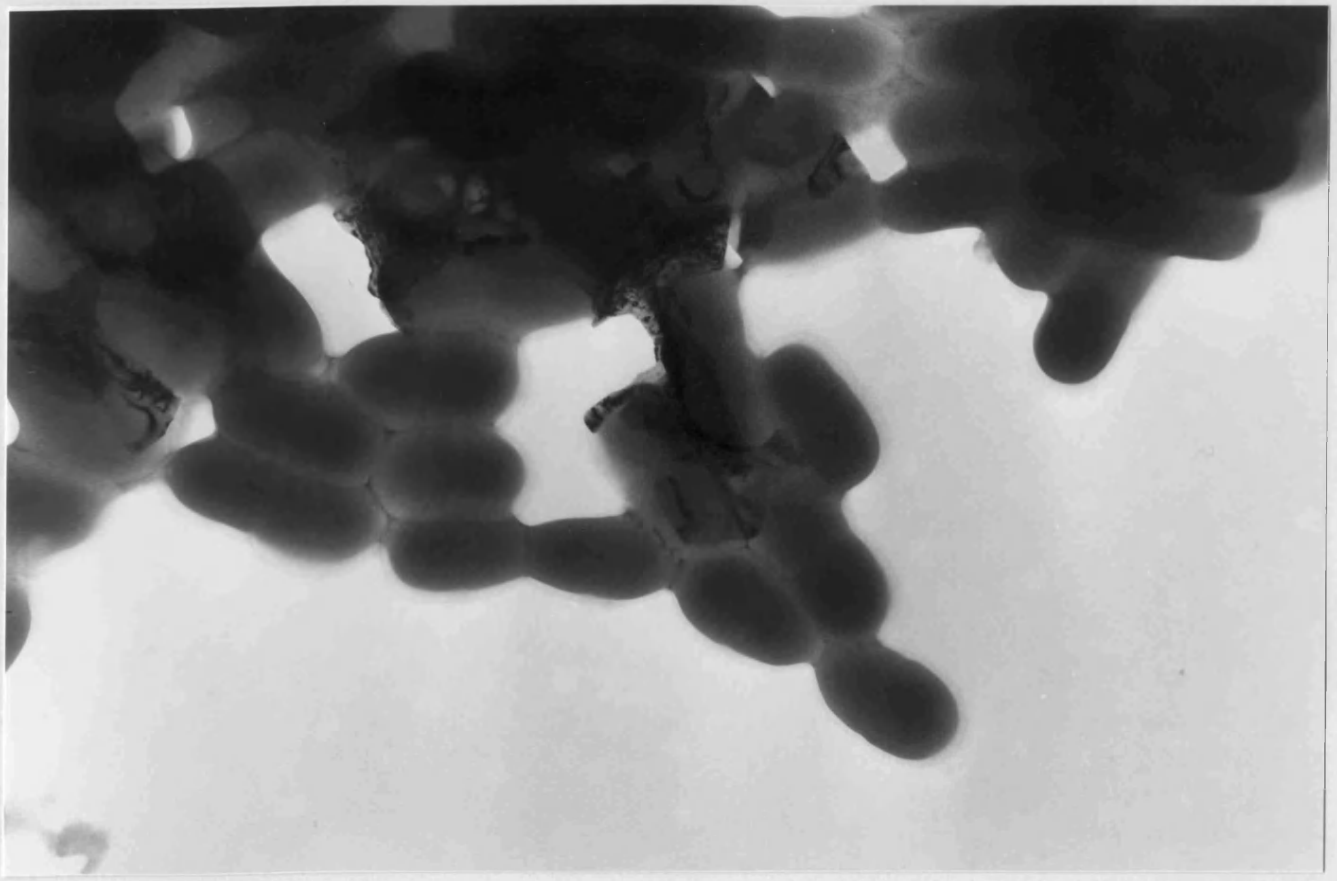

Fig. 5.15 TEM micrograph of *Streptococcus Mutans* cells exposed to $(NH_4)_2Sn$(citrate) (**54**).

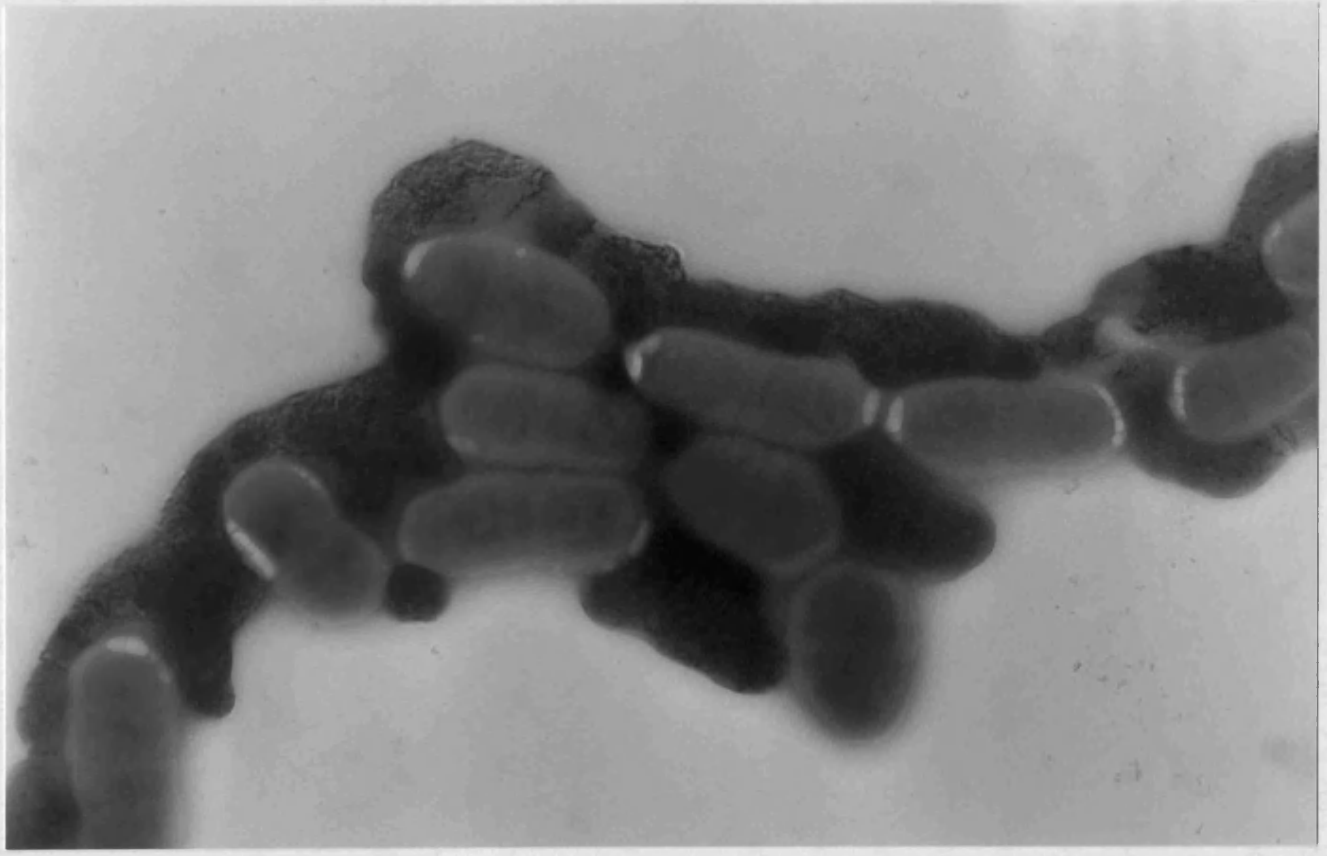

Fig. 5.16 TEM micrograph of *Streptococcus Mutans* cells exposed to ZnSn(citrate) (**56**).

5.3 The retention of stannous salts upon pellicle-coated hydroxyapatite.

A selection of highly water-soluble stannous salts were tested for their adhesion properties upon synthetic hydroxyapatite (HAP), $Ca_5(PO_4)_3OH$, the main mineral constituent of dental enamel (Section 1.2). However, the exposed surface of a tooth rarely, if ever, actually comprises of clean HAP. Therefore, in order to mimic the situation in the human oral cavity, the HAP was pre-coated with pellicle, a proteinaceous layer continuously laid down by the saliva which irrigates the teeth (Section 1.3.1). It is desirable for a small percentage of the tin compound to be retained upon the HAP for a short while after application. This build-up of anti-plaque active agents acts to inhibit plaque regrowth between brushings. However, excessive retention of stannous salts on the teeth is undesirable as it has been shown to cause unsightly staining of the surface due to reaction with certain dietary components.

In order to compare the relative deposition levels of a limited range of compounds, the following procedure was employed:-

Synthetic, spheroidal HAP (20g) was incubated overnight in sterile human saliva (50ml) in an orbital incubator at 37°C. The following morning, the HAP, now thoroughly coated in a proteinaceous pellicle layer, was carefully filtered, washed with copious amounts of water and air-dried.

Each test sample was made up as follows in 50ml sterilin containers:-

(i) 1.00g of dried HAP/pellicle.

(ii) Stannous compound equivalent to 50.0mg of Sn(II).

(iii) Nitrogen-purged millipore water (40.0ml).

Each sample solution was adjusted to pH 7.0 with 2N KOH solution. The samples were then allowed to stir simultaneously, at room temperature, for 30 minutes. After this time, the HAP was carefully filtered, thoroughly washed with

water and air-dried overnight.

250.0mg of the dried HAP/stannous compound was accurately weighed into a 50.0ml volumetric flask. The solid was thoroughly dissolved in 20ml of 20% HCl and made up to volume with more 20% HCl.

The sample solutions were subsequently analysed for total tin content to allow for oxidation during the procedure. The analysis was carried out at URPSL using Inductively-Coupled Plasma Atomic Absorbance spectrophotometry (ICP-AA). This technique uses a very hot plasma flame in order to achieve more efficient atomisation of the sample. This significantly improves the limits of detection for the atomic absorbtion technique.

If the tin(II) compound was wholly retained, i.e. 100% deposition, the total tin content would be 5.0% (i.e. 50.0mg Sn(II) in 1.00g of HAP). The results for this experiment are presented in Table 5.2.

Table 5.2 The deposition of tin(II) upon HAP/pellicle at pH 7.0.

Compound	Tin content / %(w/w)	Retention / %
Sn(αG6P) **(38)**	0.300	6.0
Na_2Sn(citrate) **(52)**	0.091	1.8
$(NH_4)_2Sn$(citrate) **(54)**	0.090	1.8

The results clearly show that the three stannous compounds are indeed retained upon the surface of the HAP. The sugar phosphate is retained to a significantly greater extent than the two isostructural mono-stannous citrates. The

extent of stannous deposition is also quite low which suggests that staining is unlikely to be a problem with any of these compounds.

A possible cause of stannous deposition is due to weak intermolecular forces between the positively-charged cation and the electron-rich functional groups of the proteinaceous layer. Proteins are large, complex amino acid polymers with complex side-chains and it is likely that many N, S and O atoms are presented to the incoming stannous moiety at the surface of the pellicle layer as represented schematically in Fig. 5.17.

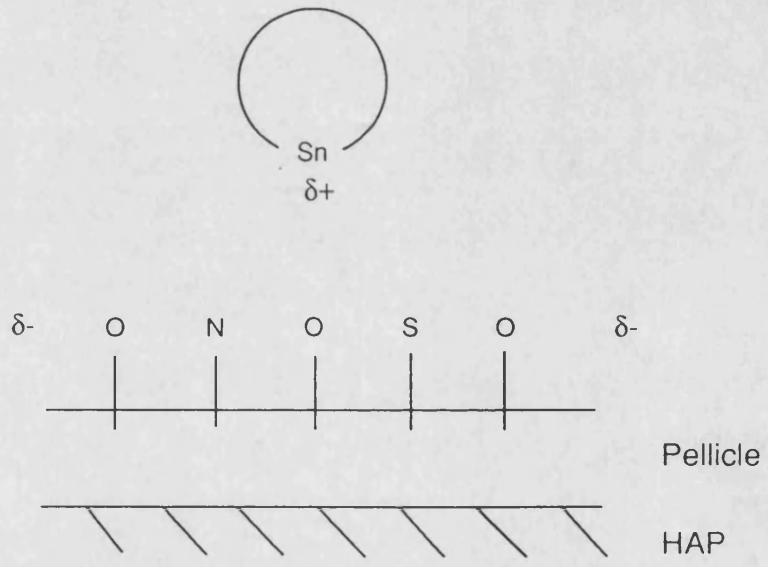

Fig. 5.17 The interaction of stannous salts with dental pellicle.

However, the stannous centre is extensively coordinated by the surrounding ligands which are bound directly to tin. Consequently, this electrostatic argument for the deposition of tin compounds onto protein surfaces is highly questionable.

Pellicle is known to contain many mucinous glycoproteins and immunoglobulins which are rich in surface binding lectin proteins.[222] The sugar phosphate group in compounds such as Sn(αG6P) and the citrate ligand in the tin(II)

citrates can play a major part in the interaction with the protein surface. These interactions can occur through complex hydrogen bonding involving the uncoordinated C(OH) and C=O groups. This is the most likely explanation of the relatively high deposition levels of Sn(αG6P) compared to the citrates. The sugar function contains many exocyclic primary OH groups by which lectin binding might occur.

APPENDIX 1. THE BACKGROUND TO EXAFS STUDIES.

The Extended X-ray Fine Structure (EXAFS) has been known for over 70 years but it is only recently that its power for structural determination has been fully recognised. The first experimental detection of fine structure past the absorption edges were by Fricke and Hertz as early as 1920.[209,210] However, the development of this technique remained relatively confused and dormant until the availability of synchrotron radiation sources of X-rays. These highly collimated, plane polarised, and precisely pulsed X-ray sources, with fluxes of 10^{12}-10^{16} photons $sec^{-1}mrad^{-1}mA^{-1}$, greatly improved the signal-to-noise ratio of EXAFS measurements by 10^3-10^6 over that obtainable from conventional sources. Synchrotron radiation is emitted when charged particles travel in curved paths in magnetic fields. It is a natural by-product of high energy physics experiments in which electrons and positrons are accelerated to speeds close to the velocity of light in an evacuated chamber of a storage ring before colliding to form new elementary particles.

Because synchrotron sources typically have X-ray intensities 3 or more orders of magnitude greater in the continuum energies than do the standard X-ray tube sources, the collection time for measuring a single spectrum has fallen drastically from around a week (Lytle *et al.*)[211] to the order of minutes. At the same time, these powerful synchrotron sources expanded the scope for the types of sample that could be successfully studied, e.g. 'dilute' systems such as biological samples.

The theory of EXAFS is exceedingly complex and the readers attention is drawn to the many detailed mathematical explanations in the literature which are beyond the scope of this discussion. EXAFS refers to the oscillatory variation of the X-ray absorption as a function of photon energy beyond an absorption edge. For atoms either in a molecule or embedded in a condensed phase, the variation of the absorption coefficient (μ) at energies above the absorption edge displays a fine structure called EXAFS. The structural content of this fine structure was first recognised in the 1970's by Stern, Lytle and Sayers.[212,213]

From a qualitative viewpoint, the probability that an X-ray photon will be absorbed by a core electron depends on both the initial and the final states of the electron. The initial state is the localised core level corresponding to the absorption edge. The final state is that of the ejected photoelectron which can be represented as an outgoing spherical wave originating from the X-ray absorbing atom. If the absorbing atom (A) is surrounded by a neighbouring atom (B), the outgoing wave will be back-scattered, thereby producing an incoming electron wave. The final state is then the sum of all the outgoing and all the incoming waves, one each per neighbouring atom. It is the interference between the outgoing and incoming waves that gives rise to the sinusoidal oscillation of μ *vs.* E, i.e. the EXAFS. The frequency of the EXAFS waves depends on the distance between the absorbing atom (A) and the neighbouring atom (B), i.e. the bond length, [A-B]. The amplitude of the EXAFS pattern depends upon the number and the back-scattering power of each neighbouring atom, i.e. related to coordination number and type of neighbouring atom. The simplest case, that of a diatomic molecule such as Br_2, is illustrated qualitatively in Fig. A1.1.

Structural determinations *via* EXAFS depend upon the feasability of resolving the oscillatory interference data into individual waves corresponding to the different types of neighbours of the absorbing atom A. The rapid advances in computer technology in recent years has permitted solutions of complex systems to be obtained using Fourier transform techniques, whereas curve-fitting was once laboriously employed. The Fourier methods provide a photoelectron scattering profile as a function of the radial distance from the absorber. In such a radial distribution function, the positions of the peaks are related to the distance between A and B while the size of each peak is related to the number and types of neighbouring atoms. EXAFS is a highly specific technique in that it can focus on the immediate environment around the absorbing species (i.e. Sn^{II} in the case of stannous compounds) generally out to *ca.* 6Å, or two to three coordination shells. Other

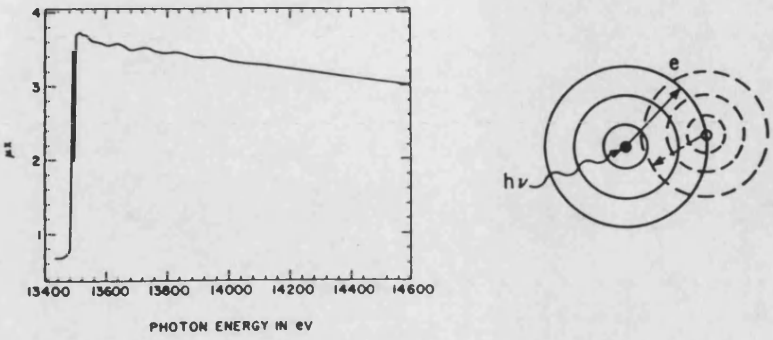

Fig. A1.1 Representation of the presence of EXAFS in a diatomic system such as Br_2.

materials or impurities in the sample which do not contain tin, or are not directly bound to tin, cause no detectable interference. An obvious deficiency of the EXAFS data is that it does not provide a full 3-D structural picture. It gives only a local structure in terms of 1-D radial distributions about each absorber.

The experimental tin(II) EXAFS results in this report were obtained on the dedicated Synchrotron Radiation Source (SRS) at the SERC Daresbury Laboratory using the 'Quick-EXAFS' facility available on Station 9.3. This research station incorporates an Si(220) monochromator with adjustable interplate separation. Solid samples were compressed into thin discs of 1cm diameter and 1mm thickness using a KBr disc press and were run in transmission mode (other EXAFS modes include fluorescence). Data collection with thicker, finely-powdered samples was investigated in order to improve signal-to-noise but inhomogeneities within the solid matrix caused a scattering effect which interfered with the spectrum. Consequently, each sample was analysed four times and the individual spectra summed. A typical EXAFS spectrometer is illustrated schematically in Fig. A1.2.

EXAFS is a useful technique in inorganic chemistry, especially when single

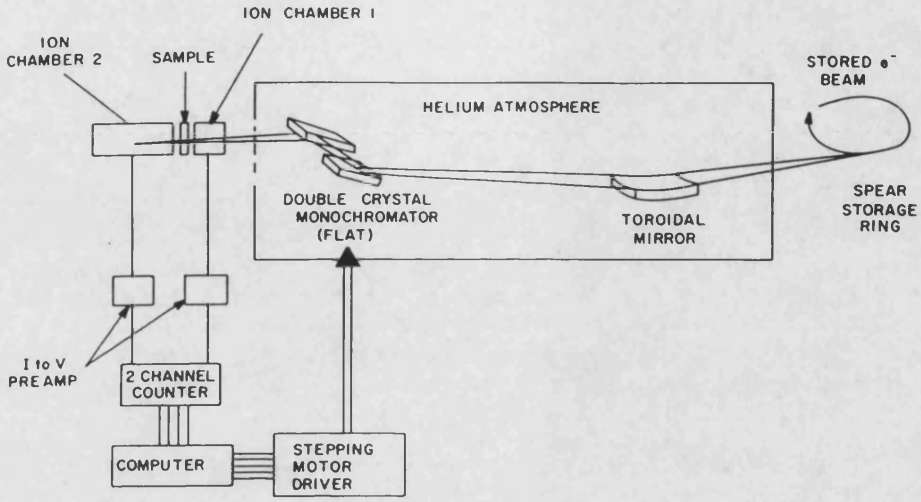

Fig. A1.2 Schematic representation of a tyical EXAFS spectrometer.

crystals are not available or when structural information in solution is sought. The technique is capable of differentiating between metal-metal and metal-ligand bonds provided that the atomic numbers of the neighbouring metal and ligand bonds is sufficiently different ($\Delta Z \geq 4$). Similarly, it is possible to distinguish between different coordinated ligands if the bound atoms are sufficiently different in atomic number. Reported examples of inorganic systems include the structural study of $[cpCoPPh_2]_2^+$ (cp = C_5H_5), $Cu(C_2O_4).1.5H_2O$, $Cu(C_6O_4Cl_2)$ and $Cu(C_6O_4X_2)(NH_3)_2$ (X=Cl, Br).[214-216] Another important use of EXAFS is the determination of local structures of the catalytic sites of homogeneous or heterogeneous catalysts.[217-219] A further application of EXAFS data is the study of biochemical systems. For example, EXAFS can be used to probe the prosthetic group of a protein, thereby allowing structure-function correlation or assessment of steric *vs* electronic effects of the active site.

APPENDIX 2. STRUCTURAL DATA FOR $Sn(Hcit)_2(NMe_4)_2.7H_2O$ (64).

Crystal data: $C_{20}H_{42}O_{16}N_2Sn$, M = 685.2 triclinic, a = 12.610(2), b = 15.571(5), c = 15.967(9)Å, $\underline{\alpha}$ = 83.24(9), $\underline{\beta}$ = 76.70(5), $\underline{\gamma}$ = 95.91(4)°, U = 2952.9Å^3, space group $P1$, $Z = 4$, D_c = 1.54gcm^{-3}, μ(Mo-K_α) = 9.40cm^{-1}, $F(000)$ = 1416.

Data were measured on the FAST system at University College, Cardiff. 11988 reflections were collected over the accessible reciprocal sphere of which 4536 were unique with $I \geq 2\sigma(I)$. Data were corrected for Lorentz and polarisation effects but not for absorption. The structure was solved by Patterson methods and refined using the SHELX suite of programs.[157,158] In the final least squares cycles the tin atoms were allowed to vibrate anisotropically. All other atoms were treated isotropically. Refinement was treated in three blocks; one block for each of the cations, the anions and finally the solvent molecules. Hydrogen atoms were not included. Final residuals after 44 cycles of blocked-matrix least squares were $R = R_w$ = 0.0513. The maximum and minimum residual densities were 0.43 and -0.62eÅ^{-3} respectively.

Final fractional atomic coordinates, isotropic thermal parameters, bond distances and angles are presented in full in the following tables.

Table A2.1 Fractional atomic coordinates ($Å^2 \times 10^3$) and equivalent isotropic temperature factors ($Å^2 \times 10^3$).

	x	y	z	U
Sn(1)	2351(1)	4523(1)	2140(1)	3
Sn(2)	7659(3)	483(2)	2862(2)	49(1)

Table A2.2 Fractional atomic coordinates ($\times 10^3$).

	x	y	z
Sn(1)	2351(1)	4523(1)	2140(1)
Sn(2)	7659(3)	483(2)	2862(2)

Table A2.3 Anisotropic temperature factors (Å x 10^3).

	U_{11}	U_{22}	U_{33}	U_{23}	U_{13}	U_{12}
Sn(1)	3	3(1)	2(1)	1(1)	2	-1
Sn(2)	52(1)	47(2)	35(2)	6(1)	-2(1)	6(1)

The temperature factor exponent takes the form:

$-2\ (U\ .h\ .a^*\ +\ \ldots\ \ +2U\ .h.k.a^*.b^*)$

Table A2.4 Isotropic temperature factors ($Å^2 \times 10^3$).

	x	y	z	U
O(1)	1003(9)	3916(8)	2633(8)	11(3)
O(2)	-447(8)	3520(7)	2615(7)	19(2)
O(3)	2219(9)	4280(8)	927(8)	11(3)
O(4)	4408(9)	3381(7)	-11(7)	23(2)
O(5)	3836(8)	3470(7)	-1255(7)	27(2)
O(6)	3362(9)	3216(8)	2019(9)	8(3)
O(7)	3387(9)	2035(9)	1404(9)	10(2)
O(8)	1342(9)	5780(8)	2063(8)	7(2)
O(9)	1163(10)	7249(9)	2102(9)	21(3)
O(10)	2496(11)	4717(10)	3294(11)	9(3)
O(11)	3760(9)	5087(8)	1773(9)	7(3)
O(12)	4505(9)	6039(8)	2296(8)	14(2)
O(13)	4979(17)	4333(15)	3479(15)	40(5)
O(14)	4300(11)	4260(10)	4854(11)	23(3)
C(1)	486(12)	3638(10)	2314(10)	17(4)
C(2)	1053(12)	3198(10)	1305(11)	12(3)
C(3)	2202(14)	3429(13)	980(13)	8(4)
C(4)	2545(12)	3229(11)	33(11)	17(4)
C(5)	3728(16)	3303(14)	-395(17)	15(4)
C(6)	3085(14)	2868(12)	1503(13)	14(4)
C(7)	1473(10)	6485(9)	2342(10)	5(3)
C(8)	1923(12)	6301(10)	3166(10)	13(3)
C(9)	2939(12)	5477(11)	3220(12)	6(3)
C(10)	3834(10)	5597(8)	2400(8)	2(2)
C(11)	3478(13)	5472(11)	3977(12)	11(3)

C(12)	4297(13)	4576(11)	4134(12)	15(4)
O(15)	9042(14)	963(12)	2299(13)	48(5)
O(16)	10566(9)	1437(8)	2604(8)	31(3)
O(17)	7791(12)	640(11)	3988(11)	31(4)
O(18)	5466(10)	1858(8)	5085(8)	33(3)
O(19)	6288(8)	1246(7)	6200(7)	22(2)
O(20)	6718(14)	1752(13)	2903(13)	40(5)
O(21)	6688(17)	3020(16)	3585(16)	53(6)
O(22)	8603(20)	-787(17)	3002(18)	69(7)
O(23)	8734(13)	-2194(12)	3046(11)	40(4)
O(24)	7438(16)	257(14)	1695(15)	35(5)
O(25)	5086(11)	685(10)	1591(10)	13(3)
O(26)	5810(18)	765(17)	120(17)	62(7)
O(27)	6300(16)	-139(14)	3291(14)	47(6)
O(28)	5668(13)	-1117(11)	2763(12)	43(4)
C(13)	9570(12)	1428(10)	2864(10)	16(4)
C(14)	8963(17)	1703(15)	3590(15)	34(6)
C(15)	7743(22)	1652(19)	4079(20)	36(7)
C(16)	7372(14)	1954(11)	4989(12)	22(4)
C(17)	6320(21)	1604(18)	5423(22)	33(6)
C(18)	6997(16)	2240(14)	3516(14)	21(5)
C(19)	8450(23)	-1462(20)	2560(20)	61(9)
C(20)	7940(17)	-1408(14)	1805(15)	36(5)
C(21)	7068(21)	-575(18)	1776(20)	40(7)
C(22)	6610(19)	-568(17)	949(17)	39(7)
C(23)	5831(15)	301(13)	826(14)	24(5)
C(24)	6250(16)	-499(14)	2716(14)	34(5)
N(1)	7665(16)	5826(15)	3055(15)	25(5)

C(25)	6774(24)	6747(20)	3243(22)	55(8)
C(26)	8392(15)	5972(13)	2229(13)	23(4)
C(27)	8436(16)	5665(13)	3702(13)	35(5)
C(28)	7093(14)	5105(12)	3091(13)	28(4)
N(2)	2336(16)	9148(15)	1875(15)	25(5)
C(29)	3245(13)	8356(11)	1788(12)	13(3)
C(30)	1540(18)	9182(15)	2812(16)	36(6)
C(31)	1726(14)	9235(12)	1174(12)	25(4)
C(32)	2804(15)	10000(13)	1785(14)	32(5)
N(3)	3132(18)	6772(16)	9126(19)	22(5)
C(33)	2148(12)	6797(11)	8768(11)	20(3)
C(34)	4163(13)	6310(11)	8582(11)	35(3)
C(35)	3119(12)	6097(11)	9938(10)	31(3)
C(36)	3274(19)	7646(15)	9192(16)	61(6)
N(4)	3124(18)	1704(16)	4212(19)	24(5)
C(37)	2211(20)	1602(17)	3721(18)	57(7)
C(38)	2976(20)	1393(17)	5118(16)	68(6)
C(39)	4238(26)	1683(21)	3489(21)	98(9)
C(40)	2900(19)	2681(15)	4481(15)	59(5)
O(1′)	-31(10)	7154(8)	670(9)	23(3)
O(2′)	100(15)	2209(13)	5741(13)	58(5)
O(3′)	475(10)	5512(8)	373(8)	44(3)
O(4′)	768(9)	452(7)	5050(7)	32(2)
O(5′)	616(18)	4674(15)	4705(16)	21(5)
O(6′)	-699(8)	3610(6)	4544(6)	31(2)
O(7)	-136(11)	1368(9)	433(9)	61(3)
O(8′)	678(20)	-138(16)	9658(18)	29(6)

Table A2.5 Bond lengths (Å).

O(1)-Sn(1)	2.095(14)	O(3)-Sn(1)	2.066(16)
O(6)-Sn(1)	2.125(13)	O(8)-Sn(1)	2.067(13)
O(10)-Sn(1)	1.958(20)	O(11)-Sn(1)	2.105(15)
C(3)-Sn(1)	2.725(25)	C(6)-Sn(1)	2.747(22)
C(9)-Sn(1)	2.731(24)	C(1)-O(1)	1.101(24)
C(1)-O(2)	1.214(19)	C(3)-O(3)	1.323(25)
C(5)-O(4)	1.198(30)	C(5)-O(5)	1.348(29)
C(6)-O(6)	1.192(28)	C(6)-O(7)	1.278(24)
C(7)-O(8)	1.291(22)	C(7)-O(9)	1.204(19)
C(9)-O(10)	1.409(26)	C(10)-O(11)	1.382(22)
C(10)-O(12)	1.187(20)	C(12)-O(13)	1.225(27)
C(12)-O(14)	1.196(26)	C(2)-C(1)	1.752(25)
C(3)-C(2)	1.537(26)	C(4)-C(3)	1.522(29)
C(6)-C(3)	1.576(29)	C(5)-C(4)	1.516(27)
C(8)-C(7)	1.521(25)	C(9)-C(8)	1.586(22)
C(10)-C(9)	1.545(21)	C(11)-C(9)	1.515(30)
C(12)-C(11)	1.553(24)	O(15)-Sn(2)	2.040(21)
O(17)-Sn(2)	1.892(21)	O(20)-Sn(2)	2.041(20)
O(22)-Sn(2)	2.062(26)	O(24)-Sn(2)	2.028(28)
O(27)-Sn(2)	2.111(24)	C(15)-Sn(2)	2.850(37)
C(21)-Sn(2)	2.853(37)	C(24)-Sn(2)	2.673(28)
C(13)-O(15)	1.563(31)	C(13)-O(16)	1.233(20)
C(15)-O(17)	1.585(37)	C(17)-O(18)	1.271(35)
C(17)-O(19)	1.295(36)	C(18)-O(20)	1.457(35)
C(18)-O(21)	1.190(32)	C(19)-O(22)	1.406(48)

C(19)-O(23)	1.323(35)	C(21)-O(24)	1.464(39)
C(23)-O(25)	1.450(25)	C(23)-O(26)	1.268(34)
C(24)-O(27)	1.151(35)	C(24)-O(28)	1.332(32)
C(14)-C(13)	1.290(27)	C(15)-C(14)	1.573(35)
C(16)-C(15)	1.513(38)	C(18)-C(15)	1.520(38)
C(17)-C(16)	1.541(35)	C(20)-C(19)	1.477(43)
C(21)-C(20)	1.485(31)	C(22)-C(21)	1.556(47)
C(24)-C(21)	1.612(36)	C(23)-C(22)	1.487(30)
C(25)-N(1)	1.603(36)	C(26)-N(1)	1.452(29)
C(27)-N(1)	1.536(35)	C(28)-N(1)	1.463(33)
C(29)-N(2)	1.461(25)	C(30)-N(2)	1.597(33)
C(31)-N(2)	1.474(33)	C(32)-N(2)	1.558(35)
C(33)-N(3)	1.471(33)	C(34)-N(3)	1.461(26)
C(35)-N(3)	1.569(33)	C(36)-N(3)	1.434(38)
C(37)-N(4)	1.580(45)	C(38)-N(4)	1.455(39)
C(39)-N(4)	1.596(39)	C(40)-N(4)	1.571(38)
C(40)-C(38)	2.129(35)	O(5')-O(5'a)	1.765(41)
O(8')-O(8'b)	1.787(47)		

Key to symmetry operations relating designated atoms to reference atoms at (x,y,z):

(a) -x,1.0-y,1.0-z

(b) -x,-y,2.0-z

Table A2.6 Bond angles (°).

O(3)-Sn(1)-O(1)	87.1(6)	O(6)-Sn(1)-O(1)	86.3(5)
O(6)-Sn(1)-O(3)	79.4(6)	O(8)-Sn(1)-O(1)	93.8(5)
O(8)-Sn(1)-O(3)	91.6(6)	O(8)-Sn(1)-O(6)	171.0(6)
O(10)-Sn(1)-O(1)	92.5(7)	O(10)-Sn(1)-O(3)	178.4(5)
O(10)-Sn(1)-O(6)	99.0(7)	O(10)-Sn(1)-O(8)	90.0(7)
O(11)-Sn(1)-O(1)	173.8(5)	O(11)-Sn(1)-O(3)	98.4(6)
O(11)-Sn(1)-O(6)	91.9(6)	O(11)-Sn(1)-O(8)	89.0(6)
O(11)-Sn(1)-O(10)	81.9(7)	C(3)-Sn(1)-O(1)	70.0(6)
C(3)-Sn(1)-O(3)	28.0(5)	C(3)-Sn(1)-O(6)	57.7(7)
C(3)-Sn(1)-O(8)	113.9(7)	C(3)-Sn(1)-O(10)	150.5(6)
C(3)-Sn(1)-O(11)	113.9(6)	C(6)-Sn(1)-O(1)	76.4(6)
C(6)-Sn(1)-O(3)	57.3(6)	C(6)-Sn(1)-O(6)	24.3(6)
C(6)-Sn(1)-O(8)	147.4(6)	C(6)-Sn(1)-O(10)	121.0(7)
C(6)-Sn(1)-O(11)	104.1(6)	C(6)-Sn(1)-C(3)	33.5(6)
C(9)-Sn(1)-O(1)	118.0(6)	C(9)-Sn(1)-O(3)	151.6(5)
C(9)-Sn(1)-O(6)	113.3(6)	C(9)-Sn(1)-O(8)	74.6(6)
C(9)-Sn(1)-O(10)	29.5(6)	C(9)-Sn(1)-O(11)	57.5(6)
C(9)-Sn(1)-C(3)	168.8(5)	C(9)-Sn(1)-C(6)	137.5(5)
C(1)-O(1)-Sn(1)	132.0(11)	C(3)-O(3)-Sn(1)	104.9(13)
C(6)-O(6)-Sn(1)	108.5(12)	C(7)-O(8)-Sn(1)	126.2(11)
C(9)-O(10)-Sn(1)	107.3(13)	C(10)-O(11)-Sn(1)	111.9(9)
O(2)-C(1)-O(1)	127.2(17)	C(2)-C(1)-O(1)	120.0(14)
C(2)-C(1)-O(2)	112.5(16)	C(3)-C(2)-C(1)	107.2(15)
O(3)-C(3)-Sn(1)	47.1(9)	C(2)-C(3)-Sn(1)	105.4(12)
C(2)-C(3)-O(3)	116.4(14)	C(4)-C(3)-Sn(1)	143.5(13)

C(4)-C(3)-O(3)	101.1(16)	C(4)-C(3)-C(2)	105.6(18)
C(6)-C(3)-Sn(1)	74.0(12)	C(6)-C(3)-O(3)	110.4(19)
C(6)-C(3)-C(2)	111.6(16)	C(6)-C(3)-C(4)	111.2(14)
C(5)-C(4)-C(3)	114.6(19)	O(5)-C(5)-O(4)	123.3(19)
C(4)-C(5)-O(4)	124.0(22)	C(4)-C(5)-O(5)	111.1(20)
O(6)-C(6)-Sn(1)	47.2(8)	O(7)-C(6)-Sn(1)	165.9(14)
O(7)-C(6)-O(6)	123.3(19)	C(3)-C(6)-Sn(1)	72.5(11)
C(3)-C(6)-O(6)	119.4(17)	C(3)-C(6)-O(7)	116.9(20)
O(9)-C(7)-O(8)	128.8(17)	C(8)-C(7)-O(8)	113.1(13)
C(8)-C(7)-O(9)	117.5(16)	C(9)-C(8)-C(7)	118.1(14)
O(10)-C(9)-Sn(1)	43.2(9)	C(8)-C(9)-Sn(1)	94.0(12)
C(8)-C(9)-O(10)	106.0(14)	C(10)-C(9)-Sn(1)	80.9(11)
C(10)-C(9)-O(10)	116.5(16)	C(10)-C(9)-C(8)	105.1(13)
C(11)-C(9)-Sn(1)	147.9(11)	C(11)-C(9)-O(10)	109.9(16)
C(11)-C(9)-C(8)	113.4(15)	C(11)-C(9)-C(10)	106.1(14)
O(12)-C(10)-O(11)	123.1(13)	C(9)-C(10)-O(11)	109.3(14)
C(9)-C(10)-O(12)	127.7(15)	C(12)-C(11)-C(9)	112.8(16)
O(14)-C(12)-O(13)	126.9(18)	C(11)-C(12)-O(13)	112.5(18)
C(11)-C(12)-O(14)	119.9(16)	O(17)-Sn(2)-O(15)	92.8(9)
O(20)-Sn(2)-O(15)	89.5(8)	O(20)-Sn(2)-O(17)	84.9(9)
O(22)-Sn(2)-O(15)	92.1(10)	O(22)-Sn(2)-O(17)	87.1(11)
O(22)-Sn(2)-O(20)	171.9(10)	O(24)-Sn(2)-O(15)	91.3(10)
O(24)-Sn(2)-O(17)	175.7(8)	O(24)-Sn(2)-O(20)	96.3(9)
O(24)-Sn(2)-O(22)	91.7(11)	O(27)-Sn(2)-O(15)	171.5(9)
O(27)-Sn(2)-O(17)	94.2(9)	O(27)-Sn(2)-O(20)	95.8(9)
O(27)-Sn(2)-O(22)	83.6(10)	O(27)-Sn(2)-O(24)	81.6(10)
C(15)-Sn(2)-O(15)	76.8(9)	C(15)-Sn(2)-O(17)	31.6(8)
C(15)-Sn(2)-O(20)	58.3(9)	C(15)-Sn(2)-O(22)	114.4(11)

C(15)-Sn(2)-O(24)	151.4(8)	C(15)-Sn(2)-O(27)	111.6(9)
C(21)-Sn(2)-O(15)	113.6(9)	C(21)-Sn(2)-O(17)	146.9(8)
C(21)-Sn(2)-O(20)	113.5(9)	C(21)-Sn(2)-O(22)	73.1(11)
C(21)-Sn(2)-O(24)	29.1(8)	C(21)-Sn(2)-O(27)	58.1(9)
C(21)-Sn(2)-C(15)	167.7(7)	C(24)-Sn(2)-O(15)	147.3(7)
C(24)-Sn(2)-O(17)	117.4(8)	C(24)-Sn(2)-O(20)	104.5(8)
C(24)-Sn(2)-O(22)	78.2(10)	C(24)-Sn(2)-O(24)	58.4(9)
C(24)-Sn(2)-O(27)	24.4(8)	C(24)-Sn(2)-C(15)	135.6(7)
C(24)-Sn(2)-C(21)	33.7(7)	C(13)-O(15)-Sn(2)	119.0(13)
C(15)-O(17)-Sn(2)	109.8(15)	C(18)-O(20)-Sn(2)	111.1(14)
C(19)-O(22)-Sn(2)	119.2(21)	C(21)-O(24)-Sn(2)	108.5(19)
C(24)-O(27)-Sn(2)	106.3(17)	O(16)-C(13)-O(15)	116.5(15)
C(14)-C(13)-O(15)	117.9(18)	C(14)-C(13)-O(16)	125.4(21)
C(15)-C(14)-C(13)	133.0(24)	O(17)-C(15)-Sn(2)	38.7(10)
C(14)-C(15)-Sn(2)	89.9(16)	C(14)-C(15)-O(17)	99.9(18)
C(16)-C(15)-Sn(2)	148.5(18)	C(16)-C(15)-O(17)	115.6(21)
C(16)-C(15)-C(14)	117.1(26)	C(18)-C(15)-Sn(2)	76.7(17)
C(18)-C(15)-O(17)	110.0(25)	C(18)-C(15)-C(14)	104.2(21)
C(18)-C(15)-C(16)	109.2(19)	C(17)-C(16)-C(15)	107.7(23)
O(19)-C(17)-O(18)	123.7(23)	C(16)-C(17)-O(18)	117.8(25)
C(16)-C(17)-O(19)	116.6(26)	O(21)-C(18)-O(20)	125.0(23)
C(15)-C(18)-O(20)	113.1(20)	C(15)-C(18)-O(21)	121.9(27)
O(23)-C(19)-O(22)	104.0(28)	C(20)-C(19)-O(22)	130.4(25)
C(20)-C(19)-O(23)	125.1(29)	C(21)-C(20)-C(19)	110.7(23)
O(24)-C(21)-Sn(2)	42.4(14)	C(20)-C(21)-Sn(2)	101.4(20)
C(20)-C(21)-O(24)	116.6(23)	C(22)-C(21)-Sn(2)	145.1(17)
C(22)-C(21)-O(24)	105.0(23)	C(22)-C(21)-C(20)	106.7(23)
C(24)-C(21)-Sn(2)	67.0(15)	C(24)-C(21)-O(24)	100.1(22)

C(24)-C(21)-C(20)	107.6(21)	C(24)-C(21)-C(22)	121.4(22)
C(23)-C(22)-C(21)	109.2(22)	O(26)-C(23)-O(25)	116.8(18)
C(22)-C(23)-O(25)	117.2(19)	C(22)-C(23)-O(26)	125.8(20)
O(27)-C(24)-Sn(2)	49.3(13)	O(28)-C(24)-Sn(2)	167.2(15)
O(28)-C(24)-O(27)	125.3(22)	C(21)-C(24)-Sn(2)	79.3(15)
C(21)-C(24)-O(27)	128.5(24)	C(21)-C(24)-O(28)	104.4(21)
C(26)-N(1)-C(25)	106.3(20)	C(27)-N(1)-C(25)	108.2(22)
C(27)-N(1)-C(26)	104.0(17)	C(28)-N(1)-C(25)	110.5(19)
C(28)-N(1)-C(26)	114.4(21)	C(28)-N(1)-C(27)	113.0(19)
C(30)-N(2)-C(29)	112.7(18)	C(31)-N(2)-C(29)	109.9(20)
C(31)-N(2)-C(30)	113.2(18)	C(32)-N(2)-C(29)	110.7(17)
C(32)-N(2)-C(30)	103.6(19)	C(32)-N(2)-C(31)	106.3(18)
C(34)-N(3)-C(33)	111.7(23)	C(35)-N(3)-C(33)	108.7(18)
C(35)-N(3)-C(34)	98.3(16)	C(36)-N(3)-C(33)	111.8(20)
C(36)-N(3)-C(34)	106.3(20)	C(36)-N(3)-C(35)	119.3(25)
C(38)-N(4)-C(37)	116.6(22)	C(39)-N(4)-C(37)	105.6(25)
C(39)-N(4)-C(38)	130.3(23)	C(40)-N(4)-C(37)	110.8(19)
C(40)-N(4)-C(38)	89.4(22)	C(40)-N(4)-C(39)	99.5(21)
C(40)-C(38)-N(4)	47.5(14)	C(38)-C(40)-N(4)	43.1(14)

Table A2.7 Selected non-bonded distances (Å).

Intramolecular:

C(1)-Sn(1)	2.948	C(2)-Sn(1)	3.465
C(7)-Sn(1)	3.014	C(8)-Sn(1)	3.253
C(10)-Sn(1)	2.917	O(2)-O(1)	2.074
O(3)-O(1)	2.867	O(6)-O(1)	2.885
O(8)-O(1)	3.039	O(10)-O(1)	2.929
C(2)-O(1)	2.492	C(3)-O(1)	2.811
C(6)-O(1)	3.039	C(2)-O(2)	2.484
O(6')-O(2)	3.040	O(4)-O(3)	2.920
O(6)-O(3)	2.677	O(8)-O(3)	2.964
C(1)-O(3)	2.999	C(2)-O(3)	2.433
C(4)-O(3)	2.199	C(5)-O(3)	2.809
C(6)-O(3)	2.384	O(3')-O(3)	2.783
O(5)-O(4)	2.243	C(3)-O(4)	2.854
C(4)-O(4)	2.401	C(6)-O(4)	2.757
C(4)-O(5)	2.365	O(7)-O(6)	2.175
O(10)-O(6)	3.107	O(11)-O(6)	3.040
C(3)-O(6)	2.398	C(2)-O(7)	3.085
C(3)-O(7)	2.437	C(4)-O(7)	2.920
O(25)-O(7)	2.656	O(9)-O(8)	2.250
O(10)-O(8)	2.846	O(11)-O(8)	2.923
C(8)-O(8)	2.350	C(9)-O(8)	2.955
C(8)-O(9)	2.336	O(1')-O(9)	3.048
O(11)-O(10)	2.666	O(13)-O(10)	3.118
C(7)-O(10)	3.122	C(8)-O(10)	2.394
C(10)-O(10)	2.514	C(11)-O(10)	2.394

C(12)-O(10)	2.845	O(5')-O(10)	2.878
O(12)-O(11)	2.260	C(7)-O(11)	3.176
C(9)-O(11)	2.389	O(13)-O(12)	3.091
C(8)-O(12)	3.178	C(9)-O(12)	2.458
C(11)-O(12)	2.839	O(14)-O(13)	2.166
C(9)-O(13)	2.837	C(10)-O(13)	2.808
C(11)-O(13)	2.317	O(21)-O(13)	2.606
C(28)-O(13)	3.093	C(11)-O(14)	2.386
C(3)-C(1)	2.650	C(6)-C(1)	3.218
C(4)-C(2)	2.436	C(6)-C(2)	2.574
C(5)-C(3)	2.556	C(6)-C(4)	2.556
C(6)-C(5)	2.992	C(9)-C(7)	2.666
C(10)-C(7)	2.980	C(10)-C(8)	2.486
C(11)-C(8)	2.593	C(12)-C(9)	2.556
C(11)-C(10)	2.446	C(12)-C(10)	3.129
C(13)-Sn(2)	3.114	C(14)-Sn(2)	3.253
C(18)-Sn(2)	2.904	C(19)-Sn(2)	3.009
C(20)-Sn(2)	3.468	O(16)-O(15)	2.383
O(17)-O(15)	2.850	O(20)-O(15)	2.873
O(22)-O(15)	2.953	O(24)-O(15)	2.908
C(14)-O(15)	2.448	C(15)-O(15)	3.104
C(14)-O(16)	2.241	O(20)-O(17)	2.656
O(22)-O(17)	2.726	O(27)-O(17)	2.937
C(13)-O(17)	2.955	C(14)-O(17)	2.417
C(16)-O(17)	2.622	C(17)-O(17)	2.906
C(18)-O(17)	2.544	O(19)-O(18)	2.262
C(15)-O(18)	2.912	C(16)-O(18)	2.412
C(18)-O(18)	2.888	C(16)-O(19)	2.416

O(21)-O(20)	2.352	O(24)-O(20)	3.031
O(27)-O(20)	3.083	C(15)-O(20)	2.484
C(39)-O(20)	3.076	C(14)-O(21)	3.095
C(15)-O(21)	2.375	C(16)-O(21)	2.800
O(23)-O(22)	2.151	O(24)-O(22)	2.933
O(27)-O(22)	2.780	C(20)-O(22)	2.617
C(21)-O(22)	2.994	C(24)-O(22)	3.023
C(20)-O(23)	2.485	O(25)-O(24)	2.917
O(27)-O(24)	2.704	C(19)-O(24)	2.997
C(20)-O(24)	2.510	C(22)-O(24)	2.397
C(23)-O(24)	2.690	C(24)-O(24)	2.360
O(26)-O(25)	2.317	C(21)-O(25)	2.829
C(22)-O(25)	2.508	C(24)-O(25)	2.810
C(22)-O(26)	2.455	O(28)-O(27)	2.207
C(19)-O(27)	3.058	C(21)-O(27)	2.498
C(20)-O(28)	2.876	C(21)-O(28)	2.333
C(22)-O(28)	2.976	C(15)-C(13)	2.628
C(18)-C(13)	3.158	C(16)-C(14)	2.633
C(18)-C(14)	2.442	C(17)-C(15)	2.467
C(18)-C(16)	2.473	C(18)-C(17)	3.080
C(21)-C(19)	2.436	C(24)-C(19)	2.784
C(22)-C(20)	2.441	C(24)-C(20)	2.500
C(23)-C(21)	2.482	C(24)-C(22)	2.763
C(24)-C(23)	3.235	C(26)-C(25)	2.447
C(27)-C(25)	2.543	C(28)-C(25)	2.520
C(27)-C(26)	2.355	C(28)-C(26)	2.450
C(28)-C(27)	2.502	C(30)-C(29)	2.546
C(31)-C(29)	2.403	C(32)-C(29)	2.484

C(31)-C(30)	2.565	C(32)-C(30)	2.480
C(32)-C(31)	2.426	C(34)-C(33)	2.427
C(35)-C(33)	2.471	C(36)-C(33)	2.405
C(35)-C(34)	2.294	C(36)-C(34)	2.317
C(36)-C(35)	2.592	C(38)-C(37)	2.584
C(39)-C(37)	2.530	C(40)-C(37)	2.593
O(4')-C(37)	3.151	C(39)-C(38)	2.769
C(40)-C(39)	2.416	O(3')-O(1')	2.554
O(4')-O(2')	2.927	O(6')-O(2')	2.874
O(6')-O(5')	2.683		

Intermolecular:

O(12)-O(5a)	2.570	O(23)-O(9b)	3.049
C(34)-O(11c)	2.957	O(7)-O(15d)	2.967
C(37)-O(16d)	3.102	O(4')-O(17e)	2.778
O(28)-O(19e)	2.674	O(2')-O(23e)	2.682
O(8')-O(24e)	2.804	C(38)-O(27e)	3.183
O(5')-C(27c)	2.992	O(8')-C(31f)	2.974
O(7)-O(1'g)	2.750	O(3')-O(3'g)	2.724
O(4')-O(4'h)	2.699	O(6')-O(5'i)	3.087
O(8')-O(7j)	2.648	O(8')-O(7h)	2.214

Key to symmetry operations

(a)	1.0-x,1.0-y,-z	(f)	x,-1.0+y,1.0+z
(b)	1.0+x,-1.0+y,z	(g)	-x,1.0-y,-z
(c)	1.0-x,1.0-y,1.0-z	(h)	-x,-y,1.0-z
(d)	-1.0+x,y,z	(i)	-x,1.0-y,1.0-z
(e)	1.0-x,-y,1.0-z	(j)	x,y,1.0+z

APPENDIX 3. STRUCTURAL DATA FOR Sn(1,3-dimethylcitrate).CH_3OH (60).

Crystal data: $C_9H_{14}O_8Sn$, M = 368.9, monoclinic, a = 9.793(6), b = 10.416(5), c = 12.849(6)Å, β = 104.21(4)°, U = 1270.6Å^3, space group $P2_1/c$, Z = 4, D_c = 1.92gcm^{-3}, υ(Mo-K_α) = 18.7cm^{-1}, F(000) = 728.

Data were measured at room temperature on a CAD4 automatic four-circle diffractometer in the range $2\leq\theta\leq22°$. 1776 reflections were collected of which 1261 were unique with $I\geq3\sigma(I)$. Data were corrected for Lorentz and polarisation effects but not for absorption. The structure was solved by Patterson methods and refined using the SHELX suite of programs.[157,158] In the final least squares cycles, all atoms were allowed to vibrate anisotropically. Hydrogen atoms were included at calculated positions on carbon atoms. Final residuals after 9 cycles of least squares were R = 0.0328, R_w = 0.0391, for a weighting scheme of $w = 0.7378/[\sigma^2(F) + 0.002599(F)^2]$. Maximum final shift/esd was 0.030. The maximum and minimum residual densities were 0.68 and -0.72eÅ^{-3} respectively in the region of the tin atom, and as such have no chemical significance.

Final fractional atomic coordinates, isotropic thermal parameters, bond distances and angles are presented in full in the following tables. Tables of anisotropic temperature factors are available as supplementary data.

Table A3.1 Fractional atomic coordinates and thermal parameters (Å).

	x	y	z	U
Sn(1)	-744.4(3)	-77.3(3)	1206.0(2)	28
O(1)	286(3)	1170(3)	33(2)	27(1)
O(2)	-784(4)	-2163(3)	1700(3)	35(1)
O(3)	3262(4)	1047(4)	57(3)	57(2)
O(4)	4458(4)	1645(4)	1683(3)	51(2)
O(5)	-1775(4)	3917(4)	-1155(3)	43(1)
O(6)	-2713(4)	3138(4)	129(3)	51(2)
O(7)	-1591(4)	-4010(3)	915(3)	36(1)
O(8)	1485(4)	-99(3)	2266(3)	42(2)
C(1)	813(5)	2442(4)	158(4)	25(2)
C(2)	2191(5)	2517(4)	1048(4)	30(2)
C(3)	3319(5)	1656(5)	858(4)	36(2)
C(4)	5611(6)	820(7)	1564(5)	62(3)
C(5)	-240(5)	3310(4)	541(4)	30(2)
C(6)	-1630(5)	3484(4)	-274(4)	32(2)
C(7)	-4100(6)	3419(8)	-545(6)	72(3)
C(8)	-1087(5)	-2922(5)	908(4)	29(2)
C(9)	2558(6)	-1026(6)	2318(5)	52(2)

Table A3.2 Fractional atomic coordinates for the hydrogen atoms (Å).

	x	y	z	U
H(8)	1616(81)	396(65)	2913(36)	93(7)
H(21)	1991(5)	2283(4)	1718(4)	93(7)
H(22)	2530(5)	3385(4)	1089(4)	93(7)
H(41)	6372(6)	881(7)	2196(5)	93(7)
H(42)	5932(6)	1088(7)	950(5)	93(7)
H(43)	5289(6)	-53(7)	1468(5)	93(7)
H(51)	184(5)	4140(4)	708(4)	93(7)
H(52)	-423(5)	2938(4)	1177(4)	93(7)
H(71)	-4806(6)	3137(8)	-193(6)	93(7)
H(72)	-4223(6)	2981(8)	-1219(6)	93(7)
H(73)	-4189(6)	4328(8)	-669(6)	93(7)
H(91)	2381(6)	-1493(6)	1654(5)	93(7)
H(92)	2565(6)	-1610(6)	2897(5)	93(7)
H(93)	3454(6)	-604(6)	2438(5)	93(7)

Table A3.3 Anisotropic thermal parameters (Å).

	U_{11}	U_{22}	U_{33}	U_{23}	U_{13}	U_{12}
Sn(1)	29.3(3)	28.1(3)	28.1(3)	-2.5(2)	7.5(2)	1.4(2)
O(1)	33(2)	22(2)	26(2)	-2(1)	8(2)	-4(1)
O(2)	46(2)	31(2)	28(2)	-3(2)	8(2)	-4(2)
O(3)	37(2)	82(3)	47(3)	-25(2)	-2(2)	11(2)
O(4)	31(2)	72(3)	43(2)	-15(2)	-5(2)	11(2)
O(5)	38(2)	54(2)	34(2)	4(2)	1(2)	0(2)
O(6)	32(2)	66(3)	55(2)	11(2)	13(2)	-3(2)
O(7)	45(2)	27(2)	35(2)	3(2)	9(2)	-9(2)
O(8)	45(2)	41(2)	33(2)	-8(2)	-2(2)	7(2)
C(1)	26(3)	25(3)	24(3)	1(2)	3(2)	-2(2)
C(2)	31(3)	29(3)	30(3)	-2(2)	7(2)	-2(2)
C(3)	31(3)	45(3)	27(3)	-2(3)	-1(3)	-3(3)
C(4)	31(3)	84(5)	65(4)	-13(4)	1(3)	22(3)
C(5)	32(3)	29(3)	29(3)	-3(2)	5(2)	-1(2)
C(6)	30(3)	25(3)	39(4)	-4(2)	5(3)	2(2)
C(7)	32(4)	105(6)	77(5)	14(4)	9(4)	6(4)
C(8)	27(3)	29(3)	29(3)	2(2)	3(2)	3(2)
C(9)	45(4)	55(4)	52(4)	-6(3)	5(3)	10(3)

Table A3.4 Bond lengths (Å).

O(1)-Sn(1)	2.393(5)	O(2)-Sn(1)	2.266(5)
O(8)-Sn(1)	2.272(6)	C(8)-Sn(1)	2.996(8)
C(1)-O(1)	1.416(6)	C(8)-O(2)	1.265(7)
C(3)-O(3)	1.198(7)	C(3)-O(4)	1.337(7)
C(4)-O(4)	1.457(7)	C(6)-O(5)	1.194(7)
C(6)-O(6)	1.339(7)	C(7)-O(6)	1.450(8)
C(8)-O(7)	1.237(7)	C(9)-O(8)	1.416(7)
C(2)-C(1)	1.542(9)	C(5)-C(1)	1.540(9)
C(3)-C(2)	1.489(8)	C(6)-C(5)	1.511(9)
H(8)-O(8)	0.960(2)	H(21)-C(2)	0.960
H(22)-C(2)	0.960	H(41)-C(4)	0.960
H(42)-C(4)	0.960	H(43)-C(4)	0.960
H(51)-C(5)	0.960	H(52)-C(5)	0.960
H(71)-C(7)	0.960	H(72)-C(7)	0.960
H(73)-C(7)	0.960	H(91)-C(9)	0.960
H(92)-C(9)	0.960	H(93)-C(9)	0.960

Table A3.5 Bond angles (°).

O(2)-Sn(1)-O(1)	137.4(1)	O(8)-Sn(1)-O(1)	83.7(2)
O(8)-Sn(1)-O(2)	84.4(2)	C(8)-Sn(1)-O(1)	120.5(2)
C(8)-Sn(1)-O(2)	22.9(1)	C(8)-Sn(1)-O(8)	97.3(2)
C(1)-O(1)-Sn(1)	129.4(4)	C(8)-O(2)-Sn(1)	113.0(4)
C(4)-O(4)-C(3)	116.0(5)	C(7)-O(6)-C(6)	115.5(5)
C(9)-O(8)-Sn(1)	128.9(4)	C(2)-C(1)-O(1)	111.1(5)
C(5)-C(1)-O(1)	109.4(5)	C(5)-C(1)-C(2)	105.4(5)
C(3)-C(2)-C(1)	113.4(5)	O(4)-C(3)-O(3)	122.1(6)
C(2)-C(3)-O(3)	125.4(6)	C(2)-C(3)-O(4)	112.5(5)
C(6)-C(5)-C(1)	114.2(5)	O(6)-C(6)-O(5)	123.2(6)
C(5)-C(6)-O(5)	125.4(6)	C(5)-C(6)-O(6)	111.4(5)
O(2)-C(8)-Sn(1)	44.1(2)	O(7)-C(8)-Sn(1)	159.6(4)
O(7)-C(8)-O(2)	125.5(5)	H(8)-O(8)-Sn(1)	114.7(48)
C(9)-O(8)-H(8)	112.7(48)	H(21)-C(2)-C(1)	108.5(4)
H(22)-C(2)-C(1)	108.4(3)	H(22)-C(2)-H(21)	109.5
C(3)-C(2)-H(21)	108.5(4)	C(3)-C(2)-H(22)	108.5(4)
H(41)-C(4)-O(4)	109.5(4)	H(42)-C(4)-O(4)	109.4(4)
H(42)-C(4)-H(41)	109.5	H(43)-C(4)-O(4)	109.5(4)
H(43)-C(4)-H(41)	109.5	H(43)-C(4)-H(42)	109.5
H(51)-C(5)-C(1)	108.3(3)	H(52)-C(5)-C(1)	108.3(3)
H(52)-C(5)-H(51)	109.5	C(6)-C(5)-H(51)	108.3(3)
C(6)-C(5)-H(52)	108.3(4)	H(71)-C(7)-O(6)	109.5(4)
H(72)-C(7)-O(6)	109.5(4)	H(72)-C(7)-H(71)	109.5
H(73)-C(7)-O(6)	109.4(5)	H(73)-C(7)-H(71)	109.5
H(73)-C(7)-H(72)	109.5	H(91)-C(9)-O(8)	109.5(4)
H(92)-C(9)-O(8)	109.5(4)	H(92)-C(9)-H(91)	109.5
H(93)-C(9)-O(8)	109.5(4)	H(93)-C(9)-H(91)	109.5

Table A3.6 Intermolecular distances (Å).

C(4)-Sn(1a)	3.825	H(41)-Sn(1a)	3.514
H(42)-Sn(1a)	3.413	Sn(1)-Sn(1b)	3.738
O(1)-Sn(1b)	2.094	O(3)-Sn(1b)	2.787
C(1)-Sn(1b)	3.014	C(2)-Sn(1b)	3.852
C(3)-Sn(1b)	3.579	O(2)-Sn(1c)	4.089
O(7)-Sn(1c)	3.999	O(5)-Sn(1d)	3.957
O(1)-O(1b)	2.499	O(2)-O(1b)	2.607
O(8)-O(1b)	3.235	C(8)-O(1b)	2.423
H(91)-O(1b)	2.976	O(3)-O(2b)	3.105
O(5)-O(2b)	3.312	C(1)-O(2b)	2.398
H(8)-O(2e)	2.752	H(21)-O(2e)	2.654
H(52)-O(2e)	2.696	H(71)-O(3f)	2.953
C(4)-O(3g)	3.235	H(42)-O(3g)	2.783
H(43)-O(3g)	2.879	C(8)-O(3b)	2.930
H(72)-O(4h)	2.717	O(7)-O(5b)	3.235
H(22)-O(5i)	2.912	H(51)-O(5i)	2.533
C(8)-O(5b)	2.932	C(9)-O(5b)	3.365
H(91)-O(5b)	2.637	C(4)-O(5j)	3.396
H(41)-O(5j)	2.437	O(7)-O(6k)	3.242
H(42)-O(6a)	2.849	H(91)-O(6b)	2.942
C(9)-O(6c)	3.362	H(92)-O(6c)	2.519
C(5)-O(7l)	3.176	H(51)-O(7l)	2.652
C(6)-O(7l)	3.020	C(1)-O(7b)	2.380
C(2)-O(7b)	2.898	H(22)-O(7b)	2.595
C(5)-O(7b)	2.982	H(51)-O(7b)	2.771
O(8)-O(7e)	2.577	H(8)-O(7e)	1.634

C(9)-O(7e)	3.393	C(8)-O(8c)	3.355
C(8)-H(8c)	2.454	C(8)-C(1b)	1.542
C(8)-C(2b)	2.515	C(8)-H(22b)	2.651
H(71)-C(3f)	2.965	C(8)-C(3b)	3.038
H(72)-C(4h)	3.078	H(72)-H(41h)	2.546
H(71)-H(42f)	2.591	C(8)-C(5b)	2.551
H(51)-H(51i)	2.517	C(6)-H(51i)	2.972
C(8)-H(51b)	2.758	C(8)-C(6b)	3.025
H(91)-C(6b)	2.711	H(91)-H(72b)	2.543

Table A3.7 Intramolecular distances (Å).

O(6)-Sn(1)	3.942	H(8)-Sn(1)	2.812
C(1)-Sn(1)	3.468	C(2)-Sn(1)	3.987
H(21)-Sn(1)	3.577	C(5)-Sn(1)	3.692
H(52)-Sn(1)	3.158	C(6)-Sn(1)	4.162
C(9)-Sn(1)	3.348	H(91)-Sn(1)	3.318
O(3)-O(1)	2.909	O(8)-O(1)	3.115
C(2)-O(1)	2.440	H(21)-O(1)	2.654
C(3)-O(1)	2.942	C(5)-O(1)	2.413
H(52)-O(1)	2.556	C(6)-O(1)	3.021
O(7)-O(2)	2.224	O(8)-O(2)	3.049
C(9)-O(2)	3.386	O(4)-O(3)	2.219
C(1)-O(3)	2.834	C(2)-O(3)	2.391
H(22)-O(3)	2.944	C(4)-O(3)	2.629
H(42)-O(3)	2.585	H(43)-O(3)	2.603
C(2)-O(4)	2.351	H(21)-O(4)	2.516
H(22)-O(4)	2.593	H(41)-O(4)	1.994
H(42)-O(4)	1.994	H(43)-O(4)	1.994
H(93)-O(4)	2.804	O(6)-O(5)	2.229
C(1)-O(5)	3.087	C(5)-O(5)	2.408
H(51)-O(5)	2.685	C(7)-O(5)	2.635
H(72)-O(5)	2.571	H(73)-O(5)	2.625
C(5)-O(6)	2.355	H(51)-O(6)	2.942
H(52)-O(6)	2.325	H(71)-O(6)	1.989
H(72)-O(6)	1.988	H(73)-O(6)	1.987
C(2)-O(8)	3.300	H(21)-O(8)	2.660

C(3)-O(8)	3.382	H(91)-O(8)	1.958
H(92)-O(8)	1.957	H(93)-O(8)	1.958
H(21)-H(8)	2.576	C(9)-H(8)	1.994
H(92)-H(8)	2.289	H(93)-H(8)	2.288
H(21)-C(1)	2.059	H(22)-C(1)	2.058
C(3)-C(1)	2.534	H(51)-C(1)	2.055
H(52)-C(1)	2.055	C(6)-C(1)	2.561
C(5)-C(2)	2.453	H(51)-C(2)	2.548
H(52)-C(2)	2.642	H(22)-H(21)	1.568
C(3)-H(21)	2.011	C(5)-H(21)	2.566
H(52)-H(21)	2.394	C(3)-H(22)	2.011
C(5)-H(22)	2.631	H(51)-H(22)	2.363
C(4)-C(3)	2.370	H(42)-C(3)	2.600
H(43)-C(3)	2.600	H(93)-C(4)	3.015
H(42)-H(41)	1.568	H(43)-H(41)	1.568
H(43)-H(42)	1.568	H(93)-H(43)	2.493
H(52)-H(51)	1.568	C(6)-H(51)	2.028
C(6)-H(52)	2.029	C(7)-C(6)	2.359
H(72)-C(6)	2.585	H(73)-C(6)	2.586
H(72)-H(71)	1.568	H(73)-H(71)	1.568
H(73)-H(72)	1.568	H(92)-H(91)	1.568
H(93)-H(91)	1.568	H(93)-H(92)	1.568

Key to symmetry operations relating designated atoms to reference atoms

(a) 1.0+x,y,z

(b) -x,-y,-z

(c) -x,-0.5+y,0.5-z

(d) x,0.5-y,-0.5+z

(e) -x,0.5+y,0.5-z

(f) -1.0+x,y,z

(g) 1.0-x,-y,-z

(h) -1.0+x,0.5-y,-0.5+z

(i) -x,1.0-y,-z

(j) 1.0+x,0.5-y,0.5+z

(k) x,-1.0+y,z

(l) x,1.0+y,z

Fractional atomic co-ordinates ($x10^4$)

	x	y	z
Sn(1)	-744.4(3)	-77.3(3)	1206.0(2)
O(1)	286(3)	1170(3)	33(2)
O(2)	-784(4)	-2163(3)	1700(3)
O(3)	3262(4)	1047(4)	57(3)
O(4)	4458(4)	1645(4)	1683(3)
O(5)	-1775(4)	3917(4)	-1155(3)
O(6)	-2713(4)	3138(4)	129(3)
O(7)	-1591(4)	-4010(3)	915(3)
O(8)	1485(4)	-99(3)	2266(3)
C(1)	813(5)	2442(4)	158(4)
C(2)	2191(5)	2517(4)	1048(4)
C(3)	3319(5)	1656(5)	858(4)
C(4)	5611(6)	820(7)	1564(5)
C(5)	-240(5)	3310(4)	541(4)
C(6)	-1630(5)	3484(4)	-274(4)
C(7)	-4100(6)	3419(8)	-545(6)
C(8)	-1087(5)	-2922(5)	908(4)
C(9)	2558(6)	-1026(6)	2318(5)

APPENDIX 4. EXPERIMENTAL AND INSTUMENTAL DETAILS.

A4.1 *Instrumentation.*

Infrared spectra: Infrared spectra were obtained as finely ground mulls in anhydrous spectroscopic grade liquid paraffin. The mull was sandwiched between windows made of potassium bromide, KBr, to produce a thin film. The spectrometer used for the majority of measurements was a Nicolet 510P Fourier transform device together with computerised data-handling capabilities. The Fourier transform spectra were obtained from 16-64 scans (dependant on sample strength) over the frequency range 4000-400cm^{-1} with a medium slit-width and a peak resolution of 4.0cm^{-1}. The lower-limit of spectra recorded in dry KBr discs is approximately 410cm^{-1} when the KBr itself begins to absorb the radiation.

Microanalytical data: Microanalytical data was obtained using a Carlo-Erba microanalyser. Typically, the furnace temperature was set to 500°C. Where possible, the results quoted are the mean of duplicated measurements. The measurements were referenced against acetanilide, PhNHC(O)CH$_3$ (Ph = C$_6$H$_5$).

Muclear Magnetic Resonance: The majority of ^{1}H and ^{13}C{^{1}H} data were obtained on a Jeol JNM-GX-270FT 270MHz Fourier transform spectrometer at ambient temperature. Occasionally, ^{1}H data was obtained on a Jeol 400MHz device in order to enhance spectral resolution. Multinuclear ^{13}P, ^{19}F and ^{119}Sn spectra were also obtained using the high field Jeol spectrometers. Solid-state MAS-NMR data was obtained in a collaboration with URPSL using the NMR facilities at Durham University.

A4.2 *Reagants and solvents.*

The tin(II) starting materials used during this project were supplied by the Aldrich chemical company and were assumed to be suitable for use without the need for further purification. The only exception to this was the commercially-available tin(II) fluoride which was found to contain substantial levels (>5%) of an unidentified stannic impurity, most probably a stannic oxy-fluoride. The impurities were found to be water-insoluble and were effectively removed by careful recrystallisation from de-oxygenated water. Subsequent application of Mössbauer spectroscopy clearly indicated that the tin(IV) impurities had been successfully removed. The majority of other solid materials were also supplied by Aldrich although citric acid was supplied by BDH, and sodium and potassium α,β-D-glucose-6-phosphates were supplied by Sigma chemicals.

The water used in all reactions was freshly distilled to remove traces of metal ions, e.g. Ca^{2+}. All organic solvents used were standard laboratory grade reagents and were stored over pre-dried molecular sieves (4Å) unless the reaction conditions required that the solvent was scrupulously dried prior to use. For example, in the preparation of tin(II) methoxide, the methanol was carefully pre-dried by distillation from magnesium turnings under an inert N_2 atmosphere. The magnesium metal required activation with a little solid iodine in order to initiate the drying process. Tetrahydrofuran (THF) and toluene were both dried immediately prior to use by distillation from sodium metal under an inert N_2 atmosphere. In order to successfully dry the THF, it was necessary to stand the 'wet' solvent over sodium wire for at least 24 hours prior to distillation. A little benzophenone was added to the distillation flask in order to indicate the level of dryness of the solvent, i.e. a deep indigo colouration indicated that the solvent was suitably dry.

APPENDIX 5. STRUCTURAL INDEX OF NUMBERED COMPOUNDS.

The following pages are intended as a quick reference guide to the numbered compounds contained within Chapters 1 to 4. For further details, refer to the relevant section within the text.

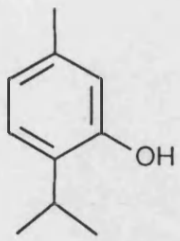

(1)

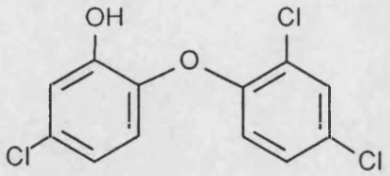

(2)

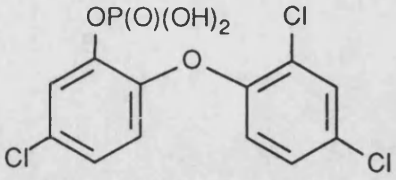

(3)

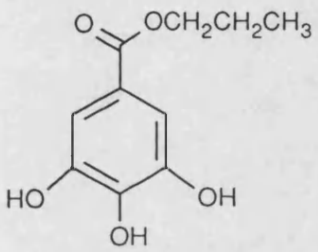

(4)

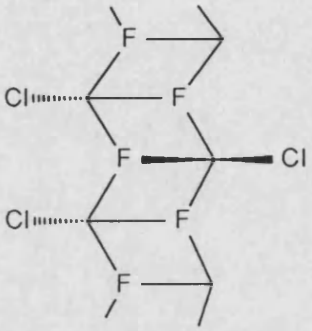

(11)

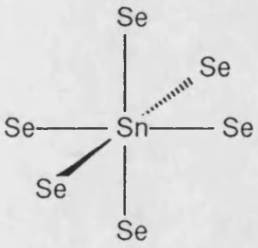

(12)

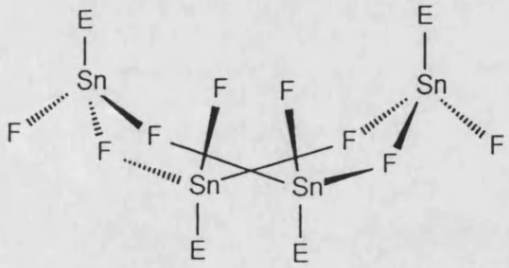

(13)

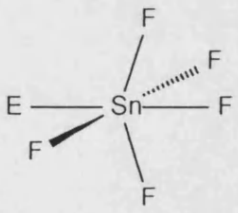

(14)

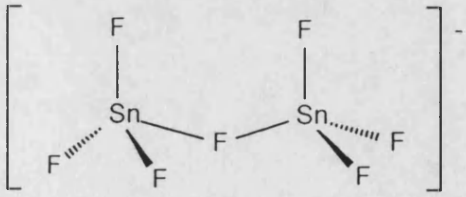

(15)

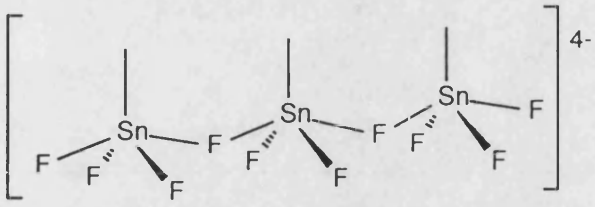

(16)

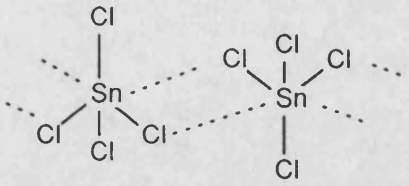

(17)

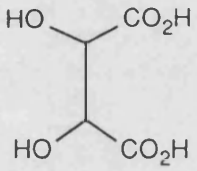

(18)

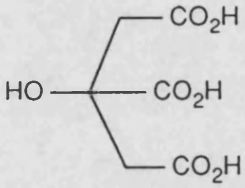

(19)

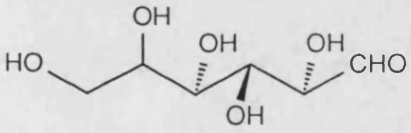

(20)

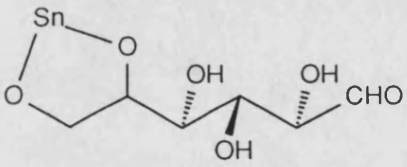

(21)

$SnHPO_3$ (22)

$SnHPO_4$ (23)

$Sn_3(PO_4)_2$ (24)

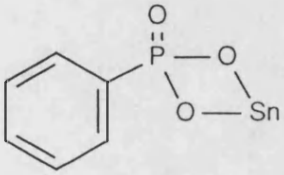

(25)

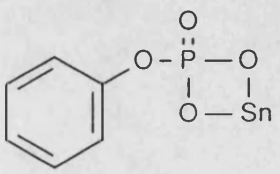

(26)

$Sn_2P_2O_7$ (**27**) $Na_2Sn(P_2O_7)$ (**28**) $ZnSn(P_2O_7)$ (**29**) $KSn_2(P_3O_{10})$ (**30**)

$Sn_2P_2O_7 + 4NaF$ (**31**) $Sn_2P_2O_7 + 4KF$ (**32**) $Sn_2P_2O_7 + 4NH_4F$ (**33**)

$Sn_2P_2O_7 + 4Bu^n{}_4NF$ (**34**) $NaSnF_3$ (**35**) SnF_2 (**36**)

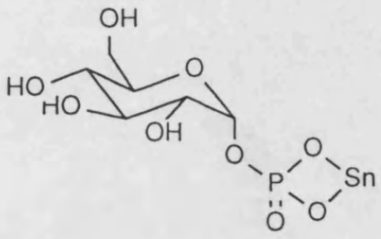

(**37**)

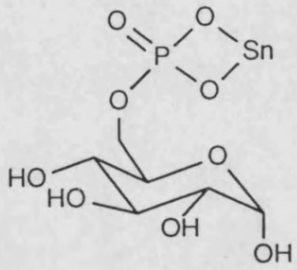

(**38**)

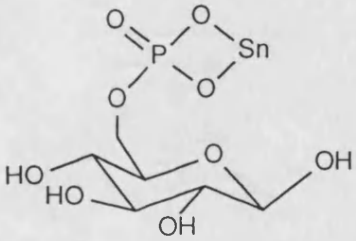

(**39**)

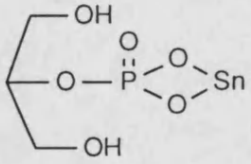

(**40**)

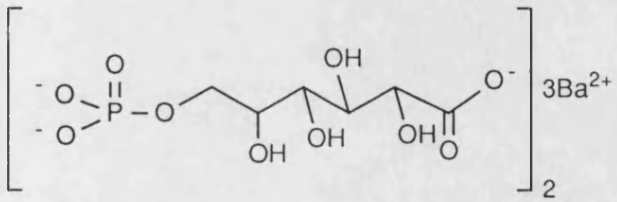

(**41**)

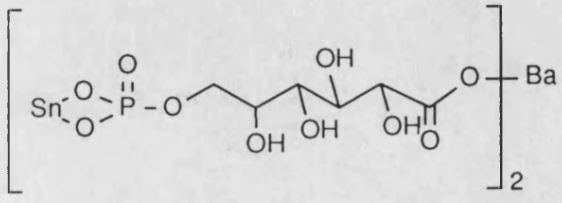

(**42**)

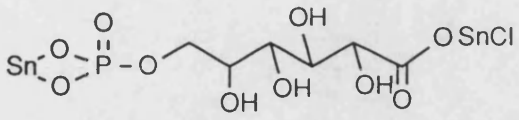

(**43**)

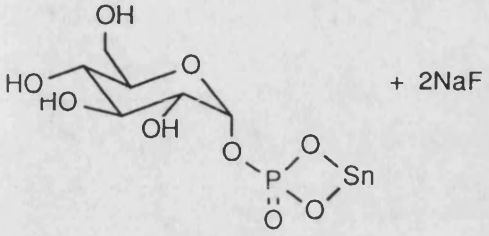

(**44**)

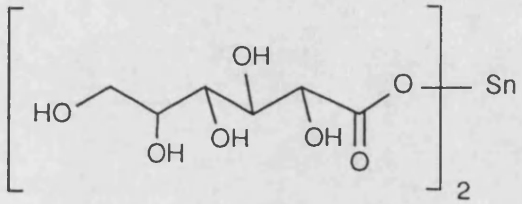

(**45a,b**)

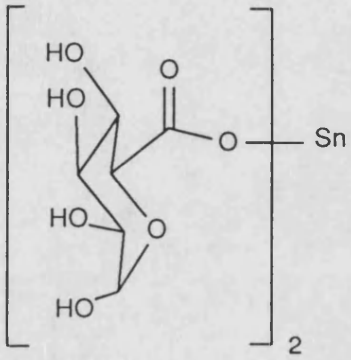

(**46**)

[D-glucose + Sn^{II}] (1:1) (**47**)

[D-fructose + Sn^{II}] (1:1) (**48**)

[D-sucrose + Sn^{II}] (1:1) (**49**)

SnF_2 + D-glucose (1:1) (**50**)

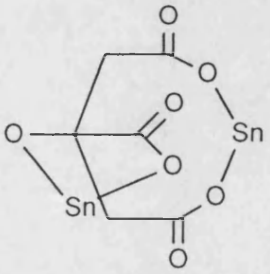

(**51**)

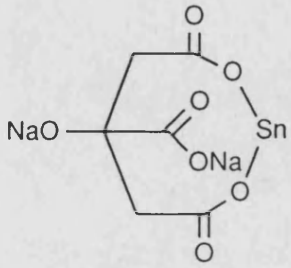

(**52**)

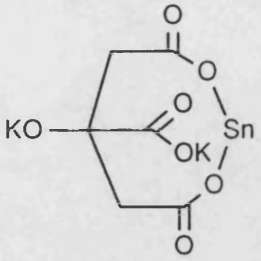

(53)

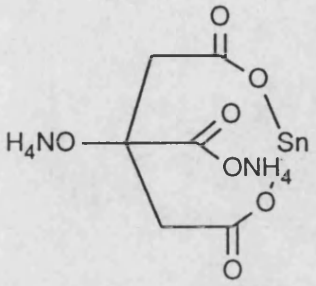

(54)

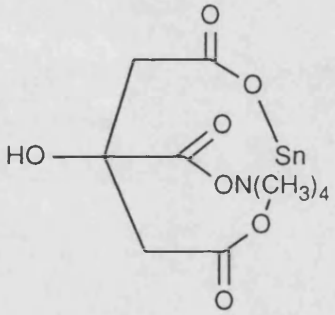

(55)

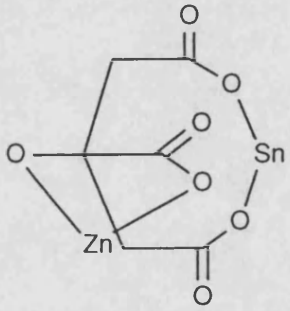

(56)

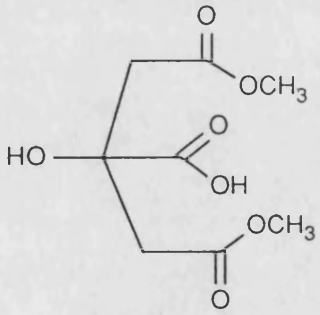

(57)

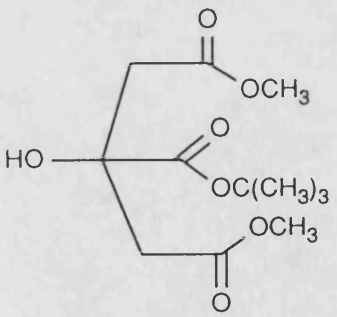

(58)

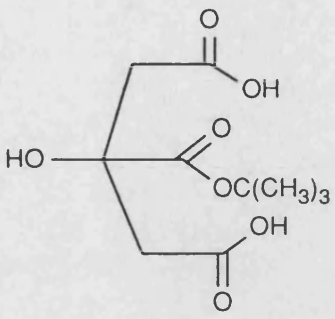

(**59**)

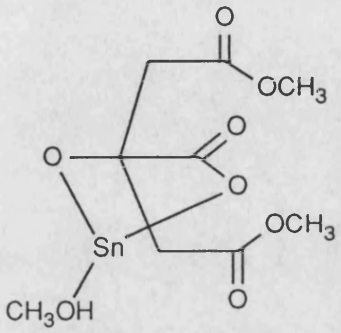

(**60**)

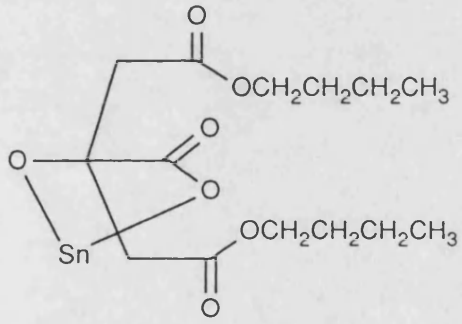

(**63**)

$Sn^{IV}(Hcit)_2[N(CH_3)_4]_2.7H_2O$ (**64**)

Sn_2(citrate) + 4NaF (**65**) Sn_2(citrate) + 4KF (**66**) Sn_2(citrate) + $4NH_4F$ (**67**)

Sn_2(citrate) + $4Bu^n{}_4NF$ (**68**)

REFERENCES.

1 K H Thoma, Teeth, Diet and Health, Century (New York), (1923).

2 The First International Conference on the Declining Prevalence of Dental Caries (Ed. R L Glass), *J. Dent. Res.*, **61**, 1301, (1982).

3 T Roseberry, Dental Science and Dental Art (Ed. S M Gordon), Lea and Febiger (Philadelphia), Ch. VIII, (1938).

4 F J G Van der Ouderaa, *J. Clin. Periodontol.*, **18**, 447, (1991).

5 F J G Van der Ouderaa, D Cummins, *J. Int. Dent.*, **41**, 117, (1991).

6 P D Marsh, *J. Clin. Periodontol.*, **18**, 462, (1991).

7 Nabi et al, *US Patent*, 4 894 220, (1990).

8 D M Francis, *International Patent*, WO 93/18741, (1993).

9 G K Watson, D Cummins, F J G Van der Ouderaa, *Caries Res.*, **25**, 431, (1991).

10 G J Harrap, C A Saxton, J S Best, *J. Periodontol. Res.*, **18**, 634, (1983).

11 C A Saxton, G J Harrap, A M Lloyd, *J. Clin. Periodontol.*, **13**, 301, (1986).

12 R M Lane, *European Patent*, 0 161 899, (1985).

13 F J G Van der Ouderaa, D Cummins, *J. Dent. Res.*, **68**, 1617, (1989).

14 C A Saxton, *J. Periodontol.*, **57**, 555, (1986).

15 C A Saxton, R M Lane, F J G Van der Ouderaa, *J. Clin. Periodontol.*, **14**, 144, (1987).

16 B Svatun, C A Saxton, F J G Van der Ouderaa, G Rolla, *J. Clin. Periodontol.*, **14**, 457, (1987).

17 C A Saxton, R J Gilbert, B Svatun, *Caries Res.*, **21**, 188, (1987).

18 C L Jones, J A Ritchie, P D Marsh, F J G Van der Ouderaa, *J. Dent. Res.*, **67**, 46, (1988).

19 C A Saxton, B Svatun, A M Lloyd, *Scand. J. Dent. Res.*, **96**, 212, (1988).

20 N Tinanoff, *J. Clin. Dentistry*, **2**, 22, (1990).

21 S H Y Wei, International Workshop on Fluorides and Dental Caries Reduction

(Eds. D J Forrester, E M Schultz), (1974).

22 T H Jordan, S H Y Wei, *Arch. Oral Biol.*, **16**, 241, (1971).

23 A F Berndt, *J. Dent. Res.*, **51**, 53, (1972).

24 M Svanberg, G Rolla, *Scand. J. Dent. Res.*, **90**, 292, (1982).

25 N Tinanoff, M A Manwell, R L Zameck, J E Grasso, *J. Clin. Periodontol.*, **16**, 284, (1989).

26 B Svatun, P Gjermo, M H Eriksen, G Rolla, *Acta Odont, Scand.*, **35**, 247, (1977).

27 K Skjorland, P Gjermo, G Rolla, *Scand. J. Dent. Res.*, **86**, 103, (1978).

28 J E Ellingsen, B Svatun, G Rolla, *Acta Odont. Scand.*, **38**, 219, (1980).

29 S L Yankell, N H Stoller, P A Green, R J Shern, *J. Periodont. Res.*, **17**, 374, (1982).

30 B Lilienthal, *Aust. Dent. J.*, **1**, 221, (1956).

31 B Svatun, A Attramadal, *Acta Odont. Scand.*, **36**, 211, (1978).

32 N Tinanoff, D A Camoski, *Arch. Oral Biol.*, **25**, 531, (1980).

33 R V Opperman, G Rolla, J R Johansen, S Assev, *Scand. J. Dent. Res.*, **88**, 389, (1980).

34 V C C Beazley, P Thrane, G Rolla, *Scand. J. Dent. Res.*, **88**, 193, (1980).

35 R L Zameck, N Tinanoff, *Arch. Oral Biol.*, **32**, 807, (1987).

36 P Glantz, *Odont. Rev.*, **20**, 5, (1969).

37 K Ota, S Kikuchi, J W Beierle, *Pediatric Dent.*, **11**, 21, (1989).

38 A Attramadal, B Svatun, *Acta. Odont. Scand.*, **38**, 349, (1980).

39 D A Camoski, N Tinanoff, *J. Dent. Res.*, **63**, 1121, (1984).

40 K Sinkiss, *Calcif. Tissue Res.*, **24**, 199, (1977).

41 H G Langer, *US Patent*, 3 227 707, (1966).

42 C H Cuhonen, *US Patent*, 4 961 924, (1990).

43 P C Waterfield, *European Patent*, 0 514 966, (1992).

44 I R Beattie, *Quart. Rev.*, **17**, 382, (1963).

45 C E Moore, *Natl. Bur. Std., US Circ.*, **3**, 467, (1958).

46 L E Orgel, *J. Chem. Soc.*, 3815, (1959).

47 I Hargittai, J Tremmel, E Vadja, A A Ischenko, A A Ivanoff, L S Ivashkevich, V P Spiridonov, *J. Mol. Struct.*, **42**, 147, (1977).

48 T Fjeldberg, P B Hitchcock, M F Lappert, S J Smith, A J Thorne, *J. Chem. Soc., Chem. Comm.*, 939, (1985).

49 D E Goldberg, D H Harris, M F Lappert, K M Thomas, *J. Chem. Soc., Chem. Comm.*, 262, (1976).

50 W Hoffmann, *Z. Krist.*, **92**, 161, (1935).

51 W J Moore, L Pauling, *J. Am. Chem. Soc.*, **63**, 1392, (1941).

52 P C Génèys, S Vilminot, L Cot, *Acta Cryst.*, **B32**, 3199, (1976).

53 R E Rundle, D H Olson, *Inorg. Chem.*, **3**, 596, (1964).

54 A G Filby, R A Howie, W Moser, *J. Chem. Soc., Dalton Trans.*, 1997, (1978).

55 M Sraummanis, C Strenk, *Z. Anorg. Allg. Chem.*, **213**, 301, (1933).

56 J D Donaldson, W Moser, W B Simpson, *J. Chem. Soc.*, 839, (1961).

57 J D Donaldson, W Moser, W B Simpson, *J. Chem. Soc., (Supp.)*, 5942, (1964).

58 J D Donaldson, W Moser, *J. Chem. Soc.*, 4000, (1960).

59 D E Fenton, R R Gould, P G Harrison, T B Harvey, G M Ometanski, K C T Sze, J J Zuckermann, *Inorg. Chim. Acta*, **4**, 235, (1970).

60 W D Honmick, J J Zuckermann, *Inorg. Chem.*, **17**, 501, (1978).

61 M M Olmstead, P P Power, *Inorg. Chem.*, **23**, 413, (1984).

62 B J Sturm, *Inorg. Chem.*, **1**, 665, (1962).

63 A A Vleek, F Basolo, *Inorg, Chem.*, **5**, 156, (1966).

64 L E Hinkel, E E Ayling, T M Walters, *J. Chem. Soc.*, 403, (1939).

65 M A Khabtak, R J Magee, *Talanta*, **12**, 733, (1965).

66 E Müller, *Meth. der Organische Chemi*, **11**, 422, (1957).

67 J E Anderson, S M Sawtelle, J S Thompson, S A Kretcher-Nguyen, J Calabrese, *Inorg. Chem.*, **31**, 2778, (1992).

68 N Benczer-Keller, T Fink, *Nuclear Physics (A)*, **161**, 121, (1973).

69 V Maenming, M Grodzicki, *Theor. Chim. Acta*, **70**, 189, (1986).

70 P R Deacon, K C Molloy, P C Waterfield, *Unpublished Results*, (1993).

71 J S Morrison, M H Haendler, *J. Inorg. Nucl. Chem.*, **29**, 393, (1967).

72 P Pascal, *Nouveau Traite de Chemie Minerale*, **8**, (1963).

73 P G Harrison, B J Haylett, T J King, *Inorg. Chim. Acta*, **75**, 259, (1983).

74 D Grdenić, B Kamenar, *Proc. Chem. Soc.*, 312, (1960).

75 B Kamenar, D Grdenić, *J. Chem. Soc.*, 3954, (1961).

76 E L Muetterties, *Inorg. Chem.*, **1**, 342, (1962).

77 H Mimi-Yeh, R A Geanangel, *Inorg. Chim. Acta*, **52**, 113, (1981).

78 NMR and the Periodic Table (Eds. R K Harris, B E Mann), 351, (1978).

79 A Bonny, A D McMaster, S R Stobart, *Inorg. Chem.*, **17**, 935, (1978).

80 P Jutzi, B Hielscher, *Organometallics*, **5**, 201, (1986).

81 P A W Dean, *Can. J. Chem.*, **60**, 2921, (1982).

82 J D Donaldson, R Oteng, B J Senior, *J. Chem. Soc., Chem. Comm.*, 618, (1965).

83 T Birchall, G Dénès, K Reubenbauer, *J. Chem. Soc., Dalton Trans.*, 1831, (1981).

84 T Birchall, G Dénès, K Reubenbauer, J Pannetier, *J. Chem. Soc., Dalton Trans.*, 1275, (1985).

85 B L Fournes, L Grannec, C Mirambet, B Darriet, P Hagenmüller, *Z. Anorg. Allg. Chem.*, **601**, 93, (1991).

86 R C McDonald, H H Hau, K Ericks, *Inorg. Chem.*, **15**, 762, (1976).

87 G Dénès, J Pannetier, J Lucas, *J. Solid St. Chem.*, **33**, 1, (1980).

88 P B Darriet, J Galy, *Acta Cryst.*, **B33**, 1489, (1977).

89 R E Rundle, D H Olson, *Inorg. Chem.*, **3**, 596, (1964).

90 J M Van den Burg, *Acta Cryst.*,**14**, 1002, (1961).

91 J Anderson, *Acta Chem. Scand. (A)*, **29**, 956, (1975).

92 R A Howie, W Moser, I C Moser, *Acta Cryst.*, **B28**, 2965, (1972).

93 V G Bergerhoff, H Namgung, *Acta Cryst.*, **B34**, 699, (1978).

94 V G Bergerhoff, L Goost, E Schultz-Rhonof, *Acta Cryst.*, **B24**, 803, (1968).

95 V G Bergerhoff, L Goost, *Acta Cryst.*, **B26**, 19, (1970).

96 P G Harrison, B J Haylett, T J King, *Inorg. Chim. Acta*, **75**, 265, (1983).

97 J D Donaldson, D C Puxley, *Acta Cryst.*, **B28**, 864, (1972).

98 R Weber, *J. Prakt. Chem.*, **26**, 121, (1882).

99 J D Donaldson, W Moser, *J. Chem. Soc.*, 1996, (1961).

100 K Jablcynski, W Weickowski, *Z. Anorg. Allg. Chem.*, **152**, 207, (1926).

101 J D Donaldson, W Moser, W B Simpson, *J. Chem. Soc.*, 323, (1964).

102 D A Everest, *J. Chem. Soc.*, 2903, (1951).

103 J Lees, P A Flinn, *Physics Letters*, **19**, 186, (1965).

104 M Mathew, L W Schroeder, J H Jordan, *Acta Cryst.*, **B33**, 1812, (1977).

105 R Klement, H Haselbeck, *Chem. Ber.*, **96**, 1022, (1963).

106 R Collins, W Nebergal, H Langer, *J. Am. Chem. Soc.*, **83**, 3724, (1961).

107 R C McDonald, K Ericks, *Inorg. Chem.*, **19**, 1237, (1980).

108 R Herak, B Preslesnik, M Curie, *J. Chem. Soc., Dalton Trans.*, 566, (1978).

109 T H Jordan, B Dickens, L W Schroeder, W E Brown, *Inorg. Chem.*, **15**, 1810, (1976).

110 T H Jordan, B Dickens, L W Schroeder, W E Brown, *Inorg. Chem.*, **19**, 2551, (1980).

111 R E Mesmer, R R Irani, *J. Inorg. Nucl. Chem.*, **28**, 493, (1966).

112 J D Donaldson, J F Knifton, *J. Chem. Soc.*, 4801, (1964).

113 A D Christie, R A Howie, W Moser, *Inorg. Chim. Acta*, **36**, L447, (1979).

114 J D Donaldson, A Jelen, *J. Chem. Soc. (A)*, 1448, (1968).

115 P G Harrison, E W Thornton, *J. Chem. Soc., Dalton Trans.*, 1274, (1978).

116 S Majeti, C B Guay, M M Crisanti, *European Patent*, 0 311 260, (1987).

117 A Jelen, O Linquist, *Acta Chem. Scand.*, **23**, 3071, (1969).

118 J C Dewen, J Silver, J D Donaldson, M J K Thomas, *J. Chem. Soc., Dalton Trans.*, 219, (1977).

119 J J Lignane, *J. Am. Chem. Soc.*, **65**, 866, (1943).

120 T D Smith, *J. Chem. Soc.*, 2145, (1965).

121 M M Besso, *US Patent*, 3 213 120, (1965).

122 T Birchall, R Faggiani, C J L Lock, V Maanivannan, *J. Chem. Soc., Dalton Trans.*, 1675, (1987).

123 J Doulezal, M Rousal, J Zina, *Microchem. J.*, **26**, 280, (1981).

124 M A Sieura-Alvarez, A Costa-Garcia, P Tunon-Blanco, S Arribas-Jimero, *J. Electroanal. Chem.*, **179**, 201, (1984).

125 J Zima, M Rousal, J Dolezal, *Microchem. J.*, **26**, 506, (1981).

126 R Gsell, M Zeldin, *J. Inorg. Nucl. Chem.*, **37**, 1133, (1975).

127 P G Harrison, B J Haylett, T J King, *J. Chem. Soc., Chem. Comm.*, 112, (1978).

128 US Pharmacopea, Assay for Stannous Ion, USP XXI 82.

129 K Nakamoto, Infrared and Raman Spectroscopy of Inorganic and Organometallic Compounds (4^{th} Ed^{n}.), 106.

130 P C Waterfield, *Unpublished results*, (1993).

131 R K Harris, P Reams, K J Packer, *J. Mol. Struct.*, **141**, 13, (1986).

132 M J Hudson, A D Workman, *J. Mat. Chem.*, **1**, 375, (1991).

133 D M McArthur, C A Beevers, *Acta Cryst.*, **10**, 428, (1957).

134 H Voellenkle, A Wittmann, H Nowotny, *Monatsch. Chem.*, **94**, 956, (1963).

135 C W Mason, E B Ashcraft, *Ind. Eng. Chem.*, **31**, 768, (1939).

136 R N Bell, *Ind. Eng. Chem*, **41**, 2901, (1949).

137 W H Baur, E Tillmanns, *Acta Cryst.*, **B30**, 2218, (1974).

138 Chemistry Laboratory Handbook (Year 1), University of Bath, 72, (1992).

139 J E Seegmiller, B L Horecker, *J. Biol. Chem.*, **192**, 175, (1951).

140 T Satoshi, H V Tochigi, T Manabu, *European Patent*, 0 400 641 B1, (1993).

141 A A Sheikh-Osman, R Bertani, A Tapparo, G G Bombi, *J. Chem. Soc., Dalton Trans.*, 3229, (1993).

142 J J Hefferen, *J. Pharm. Sci.*, **52**, 1090, (1963).

143 G Schroeter, L Schultz, *Ber. Deutsch Chem. Ges.*, **35**, 2085, (1902).

144 Milewska, Chimiak, Glowacki, *J. Prakt. Chem.*, **329**, 447, (1987).

145 L J Bellamy, The Infrared Spectra of Complex Molecules (2nd Ed.), 179, (1960).

146 L J Bellamy, The Infrared Spectra of Complex Molecules (2nd Ed.), 163, (1960).

147 L J Bellamy, The Infrared Spectra of Complex Molecules (2nd Ed.), 169, (1960).

148 S Tsuji, T Shibati, Y Ito, S Fujii, K-I Tomita, *Acta Cryst.*, **C47**, 528, (1991).

149 Joint FOA/WHO Expert Committee On Food Additives, *FAO Food and Nutrition,* Paper 4, 221, (1978).

150 S Tsuji, Y Tonagai, Y Ito, M Harada, *J. Food Hyg. Soc. Jpn.*, **26**, 357, (1985).

151 S Tsuji, Y Tonagai, Y Ito, M Fukuoka, *Eisei Kagaku*, **32**, 185, (1986).

152 Lecomte, *Rev. Optique,* **28**, 353, (1949).

153 Duval, Lecomte, Douvillé, *Ann. Physique*, **17**, 5, (1942).

154 Douvillé, Duval, Lecomte, *Bull. Soc. Chim.*, **9**, 548, (1942).

155 Duval, Gerding, Lecomte, *Rev. Trav. Chim.*, **21**, 382, (1949).

156 The Chemistry of Penicillin, (Princeton University Press), 382, (1949).

157 G M Sheldrick, SHELX86, A computer program for crystal structure determination, University of Göttingen, (1986).

158 G M Sheldrick, SHELX76, A computer program for crystal structure determination, University of Cambridge, (1976).

159 J D Donaldson, D C Puxley, *Acta Cryst.*, B28, 864, (1972).

160 P J Rentzepris, *Z Kristallogr.*, **117**, 431, (1962).

161 A Jelen, J D Donaldson, Unpublished results (J D Donaldson, The Chemistry

of Bivalent Tin, *Prog. Inorg Chem.*, 287, (1970).

162 A Streitweiser, C H Heathcock, Introduction to Organic Chemistry (3rd Edn.), 902, (1985).

163 B Coxan, *Meth. Carbohydrate Chem.*, **6**, 528, (1972).

164 P J Gorin, *Adv. Carbohydrate Chem.*, **38**, 13, (1981).

165 B Coxan, *Meth. Carbohydrate Chem.*, **6**, 538, (1972).

166 R U Lemieux, *J. Am. Chem. Soc.*, **80**, 6098, (1958).

167 G Kotowycz, R U Lemieux, *Chem. Rev.*, **73**, 699, (1973).

168 J G Buchanan, *Sugar* (Eds. J Yudkin, J Edelman, L Hough), 80, (1971).

169 J G Buchanan, D A Cummerson, D M Turner, *Carbohydrate Res.*, **21**, 238, (1972).

170 A B Deacon, R J Phillips, *Coord. Chem. Rev.*, **33**, 227, (1980).

171 B S Manhas, A K Trikha, *J. Indian Chem. Soc.*, **59**, 315, (1982).

172 J D Donaldson, A Jelen, *J. Chem. Soc.* (A), 2244, (1968).

173 A J F Boyle, D St. P Bunbury, C Edwards, *Proc. Phys. Soc.*, **79**, 416, (1962).

174 R G Bates, G D Pinching, *J. Am. Chem. Soc.*, **71**, 1274, (1949).

175 W B Jennings, *Chem. Rev.*, **75**, 307, (1975).

176 F P Van Remoortere, J J Flynn, F P Boer, *Inorg. Chem.*, **10**, 2313, (1971).

177 C D Garner, P Sutton, S C Wallwork, *J. Chem. Soc. (A)*, 1949, (1967).

178 G J Kruger, E L J Breet, R Van Eldrick, *Inorg. Chim. Acta,* **19**, 151, (1976).

179 C S Harreld, E O Schlemper, *Acta Cryst.*, **B27**, 1964, (1971).

180 J Potenza, R J Johnson, D Mastrpaola, *Acta Cryst.*, **B32**, 941, (1976).

181 J J Park, D M Collins, J L Hoard, *J. Am. Chem. Soc.*, **92**, 3636, (1970).

182 B Kamenar, M Bruno, *Acta Cryst.*, **B28**, 321, (1972).

183 B Kamenar, *Acta Cryst.*, **A34**, 16, (1963).

184 G Arena, A Coutino, S Musameci, R Purello, *J. Chem. Soc., Dalton Trans.*, 3383, (1990).

185 J Strouse, *J. Am. Chem. Soc.*, **99**, 572, (1977).

186 A Cervilla, J A Ramerez, E Llopis, *Transition Met. Chem.*, **11**, 186, (1986).

187 J C Sherlock, S C Britton, *Br. Corros. J.*, **7**, 180, (1972).

188 J D Glickson, T P Pitner, J Webb, R A Gams, *J. Am. Chem. Soc.*, **97**, 1679, (1975).

189 M T Nunes, V M S Gil, *Inorg. Chim. Acta*, **129**, 283, (1987).

190 M M Caldeira, M L Ramos, A M Cavaleiro, V M S Gil, *J. Mol. Struct.*, **174**, 461, (1988).

191 F T Greenaway, *Inorg. Chim. Acta*, **116**, L21, (1988).

192 C H F Chang, T P Pitner, R E Lenkinski, J D Glickson, *J. Am. Chem. Soc.*, **99**, 5859, (1977).

193 M Kakihana, T Nagumo, M Okamoto, H Kakihana, *J. Phys. Chem.*, **91**, 6128, (1987).

194 V I Korsunsky, P G Antonor, T P Lutsko, *Polyhedron*, **11**, 1403, (1992).

195 D E Zacharias, J P Glusker, *Acta Cryst.*, **C49**, 1727, (1993).

196 D E Zacharias, J P Glusker, *Acta Cryst.*, **C49**, 1732, (1993).

197 G Smith, D S Sagatys, R C Bott, D E Lynch, C H L Kennard, *Polyhedron*, **12**, 1491, (1993).

198 D W Hartley, G Smith, D S Sagatys, C H L Kennard, *J. Chem. Soc., Dalton Trans.*, 2735, (1991).

199 D S Sagatys, G Smith, R C Bott, D E Lynch, C H L Kennard, *Polyhedron*, **12**, 709, (1993).

200 H L Carrell, J P Glusker, *Acta Cryst.*, **B29**, 638, (1973).

201 C K Johnson, *Acta Cryst.*, **18**, 1004, (1965).

202 T L Feng, P L Gurian, M D Healy, A R Barron, *Inorg. Chem.*, **29**, 408, (1990).

203 E Asato, W L Driessen, R A G de Graff, F B Hulsburgen, J Reedijk, *Inorg. Chem.*, **30**, 4210, (1991).

204 J Strouse, S W Layten, C E Strouse, *J. Am. Chem. Soc.*, **99**, 562, (1971).

205 J P Glusker, D Van der Helm, W E Love, M L Dornberg, A L Patterson, *J.*

Am. Chem. Soc., **82**, 2964, (1960).

206 N A Yoon, C W Berry, *J. Dent. Res.*, **58**, 1824, (1979).

207 G A Ferretti, J M Tanzer, N Tinanoff, *Caries Res.*, **16**, 298, (1982).

208 T G Tornabene, H Edwards, *Science*, **176**, 1334, (1972).

209 H Fricke, *Phys. Rev.*, **16**, 202, (1920).

210 G Hertz, *Zeit. F. Physik*, **3**, 19, (1920).

211 F W Lytle, D E Sayers, E A Stern, *Phys. Rev.*, **B11**, 4825, (1975).

212 E A Stern, *Phys. Rev.*, **B10**, 3027, (1974).

213 E A Stern, D E Sayers, F W Lytle, *Phys. Rev.*, **B11**, 4836, (1975).

214 B K Teo, P Eisenberger, B M Kincaid, *J. Am. Chem. Soc.*, **100**, 1735, (1978).

215 A Michalowicz, J J Girerd, J Goulon, *Inorg. Chem.*, **18**, 3004, (1979).

216 M Verdaguer, A Michalowicz, J J Girerd, N Alberding, O Kalin, *Inorg. Chem.*, **19**, 3271, (1980).

217 J Reed, P Eisenberger, B K Teo, B M Kincaid, *J. Am. Chem. Soc.*, **100**, 2375, (1978).

218 J Reed, P Eisenberger, B K Teo, B M Kincaid, *J. Am. Chem. Soc.*, **99**, 5217, (1977).

219 J H Sinfelt, G H Via, F W Lytle, *J. Chem. Phys.*, **68**, 2009, (1978).

220 R J Batchelor, J N R Ruddick, J R Sams, F Aubke, *Inorg. Chem.*, **16**, 1414, (1977).

221 J C Machell, D M P Mingos, T L Stolberg, *Polyhedron*, **8**, 2933, (1989).

222 W F Liljemark, C G Bloomquist, G R Germaine, *Infection and Immunity*, **31**, 935, (1981).

223 C Williams, A Allerhand, *Carbohydrate Res.*, **56**, 173, (1977).

224 J V A O'Connor, H A Nunez, R Barker, *Biochemistry*, **18**, 500, (1979).

225 K Bock, C Pedersen, *Adv. Carbohydr. Chem. Biochem.*, **41**, 27, (1983).